2013-10

A Miniaturised Spectrometer Device for the Detection of Nitrogen Dioxide in an Urban Environment

Brian Devine
Technological University Dublin

Recommended Citation

Devine, B. (2013). A Miniaturised Spectrometer Device for the Detection of Nitrogen Dioxide in an Urban Environment. Doctoral Thesis. Technological University Dublin. doi:10.21427/D79594

A miniaturised spectrometer device for the detection of Nitrogen Dioxide in an urban environment

Brian Devine BSc.

A thesis submitted for the degree of Doctor of Philosophy to the Dublin Institute of Technology

Supervisor

Dr. James Walsh

Biomedical and Environmental sensing laboratory

FOCAS institute

Dublin Institute of Technology

October 2013

Abstract

Monitoring of air pollutants, such as Nitrogen Dioxide (NO_2), that are toxic or environmentally damaging is a key metric for environmental protection agencies worldwide. There is a constant need to develop new technologies and methodologies that provide real-time, low cost pollution measurements over a broad range of sampling sites, particularly in urban and industrial areas.

Typically, detection of pollutants in urban environments is performed using a variety of techniques, many of which are expensive, require complex setups and are in fixed locations. The novel system presented in this thesis is designed for portable, low cost and *in-situ* detection of pollutants such as NO_2 using Differential Optical Absorption Spectroscopy (DOAS). The basis for the system is the new generation of miniature fibre optic spectrometers that provide measurement specifications close to those of more traditional high cost DOAS instruments which are used to cross calibrate the initial data. The system can also be calibrated against other NO_2 sampling techniques such as chemiluminescence (CL) monitors. Based on laboratory calibration, the final measurement accuracy of the system in the field was less than ± 0.5 ppb over a calibration dynamic range of 0-50 ppb under typical daylight conditions. This level of accuracy was achieved with repeated measurements, n=10, of custom made calibration cells containing known concentrations of NO_2.

Laboratory experiments using a controlled light source were designed to examine the correlation between absorption and differential absorption using the NO_2 calibration cells with an algorithm based on the Beer-Lambert Law. These laboratory calibration tests verified that differential absorption determined using the novel system can be used to quantify NO_2 concentrations both in the laboratory and in the open atmosphere of a surrounding urban area. Field tests, using ambient sunlight as a source, were then conducted and compared to concurrent CL measurements. Good correlations have been confirmed between the novel-DOAS data and the established NO_2 quantification methods. Results prove that low cost spectrometer systems can be used to identify and quantify gaseous pollutants in real-time using ambient sunlight.

Declaration

I certify that this thesis which I now submit for examination for the award of PhD, is entirely my own work and has not been taken from the work of others, save and to the extent that such work has been cited and acknowledged within the text of my own work.

This thesis was prepared according to the regulations for postgraduate study by research of the Dublin Institute of Technology and has not been submitted in whole or in part for another award in any other third level institution.

The work reported on in this thesis conforms to the principles and requirements of the DIT's guidelines for ethics in research.

Signed_____ Date_____

Acknowledgements

I would like to thank my friends and family for their continued support throughout this project. I would especially like to thank Dr. James Walsh for choosing and guiding me in my PhD. A special thanks also for Dr. Jack Treacy, Dave Byrne, Leonard Bolster, all the researchers in the Biomedical and Environmental monitoring laboratory and the staff and people of the FOCAS institute, DIT and the EPA.

Contents

List of Figures

Chapter 1 Introduction

1.1 Introduction

Urban air pollution is a major worldwide concern, primarily because of the risks to human health, which include damage to the human cardiovascular system from particulate matter (PM) and damage to the respiratory system by chronic bronchitis, pulmonary emphysema, lung cancer, asthma and other conditions [1]. Another major risk factor caused by air pollutants is climate change. Green house gases, such as chlorofluorocarbons, trap infra-red radiation in the Earth's atmosphere causing increases in temperature. As a result of the dangers from these pollutants, national and international regulations have been developed for the monitoring and control of gas concentrations and emissions worldwide, particularly in urban areas[2]. To understand the sources and monitoring of these pollutants, we must have knowledge of the environment where the pollutants are and their interaction with meteorological and natural conditions.

The objectives of the research presented in this thesis were to demonstrate that a miniaturised spectrometer could be developed to measure the concentration of a gas in an urban environment. The specific aims included developing a system that is inexpensive and yet can be compared to current commercial and governmental monitoring systems. The system should also be capable of determining spectroscopically the differential absorption and hence the concentration of a gas without the need of a reference measurement.

The new system, identified as novel-DOAS, needs to be calibrated in the laboratory and in the field. In the laboratory rigorous testing with custom made gas samples are used to determine the accuracy of the analysis. Crucially, in the field, the system needs to be comparable to the existing systems used for monitoring gas pollution by the environmental protection authorities and the analysis of the data should be made in conjunction with data provided by the literature and these authorities.

For this system, the focus will be on the detection of nitrogen dioxide (NO_2) as it is a common gas pollutant found in urban areas. As it is possible to detect NO_2 in the visible range of the electromagnetic spectrum and as it is also monitored continuously by the Environmental Protection Agency (EPA) in the Republic of Ireland, it is an ideal analyte for the development of an optical based system. It is produced by vehicle exhaust and other forms of combustion. Chemiluminescence (CL) and differential optical absorption spectroscopy (DOAS) monitoring systems are the standard method for detecting NO_2 by the EPA and were used for comparisons with the results obtained by the novel detection system as it is the standard method for measuring NO_2 concentrations in urban environments. All the field measurements in this research were specific to Dublin city. It will be shown in later chapters that CL was used for comparisons with the data collected by the novel DOAS instrument proposed in this research as a result of the status of the larger DIT-DOAS instrument that was already in place.

1.2 The Earth's atmosphere

To simplify the structure of the Earth's atmosphere, it is divided up into different layers. The layers consist of complex structures divided up by their altitude and the particular chemistry of each layer. The layers are illustrated in figure 1.1 [3]. Approximately 90% of the content of the Earth's atmosphere is in the lower atmosphere, see figure 1.1. The troposphere extends to approximately 10 km above the Earth's surface in the middle latitudes of the northern hemisphere. The layer above the troposphere, the stratosphere, extends roughly 50 km above the surface. These two layers are separated by a thin layer, known as the tropopause. It is in these two layers that anthropogenic pollution enters the atmosphere. In the troposphere, the sources of the pollution derive from industrial and domestic activities. The pollution detected in the stratosphere can result from air traffic and the vertical transport of pollution due to chemical and physical processes.

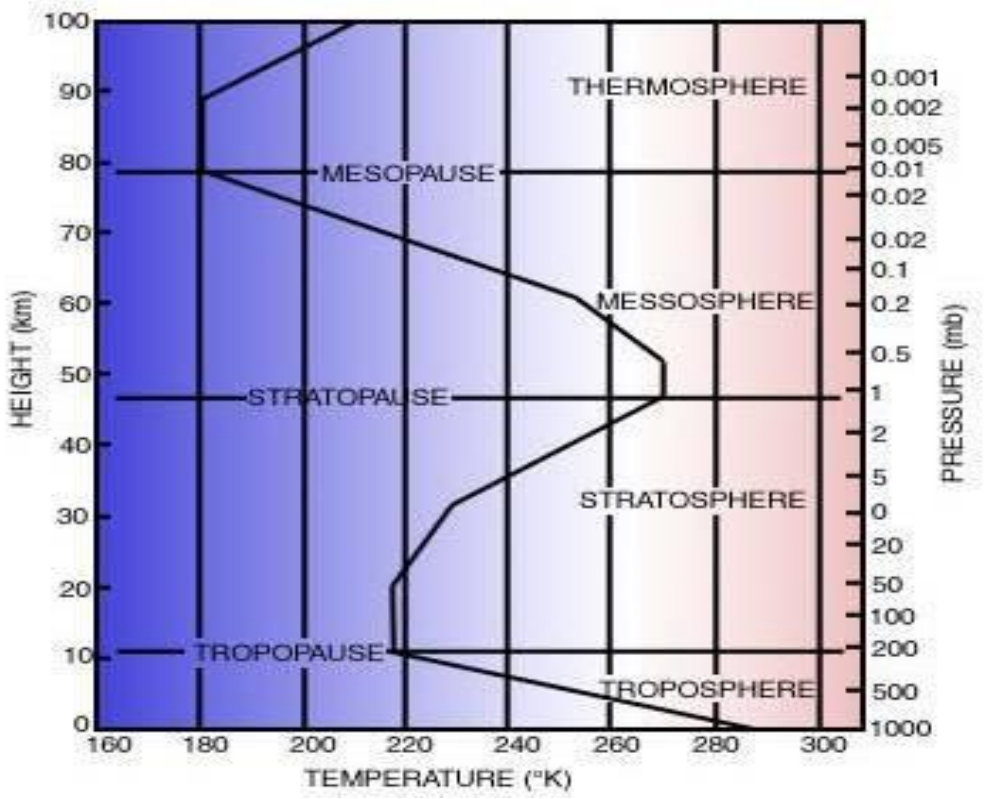

Figure 1.1 The vertical structure of the Earth's atmosphere, each layer is distinguished by temperature, pressure and altitude above the Earth's surface[4]

Close to the Earth's surface, in the lower troposphere, there is a layer known as the planetary boundary layer (PBL) which can reach a height of 1 km to 1.5 km [5]. Figure 1.1 shows how each layer is divided up by height and pressure. The figure also shows the changing temperature gradient throughout the atmosphere. The pressure, temperature and air mass in the atmosphere play a large role in the chemical reactions of gases in the atmosphere. Temperature can affect the absorption cross section of a gas (discussed in chapter 2) and the air mass can affect the transport of solar radiation (also in chapter 2) through the atmosphere [6]. Major constituents of the atmosphere are listed in table 1.1. The content of the air in the atmosphere is made up primarily of nitrogen and oxygen [1, 6]. In comparison, as much as 3% of the atmosphere can be made up of water which affects

humidity and the absorption of solar radiation [7]. Seen as an ideal gas, the air in the atmosphere obeys the ideal gas law (equation 1.1), whereby the pressure and volume of an atmosphere is directly proportional to its temperature[6].

$$PV = nRT \qquad \text{Equation 1.1}$$

where p is the pressure in Pa, V is the volume in m^3, and temperature T in Kelvin, though units can vary for each. As figure 1.1 shows, there is a decrease in pressure with increasing altitude because, as the force exerted by gravity is lower at higher altitudes, the density of the atmosphere then decreases [1]. Other physical effects on the atmosphere include solar radiation [7], the Earth's temperature and the circulation of the atmosphere by wind and the Earth's rotation i.e. the Coriolis Effect [1].

Trace amounts of nitrous oxides (NO_x) and other gases are present from gas phase processes like the carbon and nitrogen cycles [1]. For NO_x, there can be concentrations of ~1 pptv (part per trillion-volume) of NO_2 and ~50 pptv of nitrogen oxide, NO. Besides the naturally occurring trace gases, there are atmospheric constituents resulting from anthropogenic (man-made) sources *e.g.* carbon monoxide, CO, and organic compounds like Benzene.

Gas	Chemical Formula	Mixing Ratio volume (%)
Nitrogen	N_2	78.08
Oxygen	O_2	29.05
Argon	Ar	0.93
Carbon Dioxide	CO_2	0.037
Water Vapour	H_2O	0.00001-3
Hydrogen	H_2	0.00005
Nitrous Oxide	N_2O	0.00003

Table 1.1 Substantial Constituents of the Earth's atmosphere

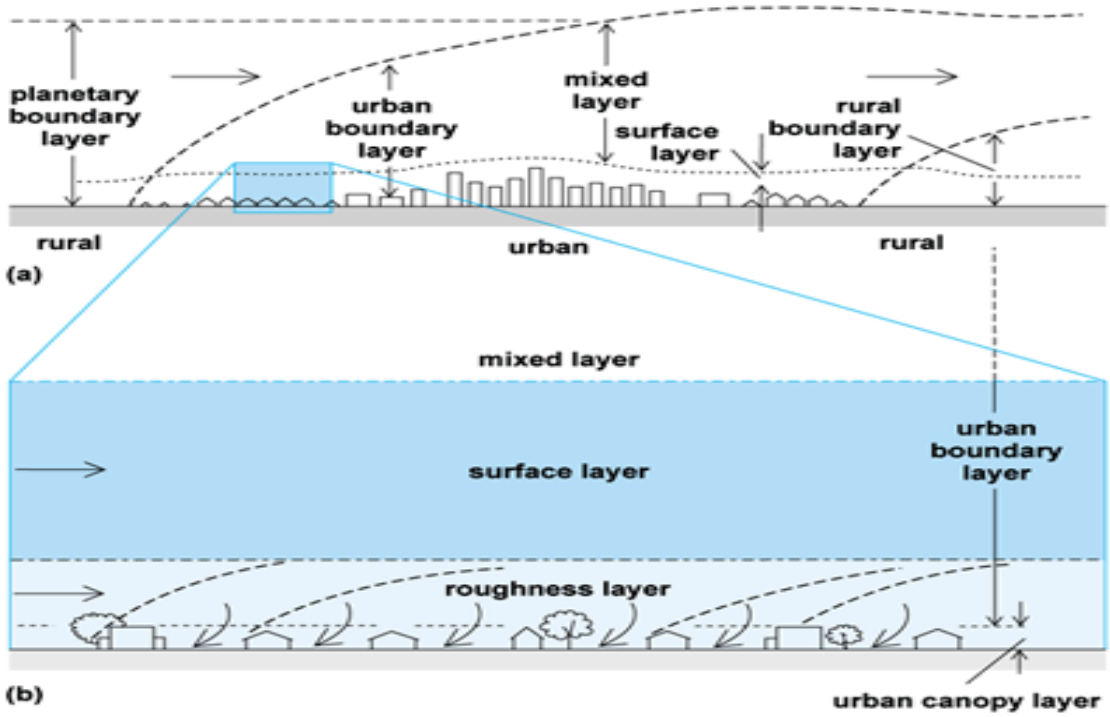

Figure 1. 2 Planetary Boundary Layer (PBL): Illustration of the (a) Planetary Boundary Layer and Urban Boundary layer (b) which has a height roughly that of the surrounding buildings.[5]

As stated in section 1.1, the PBL is approximately 1km to 1.5km in height above the Earth surface. The dimensions of the Urban boundary layer (UBL) can change depending on the velocity of the atmosphere above the surface [8], as shown in figure 1.2. The UBL can either resemble a large plume when the velocity is high, above 3 ms^{-1}, and a 'dome' above the urban area when velocities are less than 3 ms^{-1}.

In figure 1.2, the UBL that is close to the ground is where pollution levels are of most interest [9], as the human activity responsible for the emission of pollutants is below the 1-1.5km altitude and the major weather conditions that disperse the pollution occur close to the ground *e.g.* wind, rain, humidity etc.. The height of the sampling monitors used by environmental protection agencies is ~2 metres above ground [10] which covers the height of human respiration and remote sensing monitors can be situated on rooftops also within the UBL. Satellite monitoring of pollutant emissions are capable of tracking ground column densities of pollutants but are not accurate when there is extensive cloud cover in the line of site. The UBL can also be further divided up into the urban canopy layer, which extends to the height of the buildings, the surface layer above this and the mixed layer extending from the top of the surface layer to the boundary of the UBL and the rest of the PBL [8]. The novel device developed for this research is a ground based remote sensing system which should be capable of measuring the average NO_2 concentration along a path through the atmospheric layers close to the Earth's surface. Therefore, knowledge of the structure and dynamic nature of these layers is needed in the analysis of the recorded data.

1.3 Transportation of pollution

For the measurements of pollutants in an urban environment, an understanding of the atmospheric processes that transport pollutants and trace gases in the atmosphere is needed, as the distribution of pollution is governed by whether the local atmosphere is relatively calm or increasingly turbulent. An urban landscape can affect the transport of pollution because of changes in building heights and the locations of pollution sources. The scale and dimensions of street canyons are determined by the space between buildings in the urban landscape and influence turbulence in the moving air between the buildings. The magnitude of the turbulence in the atmosphere is then determined by the wind's velocity and direction [11, 12]. For traffic, the source of the pollution is dynamic and responsible for diurnal variations in concentrations.

Thermal effects also play a role in the chemical reactions of the pollutants particularly atmospheric inversions which are created by two weather fronts of different temperatures meeting. These inversions can occur laterally and vertically. Inversions mainly occur at night when the ground cools, gradually affecting the temperature at higher altitude, and the lighter pollution rises as the cold air gets heavier. The pollution will meet the inversion which can have the same temperature, preventing it from dispersing. This will create higher concentration levels in one location [1]. As pollution rises it reaches a mixing height, an altitude where a substantial amount of chemical mixing and dispersion occurs. The height of this mixing layer will vary daily and seasonally as a result of changing weather and topography [1]. Some pollutants are more susceptible to the photochemical reactions, where sunlight can cause chemical reactions with pollutants such as Ozone, O_3 and NO. As a result of the dynamic meteorological effects throughout the year, pollution

monitoring of an urban atmosphere is usually provided and correlated with the local weather conditions.

1.4 Types of pollution and the health effects

Anthropogenic air pollution includes carbon oxides, sulphur oxides, nitrogen oxides, ammonia, hydrocarbon compounds, oxidants and particulate matter [1]. Table 1.2 illustrates these different pollutants, the sources and dangers they present to human health and the environment. As can be seen from the table, there are numerous sources of man-made pollution, but not all pollutants are produced from these sources. They can be produced from reactions with other chemicals or result from physical reactions with sunlight, local temperature and even lightning.

Pollutant	Examples of pollutants	Examples of Sources	Risks to Human Health
Carbon Oxides	CO,CO_2	Fuel Combustion	Cardio-vascular damage
Nitrogen Oxides, Nitric acid	NO, NO_2, NO_3, HNO_2	Fuel Combustion	Respiratory cell damage
Sulphur Oxides, Sulphuric acid	SO_2, SO_3, H_2SO_4	Fossil fuels, smelting	Respiratory/ irritant
Hydrogen Compounds	NH_3, HCN	Decomposition/Biomass burning	Toxic, eye irritants
Hydro-carbons	PAH, VOC, CH_4	Gas phases of petrochemicals	Various toxicity from compounds
Oxides	O_3	Photochemical reactions w/ NO_x, etc.	Respiratory
Particulate Matter	PM_{10}, $PM_{2.5}$	Burning, solid waste disposal	Respiratory visibility

Table 1.2 Typical anthropogenic pollutants: sources and the potential risks to human health[1, 13]

Table 1.2 also shows that, for airborne pollutants, people with respiratory conditions are the most at risk. The dangers of the pollutants include aggravation of conditions like emphysema and asthma. Cardiovascular conditions can also be affected by compounds capable of entering the blood stream through the lungs. The human eye is at risk from exposure to larger particles in the atmosphere as well as some of the chemical compounds like the hydrocarbon benzene [14, 15].

Detection methods will be described in more detail later in this chapter (section 1.9) and subsequent chapters, but it is worth noting at this stage that several methods are required to detect and monitor the different pollutants because of the characteristic

chemistry of each pollutant. For example, particulate matter may be detectable by optical means, but for a chemical analysis of its constituents, a sampling method with chemical analysis is more commonly used.

1.5 Pollution chemistry

Carbon oxides such as carbon monoxide and carbon dioxide are produced by the combustion of fossil fuels and are particularly dangerous for human respiration. Carbon Oxides are also green house gases which are responsible for the depletion of the Ozone layer causing increases in the exposure of ultraviolet (UV) rays to humans.

Nitrogen oxides are also produced by combustion and can react with sunlight, ozone, and hydrogen. Reactions between nitrogen and hydrogen create dangerous chemicals such as ammonia, NH_3 and the cyanide ion, CN^- as well as nitric acid, HNO_3. Sulphur oxides are found in the atmosphere from combustion but also, like many other pollutants, they are present due to natural reasons; for sulphur dioxide, SO_2, volcanoes are a large natural source. SO_2 is one of three dangerous gases continuously monitored by the environmental protection agency along with ozone, O_3 and NO_2, which will be examined in more detail in the rest of this chapter and other chapters. NO_2 is the dominant pollutant used to demonstrate the effectiveness of the novel optical instrument described in this work.

Hydrogen can react with carbon and oxygen in a vast number of ways, producing a large range of organic compounds like alcohols, aldehydes and organic acids [1], some of which are collectively known as volatile organic compounds (VOCs) as they can easily be vaporised. These VOCs include solvents like benzene, which can form the basic structure behind more complex hydrocarbons known as polycyclic-aromatic-hydrocarbons (PAHs),

for example Benzene (C_6H_6) based PAHs which are in solid form under atmospheric conditions [1].

Also of interest for pollution monitoring is particulate matter or PM. Like the others mentioned, their presence in the air is from combustion but also from chemical reactions. The particulates can occur by anthropogenic activities like construction where large amounts of fine dust is produced and natural sources like plants, micro-organisms and ocean spray [1]. PM of <20 μm are also known as aerosols, because the particles are suspended in the atmosphere. Aerosols produced from chemical reactions include nitrate aerosols formed from the oxidation of nitrogen oxides, as a result of this the monitoring of these aerosol concentrations can be linked to the concentrations of nitrogen compounds *e.g.* NO_2 [16]. PM sampling instruments usually sample particle sizes of PM_{10} and $PM_{2.5}$ (10 μm and 2.5 μm).

1.6 Photochemistry of NO_2 in the atmosphere

As NO_2 is the pollutant of interest in this work, it is looked at in more detail in the following sections. The concentration of NO_2 is affected by the concentrations of other nitrous oxide gases, ozone and sunlight. O_3 concentrations are monitored at low altitudes for the risks they can pose to humans and there is some correlation between the O_3 concentrations and NO_2 concentrations because of the chemical reactions (Reactions 1.1-3)[1].

$$NO + O_3 \rightarrow NO_2 + O_2 \qquad \text{(Reaction 1.1)}$$

The O_2 in this reaction is a free radical molecule that has one unpaired electron and like NO will rapidly react when exposed to other molecules in the atmosphere. NO can be produced by photochemical reaction when light is absorbed by the molecule as in (reaction 1.2). Equation 1.2 describes the relationship between the energy needed for the reaction and the wavelength λ. For NO_2 reactions are more likely to take place at wavelengths between UV and 420 nm because light in this region has a higher energy.

$$E = hc/\lambda \qquad \text{Equation 1.2}$$

NO_2 absorbs light in the wavelength region of 350 nm to 500 nm, which is largely blue, which is why it appears as a red brown colour [1].

$$NO_2 + h\nu \rightarrow NO + O \qquad \text{(Reaction 1.2)}$$

The Oxygen formed by dissociation in (reaction 1.1) will undergo further reactions to form O_3, (reaction 1.3), where M is a molecule that accepts excess energy from the reaction *e.g.* N_2 [16].

$$O + O_2 + M \rightarrow O_3 + M \qquad \text{(Reaction 1.3)}$$

The Oxygen produced from (reaction 1.2) will react to form several photochemical products including NO_x, peroxy acetyl nitrates (PAN) and O_3. The free radicals will have low concentrations and short residence times in the atmosphere because of the high reactivity of these molecules.

Other photochemical effects are caused by aerosols and large air molecules which cause photons to scatter as they travel through the atmosphere. Large aerosol particles of

sizes ranging from 0.4 μm to 0.7 μm are largely responsible for Mie scattering where light radiation with wavelengths of the same size is scattered. This scattering can affect visibility as a haze. The air particles with sizes of 0.03 μm are responsible for Rayleigh scattering. The small size of the molecules results in scattering of wavelengths of light in the visible region and is the reason for the blue colour of the sky[1] whereas the red sky at twilight is caused by scattering at a much longer pathlength as the Sun appears to set [16]. Another form of scattering is Raman scattering, whereby there is an energy transfer between the scattering molecule and the incident photons. Raman scattering can have an effect on the solar spectrum of ambient sunlight which is used to measure pollution concentration. The processes of scattering and absorption are described in more detail in chapter two as they largely influence the appearance of absorption spectra of the atmosphere.

1.7 Pollution regulations for NO_2

The needs to scientifically quantify the concentrations and emissions of pollutants are outlined in the international and national regulations such as those developed by the EU [9] and the Irish government[17]. The Irish government environmental protection agency (EPA) is responsible for all monitoring, licensing, reporting and policy development in the area of the natural and urban environment of the Republic of Ireland under the Protection of the Environment Act 2003 [15]. The agency is also responsible for the enforcement of environmental regulations. The limits for the average and annual maximum concentrations and emissions are set by the EU. Targets are to be met by each union member within a designated period of time and failure to meet these targets can result in penalties. The EPA

is responsible for the continuous monitoring of pollutants to ensure that these targets are met.

Assessment	**Hourly limit value for the protection of human health(NO_2)**	**Annual limit for the protection of human health (NO_2)**	**Annual critical level for the protection of natural ecosystems(NO_x)**
Upper assessment threshold	140 μgm^{-3}, not to be exceeded more than 18 times a year	32 μgm^{-3} /17 ppb	24 μgm^{-3}/ 12.8 ppb
Lower assessment threshold	100 μgm^{-3}, not to be exceeded more than 18 times a year	26 μgm^{-3}/ 13.8 ppb	19.5 μgm^{-3}/ 10.4 ppb

Table 1.3 Article 35 Annex II of the Clean Air for Europe (CAFÉ) directive. The thresholds for NO_x and NO_2 established from 01-01-2010.

The EU directives outlined for NO_2 concentrations in ambient air quality assessments state the upper and lower thresholds for concentrations that were to be met by 2010 and are as shown in table 1.3. Annex VI of the CAFÉ [9]document describes the measurement methods for different pollutants. The document also outlines the long term objectives for monitoring, concentration limits for the protection of human health and the alert thresholds *e.g.* NO_2 - 400 μgm^{-3} and SO_2 – 500 μgm^{-3}. For human health it is recommended that the levels of NO_2 should not exceed 200μgm^{-3} (106.4 ppb) in one hour more than 18 times /year and 40μgm^{-3} for a calendar year. In contrast, the limit for benzene is 5μgm^{-3} in a calendar year.

1.8 Standard measurement techniques of atmospheric gases

To ensure the regulations are met, the recommended measurement methods for different pollutants can be divided up into categories where samples are extracted and examined separately, *in-situ* monitoring and remote sensing techniques. Each technique can involve instruments that are based on the same scientific method *e.g.* infra-red spectroscopy for separate examination and remote sensing. But the method chosen can be related to the chemical analyte being measured, instrument cost, location, accuracy and specifics of the measurement. The specifics of the measurement refer to measurements where sample examination is more accurately performed with a specific procedure such as sample extraction for further analysis as in the measurement of particulate matter or remote sensing when a large area needs to be monitored.

European Standard methods for different pollutants are listed below in table 1.4. The measurement techniques include sampling and remote sensing methods. The sampling methods include gas chromatography, mass spectrometry, chemiluminescence (CL) and UV photometry. The remote sensing techniques which are predominantly spectroscopic techniques include UV fluorescence, Fourier transform infra-red spectroscopy (FTIR) and DOAS. There are other techniques such as DIAL (Differential Absorption Light Detection And Ranging) and atomic absorption spectroscopy (table 1.2) that can be used for sample analysis but the methods listed in table 1.4 are designated as the standards by the European Union [9]. DOAS is not considered the primary standard for NO_2 measurement but it is popular as it can simultaneously measure several analytes accurately over a large geographical area[13].

Pollutant Compound	Principles of reference method
SO_2	UV Fluorescence
NO_x	Chemiluminescence/Differential Optical Absorption Spectroscopy
CO	Non-dispersive Infrared (IR) Spectroscopy
O_3	UV Photometry
Benzene	PM_{10} with fluorescence/gas chromatography/mass spectrometry
$PM_{2.5}$, PM_{10}	PM reference sampler
Other Heavy Metals (Ni, Cd)	PM_{10} mass spectrometry

Table 1.4 Pollutant Compounds and the standard methods employed to monitor concentrations of each one. [18]

The EPA in Ireland monitors several pollutant gases including CO, SO_2, O_3 and NO_x gases. The concentration levels of these gases are monitored by UV-photometry (tropospheric ozone), UV-fluorescence (SO_2), non-dispersive IR (CO) and CL (NO_x) [9] (see chapter 1). For monitoring, the country is divided up into four geographic zones, see figure 5.1, with Dublin and Cork cities representing zones A and B, and zones C and D representing 21 large towns and the rest of the country respectively [19].

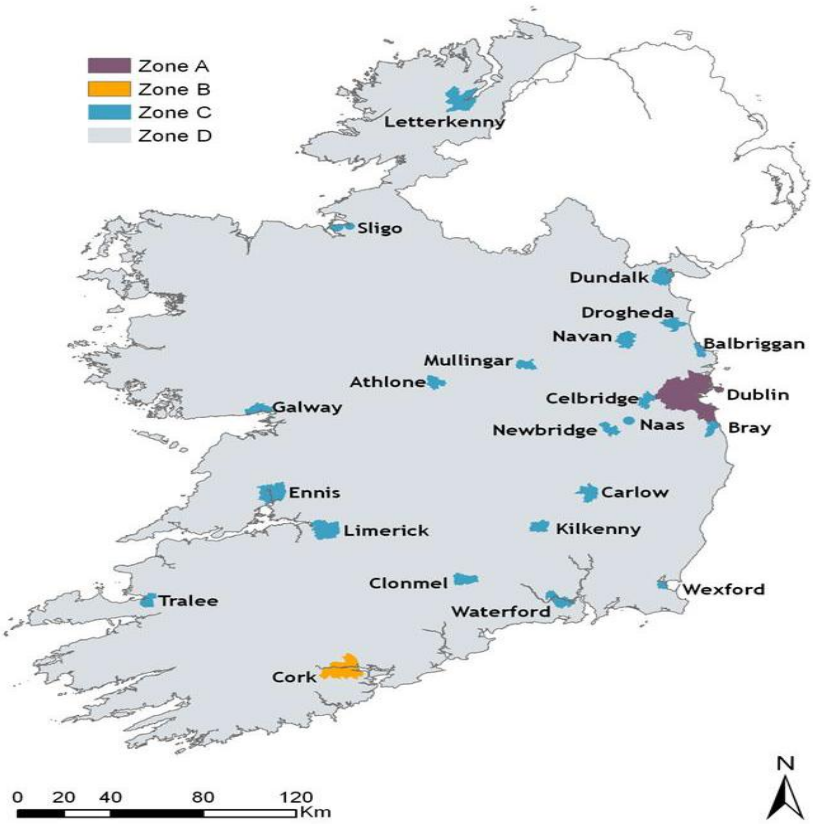

Figure 1. 3 Pollution monitoring zones A-D for the Republic of Ireland zone A covers Dublin city and most of the surrounding urban area. Greater attention is given to this area because of the dense population and activity.

Annual concentrations of pollutants are published by the EPA and are available on the EPA website (www.epa.ie/air/quality/data/rm/gas/) where they are frequently updated. Figure 1.3 [20] shows the annual NO_2 results from individual zones from 2002 to 2011. As would be expected, the concentrations are much greater in the Dublin city zone, followed by Cork in zone B, because of larger traffic congestion and the concentration of population and industry compared to zones C and D.

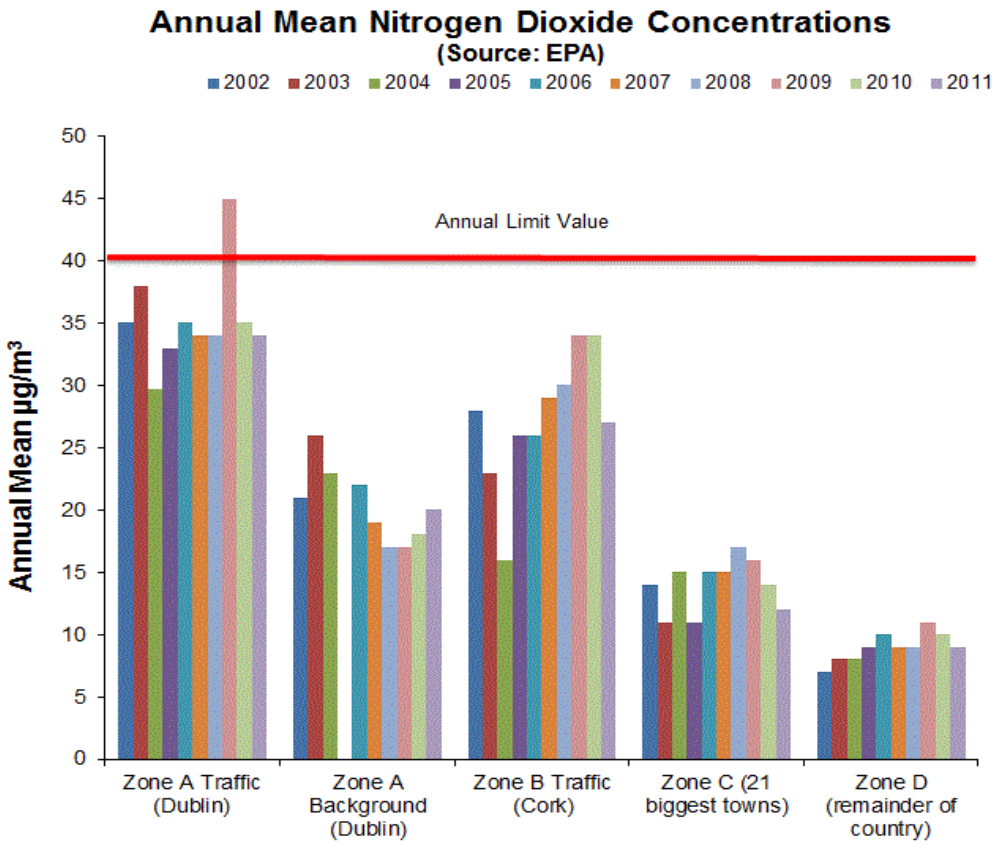

Figure 1. 4 Annual mean NO2 concentrations at each zone 2002-2011 [17]

To monitor NO_2, CL detectors are located in several locations, in Dublin, including Dun Laoghaire and Rathmines on the outskirts of the city centre and Coleraine St. and Winetavern St. in the city centre itself. The higher concentrations of NO_2 in Dublin city make it ideal for calibration of the novel system within the Republic of Ireland. Figure 1.4 shows how the data is presented daily by the EPA and past data is also available from the EPA website, both of which make it possible to compare measurements taken with the novel system to determine if the data shows any correlation.

1.9 Sampling and remote sensing methods for the detection of gas pollutants

In the following examples, the methods employed for detecting pollution by environmental agencies are described with particular attention given to methods used to measure concentrations using samples and remote sensing. Some detail is given into the methods employed to detect NO_2, specifically CL and DOAS, but these will be examined in more detail in the remaining chapters. Chapter 5 will describe how these two methods can be used to determine how well the results of each are correlated.

1.9.1 Gas chromatography

This technique involves the separation of the gas sample for identification[21]. It requires the concentrations of the compounds constituents being proportional to each other when separated by a mobile gaseous phase and a stationary phase. The output is usually combined with mass spectrometry. The method is complex but is very sensitive and can be used for a variety of compounds *e.g.* SO_2 and organic compounds.

1.9.2 Mass spectrometry

Mass spectrometry involves the separation of a sample into its mass-charge ratio. The sample is ionized and the separation is performed using an electromagnetic field

through which the ionized beam is directed. The electromagnetic field is produced by a magnet which splits the beam into different masses that are detected separately and identified when each ion signal is processed into a mass spectrum. The mass charge ratio is described in Equation 1.3.

$$\frac{M}{Q} = (E + \upsilon * B) / a \qquad \text{Equation 1.3}$$

The mass-charge ratio M/Q (kg/C) is proportional to the electric field (V/m) and the magnetic field (T) vector product, E and v*B respectively, and is inversely proportional to the acceleration (m/s^2),a, of the beam. Mass spectrometry is a powerfully sensitive technique for the identification of a sample. It is performed in the laboratory to determine particulate matter constituents, organic molecules and heavy metals. It is often performed with gas chromatography, GC-MS[22].

1.9.3 Particulate matter analysis

Particulate matter (PM) is monitored using a Tapered Element Oscillating Microbalance or TEOM[23], in which a sample is extracted through an inlet and filtered. The filter is weighed before and after extraction and the PM is identified by gravimetric means i.e. the weight difference before and after extraction. The concentration is the total PM divided by the air volume. The different size particulate matter $PM_{2.5}$ and PM_{10} can be monitored separately with PM_{10} monitors used for the detection of large molecules such as organic molecule as well as heavy metals like Lead and Nickel. The methods used to

identify the extracted samples may vary from a combined technique such as gas chromatography mass spectrometry (GCMS) to spectroscopic analysis.

1.9.4 Chemiluminescence

Measurements using CL are made using an air sample extracted through an inlet which then reacts with a molybdenum catalytic converter[24]. Light is passed through the gas and the intensity is measured by a photomultiplier tube (PMT). The concentrations of NO_x and NO are determined separately and the NO_2 concentration is then found by the subtraction of these two. CL detectors have very good sensitivity but are usually used for NO_x measurements only. They are the standard method used by the Irish EPA for nitrogen oxides, a further analysis and more detailed description of CL operation is given in chapter 5.

1.9.5 Ultraviolet photometry

Ozone can be measured with several different techniques including CL [13], DOAS and UV-photometry. UV-Photometry involves the detection of monochromatic light in the UV range passing through a sample and received by a detector. Photometry and spectroscopy involve the measurement of light. Spectroscopy specifically measures the wavelength/frequency of light from absorption and scattering processes caused by its interaction with molecules. Photometry measures the light intensity from chemical and electrochemical reactions such as the measurement of flames intensity when the sample is combusted. The analysis is performed using the Beer-Lambert law (see chapter 2) which

determines the concentration by comparing the amount of light absorbed with the total light emitted taking into account the length of the cell. The exact mathematical description will be explained in more detail in the next chapter as it is used for DOAS. The gas temperature, pressure are usually recorded simultaneously [25]. Measurements of O_3 by the EPA record the concentrations in μgm^{-3} but O_3 measurements are also performed using remote sensing methods where Dobson units (molecules cm^{-3}) are used [26].

1.9.6 Ultraviolet fluorescence

UV fluorescence is used in the detection of sulphur dioxide[21]. The method is based on the principle of fluorescence, whereby light of high energy (UV) is absorbed and after undergoing electronic and vibrational transitions (chapter 2) at high energy levels it emits light of longer wavelengths (visible) as it returns to lower energy levels. The emitted radiation is then detected and used to determine sample concentration. In practice, a light from a single source can be absorbed and the emitted light, consisting of several wavelengths, can be directed through an emission monochromator before reaching the detector. In practice, it is ideal for the detection of species with small molecular cross sections such as free radicals[6]. For pollution monitoring, it is the standard method for the detection of sulphur dioxide.

1.9.7 Non-dispersive infra-red (ND-IR) spectroscopy

Carbon Monoxide can be detected in the longer wavelengths of the infra-red region of the electromagnetic spectrum. For ND-IR spectroscopy, a broadband IR beam is emitted by a heated coil. The beam passes through a glass filter wheel and is split into two beams. One beam passes through a measure cell of nitrogen gas and the other passes through a reference cell with a mixture of CO and N_2. The sample cell with the CO folds the light beam giving it an effective absorption path length of up to 16 m [27]. Upon exiting the sample cell, the beam travels through a band-pass filter cell which narrows the beam to wavelengths where the CO would have absorbed the most. A detector then receives the beams from the measure and sample cells and converts the light signals into voltages which represent the different intensities. Software is used to represent the intensity as a spectrum where different features can be identified at different wavelengths or frequencies. The differences in the two intensities at wavelengths where CO is known to absorb light are used to determine the CO concentration.

1.9.8 Differential optical absorption spectroscopy (DOAS)

Like ND-IR, DOAS is primarily a spectroscopic technique[13]. The operation of the instrument is based on the principle of light received by a detector being absorbed at specific wavelengths. These wavelengths can then be used to identify the components of the medium through which the light has passed. The amount of light absorbed is determined by the ratio of the intensity of the emitted light without any absorber present to

the intensity of the light received after it has passed through the absorber. For differential absorption, the original light intensity before absorption is not known, so a differential absorption is determined mathematically using the attenuated features in the raw intensity spectrum. If the path distance the light takes through the absorber and the wavelengths of the attenuated features in the measured spectrum are known, the concentration of the absorber can be determined. The DOAS technique, described in more detail in chapter 2, involves the detection of a broadband light beam from a source or emitter by a receiver. The receiver converts the light into an electrical signal. The broadband signal is then analysed mathematically by the systems software. The commercial systems determine concentrations of several gases including SO_2, NO_2, O_3[28] and volatile organic compounds (VOCs).

It is worth mentioning other optical methods used to determine the concentrations of gases in the atmosphere, such as LIDAR (LIght Detection And Ranging), photoacoustic spectroscopy and cavity enhanced absorption spectroscopy. These techniques are effective and accurate but do require light sources that are stable and coherent. The photoacoustic and cavity enhanced methods in particular are performed with collected samples rather than by remote sensing [29], [30, 31]. Individual wavelengths of the signal can also be analysed separately to determine the concentration of one analyte.

The DOAS method can also be applied in numerous ways for the remote sensing of pollutant concentrations where no fixed source is used [32]. In these setups, the pathlength is not always known, so the data is measured as a column density *e.g.* m^2/kg. DOAS is the main method used for this research and is described in further detail in the next two chapters. The novel-DOAS device proposed in this research will be designed and

constructed to measure NO_2 using relatively inexpensive equipment and a specially designed algorithm for calculating the differential absorption.

1.10 Summary and thesis structure

The detection of pollution in the atmosphere has become vital in the last 100 yrs as it has been identified as a danger to human health, the environment and the atmosphere. Of particular danger to human health is pollution in the lower troposphere, especially the urban boundary layer because of its proximity to dense urban structures and constant commercial, domestic and industrial activity. The consequences of increased anthropogenic pollution in the lower atmosphere include increasing respiratory, pulmonary and cellular damage to humans.

As well as the chemicals released into the atmosphere, there are several chemical and photochemical reactions that produce dangerous molecules *e.g.* NO reaction with water producing nitric acid which can fall as acid rain under specific meteorological conditions. Regulations to monitor pollution are outlined by the European Union and the Irish Government and the monitoring is performed by the Environmental Protection Agency. Several techniques are employed in the detection of pollutants depending on the type of molecules, size of particulate matter and specific wavelength absorption.

In this thesis, the monitoring of pollutant NO_2 by a novel-DOAS system will be examined. Particular attention will be given to the differences between Passive and Active DOAS. As the portable novel-DOAS system being described is designed to use ambient sunlight (Passive system) the difficulties and advantages this approach will be described in

detail. The history and development of DOAS will be described in chapter 2, as well as the mathematical derivation of the Beer-Lambert law and the effects of light scattering on the atmospheric measurement.

Chapter 3 describes current commercially available DOAS instrumentation as well as descriptions of the software applications, viewing geometry, meteorological aspects and the comparative instruments used in Passive DOAS. Chapter 4 describes the equipment and rigorous setups employed for the laboratory and atmospheric measurements that were performed. Chapter 5 pays particular attention to how Passive DOAS compares to CL, the standard technique for NO_2 monitoring employed by the EPA. The methods used to compare the portable system to the local CL system are also described.

The results of the laboratory and field measurements in chapter 6 demonstrate the effectiveness of the determination of the differential absorption by analysis of the atmospheric spectra. The laboratory results will show how well the differential absorption compares to absorption determined with a reference measurement and the field data will illustrate how the system can be calibrated outside the lab and how comparisons of CL data recorded by the EPA can be achieved.

CHAPTER 2 Differential Optical Absorption Spectroscopy

2.1 Introduction

In this chapter, closer attention is given to differential optical absorption spectroscopy (DOAS). A description is given of how the concentration of an analyte such as NO_2 is measured using the absorbed light along a fixed pathlength. The mathematical determination of gas concentration is performed in DOAS by the Beer-Lambert Law which requires a constant known as the absorption coefficient.

The absorption coefficient for NO_2 can be known for a range of wavelengths but, for the analysis method used in this thesis, a single value for a range of wavelengths is required and a description is provided here on how that value is obtained.

An analysis is also provided of the theory behind the two forms of DOAS measurements that can be achieved with and without a fixed light source and a known pathlength.

2.2 Light scattering effects

Measuring a gas using absorption spectroscopy requires an understanding of the physical processes that affect electromagnetic radiation, light, as it travels through an analyte. The interaction of light with the atmosphere is typically described as extinction

processes. Extinction can occur in three different ways, from elastic scattering of the light, inelastic scattering and absorption [12]. Elastic scattering occurs when a photon collides with a molecule in the atmosphere and is scattered away from it. The energy of this scattered photon is equal to the energy of the incident photon before the interaction. There are two types of elastic scattering: Rayleigh scattering where the scattering particles are of a relatively small size compared to the wavelength of light, for example molecules of N_2 and O_2. Larger particles such as those found in particulate matter (PM) cause the type of elastic scattering known as Mie scattering.

Inelastic scattering is caused by a photon colliding with a molecule where a fraction of its energy is lost as it is transferred to the molecule. The molecule may also transfer a portion of its energy to the photon. Raman scattering is inelastic scattering where the scattering particle is smaller than the wavelengths of the incident and scattered light. Raman scattering can be explained in quantum mechanical terms as occurring as rotational when the angular momentum, J, of the particle is affected by the interaction and vibrational when its harmonic oscillation is affected[6]. The vibrational Raman scattering is the weaker of the two forms of Raman scattering.

2.3 Determination of gas concentration by absorption

Joseph von Fraunhofer was the first to observe dark absorption lines in solar spectra using spectroscopic gratings[33]. These lines where later identified as the absorption of light at different wavelengths in the Sun's atmosphere. Figure 2.1 shows the spectrum of a 6000 K black body radiator (red) compared to the extraterrestrial solar spectrum (blue) and

figures 2.2 shows the difference between the extraterrestrial solar spectrum (blue) and a direct spectrum (green). These images are from a DIT Matlab file developed from data found in the Simple Solar Spectral Model for Irradiance [7].

Direct solar radiation occurs when the sunlight is perpendicular to the Earth's surface. Indirect, diffuse solar radiation is sunlight scattered by clouds, PM and water vapour. Indirect scattering is responsible for daylight, even on overcast days, but the path the light travels through the atmosphere can vary depending on the atmospheric conditions [34].

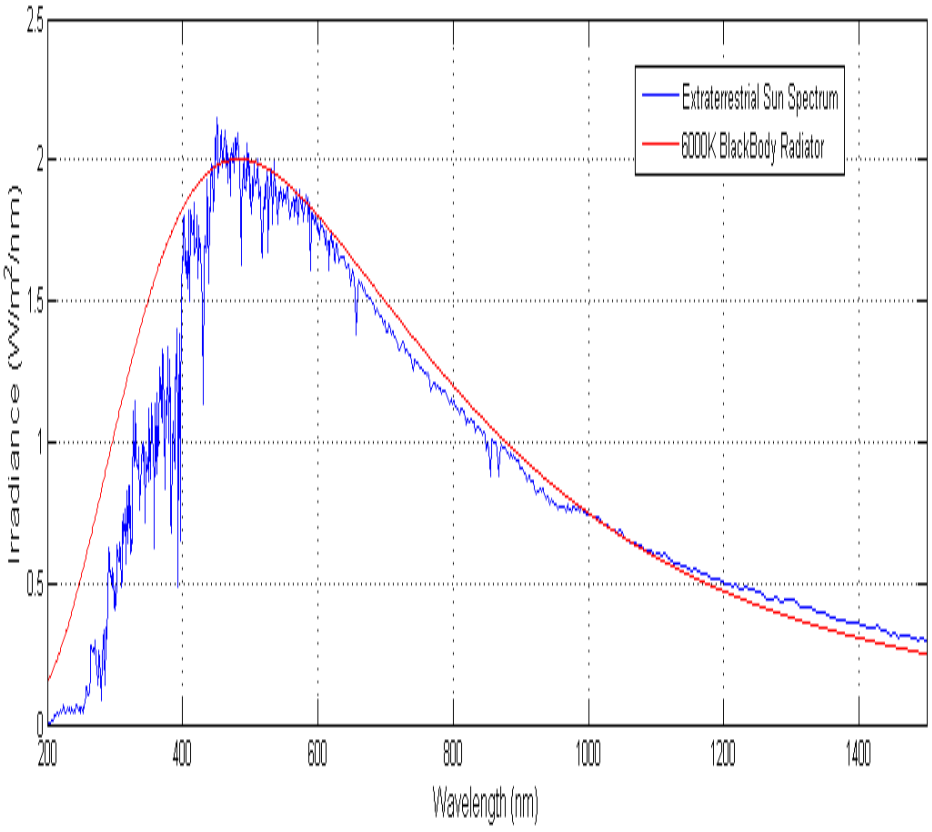

Figure 2.1. Extraterrestrial Sun spectrum (blue) and the spectrum of a 6000K blackbody radiator (red). The features in the extraterrestrial spectrum are caused by the scattering and absorption of the light at the surface of the Sun[7].

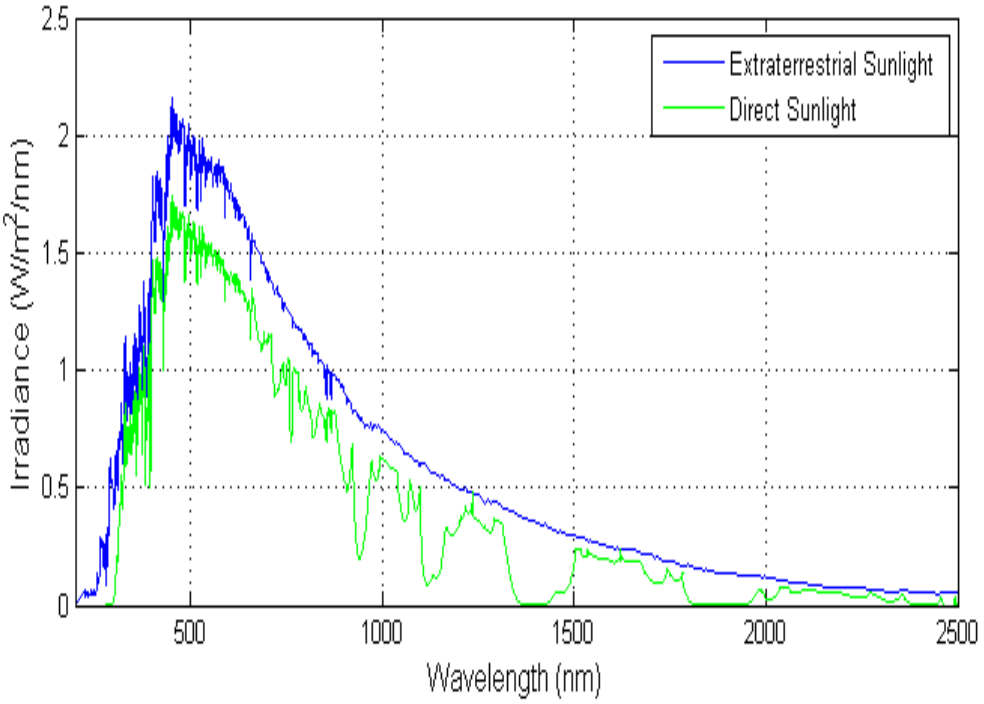

Figure 2.2 Extraterrestrial (blue) Sun spectrum and direct (green) Sun spectrum [7] . Note the attenuation of the spectrum especially in the infrared region 800 nm to 2500 nm

As figures 2.1 and 2.2 show, Fraunhofer features are abundant throughout the solar spectrum and must be taken into account when a measurement of atmospheric pollutants is determined using wavelength dependent variables. Figure 2.3 shows dominant Fraunhofer lines between 340 nm and 460 nm. The letters N, L, K, H, e and G are the alphabetical labels of the Fraunhofer lines used represent the elements iron, Fe (letters N, L and e), calcium, Ca, (K) and nickel, Ni which cause absorption at each wavelength [35]. Figure 2.3 shows both the alphabetical designation and the chemical symbol for significant lines between 340 nm and 460 nm.

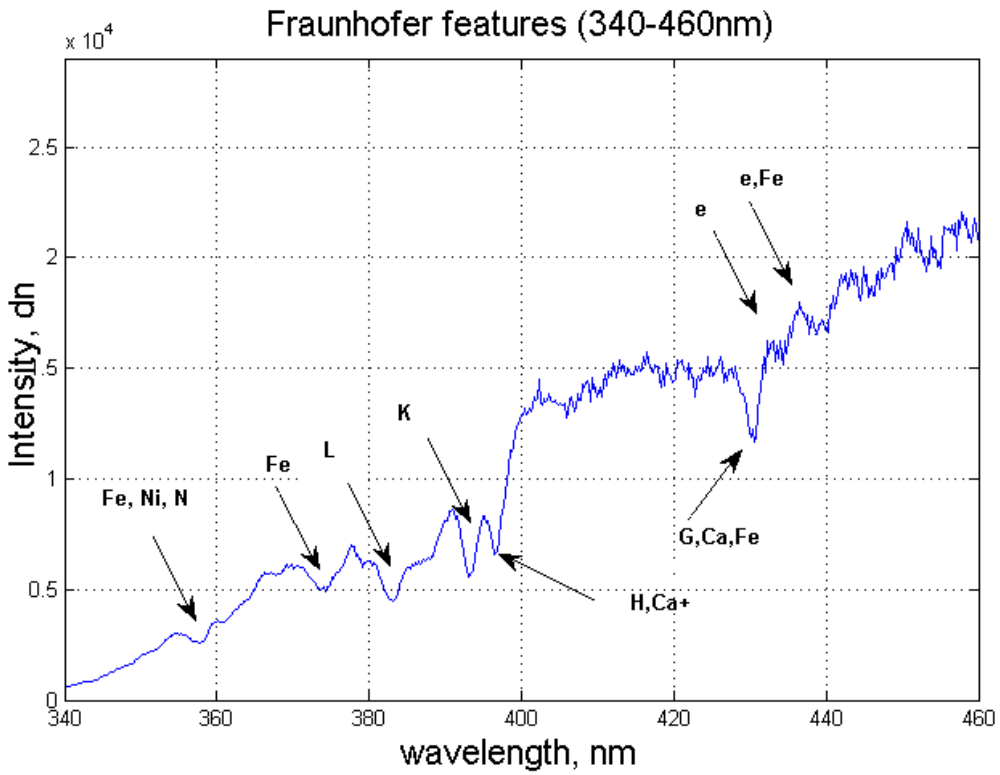

Figure 2.3 Solar Spectrum with Fraunhofer (FH) lines (measured with USB4000 spectrometer). Significant FH lines between 360 nm and 400 nm, between 420 nm and 460 nm the most significant FH line is near 435 nm.

An effect of Fraunhofer lines is the "Ring" effect which is most likely caused by rotational Raman scattering, whereby the angular momentum of the molecules in the atmosphere are affected by collisions which can cause changes in the wavelengths of Fraunhofer lines depending on the molecules with which the incident light interacts [36-38]. The effect can also be described as a "filling in" of the Fraunhofer features in direct sunlight more than those in indirect sunlight and can be seen as the features appear deeper or more skewed than features with little influence from the Ring effect. The effect can be

approximated using a spectrum which is the reciprocal of a reference direct sun spectrum taken at noon or as a fraction, as in equation 2.1.

$$I_{ring} = I_{inelastic} / I_{elastic} \qquad \text{Equation 2.1}$$

The Ring effect is of concern when spectral analysis is made of a broad spectral range, but can be minimised when only a few wavelengths are used for the analysis, as absorption features can be chosen that have no or negligible interference from Fraunhofer lines but are still known to show absorption features of atmospheric gas under investigation.

The absorption of a photon by a molecule differs from the scattering effects as the number of photons changes after the collision. An absorber such as NO_2 will absorb colours in the visible range of wavelengths, except the longer wavelengths which is why it has a brown reddish colour. The energy is mathematically related to the wavelength of the incident and emitted light by equation 2.2 (equation 1.2 chapter1).

$$E=hc/\lambda \qquad \text{Equation 2.2}$$

where the speed of light, (italic *c*)**,** in ms^{-1} is equal to the product of the lights wavelength, (**λ**), in nm and the frequency (f), in Hz.

$$c=f\lambda \qquad \text{Equation 2.3}$$

The intensity of incident light on a medium where light is absorbed can be attenuated by the medium at certain wavelengths that can be used to identify the absorber.

2.4 Beer-Lambert law

The transmission of light through an absorbing medium is proportional to the ratio of the intensity of light before it passes through the medium to the light after it is absorbed, see equation 2.4. Where ε is the molar absorptivity (m^2/mol) and N (cm^{-3}) is the number density of the specific absorber under investigation.

$$\log_{10} T = \log_{10} I / I_0 = -\varepsilon NL \qquad \text{Equation 2.4}$$

$Log_{10}T$ is also commonly referred to as the Optical Density. Alternatively, the Lambert-Beer law is commonly expressed as.

$$\ln T = -\alpha L \qquad \text{Equation 2.5}$$

where α is the absorption co-efficient of the material, in units of cm^{-1}. α can also be expressed in terms of the number density of absorbing species per unit volume, N (cm^{-3}) as $\alpha = \sigma N$, where σ is the absorption cross section per species, in units of cm^{-2}. Relating equations 2.4 and 2.5, $\varepsilon c = \alpha \log_{10} e = \sigma N \log_{10} e$. Thus [39].

$$\ln T = -\varepsilon NL \log_{10} e \qquad \text{Equation 2.6}$$

According to Beer's law, the absorber concentration is directly proportional to the absorption which is also proportional to the ratio of the incident light and the transmitted light at wavelengths λ[13]. In equation 2.7, I_o (λ) represents the light incident on the absorber and I (λ) the attenuated light, the fraction of I_o/I is directly proportional to c.

$$\frac{Io(\lambda)}{I(\lambda)} \approx N \qquad \text{Equation 2.7}$$

J.H. Lambert showed that the fraction of transmitted light and light collected is also proportional to the thickness of the absorber[6], or more specifically, the path taken by the light through the absorber as shown in equation 2.8. Figure 2.4 illustrates the light transmitted from an emitter (lamp) to receiving optics and detector with no absorber (a), and the light transmitted through an absorber in (b). The light attenuated by the absorber in (b) is illustrated by the broken line.

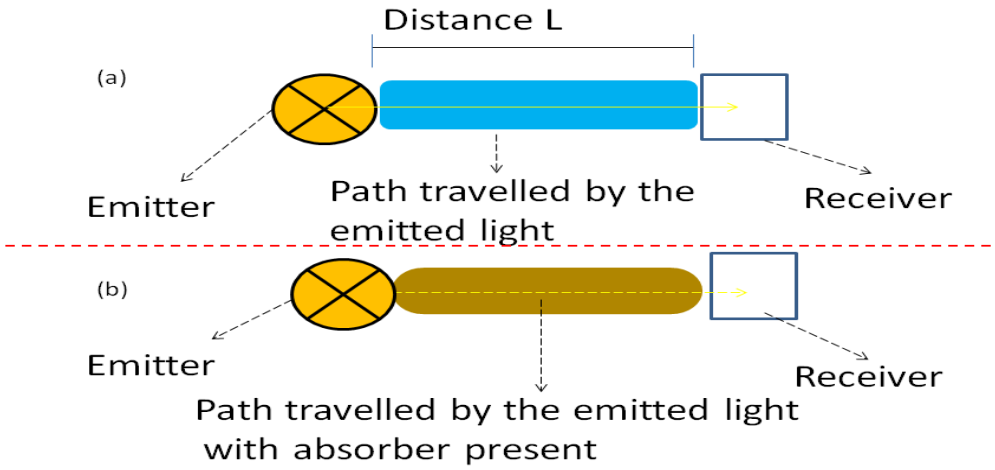

Figure 2.4 (a) light transmitted from an emitter lamp to a receiver over a distance L with no absorber (b) light attenuated (broken line) by the absorber.

$$\frac{Io(\lambda)}{I(\lambda)} \approx L \qquad \text{Equation 2.8}$$

The absorption of the light (A) by the absorber is determined mathematically as the natural logarithm of the fraction of light emitted I_o (λ) to the light absorbed I (λ) because

the attenuation of the beam of light by the absorber over the pathlength L is decreased exponentially.

$$A(\lambda) = -\ln(\frac{I(\lambda)}{I_0(\lambda)}) \qquad \text{Equation 2.9}$$

Taken together equations 2.7 to 2.8 show that the total absorption is directly proportional to the product of concentration of the absorber and the pathlength traversed by emitted light towards the receiver, equation 2.10.

$$A(\lambda) = \ln(\frac{Io(\lambda)}{I(\lambda)}) \approx NL \qquad \text{Equation 2.10}$$

To determine the concentration of a gas absorber for more than one wavelength, over pathlength L, the nature of the absorbing medium and the characteristic absorption cross section, $\sigma(\lambda)$ at specific wavelengths, needs to be known. For measurements of gas pollution, the absorption cross section represents the characteristic absorption profile of the gas. It is used to identify the dominant wavelengths or frequencies at which light is absorbed by the pollutant. Equation 2.11 shows the Beer-Lambert Law with the absorption cross section, $\sigma(\lambda)$, which has units of cm^2 $molecule^{-1}$. The concentrations of gaseous pollution are measured by the environmental protection agency (EPA) in gravimetric units i.e. $\mu g\ m^{-3}$, the absorption cross section should be converted to $m^2\ \mu g^{-1}$, with $\sigma(\lambda)$ replaced by the absorption coefficient $\alpha(\lambda)$, as seen in equation 2.12. The absorption $A(\lambda)$, $\sigma(\lambda)$ and $\alpha(\lambda)$ are all wavelength dependent.

$$A(\lambda) = \ln(\frac{Io(\lambda)}{I(\lambda)}) \approx \sigma'(\lambda)cL \qquad \text{Equation 2.11}$$

Rewriting 2.11 with the absorption coefficient α(λ):

$$A(\lambda) = \ln(\frac{Io(\lambda)}{I(\lambda)}) \approx \alpha(\lambda)L \qquad \text{Equation 2.12}$$

To convert the units from cm^2 $molecule^{-1}$ for σ(λ) to m^2 μg^{-1} for the coefficient α(λ), the conversion factor, a numerical value of 1.3×10^{12} is used. For example typical values for an absorbing NO_2 feature at 435 nm - 440 nm are $\sigma' = 2.6 \times 10^{-19}$ cm^2 $molecule^{-1}$ which converts to 3.4×10^{-7} m^2 μg^{-1}, see section 2.6.

For NO_2, the dominant absorbing wavelengths in the UV-visible range extend from 350 nm to 600 nm. Within this range of the absorption spectrum of NO_2, the transitions between states are electronic in nature but are enriched by vibrational and rotational substructure[40]. Figure 2.5 shows the typical profile of NO_2 determined using an Ocean Optics miniaturised spectrometer. The accuracy of the measurement depends on the resolution of the instrument's detector. The absorption is calculated by the instrument software using equation 2.6 for the wavelength range 200 nm to 1100 nm.

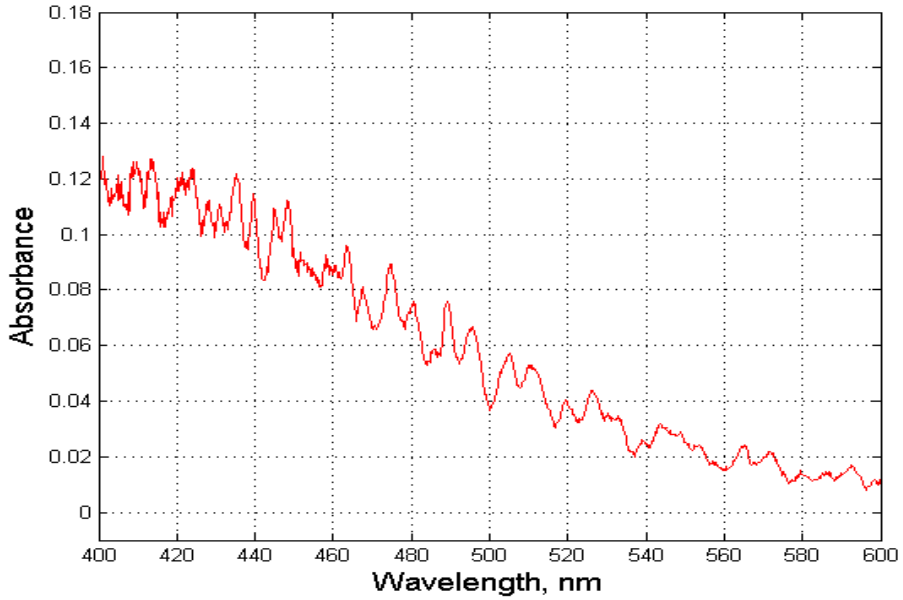

Figure 2.5 Absorption profile of NO_2 between 400 nm to 600 nm NO_2 has prominent absorption features in the visible region. This image was developed using a USB 4000 miniaturised spectrometer.

The absorption coefficients of NO_2 for each of its absorption features can be determined from the literature, and several examples are available such as Schneider (1987), Burrows (1998), Vandaele (1998) and Bogumil (2003) [4, 41-44]. Each of these examples may have different instrument resolutions [45] depending on the technique used to determine α. Therefore, a value for the absorption coefficient should be measured in the laboratory using a sample with known concentration, c, over a fixed pathlength. L. The absorption calculated from a single feature is modified to equation 2.13, where α (λ) represents the absorption coefficient determined for the same three wavelengths.

$$A(\lambda) = \ln(\frac{Io(\lambda)}{I(\lambda)}) \approx \alpha'(\lambda)L \qquad \text{Equation 2.13}$$

To determine the concentration from a single absorption feature, A(λ) is determined from three intensities that correspond to three wavelengths on the absorption feature. The three points are the peak (P1) and either side of the base of the feature (B1 and B2) at ~440 nm illustrated in figure 2.6.

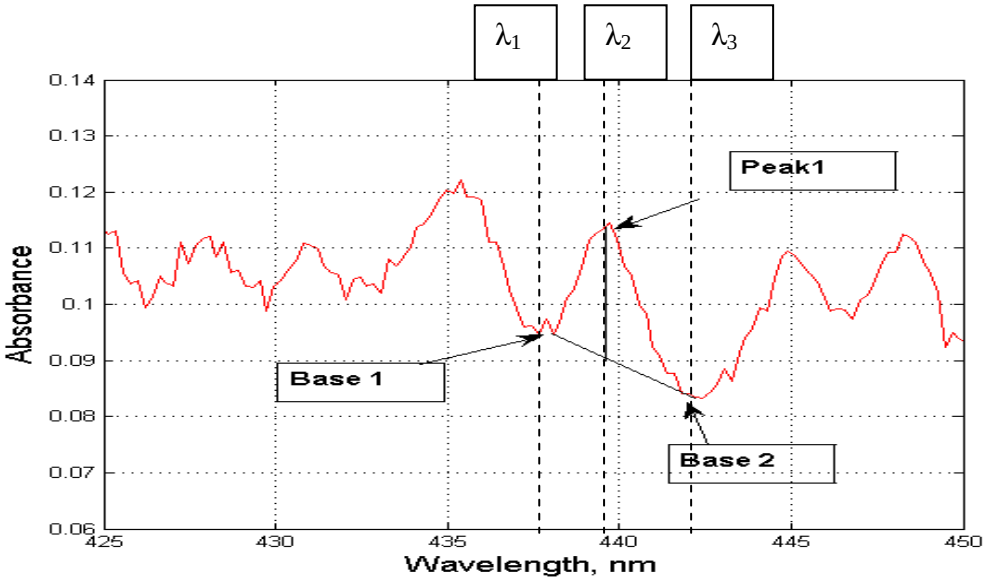

Figure 2.6 Determination of the absorption using a single absorption feature at 440 nm detected by a USB 4000 spectrometer

$$A(\lambda) = P_1 - \left\{ B_2 + (B_1 + B_2) \times (\frac{\lambda_2 - \lambda_1}{\lambda_3 - \lambda_1}) \right\} \qquad \text{Equation 2.14}$$

The wavelengths λ_1 to λ_3 in equation 2.14 represent the wavelengths of the absorption feature in fig. 2.6. These are 437 nm, 439.5 nm and 443 nm. In the laboratory, the light measured where no absorber is present, $I_o(\lambda)$, is known as the reference

measurement. This can be measured by ensuring that there is none of the absorber under investigation in the light's path.

2.5 Differential absorption of NO_2

Absorption spectroscopy is an established method for identifying and quantifying various analytes which involves comparing a reference spectrum to spectra of different absorbers. However, under conditions where the absorber cannot be removed, *e.g.* atmospheric measurements in which background concentrations are always present, then a reference measurement is not possible. To overcome this, several methods of determining a mathematical reference $I_o'(\lambda)$ have been developed as described in the following section.

As described in section 2.3, absorption spectra are commonly found by dividing a broadband reference spectrum measured with no absorber present, $I_o(\lambda)$, divided by a spectrum measured with an absorber, $I(\lambda)$, or absorbers, according to equations 2.7 to 2.11. To determine the absorption without reference spectra requires a mathematical analysis of the measured spectra that contains attenuated features caused by the absorbing substances. This approach can be used for liquids and solids but the description here is focussed on spectroscopy of NO_2 gas.

To determine what is known as the differential absorption, the prominent absorption features of NO_2 need to be identified. These features are used to locate the attenuated features of NO_2 in raw intensity spectra of a gas sample in the laboratory. The features can

be identified using typical absorption coefficient spectra from the literature [4, 41-44]. As stated in section 2.4, the prominent features for NO_2 are between 350 nm and 600 nm, as shown in figure 2.5.

The same features are then identified in the raw intensity spectrum obtained from the receiver optics after light has passed through the NO_2 gas sample, as shown in figure 2.4 (b). The chosen features should be free from interference by any other absorbers and instrumentation effects on the measured spectrum. The effects of these can be filtered out in the analysis of the spectrum if the other absorbers are known and the instrumentation effects are understood.

The measured spectrum can be analysed for a broad range of wavelengths using a polynomial fit to the spectrum. This essentially acts as a mathematically constructed I_o. The differential absorption can also be determined using one of the features in the spectrum similar to the determination of absorption using one feature described in figure 2.6 and equation 2.14. The differences between each spectral analysis are described in section 3.5 of chapter 3, with the advantages and disadvantages shown in table 3.5.

Figure 2.7 shows how the features in the raw spectrum appear compared to a reference spectrum. The blue line represents the reference spectrum taken with no NO_2 between a light source and detector. This is labelled in the figure as True $I_o(\lambda)$. Using the three intensities I_1, I_2 and I_3, the mathematical $I_o'(\lambda)$ can be obtained and from this the differential absorption D, equation 2.15 [13]. $I_o'(\lambda)$ is calculated using intensities 1 to 3:

$$I_o'(\lambda) = I_1 - \left\{ I_3 + (I_3 + I_1) \times \left(\frac{\lambda_2 - \lambda_1}{\lambda_3 - \lambda_1} \right) \right\} \qquad \text{Equation 2.15}$$

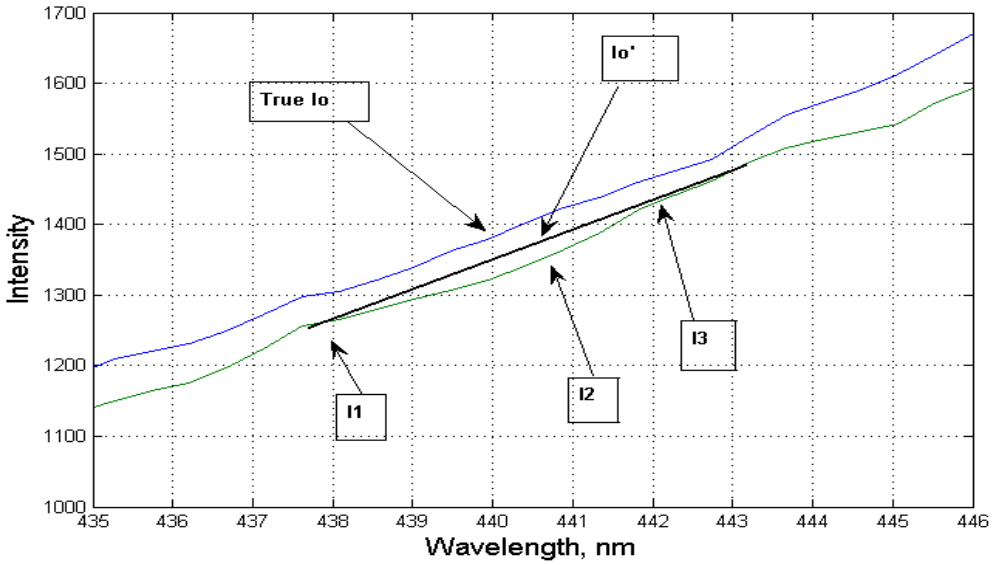

Figure 2.7 Comparison of reference (blue) and measured spectra (green). With labelled intensities of an attenuated feature used in the determination of differential absorption D.

As in equation 2.16, the wavelengths represent the corresponding intensities I_1 to I_3. The differential absorption $D(\lambda)$ is then found from equations 2.15 to 2.17 [13].

$$I(\lambda) = I_2 \qquad \text{Equation 2.16}$$

The Beer-Lambert Law, derived for the determination of differential absorption with each term for the mathematically determined $I_o(\lambda)$ and the absorption coefficient $\alpha'(\lambda)$, is shown in equation 2.17.

$$D(\lambda) = \ln\left(\frac{Io'(\lambda)}{I(\lambda)}\right) = \sigma'(\lambda)cL \qquad \text{Equation 2.17}$$

2.6 Differential absorption coefficient α' of NO_2

The Beer-Lambert law in equation 2.17, states that the absorption is directly proportional to the product of concentration of a gas and the fixed path length over which the measurement takes place. The spectrum of α is proportional to the absorption spectra of the gas being measured so each value of α corresponds to the same absorption feature at the same wavelength related by the Beer-Lambert law.

The Differential Absorption is determined using more than one wavelength, as shown in figure 2.7. So the wavelength dependent σ(λ) is replaced with the differential form of σ'. Using the characteristic spectra of (λ) shown in figure 2.4 [26, 46] and choosing a feature within 400 nm to 500 nm then with equation 2.18, a value for differential absorption cross section σ' can be calculated:

$$\sigma'(\lambda) = \sigma_1 - \left\{ \sigma_3 + (\sigma_3 + \sigma_1) \times \left(\frac{\lambda_2 - \lambda_1}{\lambda_3 - \lambda_1} \right) \right\} \quad \text{Equation 2.18}$$

Figure 2.8 shows the characteristic absorption cross section (coefficient) spectra (in gravimetric units $m^2\mu g^{-1}$) for NO_2 compiled by the five different studies from 1987 up to 2003 referenced in Section 2.4. It shows prominent features between 430 nm and 440 nm. The significant features with data-tips indicating each wavelength peak and trough are displayed. The constant α' can be used to determine the mass concentration in μgm^{-3}.

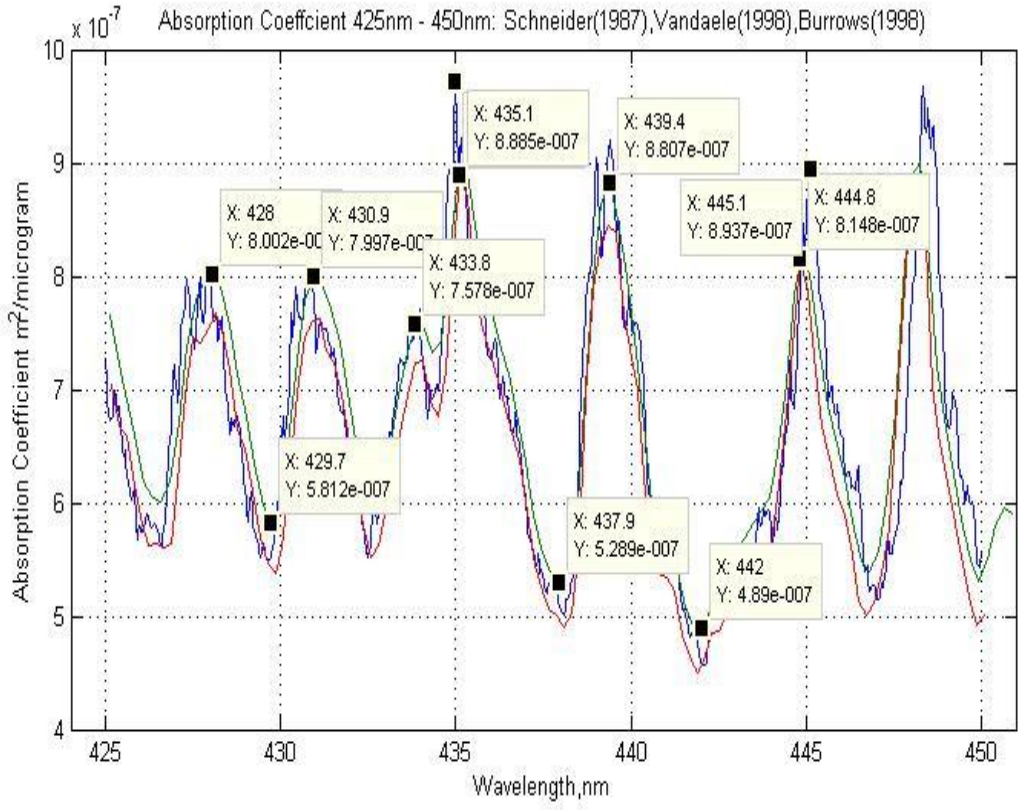

Figure 2.8 Absorption Coefficients, *α*, data from literature sources Burrows 2000, Schneider 1987, Vandaele, Burrows 1998, Bogumil 2003 cm^2mol^{-1} ($x10^{-19}$). The largest differences are between Schneider data and the others as the data is much older and the resolution of the instrument used was not as sophisticated as the others. [4]

Converting from concentrations in c_n ($molec.cm^{-3}$) to c_m (μgm^{-3}) (see section 1.5) is sometimes necessary when comparing data described in the DOAS literature and can be done using the conversion formula (Equation 2.19).

$$N_m = N_n \times \frac{M}{N_A(10^3 \times 10^9)^{-1}} \qquad \text{Equation 2.19}$$

M=Molar mass *e.g.* NO_2 = 46 $gmol^{-1}$, N_A=Avogadro's number 6.02 x 10^{23} molecules, unit scale conversion (i.e. mg to µg and mol/L to $\mu g/m^{-3}$) = $(10^3 x 10^9)^{-1}$.

It may be necessary to convert from ppb to $\mu g/m^{-3}$, which is performed by multiplying the ppb concentration by 0.532. If $\sigma'(\lambda)$ and I (λ) can be calculated for a concentration over a known pathlength L, then a method for measuring a gas without a known reference is possible. This method using equations 2.15 to 2.18 forms the basis of the algorithm designed for this research.

2.7 History of differential optical absorption spectroscopy

DOAS has been in use as a technique for monitoring gaseous pollution since the 1970s [46], although earlier spectroscopic methods to measure light absorption to determine ozone distribution had been developed as early as 1925 by Dobson et al [26] based on observations of the ozone absorption lines in the atmosphere by John William Strutt [6]. These early techniques relied on two wavelengths and the Beer-Lambert law to determine the height of the ozone layer in the atmosphere. Advances in spectroscopic techniques and technology led to greater accuracy in atmospheric measurements whereby several wavelengths could be used with broadband artificial light sources and long term measurements could be taken of several pollutants in urban areas.

The technology developed in the 1970s by Noxon (1975), Perner (1979) and others involved using several wavelengths to determine concentrations of ozone and nitrogen dioxide in the atmosphere. Platt and Perner [47] developed DOAS with an artificial light

source over a long path of up to 10 km for conditions with high visibility. For a path of 3.9 km they were able to detect NO_2 at 5 ppb or 10 µg m^{-3}.

Over the last thirty years, DOAS has been developed further with advances in spectrometer sensors such as charge coupled devices and photodiode arrays [48] as detectors and light emitting diodes as emitters [49]. These developments have been largely focussed on scientific studies of the atmosphere and volcanic emissions, but there has also been a focus on urban pollution [5]. The DOAS method has also been used as the basis for remote sensing devices such as balloon measurements and satellite measurements [50, 51]. It is worth comparing the various ways in which DOAS can be applied. Section 2.8 explains the two main approaches to DOAS, active and passive. Section 2.9 explains some of the theory behind light scattering measurements in the atmosphere and the more recent methods employed using DOAS and how they relate to the method developed for this research will be covered in chapter 3.

2.8 Active and passive differential optical absorption spectroscopy

There are various methods for detecting pollution concentration using DOAS. Among these techniques are those that use a fixed artificial light source with a known pathlength and those that use natural light where the pathlength may vary.

What follows is an explanation of these types of measurements and the various forms the results can take. As our system is also being developed to detect NO_2, particular attention is given to how well they are suited for measurements of its concentration in the atmosphere. It is worth noting that this research aims to ultimately measure concentration of NO_2 pollution, although some of the methods described here produce results as a product of c and L known as column density. Measurements have been performed using the developing system to examine some of these methods and how they could be used to reach the objectives of this research. The most common forms are illustrated in Table 2.1 [50].

	Method	**Light Source**
1.	Commercial DOAS	Xenon Lamp
2.	Direct Sunlight DOAS	Sunlight
3.	Solar Zenith measurement	Vertical measurement of Troposphere and Stratosphere
4.	MAX-DOAS	Ambient Solar Light
5.	Satellite	Sun, Moon and light reflected off the Earth's surface

Table 2.1 Various DOAS methods and the light sources employed

2.8.1 Active DOAS

In table 2.1, method 1 relates to the commercial methods developed by companies such as OPSIS in Sweden which use a high power xenon lamp to emit a focussed beam of light along a fixed path. The xenon lamp has a broad spectrum from below 300 nm to 1100 nm. This source is suitable for the detection of a variety of analytes including NO_2, SO_2, O_3 and organic molecules like Benzene. The light from the lamp is directed towards a receiver

or retro-reflecting mirror using a collimating mirror positioned ~ 74 cm from the lamp, as shown in figure 2.9. The lamp and mirror are enclosed in a stainless steel tube to protect them from bad weather conditions.

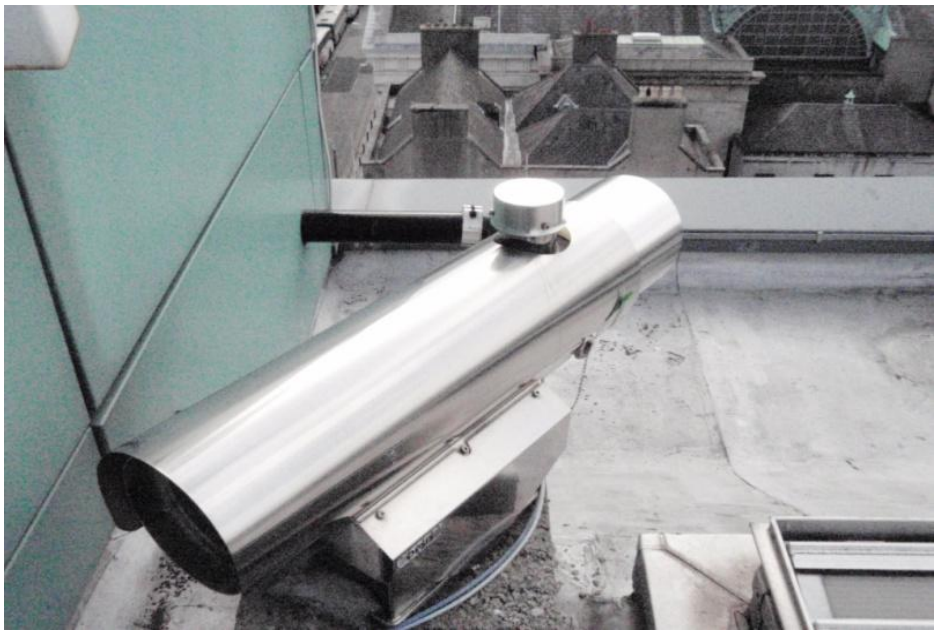

Figure 2.9 OPSIS system emitter housing on the roof of DIT Cathal Brugha Street

The receiver is enclosed in another tube with a collimating mirror to receive the beam and direct it onto an optical fibre. The other end of the fibre is connected to an analyser and transmits the received light onto a diffraction grating. The grating divides the light up into its constituent wavelengths much like a prism and this light is reflected onto a PMT that converts the received light into an electrical signal. The intensity of the signal is measured and used to form a spectrum of the light received by the PMT. This spectrum is analysed using a fitted 5^{th} degree polynomial across the range of wavelengths measured which acts as a substitute value for I_o. The pollutants being analysed are identified by the

operator so that the software can then determine the average concentration of each pollutant over the fixed pathlength, L. The software already will contain a database of the absorption coefficients for each analyte. In chapter 3, section 3.2 the applications of active DOAS and its disadvantages are described.

2.8.2 Passive DOAS

The methods 2-5 in table 2.1 use ambient or direct sunlight to determine gas concentration. Platt describes the methods using ambient light as Passive DOAS as opposed to those using artificial sources as Active DOAS [6]. These Passive methods have been primarily used for scientific research and the instrumentation used is also described in more detail in chapter 3. One factor that these methods have in common is the problems of determining accurate concentrations with a varying pathlength.

Column density is one way in which the need for determining a path length is avoided by calculating instead the product of the concentration, c, and the path length, L. The columns used then are either the Vertical Column Density (VCD), seen in equation (2.19) where the instrument is directed toward the zenith, or the Slant Column Density (SCD) as in equation (2.18). As column density is the product of c and L its units are usually given in modified D.U. molecule cm^{-2} (mass equivalent: $m^2 \mu g^{-1}$).

The Vertical and Slant column densities are related by the Air Mass Factor or AMF as described in (2.20). This is a quantity used to describe the thickness of the atmosphere. The magnitude of the AMF has been shown to be dependent on aerosol concentration and altitude. It can be determined with accurate measurements of Oxygen molecules different altitudes.

$$AMF = \frac{SCD}{VCD} \qquad \text{Equation 2.20}$$

Comparing the terms SCD and VCD to the two forms of the Beer-Lambert law described in equations (2.13) and (2.17), we can see mathematically how the forms of ambient light measurement techniques in table 2.1 and the results obtained are related.

$$SCD = \frac{\log(\frac{Io}{I})}{\alpha} \qquad \text{Equation 2.21}$$

$$VCD = cL \qquad \text{Equation 2.22}$$

The AMF can be determined geometrically from the Solar Zenith Angle (SZA) the angle between the Sun and the Zenith of the ground based instrument [6]**.**

$$AMF \approx \frac{1}{\cos(sza)} \qquad \text{Equation 2.23}$$

2.9 Light scattering effects on the pathlength measured by DOAS instruments

Scattering of sunlight occurs as it travels through each layer of the atmosphere. DOAS measurements with sunlight can be achieved in three different ways: Direct sunlight, zenith scattered light (ZSL) and off-axis measurements. Direct sun measurements require the detector to be aligned directly with the Sun throughout the day. This can be difficult to do, as the instrument would need to be capable of tracking the Sun as it moves across the sky. But the AMF in this approach is inversely proportional to the elevation

angle of the detector (equation 2.20). ZSL and off-axis measurements measure indirect as wells as direct sunlight. A disadvantage of using indirect sun measurements is that the light passing through the atmosphere can be scattered in directions where the path taken is less than the path taken were no scattering occurs. Because of this the value for the column density is lower than actual column density. This is illustrated in figure 2.10, where the pathlength taken by the light received by the detector at elevation angle α_1 is shorter than that received by the detector at elevation angle α_2.

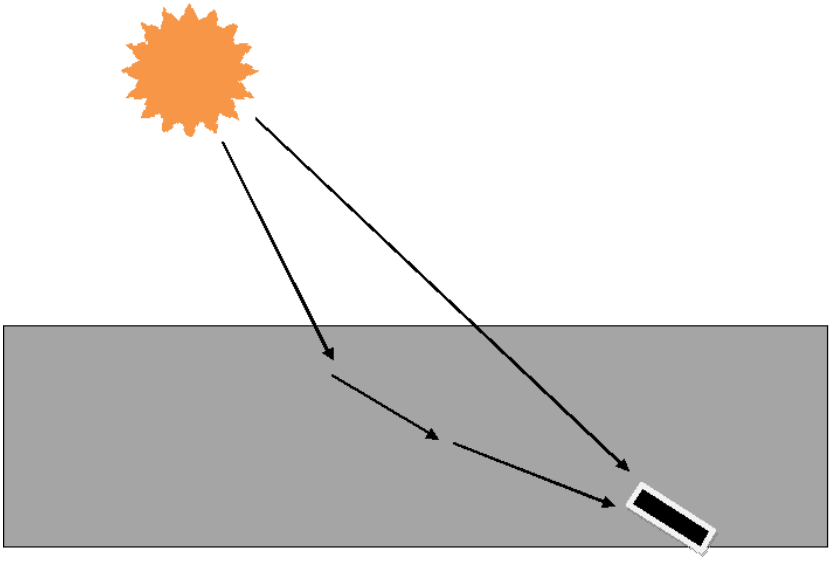

Figure 2.10 Lower scattering altitudes of sunlight entering a DOAS receiver. Note the different pathlength of the lower elevation angle as a result of scattering in the trace gas layer. [32]

Zenith scattered light (ZSL) measurements involve directing the detector perpendicular with the horizon. These measurements are predominantly used for stratospheric measurements of the atmosphere [46, 52] where the column densities were determined by the thickness of the atmospheric layers, air mass and viewing geometries at

different elevation angles and solar zenith angles (SZA). The SZA is the angle between the zenith of the detector and the Sun.

Off-axis measurements are conducted by recording spectra at angles between the zenith and the horizon. The zenith measurement will contain data of the troposphere and stratosphere and the horizontal measurement will predominantly be the troposphere, so a differential slant column density can be determined by subtracting the zenith SCD from the horizontal SCD. This is assuming that the zenith measurement only contains a fraction of the tropospheric content. A more sophisticated version of off-axis measurement is the Multi-Axis Differential Optical Absorption Spectroscopy or MAX-DOAS. These measurements are made using several detectors positioned to monitor several elevation angles between the horizon and the zenith [32]. The modern miniaturised spectrometers are ideal for this concurrent measurement [48].

2.9.1 Atmospheric measurements with light scattering effects

Taking into account the scattering by different sized particles allows the terms for Rayleigh, ε_R, and Mie, ε_m, scattering to be included in the Beer-Lambert equation 2.24 as follows:

$$\ln \frac{Io(\lambda)}{I(\lambda)} = \alpha(\lambda)cL + \varepsilon_R + \varepsilon_m \qquad \text{Equation 2.24}$$

The ε_R and ε_m terms represent broadband scattering as opposed to the narrowband absorption features of gases such as NO_2 . Therefore they can be ignored when using the calculation on an individual feature.

The scattering in the atmosphere is described by Honniger et al [32] as occurring in trace gas layers in the stratosphere (figure 2.11 top) and close to the Earth's surface where there is greater air density(figure 2.11 bottom). In each scenario shown in figure 2.11, the path taken by the light through the trace gas layers, ds, is longer than the thickness of the layers, dz, and the column densities of each are related by the AMF. The Albedo, which is the reflection of sunlight off the surface back into the atmosphere, can increase the amount of scattering and as a result will increase the pathlength through which the light received by a detector travels.

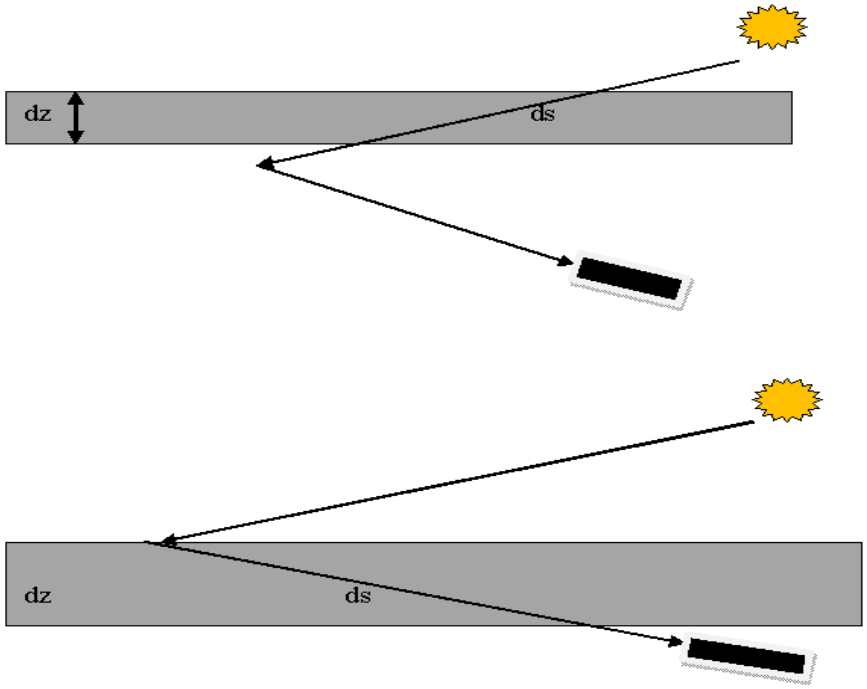

Figure 2.11 Scattering altitudes of the light entering a DOAS receiver, the darker areas represent two trace gas layers through which the light travels. The slanted path is represented by ds and the vertical path by dz. [32]

2.9.2 Radiative transfer models, RTMs

To make accurate studies of the atmosphere using ambient sunlight, as in zenith scattered and off-axis measurements, the light received by the detector can be modelled as it passes through the atmosphere. The models can use two types of scattering that occur which are single-scattering [53] and multiple-scattering [54] of the light depending on the

atmospheric conditions. Some of these models can be complex and involve sophisticated mathematical techniques; various models used include SCIATRAN (Bremen-Germany , single and multiple scattering) [55] and TRACY (Heidelberg-Germany, single and multiple scattering) [48, 55] and MCARaTS (Monte-Carlo Radiative Transfer Model (RTM), Iwabuchi [56] 2006). An intercomparison of RTMs by Hendrik et al (2005) [55, 57] shows that there is very little difference between the single and multiple scattering models for NO_2 compared to BrO, most likely due to the wavelengths used to determine the slant column densities (352 nm for BrO and 422 nm for NO_2). Hendrik et al. also show that there is an increase in NO_2 concentration at high solar zenith angles i.e. when the Sun has dropped below the horizon.

2.9.3 Diurnal variation in slant column density

Figure 2.12 shows the variation of the differential slant column densities determined by variation in slant column density for NO_2, O_3 for 20 May 2004 by Leigh et al [58]. The darker blue line in each of the graphs represents the zenith and the light blue, green and yellow represent 15^0, 10^0 and 5^0 detector elevation angles. The differences between the zenith and lower elevation angles show the how the stratospheric SCDs can contrast with the tropospheric SCDs. For example, the O_3 measurements (b) show no significant differences between the stratospheric and tropospheric variation at the beginning and end of the day. The increases and decreases for O_3 are primarily due to the changing solar zenith angle at sunrise and sunset. The NO_2 in (2.12 a) displays a high SCD (molecules/cm^2) in the morning and again in the evening for each elevation angle. This is most likely due to

photochemical effects, as the sunlight is parallel to the Earth's surface during twilight. The strong peaks between 8am and 12pm are likely caused by higher traffic congestion which would also play a part in the late evening increases. The dark blue colour represents the zenith measurement and the light blue, green and orange represent the elevation angles 15^0, 10^0 and 5^0 respectively.

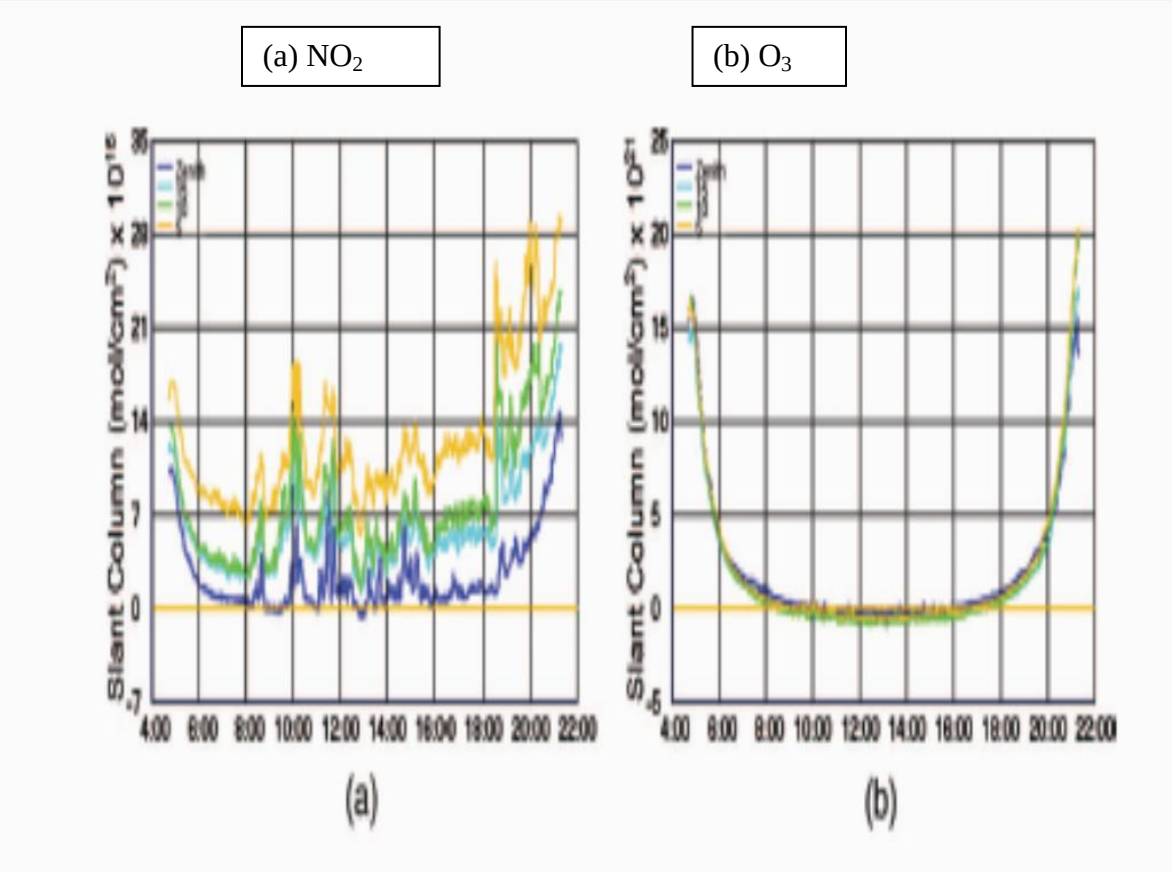

Figure 2.12 Variation in slant column density for (a) NO_2, (b) O_3 for 20 May 2004 in Leicester in the UK Leigh et al [58] from 4am to 10pm. The O_3 has maximum column densities at night (see text). During the day they mix with other molecules such as NO forming NO_2 so their column densities are near 0 during the day.

2.10 Summary

To develop a method to detect NO_2 concentrations in the atmosphere using ambient sunlight, the processes governing the transmission and absorption of the electromagnetic radiation in the atmosphere need to be understood. It has been shown that the major scattering effects on sunlight in the atmosphere are the elastic scattering (Rayleigh and Mie) and the inelastic scattering (Raman).

Rayleigh and Mie scattering are the result of photons colliding with small molecules and PM in the atmosphere. The energy of the scattered photons is the same after scattering. Inelastic Raman scattering occurs when a fraction of the photon energy is lost or transferred to a molecule, which is smaller than the incident light's wavelength, in the atmosphere. Light can also be absorbed in the atmosphere when incident photon energy is changed by molecules after a collision. The solar spectrum measured from the ground can be used to monitor scattering and absorption. However the spectrum will also contain features of Fraunhofer lines that are caused by sunlight absorbed by elements in the outer layer of the Sun.

The amount of light absorbed by gas pollutants like NO_2 in the atmosphere is determined using the Beer-Lambert law (equation 2.8). The absorption coefficient $\alpha(\lambda)$' is used to determine the magnitude of the gas concentration using the Beer-Lambert law. The profile of the absorption coefficient spectrum is also the characteristic absorption profile i.e. the characteristic absorption wavelengths of the gas, NO_2. To determine a value for absorption a reference measurement is required with no absorber present. However, in the

Earth's atmosphere there is always some trace amount of pollutant gases due to chemical mixing in the atmosphere.

DOAS has been proven to be a successful alternative when the reference measurement cannot be found, equation 2.14. The technique involves the calculation of a mathematical value I_o' from the observed spectrum which will show attenuated features caused by absorbers. The differential absorption is determined using equations 2.12 to 2.14. For NO_2 the wavelengths in the near-uv to visible region of the e/m spectrum are 350 nm to 580 nm (see figure 2.5), with dominant features between 400 nm and 450 nm. The differential absorption coefficient at 400 nm to 500 nm is used for this region is $\sigma(\lambda)' = 2.6 \times 10^{-19} cm^2/molec.$ (3.4×10^{-7} $m^2 \mu g^{-1}$ in gravimetric units)[13].

It has also been shown that DOAS can be employed as either an active or passive approach. The active version uses artificial light sources positioned a fixed distance from receiving optics, sensor and datalogger. The passive system uses ambient light to determine concentrations or column densities of gas pollution. The novel-DOAS system developed in this research is being developed as a passive DOAS system to measure NO_2 concentrations but can also be adapted to use artificial light sources for low light level measurements. One major difficulty in measuring ambient sunlight for DOAS is the scattering effects on the pathlength travelled by sunlight through different layers of the atmosphere. Several attempts have been made in the last few decades to explain the scattering effects on absorbers using radiative transfer models and carefully selected reference measurements. Chapter 3 will describe in further detail the latest technologies used to monitor NO_2 in the atmosphere and the various ways that passive DOAS techniques can be employed.

CHAPTER 3 Active and passive DOAS instrumentation for NO_2 detection

3.1

3.1Introduction

The developments in the past few decades of inexpensive DOAS methods have made it possible to develop a portable novel-DOAS system that is adaptable and comparable to established monitoring techniques. Current miniaturised spectrometers are low cost and allow a variety of optical arrangements for gas monitoring in the laboratory and outside in urban environments. Section 3.2, 3.3 and 3.4 outline the different DOAS applications and developments that have occurred in recent decades and the satellite and correlation spectrometry (COSPEC) methods that use optical absorption spectroscopy[6]. Sections 3.4 to 3.7 will describe the specific issues that are required in the development of an inexpensive portable novel-DOAS system with flexibility in application.

3.2 Current DOAS applications for NO_2 detection

DOAS has been developed for commercial and scientific applications since the method was first used to monitor atmospheric gases [26]. The commercial applications of

DOAS have been primarily for urban traffic and industrial monitoring. Table 3.1 lists the disadvantages for a commercial DOAS operation.

System requirement	Disadvantage
Location	High building roof tops Fixed positions Requires locations for receiving and emitting components
Power supply	Permanent mains supply needed for PC and spectrometer Mains supply also required when receiver is motor operated
Calibration	Calibration performed by industry professional Calibration cells needed for each analyte
Maintenance	Instrumentation needs to be operated by trained professionals Replacements of lamps and software packages are expensive
Concurrent data systems	DOAS systems usually operate with a datalogger, controller unit, wind speed monitor and light level monitor.

Table 3.1 System requirements and disadvantages of commercial DOAS instrumentation

The instrumentation for these systems has been primarily based on active DOAS i.e. with artificial light sources over a fixed pathlength, as seen table 3.1 [28, 59]. There are also more recent commercial passive DOAS systems, table 3.5, such as the Hoffmann Messtechnik GmbH [60] mini-MAX DOAS. Other remote sensing methods are similar to passive DOAS, like COSPEC and the recent flyweight correlation spectrometry FLYSPEC which uses miniaturised spectrometers and there are other applications in which DOAS is used other than ground based monitoring such as satellite and high altitude balloon measurements, see table 3.4.

Single /Double path	1970s-present
Multiple Path	1980s-present
Multiple reflection cells	Late 1980s-present
Multiple path tomography (2D-3D)	1990s-present

Table 3.2 Active DOAS developments from the 1970s to the present

Commercial active DOAS systems such as OPSIS AB (Sweden) and SANOA (France) are capable of monitoring such gases as SO_2, O_3, and NO_2 and volatile organic molecules like formaldehyde (CH_2O) and Benzene (C_6H_6). The detection limits for various compounds using the SANOA instruments are listed in table 3.3[61].

Compound	**Chemical Formula**	**Detection Limit, ppb**
Sulphur Dioxide	SO_2	0.2
Nitrogen Dioxide	NO_2	0.6
Ozone	O_3	0.6
Benzene	C_6H_6	0.9
Formaldehyde	CH_2O	1.1
Nitrous Oxide	HNO_2	0.9
Nitric Oxide	NO	1.5

Table 3.3 Typical detection limits for the SANOA commercial DOAS system

To put this into perspective the annual average for NO_2 between 2002 and 2011in Ireland was no greater than 25 ppb and no less than 2.5 ppb [17]. Although the active

systems are very accurate, they also have significant disadvantages for long term applications, both economic and instrumental. In section 3.8, a cost analysis of the different methods described is provided. The sources of the instrumental disadvantages of large commercial DOAS include the choice of location, power supply, calibration, maintenance and concurrent data systems.

These systems require elevated locations, usually roof tops above the average building height in an urban location. The receiving optics is connected by an optical cable to a spectrometer located inside the building which is in turn connected to a PC used for analysis. The PC and spectrometer are powered by the mains power supply. The PC is used to specify the gases to be monitored and the pathlengths under investigation. The OPSIS software also allows the user to troubleshoot to determine causes of malfunctions [28]. But the software and physical components are expensive to replace and space and access are needed for operation. The rooftop locations may also have health and safety issues depending on their specific locations.

The passive DOAS methods have been used in various ways to monitor gas densities and concentrations using ambient light. Tables 3.4 and 3.5 summarize some of the various applications that have been studied. The different compounds O_3, BrO, SO_2 and NO_2 can be used to illustrate the development of passive DOAS applications. O_3 has a well known absorption profile and Bromine monoxide (BrO) [62, 63] has been shown to reduce stratospheric ozone levels and has been detected in the stratosphere by DOAS since 1989. SO_2 is present at high concentrations in volcano emissions as well as being in urban areas and can be very harmful to human health at high concentrations. Several variations of the DOAS technique have been employed to monitor SO_2 emission and notable results and advances in DOAS have been developed from volcano measurements [64]. NO_2 has been

monitored since the 1970s *e.g.* Kroon, Noxon, etc., using DOAS techniques. Like SO_2, it is a harmful pollutant affecting respiration. As it absorbs light in the uv-visible region of the spectrum, 350 nm to 460 nm, it can be detected using ambient sunlight and a range of available light sources. NO_2 is also a secondary pollutant because it can form NO and O_3 in the presence of sunlight. The O_3 can then react with NO to form NO_2 in the photolysis cycle (as seen in chapter 1) and has been measured spectroscopically using ambient light since 1926 by Dobson [26].

Direct Sunlight	Dobson O_3 (1930s) Moonlight, aircraft (1980s – present) Balloon(O_3, NO_2, SO_2) (1990s-present)
Zenith Scattered	Brewer (O_3, NO_2) (1980s-present)
Off-Axis	(1980-1990)
Satellite	(1990s-present) GOME, SCIAMACHY etc.
MAX-DOAS	(1990s-present) pollution, stratosphere, volcanoes, commercial use
Imaging	2000s-present NO_2, SO_2, volcanoes

Table 3.4 Passive DOAS development from 1930 to the present

No.	Application of MAX-DOAS, off-axis DOAS	Source and location
1.	Trace gas profiles	Von Freideburg, Wagner et al 2002, Heidelberg [54]
2.	Comparison of NO_2 and commercial DOAS	Morales, Walsh, 2005 Dublin city[5]
3.	Tropospheric NO_2	Honniger, Platt 2002, various locations arctic boundary layer, Heidelberg[32]
4.	Aircraft mounted off-axis DOAS	Petritoli, 2002, Argentina[65]
5.	Volcanic emissions of BrO	Bobrowski, et al 2003, Soufrière Hills volcano (Montserrat)[66]
6.	Pollution transport	Melamed, Mexico City 2009[67, 68]
7.	Sun-illuminated targets to detect various trace gases	Frins et al, Heidelberg, 2006[68]
8.	NO_2 observations from research vessel	Takashima 2011 Western Pacific and Indian ocean[69]
9.	Intercomparison of MAX-DOAS and zenith sky for NO_2 and O_4 using 22 variations of DOAS measurement	Roscoe et al 2010 Lopik the Netherlands[48]

Table 3.5 Summary of some of the various applications of passive DOAS which illustrate the versatility of method

To detect these trace gases, several DOAS approaches have focussed on the vertical profile of gases such as O_3 and NO_2. The development of inexpensive, robust miniaturised spectrometers has meant that significant advances have been made in applying the DOAS method to atmospheric monitoring. With charge coupled device (CCD) sensors that provide

spectral resolution that is suitable for the identification of the common trace gases, ground based measurements using zenith viewing DOAS, off-axis and multi-axis measurements have been combined with results from DOAS instruments on aircraft [65], balloons [6] and satellites [70]. Studies have been performed of the effects of light scattering by clouds [71], light reflection off buildings [72] and comparisons with other ground based instruments [73]. Overall these studies have proven passive DOAS applications to be incredibly versatile and flexible in application for scientific studies. It has the advantage that it can be developed for specific purposes *e.g.* volcanic observations and marine atmosphere observations. For commercial application of MAX-DOAS, there has been relatively little achieved in applying these methods [60]. The disadvantages of the passive DOAS methods can depend on the specific application, the analytes examined and the section of atmosphere under observation. The passive approach can be affected by meteorological conditions which cause scattering of light traversing the atmosphere (section 3.6) and interfering species are difficult to identify when analysing the complex spectrum of direct and indirect sunlight, see table 3.7.

3.3 Satellite monitoring of NO_2

A major application of passive DOAS has been its use in satellite instruments for several international missions. Table 3.6 summarizes the different missions responsible for the detection of NO_2 although there are other satellite platforms for other atmospheric gases and pollutants [50, 70, 74, 75]. Not all the satellites in table 3.6 are currently operational but future missions will include NO_2 monitoring instruments.

Instrument	Platform	Year	Orbit
ATMOS-atmospheric trace molecule spectroscopy	ATLAS	1992-1994	Inclined
GOME-global ozone monitoring	ESA, ERS-2	Present	Polar, sun synchronous
GOME-II	METOP1-3	06-10/11	Polar, sun synchronous
GOMOS-global ozone monitoring by occultation of stars	ENVISAT	2002 to 2012	Polar, sun synchronous
ODUS-ozone dynamic UV spectrograph	GCOM-A1 Japan	2005	Inclined
OMI-ozone monitoring instrument	NASA-EOS	2004	Polar, sun synchronous
OSIRIS-optical spectrograph and IR imaging system	ODIN-Sweden	2001-present	Polar, sun synchronous
POAM II-III polar ozone aerosol measurement	SPOT-3, SPOT-4	1993-1996, 1998-present	Polar, sun synchronous
SAGE I-III stratospheric aerosol gas experiment	I-NASA atmospheric explorer II-Earth radiation budget satellite III-Meteor 3M international space station	I-1979-1981, II-1984-present, III-2001-present	Inclined
SCIAMACHY-scanning imaging absorption spectrometer for atmospheric cartography	ESA –ENVISAT	2001-2012	Polar, sun synchronous

Table 3.6 Satellite Monitoring instruments for NO_2 and O_3 [6]

DOAS is an ideal method for monitoring the atmosphere remotely by satellite when ambient sunlight is the primary available light source. Satellite orbits for scientific monitoring of the atmosphere are described as Low Earth Orbits (LEO). The satellites are positioned approximately 100 km above the Earth's surface at an angle of 96^0. The angle position is to maintain a Sun synchronous orbit where the satellite passes the same location

at the equator on every orbit at the same local solar time. This ensures that the same shadow positions are observed each season. The orbits travel from pole to pole taking over 90 mins to traverse the complete each time.

The satellite observations are made either by nadir or limb or in the case of the SCIAMACHY measurements were made for both. The nadir viewing is taken when the satellite instrument is looking directly down over the Earth and the limb viewing is a measurement through the atmosphere of the Earth's surface. The spatial resolution of the satellite's view is determined by the length and width of the track it monitors. For example, the OMI has a spatial resolution of 13 km along its track and 24 km across the track (nadir). The GOME-II has a spatial resolution of 40 km (along) and 80 km (across track) with a complete global coverage of 1.5 days. The SCIAMACHY had a spatial resolution of 30 km by 60 km and a coverage of 6 days because it alternated (discontinued in 2012) between limb and nadir views[76]. During orbit, the ENVISAT satellite carrying the SCIAMACHY payload would view the Sun directly. This is the occultation mode were the data recorded is as a reference with the data collected from nadir and limb viewing. The occultation viewing will also be made of the Moon in the southern hemisphere [77]. As these measurements use scattered sunlight as a source for DOAS measurements, the pathlength is impossible to determine so the data is represented as a column density, i.e. molecule/cm^2. The SCIAMACHY instrument was capable of gathering data on a range of molecules *e.g.* O_3, NOx and CO_2 as well as aerosols and cloud density. The broadband wavelength range observed by SCIAMACHY was between 214 nm to 1773 nm with narrow bands 1934 nm to 2044 nm and 2259 nm to 2386 nm.

The image in figure 3.1 shows the monthly mean tropospheric NO_2 column density taken by the GOME II which has the same orbit as the ENVISAT (SCIAMACHY). The NO_2 data is recorded in units of 10^{15} molecules/cm^2 for May 2013. The blue and light blue over Ireland indicates a low column density average for NO_2 with higher densities other regions *e.g.* northern Italy and northern Germany. The highest pollution regions of the planet are invariably close to major cities.

The satellite pictures are constructed by creating an image using numerous sensors designed to measure a broad spectral range. Narrow band ranges are also used to create the spectral and radiometric detail in the images. Each pixel is directly proportional in size to the area on the Earth's surface being observed. It is crucial for the satellite sensors to have reasonably high resolution to create as detailed an image as possible. They should also have a high signal to noise ratio [42].

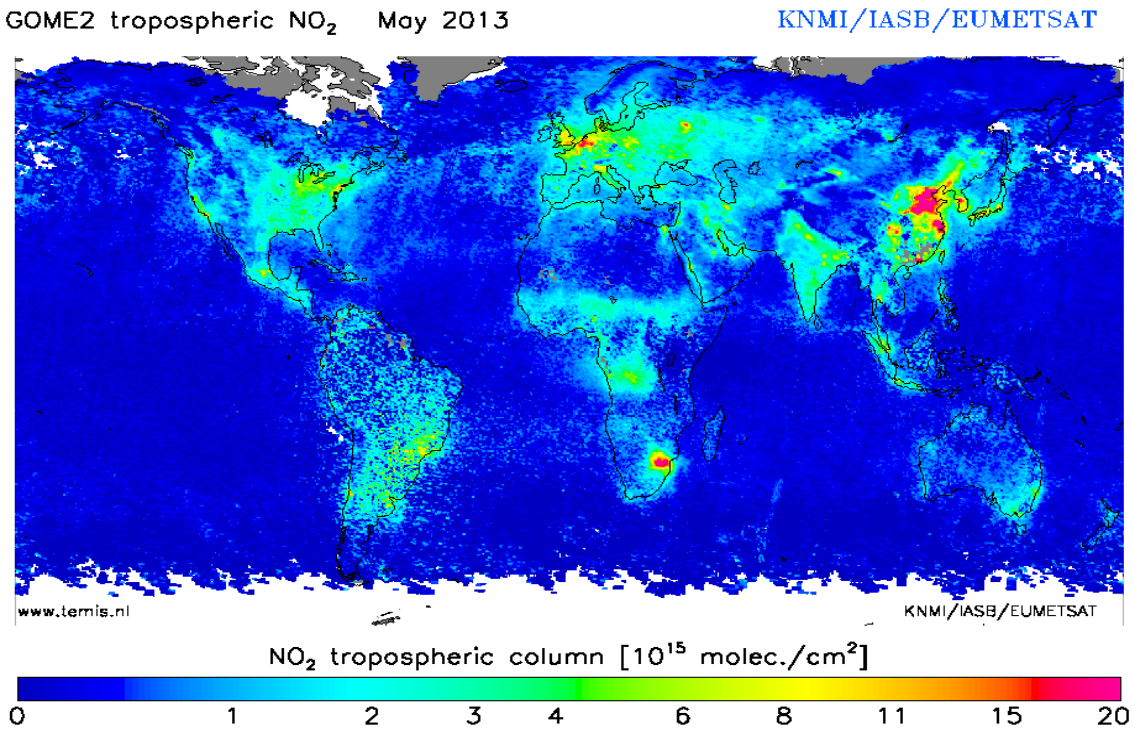

Figure 3.1 Monthly mean tropospheric column density of NO_2 May 2013 obtained by GOME II satellite[78]. The highest column densities have a red/pink colour.

The accuracy of satellite data as a remote sensing technique for monitoring the Earth's atmosphere relies significantly on clear skies and exact positioning of the satellite. The satellites in table 3.4 are in polar orbits and are used to monitor the entire Earth surface so a real time continuous update of NO_2 above countries with large cloud cover like the Republic of Ireland is not possible. The lifetime of the instrument depends on the equipment used which is expensive and is based on tightly controlled timetables by the relevant space agencies.

3.4 Correlation spectroscopy using miniaturised spectrometers

COSPEC [79] was developed in the 1970's in Canada to monitor industrial smoke stacks. In figure 3.2, the apparatus for a correlation spectrometer is shown. The instrument operates by taking measurements and comparing them in real time to samples that rotate within the path measured by the detector. This allows the instrument to continuously assess the accuracy of each measurement and correct for any interference such as cloud cover reducing the light level. COSPEC has been successfully applied to the monitoring of volcanoes in the last few decades. The early systems used for this application, however, were vehicle mounted. Because of the conditions and locations of some volcanoes, miniaturised spectrometers have been used instead. These spectrometers have also made it

possible to reduce the size of the COSPEC apparatus leading to a smaller portable device known as a FLYSPEC [79].

3.5 DOAS software applications

Analysis of recorded spectra by software has led to different approaches. The OPSIS and SANOA commercial systems use their own platforms recently based on the windows operating system. Early versions of the OPSIS software were DOS based with input parameters required for the path length and which analytes where to be monitored. The OPSIS software (EmVision) records a spectrum of the received light from a Xe lamp source which is fitted to a pre-recorded lamp spectrum in the system memory. The measured spectrum is divided by the lamp spectrum and a raw spectrum is left with an absorption spectrum with broadband and differential features as described in chapter 2. A 5^{th} degree polynomial is fitted to this spectrum and divided into the absorption spectrum. The result represents the differential spectrum from which the pollutant concentration is calculated. The DOS operating system could record a spectrum every 60 seconds but could operate slower to match EPA standard methods (every 5 minutes).

Current passive DOAS systems use various software applications such as DOASIS to analyse measured spectra. The software records the spectrum of light received by a miniaturised spectrometer and allows the user to perform several mathematical functions to determine the SCD of the analyte.

DOASIS is capable of keeping a Fraunhofer spectrum and reference spectra on file for whole spectrum analysis. The WinDOAS [80] system is a Belgian spectral analysis

program that operates similarly to DOASIS. In recent years, WinDOAS has been updated to QDOAS [48], which is a multi-platform derivative of WinDOAS. Both programs perform the analysis of atmospheric spectra using sophisticated software analysis including such techniques as wavelength calibration, convolution and other various cross section analyses to eliminate small wavelength variations caused by the Ring effect (section 2.3) and changing solar zenith angles. Instrumental effects such as offset and dark current are also accounted for in the analysis.

The output of these analytical approaches to MAX-DOAS is the vertical column density, with the AMF determined using RTMs which determine the AMF using the known profiles of absorbers such as O_4. An intercomparison of RTMs performed by Hendrik et al (2005) showed that, although there were large differences between RTMs for aerosols (large oxygen molecules) there was little differences when the ground albedo (reflection from ground surface) and relative azimuthal (direction measured by the detector) was used to determine the AMF.

An alternative simplified method to these software packages can be achieved using other software such as Matlab-2007a, further detail in chapter 4 and Appendix II, which is used to analyse narrowband features only. As in the early methods to determine ozone concentration and density developed by Dobson (1931) and Gőtz (1926), an "Umkehr" method [81], using the variation between the intensity of more than one wavelength, can be used. Once the coefficient α profile is known and the instrumental dark and offset can be accounted for, the unique absorption features can be identified and, using the equations in chapter 2 (equations 2.12 to 2.15), the differential absorption can be computed. Table 3.7 outlines the advantages and disadvantages between the different methods. The polynomial smoothing and cubic spline methods are very accurate and allow the user to calculate

concentrations of absorbers along a broad wavelength region. But their results can be affected by interfering species and variations in the attenuation features of the raw intensity spectrum by Fraunhofer lines and the Ring effect. The single feature approach is focussed on the analysis of the attenuation at a minimum of three wavelengths. To minimise any possible errors in the single feature approach, the detector must have a high signal to noise and good resolution for the identification of attenuated intensities.

Method	Advantages	Disadvantages
Single feature analysis	**Simple and quick**	**S/N: worse by subtraction of two measured values**
Polynomial Smoothing	**Polynomial derivation, degree of polynomial**	**Loss of measured points, end of spectrum, problems with sharp peaks**
Cubic Spline	**Entire Spectrum, good linear**	**Large influence from chosen parameters**

Table 3.7 Advantages and disadvantages of spectral analysis methods using one or more attenuation features in the raw intensity spectra

3.6 Viewing geometry and the optical pathlength through the atmosphere

Determination of the pathlength in passive DOAS within the troposphere relies on several factors, including an estimation of the height of the urban pollution layer (UBL, see chapter 1) above the ground, atmospheric conditions and local topography[82]. The MAX-DOAS technique uses a detector directed at varying elevation angles. For this, the

pathlength depends on the elevation angle of the detector and the photon path length through the troposphere. Figure 3.2 illustrates how direct sunlight without scattering (a) where the light received by the detector travels through the lower atmosphere once, whereas in (b) there is multiple scattering so the light has passed through the lower atmosphere several times. RTMs [57] have been developed to determine paths of light for multiple and single scattering, *e.g.* SCIATRAN etc., see section 3.3.

When the detector is directed parallel to the horizon, the path length is much greater than when pointing at the zenith [82]. The mathematical approach used in MAX-DOAS is described in equations 3.1 and 3.2 and is covered in detail in Platt, S., *Differential Optical Absorption Spectroscopy: Principles and Applications*. 2008: Wiley in several chapters[6].

$$SCD = (SCD_{trop} / \sin\theta) + (SCD_{strat} / \cos sza) \qquad \text{Equation 3.1}$$

$$SCD = VCD(\theta / \sin\theta + (1-\theta) / \cos sza) \qquad \text{Equation 3.2}$$

In equation 3.1, SCD_{trop} represents the slant column density through the troposphere and SCD_{strat} represents the slant column density through the stratosphere, thus showing that the light measured along the horizon is made of two components, the density of the gas in the stratosphere and in the troposphere. Angle θ represents the elevation angle of the instrument and SZA is the solar zenith angle of the Sun. The AMF (equation 2.17) can be estimated if the pathlength is determined using the relatively well known vertical profiles of oxygen molecules [6, 52]. Because of the scattering and various viewing directions used in

MAX-DOAS (figure 3.2) measurements the SCD is usually converted into VCD the vertical column density.

The lower atmosphere, the urban boundary layer, is where the greatest concentration of pollution responsible for damage to human health is located. Therefore, NO_2 measurements may only be needed within the urban boundary layer where concentrations are significantly higher than in the stratosphere [32]. Measurements of NO_2 across the horizon would be comparable to commercial long path DOAS measurements, which could be used as an accurate reference method to determine the accuracy of a much simpler setup. Techniques have also been developed involving the reflection of sunlight by buildings and optically similar targets known as ToTaL DOAS [72, 83] where the total SCD is the sum of the SCD through the atmosphere and the SCD between the building and the detector. Mathematically this is similar to equation 3.1.

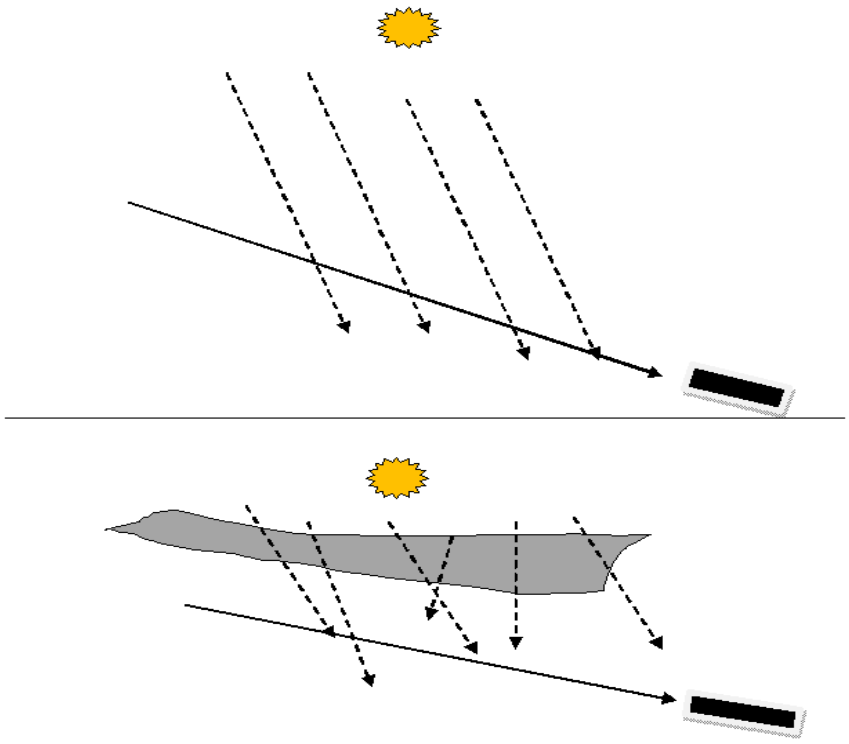

Figure 3.2 MAX-DOAS under clear sky (a) and cloudy conditions (b). The clouds cause the light to scatter resulting in variations in the optical pathlength of the light through the PBL and UBL where NO_2 concentrations are measured. [84]

Urban boundary layer heights (see section 1.2, figure 1.2) have been extensively studied and the height of the pollution layer and vertical profile of NO_2 in the UBL has been estimated so that accurate representations of the NO_2 concentrations could be known [6, 29, 32, 52, 84-86]. Measurements of the NO_2 concentration in the lower atmosphere suggest a large concentration up to 1 to 1.5 km in altitude (section 2.9 figures 2.10 -2.11) [87]. Taking this height as the vertical height of NO_2 in the UBL means, the horizontal gas profile through a known pathlength, with the detector at angle θ above the ground, could be calculated using a simple geometric approach as shown in figure 3.3 [52, 53, 88]. In the

diagram, in figure 3.3, h is the height above the ground of the observer and an approximate value for d is calculated distance observable through the Earth's atmosphere at that height.

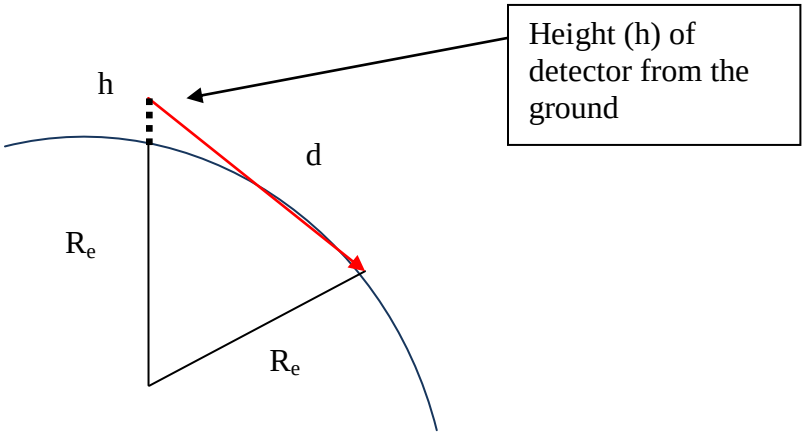

Figure 3.3 Viewing geometry of the front end optics of the novel system. The determination of d, pathlength, is found using the radius of the Earth, R_e.

$$d = \sqrt{h^2 + 2R_e h} \qquad \text{Equation 3.3}$$

where, h is the height of the observer and d the pathlength observed. R_e is the radius of the Earth ~ 6371 km. The angle, between R_e and distance d is a right angle, so for a height of 10 m (0.01 km) from the ground, d ~ 11.29 km. The measurements made using this approach could then be compared to established methods such as long path DOAS, UV absorption measurements and CL and even satellite data [5, 89, 90]. Hao-yi et al [88] show that the Differential Absorption D can be approximated if the angle between the observed columns through the atmosphere is equal to the solar zenith angle then the value for D is:

$$D = \ln(\alpha(\lambda)(\frac{VCD}{\cos\theta}) \qquad \text{Equation 3.4}$$

3.7 Meteorological and topographical influence on DOAS measurements

Pollutants such as NO_2 are affected by annual weather and seasonal changes. NO_2 can react with moisture to form nitric acid and sunlight is responsible for certain photochemical reactions in the atmosphere, as described in chapter 1. Therefore, seasonal increases in sunlight can be responsible for changes in the pollutant concentrations. The overall air mass volume varies with changing temperature and pressure depending on the local climate which can lead to a reduction in height of the boundary layer. O_2 molecules and PM affect the scattering of light radiating through the atmosphere which can increase the optical pathlength. Cloud cover can also affect the AMF as it can be responsible for increased scattering in the atmosphere [71, 91]. According to Wagner et al 1998 [91], optical pathlengths through clouds may be responsible for both enhancing and reducing the optical path taken by sunlight. They also concluded that optical pathlengths in the visible region of the spectrum are more accurate because of the longer wavelengths.

Local landscape influences on DOAS measurement depend on geographical location, landscape topography and the height profile of buildings within the measured pathlength. A mountain range or valley may protect an urban area from high winds preventing any pollution dispersion in contrast coastal areas have higher winds increasing the dispersal. Urban canyons can shield high concentrations of traffic from wind again

reducing dispersion the high temperatures associated with urban areas can also reduce the dispersion of pollution by wind [92].

As this project involves the development of a portable measurement system to determine NO_2 concentration in an urban environment, specifically Dublin city, a brief description of the weather conditions expected there is now given. The city is situated along Ireland's east coast with the River Liffey running through its centre. There is a low mountain range located to the south and the remaining landscape to the west and north of the city is low lying, where agricultural activity is the main source of industry. The city is approximately 115 km^2 in area. The diurnal variation of wind speed in Ireland is considerable. The variation is more pronounced in the summer months than in winter [93]. This is caused by the land surface heating early in the day, which increases the mixing of the faster-moving air at higher altitude than with the air near the surface. The strong winds are responsible for the pollutant gases like NO_2, mixing in the atmosphere and the transportation of the gases throughout the country [11]. In the average day, specifically the late afternoon and evening, the surface heat of the land diminishes which causes the wind speed to decrease during the night. This effect is more noticeable during the summer months. Variation in the wind direction in Ireland is mostly westerly and southerly from the Atlantic, but there may be northerly and easterly winds at other times of year. The average maximum temperatures in Ireland range from only 18^0 Celsius in the summer to 8^0 in the winter with on average less than 10 days of frost on the coastal areas. This variable weather in Dublin and Ireland [93], with a moderate climate, show that the transport of pollution is dominated by wind direction from the west, off the Atlantic, and with the variable temperature there is good atmospheric mixing of gas pollutants. The weather conditions

and the resultant effects on pollutant mixing in the lower atmosphere justify the need for constant monitoring of pollution concentrations.

The strong winds which cause the transportation of the pollution in urban areas (section 1.5) validate the need for a portable, inexpensive spectroscopic system to record local gas concentrations.

3.8 Cost analysis of commercial and mini-DOAS systems

A comparison of the expense of commercial DOAS and the passive DOAS systems shows considerable differences between the two. However the larger expense required for commercial systems would be worthwhile if accurate measurements of a complete diurnal variation of more than one analyte were required. Larger Commercial DOAS expense is not just from the cost of the system itself but also from the fixed light sources or retro-reflectors and installation of the spectrometer and the receiver/transceiver. All light sources and the spectrometer will require mains power supply. The Xenon lamps used in DOAS typically have a lifetime of 2000 hours and can cost up to €500. Calibration of commercial DOAS will also require considerable expense as a specially designed calibration cell is used to meet the dimensions of the overall system. Overall the system can range in value from a basic package of €50,000 up to €200,000 including calibration gases and lamps[94].

In contrast, the passive DOAS miniaturised spectrometers are relatively inexpensive and can range from €2000 to €5000 and optical fibres and lenses can be purchased for less than a few hundred euro. Software packages for DOAS spectral analysis can also be performed with existing software that may already be available *e.g.* Matlab,

Simulink and LabView. Alternative inexpensive light sources can possibly be employed for nightly measurements of NO_2 or other analytes. Light emitting diodes are ideal as they are inexpensive, can be powered independently of the mains output and are relatively inexpensive compared to other sources.

3.9 Summary

Current Active and Passive instrumentation show how DOAS can be applied to the measurement of NO_2, in particular, the various applications of Passive DOAS used to measure both tropospheric and stratospheric NO_2. Satellite data collected by NASA and the ESA provides additional data on the vertical column density of NO_2 and other analytes which have been shown to correlate with ground based instruments. Another application of optical absorption spectroscopy is COSPEC and the flyweight system FLYSPEC which is similar to DOAS but has been predominantly used for volcanic measurements.

The development of the Passive novel-DOAS instrumentation requires software for data analysis of measured spectra, which can be very sophisticated, however, using a simplified approach to the determination of D, means that commonly available software such as Matlab can be used. The viewing geometry of the instrument is crucial to determination of NO_2 concentration in either the stratosphere or the troposphere. Meteorological conditions and light scattering by particles in the air can affect the pathlength of the received light but comparative methods such as CL or Active Long Path DOAS could provide data for correlation.

The passive novel-DOAS system for the measurement of NO_2 in the lower atmosphere close to the surface would provide results that would be of benefit to scientific research and air quality monitoring. The instruments can be devised using inexpensive hardware and commonly used software applications. Data retrieved could be compared to existing methods to determine correlation and an estimation of the optical pathlength being used. Cost effective light sources such as LEDs may also be utilized for night or low light level measurements increasing the flexibility of an inexpensive instrument.

CHAPTER 4 Materials and methods

4.1 Introduction: Portable *in-situ* detection system

Typical DOAS systems described in the previous chapters are divided up between the large setup of commercial systems and scientific DOAS apparatus designed for long term atmospheric or volcanic research. The instrument described in this chapter was developed from rigorous optical bench tests, laboratory tests of gas samples, light sources and optical alignment. An algorithm shown in Appendix II, was designed using Matlab software to analyse the spectrum of light passing through a gas sample determining the absorption and differential absorption and tests were repeated to compare these results. Ultimately the instrument will be unique in its ease of use and portability, thus allowing greater flexibility for future applications and greatly reduced cost for NO_2 detection.

4.1.1 Instrumentation and sample requirements

The choice of detector for DOAS applications can vary as the technique is capable of detecting analytes across a broad wavelength range. As the work described here focuses on the detection of nitrogen dioxide the wavelength range is determined by the NO_2 absorption cross section as described in literature (Schneider [41], Vandaele [43], Burrows [75], Bogumil [44]). There are significant absorption features for NO_2 in the range 400 nm

to 500 nm, particularly at 435 nm and 440 nm, so a detector operating in the visible range would be ideal. This makes it suitable for laboratory experiments as readily available visible light sources can be used to test the samples.

The optical alignment of the detector should be adjustable to measure different parts of the sample if necessary. This is easily achieved in the laboratory. The following are features of the proposed system. The detector required to analyse the spectral range where absorption is known to take place must have low power needs, portability and have a suitable spectral range and optical resolution for the detection of NO_2. One of the most common spectrometers used in Multi-Axis-DOAS is the USB miniaturised fibre optic spectrometers produced by Ocean Optics [95], several of which have been used in DOAS measurements from the earlier S2000 to the later HR4000 spectrometers (Ocean Optics, Dooly(HR2000) [96], Fitzpatrick(S2000) [97], Chen(HR4000) [98]). The work here describes tests performed with three spectrometers specifically the USB2000, USB4000 and the Maya2000 models available from Ocean Optics. Initially, the optical alignment of each of the spectrometers was tested with an optical fibre and collimating lens attached and then the setup was adjusted for different samples and a field apparatus was developed.

The first samples used in the laboratory tests in this research were gas filled polypropylene (PP) bags. Each bag was filled with air with known amounts of nitric oxide injected. This mixes with the air to form nitrogen dioxide at predetermined concentrations. The experimental procedure used a tungsten halogen lamp as a broadband light source fixed with an optical fibre and a collimating lens to produce a collimated beam through the sample. The lenses are coupled to the fibres and each sample is placed between the emitting and receiving lenses. Figure 4.1 shows a schematic of the bench top setup for the bags and

the fibres which are attached to stands which can be adjusted to improve the alignment of the light through the sample. A rail was also used to manoeuvre the setup with each bag sample.

To improve the accuracy and precision of the novel-DOAS system, custom designed calibration cells were eventually used as samples with known concentrations that were a suitable size to be placed in front of the receiving optics, as shown in figure 4.1. Initially, baseline tests were performed on the receiving optics including a determination of the field of view (FOV) of the collimating lens when attached to an optical fibre [95]. The alignment of the receiving setup is collimated with a beam from the emitter. The lens is also compared to a diffuser (also known as a cosine corrector [95]) which has a field of view of 180^0. The spectral range of the lens and optical fibre, when coupled to each spectrometer, were also examined with a broadband light source. Finally, the affect of an adjustable aperture and collimating cylinder attached to the lens were used to control the amount of light entering the optical system to avoid saturation and control the viewing direction. An examination was made throughout of the spectral analysis algorithm to confirm the absorption profile of NO_2 was analysed as accurately as possible.

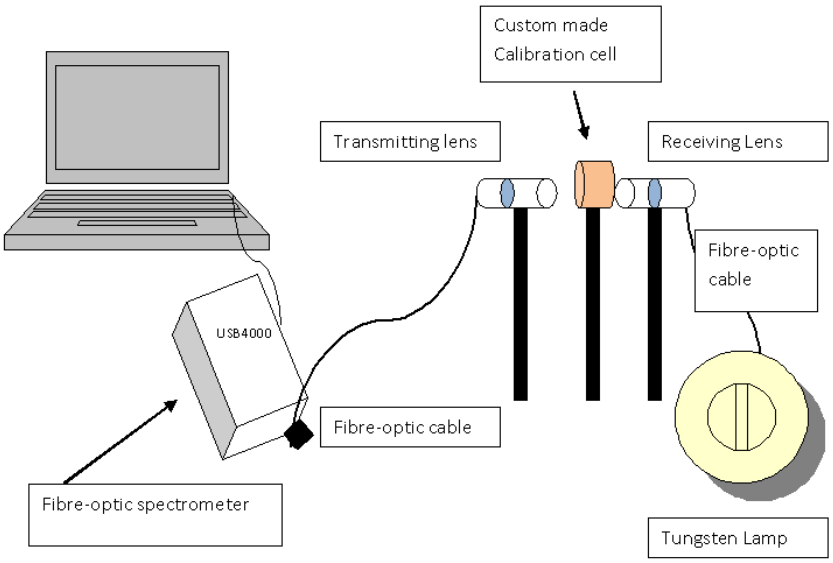

Figure 4.1 Optical fibres coupled to collimating lens aligned with each other on a bench. The bench allows the adjustment of the emitting and receiving fibres for alignment on either side of the polypropylene bag.

4.2 Optical instrumentation

The optical components of the detector need to be capable of detecting a large sample volume that will provide enough information to determine the average concentration of the analyte. For DOAS, the commercial optical system can detect the light emitted by a xenon lamp over a path of up to 2 km or, if retro-reflectors are used, up to 10 km. The optical system of the OPSIS commercial system, as described in chapter 3, uses mirrors of 100 mm in diameter for the emitting and receiving optics, with beam divergence of ~4 mrad. The system developed for this research requires a smaller optical setup but will

still need to detect a large cross section of the light path being monitored. The area viewed by the receiving optics is known as the FOV. For the active DOAS systems, the optics are designed so that the FOV is compatible with the path lengths that are possible using the artificial light sources. For the passive systems, the FOV needs to be maximised for measurements of the layers of the atmosphere under investigation.

The laboratory measurements were designed to detect NO_2 concentrations through both PP bags and calibration cells. The light source could be fitted with an optical fibre and lens for a clearly visible beam of light to pass through the sample or without the fibre and lens for a broad beam illumination of the sample (seen in figure 4.1). As stated, the optical elements will determine the alignment and focal length of the system. The receiving optics needs to be able to detect the light with minimal adjustments and, for the laboratory specifically, the setup needed to be stable for repeat measurements. The FOV could be determined by using the same receiving optics attached to a source and measurements then made of the divergence of a focussed beam through the lens and focal length. Overall, the optics chosen must be capable of viewing the samples or atmosphere adequately and detect light in the same wavelength range where the DOAS calculation will be performed.

The optical characteristics of the collimating lens are determined by the size and manufacturing material, usually silica for transmission of UV and visible light, such as the BK-7. Made from a Boro-Silicate, crown glass can be more suitable for visible measurements. The lenses are designed with a thread to fit onto the ferrule connecting them to Ocean Optics fibres. The focal length is determined from Equation 4.1, where f is the focal length, typically in cm or mm, and u and v represent the object distance between the lens and object and the image distance between the lens and a focussed image.

$$\frac{1}{f} = \frac{1}{u} + \frac{1}{v} \qquad \text{Equation 4.1}$$

The divergence of the beam from the lens is related to the diameter and the focal length. The 74-UV Ocean Optics lens has a diameter of 5 mm and a focal length of 10 mm and an estimated acceptance angle of 25^0. The divergence of the 74-UV is ~26.5^0 and thus it has a half-angle divergence of 13.25^0.

The optical fibres use the principle of total internal reflection to transmit light from one end of the fibre to the other. Figure 4.2 shows the transmission of light in the fibre. The fibre is composed of the central core and the outer cladding layer. The light entering the core of the fibre is internally reflected at a critical angle and subsequently reflected off the cladding lining the inside of the fibre. The fibre f-number, f/#, is related to the size of the entrance aperture where an aperture with f/# of f/2 is larger than f/4 for a narrower aperture (equation 4.2).

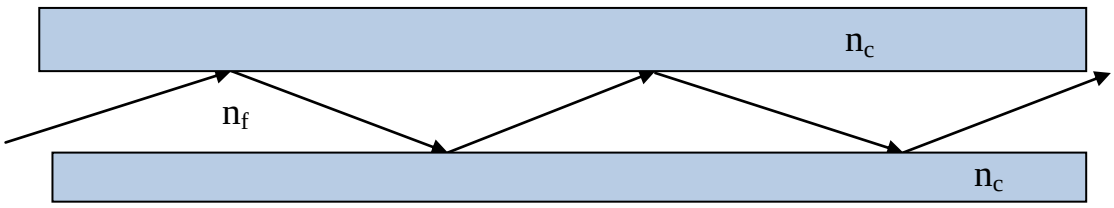

Figure 4.2 Transmission of light in optical fibre occurs as the light enters at the critical angle and subsequently reflects off the cladding as it travels to the opposite end.

The square root of the Numerical Aperture (N.A.) of an optical fibre is related its gathering power and is calculated from Equations (4.3 , 4.4) [99].

$$\mathbf{f/\# = f/Diameter} \qquad \text{Equation 4.2}$$

Equation 4.2 is used to calculate the f/# using the focal length of a lens and the diameter of the lens. For optical fibres the f/# equation 4.3 is used.

$$f/\# = \sqrt{N.A} \qquad \text{Equation 4.3}$$

The numerical aperture can also be calculated from the refractive indices of the fibre core and cladding (4.5). For the novel system to have an effective field of view, N.A. must be close to the effective N.A. of the rest of the instruments optical configuration. In equation 4.4 θ represents the acceptance angle of the fibre optic, the half-angle divergence of the lens should then be close to the same magnitude of this angle for an ideal field of view.

$$N.A. = n\sin\theta \qquad \text{Equation 4.4}$$

$$N.A. = \sqrt{(n_f^2 - n_c^2)} \qquad \text{Equation 4.5}$$

The numerical aperture of the fibres used in this research was 0.22 with core diameters of 600 μm. The acceptance angle of the fibre is then ~ 12^0 almost equal that of the half-angle divergence of the lens.

4.3 Optical alignment

The optical throughput of the overall receiving system consists of the collimated light from a transmitting optical setup entering the lens of the receiving optics. For the system being described here, the entrance optics consists of a collimating lens connected to a fibre by standard Ocean Optics SMA905 connector. The light propagates through the fibre and into the spectrometer, as shown in figure 4.3, the shaded area indicated by the box and red lines represents the optical fibre ferrule and frame of the lens. The combination of the entrance slit of the spectrometer, the mirrors, which direct the light onto a grating and towards the CCD detector, the size and alignment of the grating and size of the detector determine the amount of light exposed to the detector elements. The complete optical arrangement of the entrance optics determines the signal developed measured by the spectrometer. The relationship of each optical element in the whole optical system can be determined as the product of all the optical components from the size of the entrance aperture to the area of the CCD detector inside the spectrometer.

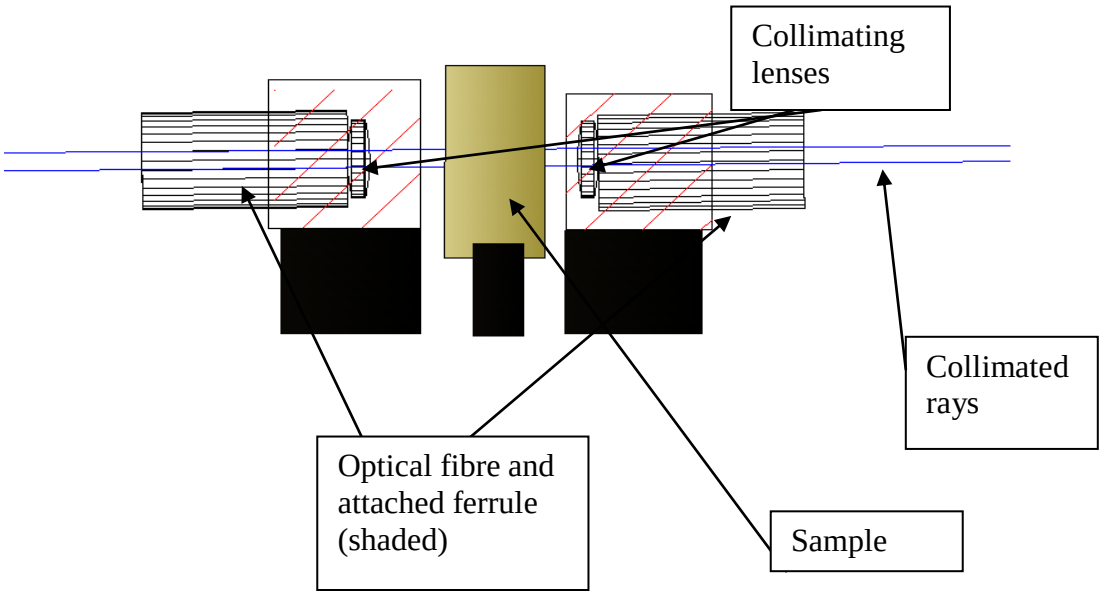

Figure 4.3 Schematic of how light rays passing through a sample are collimated by lenses and optical fibres.

As discussed in chapter 2, modern DOAS measurement devices use a variety of detectors, from the PMT of the larger commercial systems to the photodiode array and charge coupled devices of smaller detectors. PMTs detect light which is converted to an electrical signal by the photoelectric effect. They are able to detect very low light levels, which are directed at several electrodes increasing the signal, making them ideal for the detection of the xenon lamp source over the long light paths used in active DOAS systems. Photodiode arrays are, as the name suggests, arrays of light sensitive semiconductor devices used for the detection of specific light wavelengths or a range of wavelengths. These can be designed to detect specific wavelengths associated with a chosen analyte.

4.4 Miniaturised spectrometers and charge coupled devices

The typical miniaturised spectrometer used in modern DOAS applications is the type manufactured by Ocean Optics and Acton. The Ocean Optics spectrometers use a Czerny-Turner design, see figure 4.3.

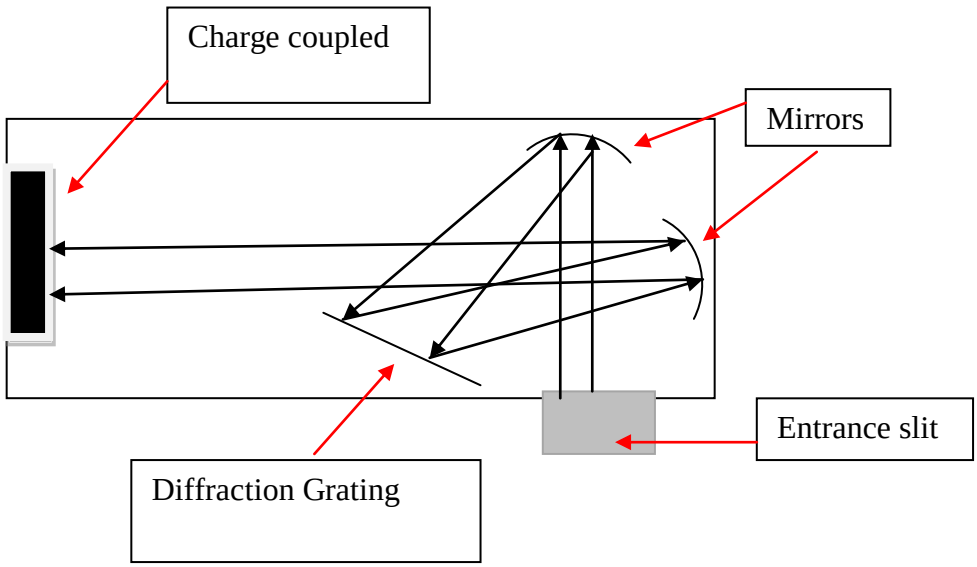

Figure 4.4 Czerny Turner spectrometer design. The light enters at the aperture where the optical fibre is coupled to the spectrometer. The light reflects off the opposite mirror onto the diffraction grating, the diffracted light is then collimated by the second mirror and reflected onto the CCD detector.

The main components of this design are shown in figure 4.3. They include the entrance slit, diffraction grating and charge coupled device (CCD) detector. The entrance slit is chosen for the best optical resolution for the spectrometer that is used. The diffraction grating will have a chosen spectral range depending on the material and blaze angle and the

dispersion, lines/nm, is determined from this range divided by the number of detector elements. The optical resolution is the product of the dispersion and the pixel. For example, the resolution of a USB4000 with 3648 detector elements and a slit width of 25 microns and optical resolution of ~1.34 nm will have a pixel resolution of ~7.5 pixels. Alternatively, the USB2000 spectrometer has 2048 detector elements and is also a front illuminated spectrometer; the differences between front illuminated and back illuminated spectrometers are outlined in detail in this section and section 4.5. The resolution provides more detail in each recorded spectrum making it possible to identify the attenuated features of each spectrum which is caused by gas absorption. But the USB4000's greater resolution allows for a greater accuracy in the determination of differential absorption (D) as the absorption and attenuated features are more readily identifiable.

Diffraction gratings can be either transmission gratings or reflection gratings. Transmission gratings consist of slits for light to pass through or a transparent material with grooves etched into one side. The reflection gratings have ruled grooves into the reflecting surface. The density of these grooves determines the dispersion and therefore the spectral resolution. Modern diffraction gratings for spectroscopy use reflection gratings with blazed [99] rulings that have sharp edges to reduce the amount of light wasted in their operation, making them ideal for applications like the one described in this research.

The ideal detector used in the miniaturised optical fibre detector is the Charge Coupled Device semiconductor detector. Charge coupled devices (CCDs) are sensor devices developed by GE Smith and WS Boyle for Bell laboratories in the 1970s. Originally designed for image sensing, they have numerous applications including commercial applications like memory and cameras. The principle of operation behind the

charge coupled device involves light illuminating the surface of a solid state material (*e.g.* a metal oxide) and then the excited charge is transferred through the semiconductor in a discrete form to an adjacent area where the charge is stored [100]. The metal oxide layer is known as a potential well which forms when the electronic charge is applied to the device. CCDs in miniaturised spectrometers can have a lens close to the surface of the detector to maximise the light sensing of the detector.

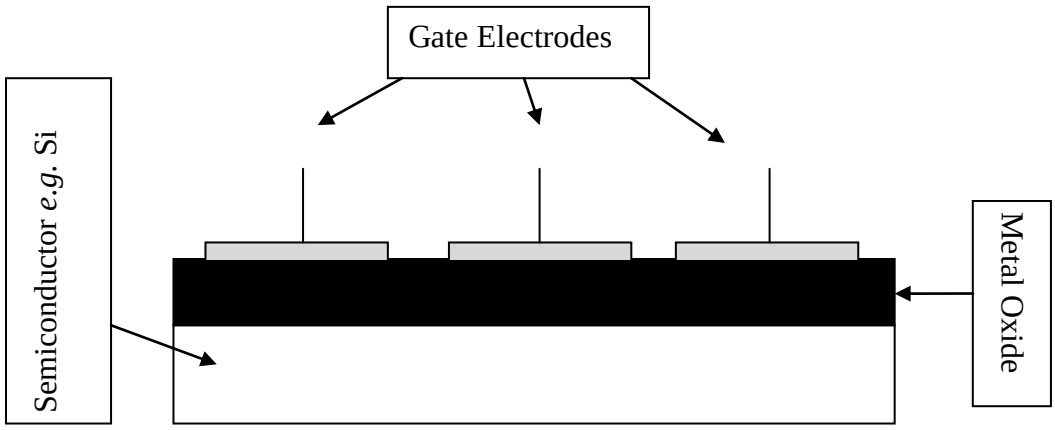

Figure 4.5 Structure of charge coupled device with three electrodes, a potential well is formed under each electrode where the electronic charge is built up before conversion into an electronic signal.

The potential wells transfer the accumulated charge through the semiconductor layer. As indicated in figure 4.4, the potential well is formed beneath the middle electrode when a positive voltage is applied while the others electrodes have a zero applied voltage. The difference in the electrodes creates a potential barrier confining any charge carrying electrons. By adjusting the potential in sequence, the charge is sequentially

transferred through the semiconductor material to the output. The 3 electrodes (figure 4.4) form a pixel which can be grouped in sets and when a series of these pixels are formed they create what is known as a vertical and horizontal register. The CCD is operating as a charge transfer device throughout this process. The vertical register consists of a photosensitive column, *e.g.* 64-128 or more pixels that transfer the charge to the horizontal register. The charge is then transported to an amplifier and converted to a voltage see figure 4.5.

Although there are a few different ways that the transfer process is used, the most common for spectroscopy is the Full Frame Transfer (FFT) process. Frame transfer in CCDs uses two vertical shift registers, a photosensitive and a storage section as well as the horizontal register and the output section. Once the charge builds up in the potential well, it is transferred to the vertical photosensitive section which converts light into electronic charge. The frame transfer is processed in this vertical register, and then transferred to the horizontal register and from there to the output. All parts of the device except for the photosensitive section are protected from light by an opaque material. FFT CCDs are designed without the storage area so the collected light is transferred directly from the photosensitive section to the horizontal register as shown in figure 4.5.

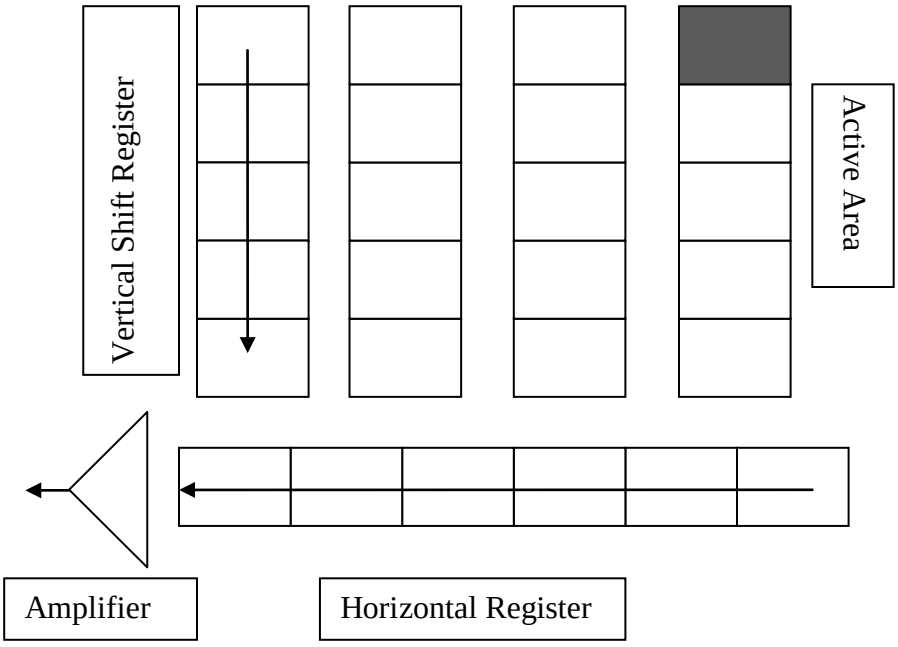

Figure 4.6 Full frame transfer process of a CCD detector. The electronic signal builds up in the vertical shift register and passed to the active area. From here it is transmitted to the horizontal register followed by the amplifier.

4.5 The back illuminated charge coupled device

The structure of CCDs can also vary according to how the light passes through the semiconductor. Back illuminated CCDs (BI-CCD) for spectroscopy e.g. Maya2000 are ideal for low light levels and are responsive in the UV region of the spectrum. The principle of operation compared to the front illuminated CCD (FI-CCD) is, as the name suggests, the illumination of the back of the CCD array. This means the light enters the detector through the silicon before reaching the electrodes. No light is lost by reflection or absorption as in

the FI-CCD, so the BI-CCD has a much higher quantum efficiency [101]. BI-CCD detectors are usually thinned to reduce the distance the light travels. However, the layers of Silicon the light passes through create optical cavities that result in Fabry-Perot etalon features in the viewed spectrum especially in the near-IR [102]. The structural differences are shown in figure 4.6. The etaloning is in spectral and the spatial features.

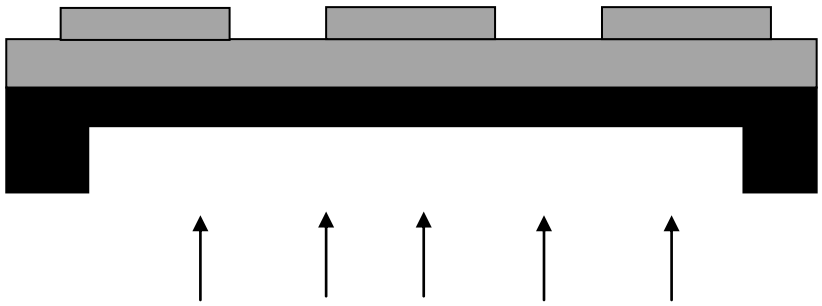

Figure 4.7 A Back illuminated charge coupled device. Note thinned silicon layer where the spectral etaloning is known to occur.

The spectral etaloning causes the intensity to vary in magnitude with wavelength. This occurs because when the light reaches the poly-silicon electrode layer there is a change in refractive index, reflecting light back into the CCD. For some wavelengths the light will be reflected back several times. This effect enhances the quantum efficiency of the CCD because more light is turned into signal but it reduces the amplitude of the signal due to absorption and reflection. In spatial etaloning there is also a variation in intensity amplitude with the thickness of the CCD especially if the thickness of the silicon is not consistent.

As well as spectral and spatial etaloning, there can be spectroscopic etaloning where the wavelength of the light changes across the BI-CCD. Most of these effects in BI-CCDs

occur in the longer wavelengths of the near infra-red region. Spectroscopic binning can counter these effects where the vertical and horizontal shift registers sum their pixels before moving to the next stage. This action along the two columns will average out the interference patterns created by the features in the Near IR. Anti-reflective coatings can also be used to optimize these longer wavelengths. The vertical line binning operation can also reduce the signal readout time. The disadvantages of the etaloning in the recorded spectrum of the Maya2000 are illustrated in the results chapter 6. Ultimately, of the three spectrometers, the USB4000 was chosen because of its optical characteristics and how well the absorption spectrum of NO_2 compares to NO_2 spectra from the literature.

4.6 Dark current and noise

The types of noise encountered when using CCD spectrometers are caused by both electronic and physical effects. The dark current is the observable signal present when no light is being received by the spectrometer. It is a thermal effect occurring in the different regions of the CCD. Within the dark current, both the signal received with no light and the noise in the system is present. This noise in the signal is dependent on the integration times being used which can be reduced by varying the integration time without losing any information when taking measurements. To reduce the effects of thermal noise, it is important that the spectrometer CCD should not be allowed to overheat. This can be difficult for long term measurements but there are several ways to counter this, such as cooling with a combined Peltier element and heat sink or with a D.C. fan. If the sunlight being acquired for atmospheric measurements is changing quickly, and/or if the wind speed

is high and cloud cover is rapidly changing, then low integration times are needed. The signal-noise ratio, S/N, of the detector is the total signal divided by the noise. The number of scans made by the detector can be used to improve the S/N, which increases as $1/\sqrt{n}$, where n is the sum of spectra added [101, 103].

Readout noise is a type of noise created in the output stage of the CCD. The metal oxide semiconductor field effect transistor (MOSFET) amplifiers produce an electrical noise that determines the lower limit of detection of the detector. The Dynamic Range, DR, of a CCD detector is dependent on readout noise by equation 4.5.

$$\text{Dynamic Range} = \text{full well capacity}/\text{readout noise} \qquad \text{Equation 4.5}$$

Other forms of noise affecting the system operation include:

- Fixed pattern noise caused by the variation in the response of neighbouring pixels.
- Shot noise affected by the statistical changes in the number of photons incident on the detector.
- Dark Shot noise when the dark current is affected by shot noise. Reducing the dark current will lower the effects of dark shot noise.

The overall noise of the system can be reduced by keeping the detector at a low temperature and using an integration time that yields information about the analyte but is not heavily laden with noise effects. Typical noise and dynamic ranges for the miniaturised spectrometers used in this work are described in table 4.1 below.

Parameter	USB2000	USB4000	Maya2000
CCD Model	Front Illuminated-CCD	Front Illuminated-CCD	Back Illuminated-CCD
No. of pixels	2048	3648	2048 x 14
Readout (dark) noise	2.5	50	13
S/N ratio	250:1	300:1	350:1
Quantum Efficiency %	~40-50	~40-50	~90
Spectral Range	650nm	650nm	~935nm
Dispersion nm/pixel	0.32	0.18	0.45

Table 4.1 Characteristics of the three miniaturised spectrometers used in the development of the novel DOAS device

4.7 Power and software requirements

The basic power requirements for a portable DOAS system will come from the supply of the computer used to record and control the spectrometer measurements. Miniaturised spectrometers like the Ocean Optics models use low power from 250mA to 500mA at 5 Volts with a D.C. supply. The system described here uses a laptop connected to the spectrometer by USB cable which powers the spectrometers. The laptop can operate on its own in-built battery or from a mains supply when recharging. The battery lifetime for any laptop can vary and may decrease over time, but if operating well can last up to 7 hours in newer models. As the software needed to run the spectrometer can be added easily to the laptop operating system, any laptop can be used. So for long term measurements, when a mains power supply is not readily available, more than one laptop could be used.

The requirements for the software used to collect spectra for DOAS analysis are that it should be capable of representing the data as raw intensity, absorption and it should be

possible to save the data in a common format *e.g.* text files. The primary software used with Ocean Optics spectrometers is SpectraSuite. This software allows the user to control the integration time and the number of scans for each. SpectraSuite also allows the user to save the data in several ways including text files and can present the data in raw intensity, transmission, irradiance and absorption. Figure 4.8 shows a screen shot of typical data of gas samples measured using the USB4000 spectrometer [95], the data is presented in intensity versus wavelength in a) and absorption versus wavelength in b). The units for the intensity and absorption spectra are a digital number on the y-axis and wavelength in nanometres for the x-axis the wavelength range shown is between 300 nm and 700nm.

a)

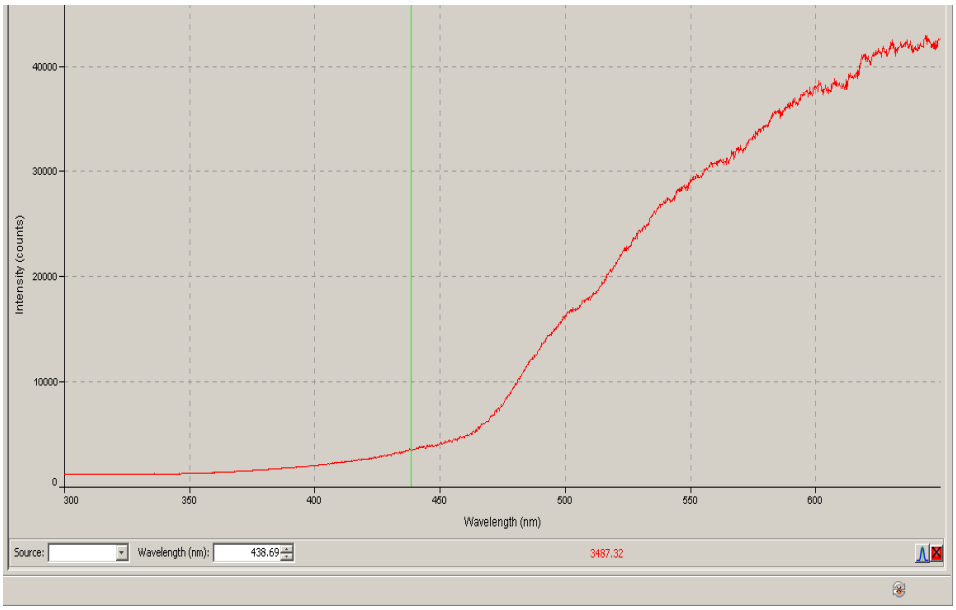

b)

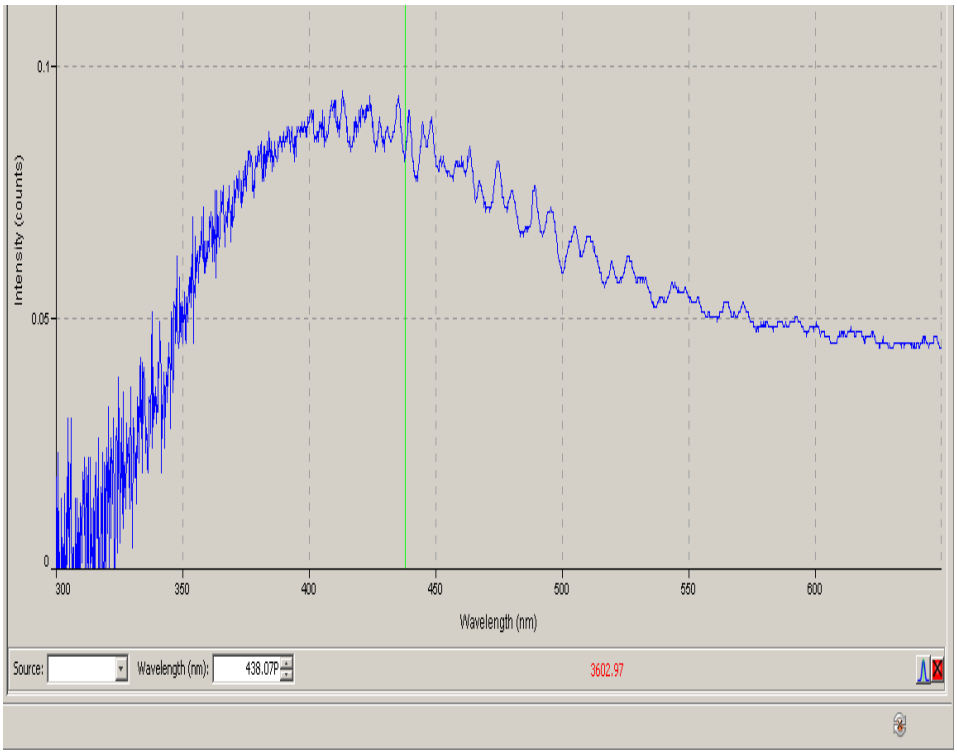

Figure 4.8 Raw intensity spectrum (a) of a tungsten light source used in the laboratory as a reference measurement I_o and an absorption spectrum (b) for NO_2 with wavelength on the x-axes is between 300 nm and 700 nm.

The absorption spectrum shown in 4.7 (b) is calculated for NO_2 using a visible light source with a peak wavelength between 500 nm and 600 nm. The spectrum of the lamp in 4.7 (a) is low between 400 nm and 300nm. The effect of this low signal produces a noisy signal in the absorption spectrum, 4.7 (b) in this range. However, the NO_2 features are identifiable between 400 nm and 600 nm with significant peaks between 435 nm and 500 nm.

For measurements over several days, the software allows the user to control measurements taken for designated times which are saved in one folder. Dark subtraction can be done either with SpectraSuite or during the data analysis with Matlab or other

software. A dark current file should be saved often for continuous analysis. Other SpectraSuite functions include stray light correction and spectra overlay for comparing different results. Data can also be reformatted if necessary using the SpectraSuite menu to convert files to text etc.

4.8 Final setup for laboratory and field measurements

In chapter 6 the results of measurements taken with the miniaturised spectrometers used for this research are described. The results will show that the USB4000 was chosen for the final setup of the novel-DOAS because of the accuracy of the results with the calibration cells.

The experimental setup used to test the spectrometers for this research consisted of adjustable stands attached to an optical bench (see figure 4.1). For tests of path changes between the source and detector, a metre long rail was used. The stands are attached to either the bench or rail and adjusted to improve the optical alignment and counter any saturation of the signal or refraction by the sample material and NO_2 gas. The primary light source used in the laboratory is a tungsten lamp with a broad profile and initial tests were done with the USB2000 spectrometer.

4.8.1 Sample preparation and measurements

The procedure is developed with PP bag samples that are filled with air and small amounts of NO added to create a concentration of NO_2 that will be used to determine if the detector can identify the characteristic profile of the gas in air. Several tests are performed

with the bags and the USB2000 to develop a comparison of absorption (A) and differential absorption (D). To improve the accuracy of the measurements, the USB4000 and Maya2000 are later used. Ultimately, the USB4000 spectrometer was chosen because of improved resolution. The signal to noise ratio and the results of tests performed on the calibration cells are described in more detail in chapter 6.

For the PP bags, the pathlengths are taken to be the width of the sample. The bag widths are between 18cm and 20cm, approximately the thickness when the bag is fully inflated. Preparation of the NO_2 bag samples involved pumping air into the bags until they are half full then injecting millilitres of NO into each bag which would then be filled with more air. Usually three samples are prepared and a bag filled solely with air is used as a reference sample.

Eventually, the calibration cells took the place of the bags because of the accurate concentrations and the suitable size compared to the optical setup. The final optical setup consisted of a spectrometer with a 1 metre or 2 metre optical fibre, collimating lens, collimating tube and adjustable aperture. The whole apparatus was fitted to a camera stand with a rotational platform for measurements of various azimuthal and elevation angles.

4.8.2 Optical bench measurement procedures

The procedure for testing each sample involved placing the reference sample (air sample) into the path of the detector with the light from the source directed at the receiving optics. The integration time and sampling average are chosen and the appropriate settings

made. A dark current measurement is recorded while the lens is covered this will later be subtracted from each recorded intensity spectrum. The raw intensity spectra are then recorded as a reference spectrum and saved. The reference sample is then removed and the NO_2 samples are placed in the path. A spectrum is recorded for each and then the procedure was repeated 5-10 times. For measurements of A, an absorption spectrum is recorded after each NO_2 sample is measured. Once the data was collected it is examined in a Matlab file which used a purpose built algorithm to determine the dark subtraction, mean and standard deviation, D and A for each sample. More than one dark spectrum is taken for all measurements, as the dark current could vary while the spectrometer is in use. Figure 4.8 shows a bag filled with air placed in the optical bench apparatus. The concentration of NO_2 in the bags is calculated with a known path length and α' which is determined from the literature and this concentration could be compared to the expected concentration value.

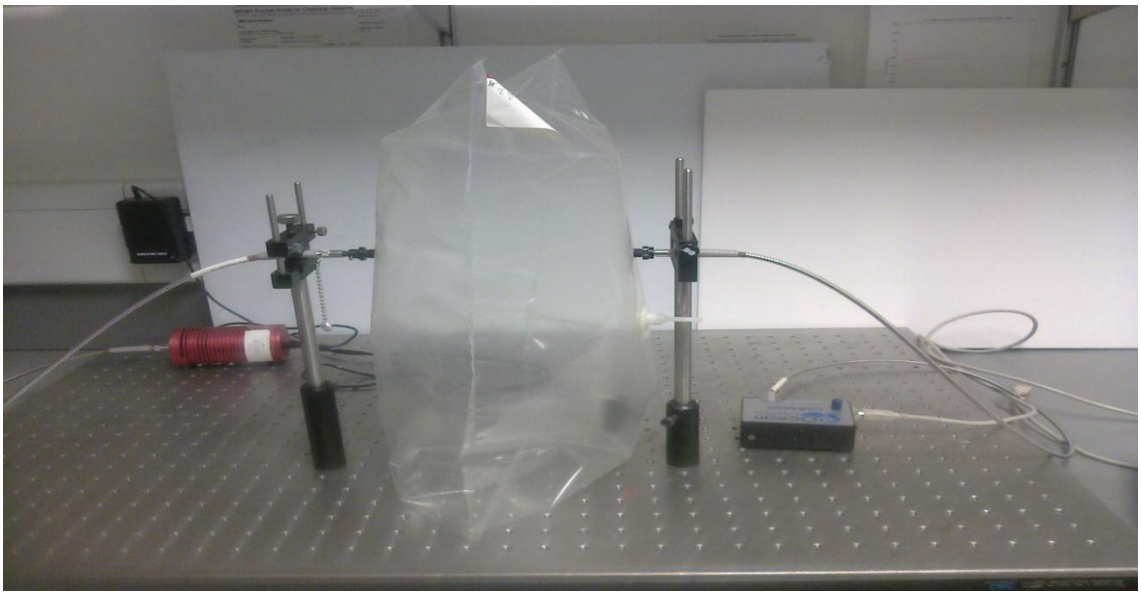

Figure 4.9 Polypropylene bag placed in the path of a collimated light beam produced by a tungsten source, optical fibres and collimating lenses, detected by a USB4000 detector.

The bags are also tested for their stability over time with absorption measured over periods of time of a few minutes after preparation, hourly and once a day for one week. These tests are used to determine if the actual concentration is above or below the expected results and by how much the concentration changes for periods of time. It is expected that the concentration immediately after mixing would be low for a half hour. When the NO is converted to NO_2, the concentration should have some stability for a minimum of a couple of hours until the gas chemically reacts with light or begins to form a deposition layer on the bag itself. The rate of reaction for each bag is monitored with particular attention to low concentrations in case they drop below the limits of detection before accurate examination of the sample could be performed. Once filled, different paths through each bag are tested to compare if each pathlength had the same concentration this would confirm that the concentration is uniform throughout the bag.

Initial tests of the bags show large differences between the expected concentrations and the measured results. Tests were conducted on diluted bags with a CL instrument to determine if the results which required lower concentrations were independent of the instrument and a result of the bag material (polypropylene) or the filling procedure.

4.8.3 Calibration

The calibration cells were chosen as an alternative to the PP bags because of the stability of the cells and their use for similar methods like COSPEC [79] described in chapter 3. The calibration cells were manufactured by Resonance Ltd [104]. Each cell has a quartz body with a short stem, a diameter of 22 mm and a thickness of 14.5 mm. The cells

are ideal for testing with the new system (section 6.4) because the size of each cell means it is possible for placement in front of the system optics in a way that is not as cumbersome as the PP bags. Four cells were purchased with concentrations equivalent to typical atmospheric concentrations for NO_2. Table 2 shows the differences in concentration for 1 metre and 10 km for each cell. Tests performed with the calibration cells include accurate determination of each cell NO_2 concentration and tests of the NO_2 concentration stability over time with exposure to a light source. The cells are expected to have a stable concentration of up to two years, according to the manufacturer. The absorption of light in the 430nm – 445nm range is measured and recorded and the mean and standard deviation was determined. In chapter 6 it is shown that the known concentration of the cells allowed for an assessment of the three miniaturised spectrometers and showed that the USB4000 spectrometer (section 6.6) yielded the most accurate results, justifying its use in the field measurements described in chapter 6, section 6.9.

	Cell concentration. Equivalent for 1m path length	**10km path length**	**Concentration error %**
1	Atmospheric air	0 ppb	0
2	5ppm-m	0.5ppb	±10
3	20ppm-m	2ppb	±10
4	50ppm-m	5ppb	±10

Table 4.2 Concentrations of calibration cells for 1m in the laboratory (in ppm) and a 10km pathlength (in ppb) equivalent to those that can be measured in the atmosphere

The mean values of A(λ) for each cell are compared to the mean values for D(λ) with standard deviation for 10 measurements of each cell. The cells, shown in figure 4.9, have a fixed concentration so the spectrum of α could be determined with a fixed path length. The differential α(λ)' can be found from significant features in the wavelength range mentioned above. This coefficient α(λ)' would be more instrument specific than the values taken from the literature. For example, the instrument resolution between the results of Solomon [52], which were taken in 1987, would be very different to those of Bogumil (2003) [44] and the USB4000, but α(λ)' should still be within a small margin of error of the literature values.

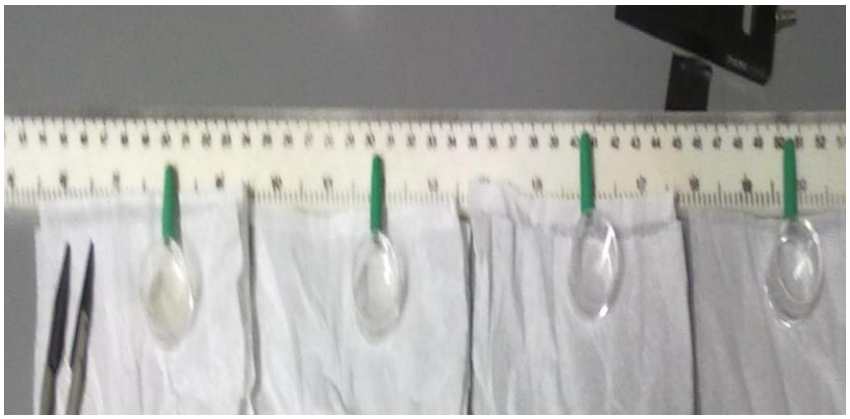

Figure 4.10 Gas calibration cells. Each cell is 1.4 cm thick and each one is fitted with a stem for placement in front of the detectors lens.

The cells are also tested for changes in light intensity using neutral density filters (NDF). It was expected that D(λ) would be independent of the light intensity except at very low light levels close to the limit of detection (LOD) where the signal to noise is low.

4.8.4 Urban measurement of NO_2 with the novel-DOAS

To test the effectiveness of the novel instrument for measurements of the urban atmosphere, several tests were developed to determine the instruments ability to profile the UBL NO_2 variation and the vertical variation (see sections 6.8 and 6.9). These measurements are also used to determine the differences between clear and cloudy days and for comparisons with existing methods to determine the approximate LOD of the USB4000. The spectra of sunlight are examined in detail to identify the ideal wavelengths for analysis, specifically, wavelengths where there was minimal interference from Fraunhofer lines and therefore the Ring effect [37]. The chosen range would also have low interferences from other species and still be a significant feature for the identification of NO_2 and determination of its wavelength. For the determination of $D(\lambda)$, equation 2.14, the feature at 439 nm – 441 nm was chosen, as it had only small interference from Fraunhofer features unlike the feature at 435 nm.

Measurement of NO_2 in the atmosphere above Dublin city required a clear view of a path above the city. For measurements conducted over several days, only one elevation angle is needed so the main requirements included an unblocked view of a large area of the city preferably with an EPA-CL [24] monitor within the path. The benefits of the CL monitor will be explained in more detail in the next chapter. The main objective of measurements using solar light is to determine a profile of the diurnal variation of NO_2 in the atmosphere and compare the results to similar measurements in the literature, available commercial DOAS systems as well as CL data. The measurements are expected to show that the gas concentration will vary throughout the day with high concentrations occurring

at sunrise and sunset due to rush hour traffic and the photochemical reactions of NO_x gases with ozone when the Sun is at its highest solar zenith angles.

To measure concentrations that are comparable to the EPA standard requirements for NO_2, most of the measurements are setup for low elevation angles. The path length is approximated from typical viewing geometries found from the literature and by making comparable measurements with the CL data made available by the EPA. The USB4000 was set to measure automatically for several days with frequent dark currents recorded. In the analysis, the dark current is subtracted and the readings recorded at low light levels and during the night are ignored. Measurements are recorded every 10 to 15 minutes, the data then can be presented as the half-hourly or hourly change throughout daylight hours. The daily mean can also be determined from the data analysis.

For measurements of more than one elevation angle, the ideal locations are roof tops of city buildings. For this research DIT buildings are the primary locations [105]. Measurements of the different elevation angles should provide data on the vertical profile of NO in the atmosphere from the troposphere to the lower stratosphere. The integration time of the USB4000 was set at 10ms for 100 to 500 scans averaging over 1 second to 5 seconds. The measurement of each elevation was conducted in a way to reduce the amount of time between each measurement, as the NO_2 concentration will vary with wind velocity and the light scattering in the atmosphere can affect the length of the path length. An adjustable rotation stage was attached to the field apparatus to ensure that the measurements of each angle can be controlled. The rotation stage is graded with 360^0 angles with 90^0 aligned to the zenith position. Figure 4.11 shows the front-end optics of the field apparatus. For azimuthal angles the stand is adjusted so that the stage can show the

azimuthal changes. Where more than one azimuthal angle is needed, a clear view of multiple paths is ideal. Measurements of the different azimuthal directions can be conducted to compare any changes in concentration in different areas of the city at any one time. These measurements were all taken at the lowest elevation angles. A more detailed examination of elevation and azimuth can be done with multiple spectrometers simultaneously.

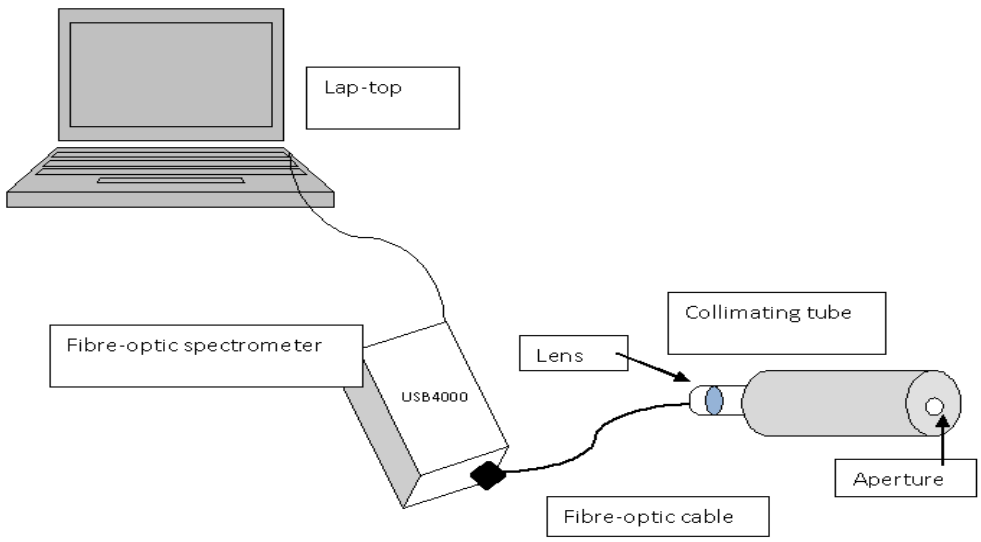

Figure 4.11 Schematic of the field apparatus of the novel-DOAS with the collimating tube and adjustable aperture fixed to the collimating lens and fibre

The calibration cells were placed in front of the USB4000 to see the effect made when a known concentration is placed in the path, the air sample is used as a reference for any additional effects caused by the quartz cell. If the increase in the value of D, for the known attenuation feature where NO_2 is known to absorb sunlight, corresponds to the

increase in concentration of each cell, then it can be assumed that the system is capable of detecting increases in NO_2 using ambient sunlight. If there is a noticeable effect when the smallest concentration is placed in the path then the LOD of the system can be determined and a calibration procedure developed.

Several measurements were taken comparing the light being received by the USB4000 under different meteorological conditions. Direct measurements are taken to compare direct sunlight spectra with the measurements of indirect light and a value of D was calculated from each.

Different geographical locations were compared, but these cannot be done simultaneously because of the distances involved, the number of instruments and the meteorological conditions. Landscape comparisons can be performed with the USB4000 directed at nearby mountains and towards the sea and at urban areas to determine if any notable changes in D could be detected.

4.9 Summary

As described in chapter 3, modern miniaturised spectrometers can be used to record spectra with enough detail to accurately make a determination of the D at specific wavelengths. A system consisting of a USB spectrometer with a lens, optical fibre and collimating cylinder attached to a portable stand is ideal for measurements of different locations without difficult installation at each location. Power usage can be kept to a minimum and more than one system can be used to monitor a larger area if necessary. To determine the LOD of the instrument laboratory tests were performed, tests were conducted

to explore the possibility of determining the correlation between absorption measurements and differential absorption. To perform the laboratory experiments, a broad band tungsten light sources are used to simulate the broad solar spectrum. Samples of NO_2 prepared in PP bags are used but for more accuracy quartz calibration cells are more ideal. The individual features in a specific spectral range are where light is attenuated by the gas these are used to determine the differential absorption and the absorption.

Atmospheric NO_2 measurements are done with the novel setup. A survey of different azimuthal directions and elevation angles are also performed. The vertical profile of the lower atmosphere can be determined if the O_3 and aerosol profile are known however the possibility of making an estimate of the profile using the cheaper portable system is examined. Data was collected during daylight hours for several weeks and compared to other methods mainly CL. s

Chapter 5 will describe in further detail the comparison and correlation between Passive DOAS and CL measurements. Along with a summary of the literature on DOAS and CL comparisons, a description is given of the tests performed using the portable novel-DOAS instrument and what the results of these tests were expected to reveal.

CHAPTER 5 Comparison of chemiluminescence and DOAS for monitoring of NO_2

5.1 Introduction

In order to calibrate the novel-DOAS system, it was first required that CL and DOAS can be demonstrated to produce correlated results. The following chapter explores the distribution of the monitoring stations employed by the EPA in Ireland and how CL is used throughout Dublin city to monitor the concentration of NO_2. Initially the results of CL data and an old DOAS instrument used by DIT (section 5.3) are compared, and comparisons in DOAS literature where both methods were used to make concurrent measurements are reviewed. As described in chapters 2 and 3 of this thesis, determination of the pathlength, L through which the scattered light travels can be the source of substantial error in the calculation of the NO_2 concentration using DOAS. In chapter 3, section 3.6, the pathlength, assuming the detector is ~10 m off the ground is approximately 10 km. With this value, the concentration of a pollutant in the local atmosphere can be estimated from the calculated values for differential absorption, D. However, the effects of scattering light, described in chapters 2 and 3 illustrate how difficult it is to rely on fixed values for the pathlength. Therefore, a comparison of the novel-DOAS system with a known accurate method like CL will improve the estimates for L and the effectiveness of the novel system to measure the concentration of NO_2 in the atmosphere.

A detailed description of the CL instrumentation and its operation is given and of how the results of a CL device, used by the EPA in Dublin, were compared to the novel -OAS system being developed for this research.

5.2 Summary of literature for DOAS and CL comparisons

A comparison of UV absorption, CL and a multi-path DOAS system was made by Williams et al (2006) in three locations in the U.S.A., Nashville Tennessee, Houston Texas and the north east coast of the U.S., the gulf of Maine [89]. The study describes measurements made to assess the correlation of the UV absorption data to the other methods. The results showed that there was a good correlation between the UV system and the CL system with some discrepancies at night and early in the morning. However, comparisons of the Multi-path DOAS and the UV system showed very good correlation with a variation of ±7%.The data was compared for the period between 10am and 6pm in the evening.

Good correlations between CL and DOAS were also observed by Leigh et al. (2006)[106]. An *in-situ* CL system was compared to a concurrent-multi-axis DOAS (CMAX-DOAS) set up in Leicester (UK). The CMAX-DOAS measurements appear to be recorded between 5am and 9pm and the weekly variations, including lower concentrations on Sundays, are shared by the CL results.

More recent comparisons made by Chan et al. (2011) [49], Dunlea et al. [107] comparing Tunable IR Laser Diode Absorption Spectroscopy (TDLAS) to DOAS and CL.

Other comparisons include those conducted by Vlemmix et al. [108], which were done with the regional Lotos-Euros air-quality model in the Netherlands.

5.3 Dublin Institute of Technology DOAS monitor

Research has been conducted by the Dublin Institute of Technology (DIT), which had an operating OPSIS-DOAS system with the receiver located on the roof of the Kevin Street building as well as several emitters located in different locations around Dublin city [5, 105, 109, 110]. Figure 5.1 shows the locations of the receiver and the 5 paths between the receivers and the emitters.

The emitters where fixed in position on the roofs of current and former DIT buildings and local government buildings. Due to the increased construction around the city in the last two decades and change in ownership and use of these buildings, not all the emitters were available for use in this project.

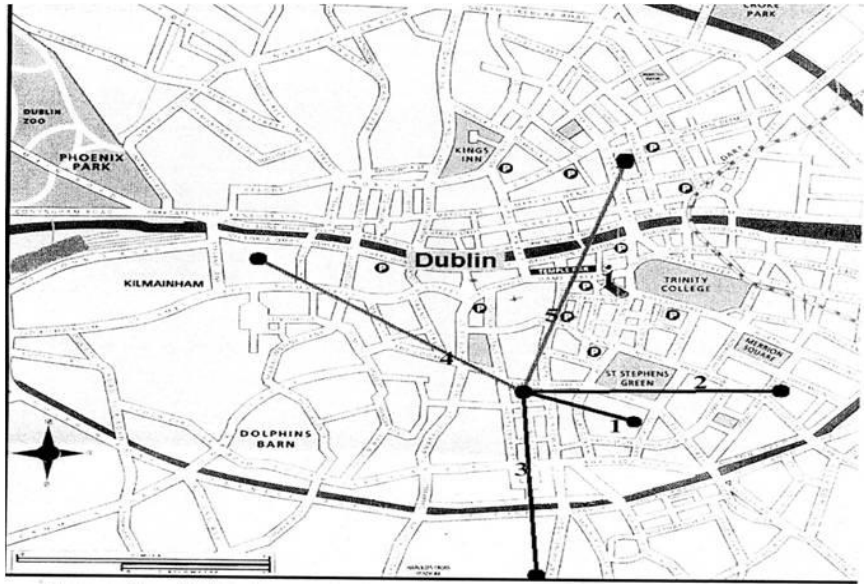

Figure 5.1 Map of Dublin area that includes the paths of the DIT-DOAS system. Only the Cathal Brugha street path is still available but it is nearly 2 km from Kevin Street and alignment is difficult [105].

Part of this project involved both an examination of the existing DOAS system in DIT and a determination of its status with a view to recommissioning the instrument if possible. Several reasons made this difficult: one was the increase in construction as already mentioned, the system's electronics were in need of replacement, a new location needed to be sourced for the spectrograph, the cost of recalibration was particularly high and for health and safety reasons not all the external systems were easily accessed. At the beginning of this project, a lamp was installed in the emitter on the roof of DIT Cathal Brugha Street, which is path number 5 in figure 5.2, to the north of Kevin St. The pathlength was approximately 1.8 km long and was difficult to identify during daylight hours. Efforts to align it with the receiver and the portable system at night were not possible

as the low power of the 150W lamp over that distance made it too difficult to detect. According to OPSIS, any calibration of the OPSIS system is best done with a pathlength of 300 m to 1 km. It was also determined that the software of the system needed to be extensively updated and the spectrometer would most likely require replacement components[28].

Older data saved electronically on the DIT DOAS system did show correlation between DOAS concentrations and Dublin based EPA CL devices, however, as shown in figure 5.4. The graph shows how the diurnal variation of the results taken by the EPA showed a very similar trend to the results of the DOAS. The DOAS concentrations appear higher overall, which may be due to the DOAS results representing measurements of the average concentration over a distance of 600 m to 1 km. It was decided that a comparison of the portable system and the local EPA data could be used to determine the accuracy of the new device for measurements of the local atmosphere.

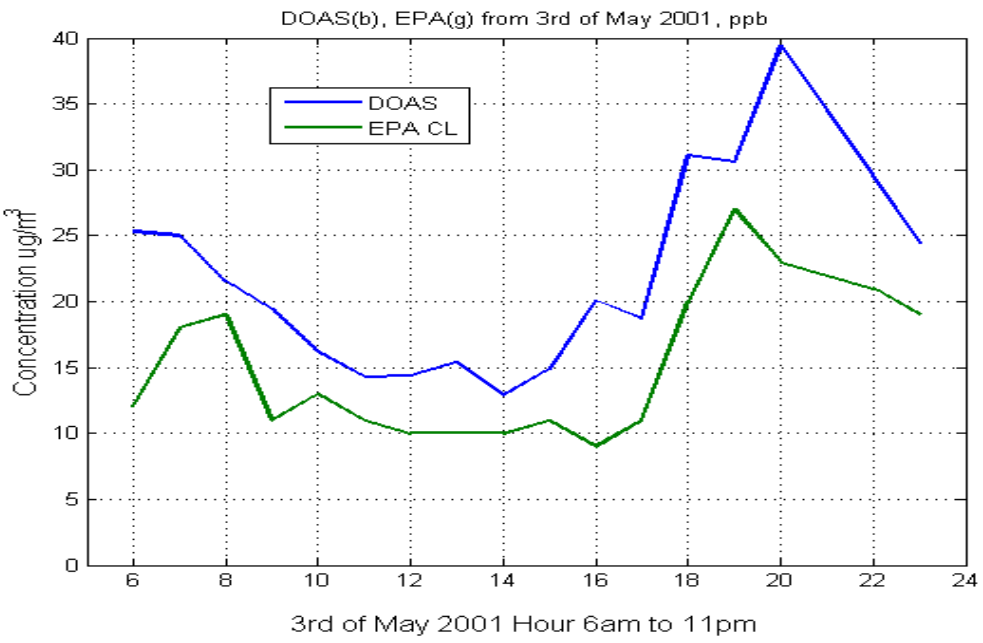

Figure 5.2 Comparison of the data obtained from DIT-DOAS and EPA-CL instruments for 03-05-2001

Figure 5.3 shows the CL data presented by the EPA for the Rathmines site on Wynnefield Road. The data shows the variation in concentration for 6 days in October 2012 for O_3, SO_2 and NO_2. It is worth noting the lower SO_2 concentration in comparison to the other two gases and how the NO_2 and O_3 levels vary with an apparent inverse relationship, most likely due to the photochemical reactions described in chapter 1. The few days presented in figure 5.3 are for the October bank holiday weekend. The data shows the day and night variation of all three of the gases, with the daily variation appearing between the dates marked on the horizontal x-axis. There is some reduction in the NO_2 concentration during the daylight hours and much higher concentrations during early morning and evening. The low concentration on Sunday the 28/10/12 is due to lower traffic congestion and the increased photolysis of the NO_2 gas. It can be compared to the higher concentrations on the Friday 26/10/12 where the NO_2 reaches 50 μgm^3. This is most likely

driven by the typical traffic congestion at the end of a working week at the beginning of the bank holiday.

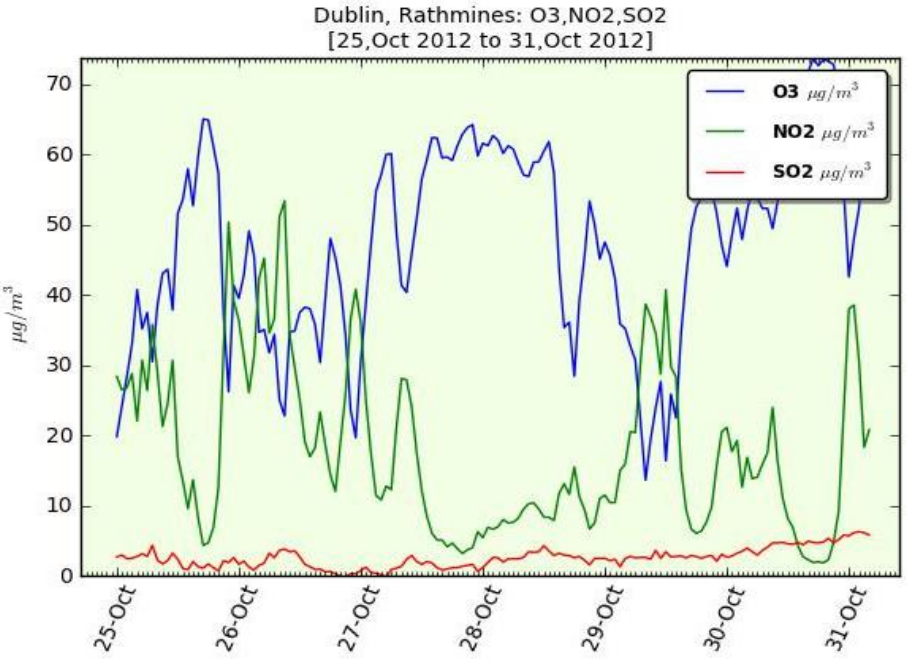

Figure 5.3 Real-time data from the Rathmines monitoring station (25th to 3rd of October 2012). The NO (green) O (blue) and SO (red) data are available from the EPA website [17]

5.4 Chemiluminescence instrumentation

As previously stated in chapter 1, the European Union regulations advise [9] that the standard method for the monitoring of NO_2 can be done by CL. CL [10] is a point sampling technique which takes a sample of the atmosphere through an intake tube and then the concentration of NO_x, NO and NO_2 are determined using a molybdenum catalytic converter and PMT detector. Figure 5.4 illustrates the process the NO_x gas takes inside the CL

instrument. Alternatively the DOAS method of measuring pollution is a remote sensing method that can be setup to measure many pollution concentrations over long paths in a typical urban environment. The two methods are worth comparing (section 5.5) as they each have their advantages and disadvantages and have previously been shown to complement each other [49, 89, 106, 107].

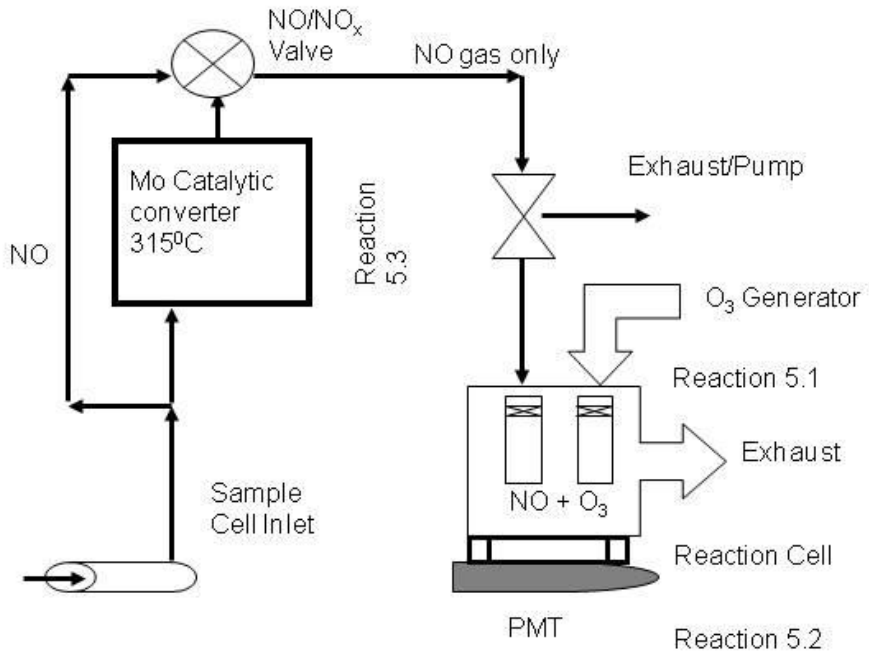

Figure 5.4 CL monitor operation. Air is sampled at the inlet and the PMT measures light through NO or NOx gases. NO2 is then found by subtraction.

The process of CL occurs when the samples are extracted from the atmosphere in a gas phase. In this state, they undergo chemical reactions that emit light. The reactants transfer energy during the reaction and undergo electronic transition up to higher energy

levels. When the excited electrons return to lower states they release energy in the form of photons.

The CL monitoring instrument operates by sampling the local atmosphere through a narrow inlet tube. The nitric oxide (NO) in the air sample reacts in a cell with ozone produced by the instrument (Reaction 5.1). The following reactions describe the order that the NO and O_3 gases are introduced to each other (Reaction 5.1 – 5.3) and their products as well as the reaction of NO_2 with the molybdenum (Mo) converter.

$$NO + O_3 \rightarrow NO_2^* + O_2 \qquad \text{(Reaction 5.1)}$$

$$NO_2^* \rightarrow NO_2 + h\upsilon \qquad \text{(Reaction 5.2)}$$

$$3NO_2 + M_o \rightarrow 3NO + M_oO_3 \qquad \text{(Reaction 5.3)}$$

Single molecules of NO_2 and oxygen are produced, with the NO_2^* molecule retaining excess energy that is emitted as infra-red light (Reaction 5.2). The light emitted is in the wavelength range 600 nm to 3000 nm with a maximum (IR) peak at 1200 nm and is detected by the PMT. The sample is then directed through the Mo converter at a temperature of 315 ^{0}C (Reaction 5.3), which chemically separates more NO from the sample. This is then passed through the same reaction cell and the emitted light is measured again by the PMT, see figure 5.6. This second measurement represents the amount of NO_x gas in the sample as the amount of photons released should be directly proportional to the NO concentration. Finally, the NO_2 concentration is determined by subtracting the NO concentration from the NO_x concentration [10, 24, 27].

5.5 Comparison of *in-situ* DOAS and CL

As has already been shown, there is good correlation between DOAS and CL, (figure 5.4, and results described in the DOAS literature). Because of this and the lack of availability of a local DOAS system, comparisons were made of CL and the novel optical system to determine NO_2 concentrations and the optical system's LOD. For this research, some comparison was made between the results obtained by the novel DOAS system and a CL instrument used for another research project conducted by Trinity College Dublin. Extensive comparisons were also made between the DOAS system and the EPA monitoring station in Rathmines, an area in South Dublin.

The CL monitor was a Teledyne API 200A chemiluminescence analyser[24]. These systems are designed to monitor nitric oxide, NO_2 and NO concentrations. The API 200A monitor is 18 cm by 43 cm by 60 cm in size with inlet tubing and external vacuum pump connections. It is powered by a mains supply or a portable generator. The API 200A instrument has a range from 50 ppb to 20,000 ppb (20ppm), and a inlet tube flow rate of $500cm^3$/min so approximately half a litre is extracted from the atmosphere each minute and it has an operating temperature of 5 to 40 ^{0}C. Its central processor has several functions that allow the operator some selectivity this is possible with the 'multi-tasking software'. Calibration was performed with a standard gas of known concentration held in an external cylinder.

Overall, the CL systems are reliable and accurate but they are a fixed system requiring mains access and protection against the weather and theft. CL is very accurate and is comparable to other measurements made by CL within Ireland and the rest of the EU. It is less susceptible to interference by other trace gas species as the measurement is specifically designed for NO_x/NO and NO_2. But this also means that other instruments need to be employed for the identification of other species which is not the case with the DOAS method, which can determine concentrations using the spectral data obtained for a broad wavelength range.

It is also worth noting that CL is a point sampling method that may be influenced by unusually strong sources nearby and does not represent average concentrations over a large area. As the results will show, tests were performed on the portable DOAS system to demonstrate how it could be used as an inexpensive, portable, flexible instrument that can measure average concentrations over a path length and can be compared with other established methods such as CL. A DOAS device could also determine the necessity or even suitability of a monitoring site for longer term measurements by a larger, expensive, permanent DOAS system or CL monitor. The CL instrumentation, commercial DOAS and novel-DOAS instrumentation and limits of detection are summarised in table 5.1.

Chemiluminescence	Commercial DOAS	Proposed System
Intake tube	Average conc. along fixed path	Average conc. along an open path
Series of reactions	PMT, CCD	CCD
50ppb → 20,000ppb	L=500m 1ppb	L=500m ~10ppb
NO, NOx, NO_2	NO_2, SO_2, O, Benzene, PM	NO_2

Table 5.1 Comparisons of the CL measurement limits with commercial DOAS system and the proposed novel-DOAS instrumentation

5.6 Experimental procedure with TCD-CL

The experimental procedure of measurements of the atmosphere using the novel-DOAS and the CL monitor involve comparing results to assess the ability of the DOAS system to make concurrent measurements with a known method. Results are obtained simultaneously with the DOAS instrument and the Trinity and EPA systems when they are situated in the line of sight of the novel-DOAS device. The results are examined using an approximation of the pathlength measured by the DOAS method and the data provided by the Trinity system and the EPA.

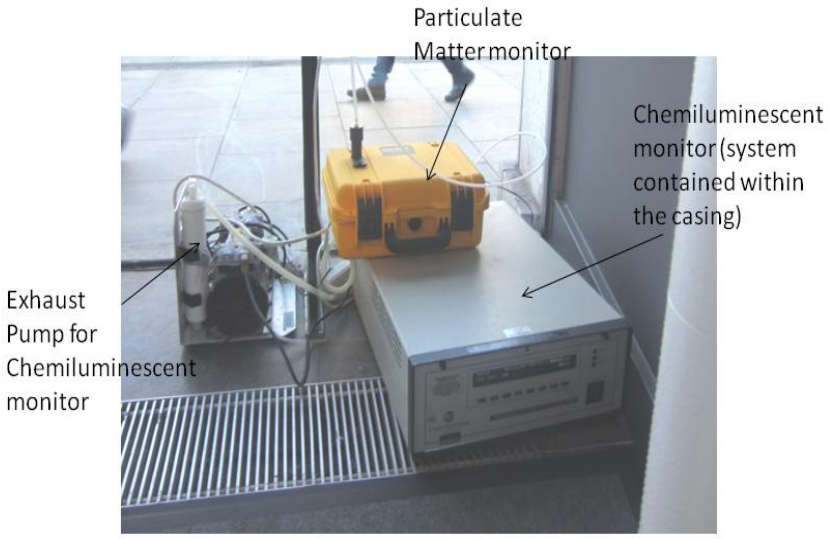

Figure 5.5 CL monitor setup for field research with PM monitor (yellow case) and vacuum pump for extracting the air into the sample cell inlet (figure 5.6)

As the DOAS method employed in this project uses ambient sunlight and needs a clear line of sight without obstruction from nearby buildings, trees etc. the results are recorded for daylight hours from both the roof top of DIT Kevin St. and the second floor of the FOCAS (Facility for Optical Characterisation and Spectroscopy) building which is part of the DIT Kevin St. campus.

The measurements carried out with the TCD CL monitor, as can be seen in figure 5.5, were designed to compare PM and NO_x concentrations in three different locations on the Kevin St. campus: 1) the roof of the Kevin St. building, 2) the front of the building at ground level and 3) inside a laboratory on the top floor of the same building. The TCD CL system was first placed on the highest part of the Kevin St. building with a PM monitor attached and then moved to the ground. The system required a mains power supply for the pump and needed to be protected against rain and theft which is an example of how the CL

instrumentation is not easily relocated compared to the optical system which only requires an accessible location. DOAS measurements from the north facing balcony of the FOCAS building with the CL monitor in the path of the optical instruments line of sight.

5.7 Analysis of the novel-DOAS with EPA-CL data

Comparisons of the DOAS device measurements and an EPA CL monitor were conducted with a significant set of data taken during the summer of 2011. The CL monitor is located on Wynnefield Road in Rathmines south of Dublin City Centre and the DOAS device was set up (in 2011) at the DIT FOCAS building. Spectra were recorded by the DOAS device for 24 hour period, and these were later analysed using the specially designed DOAS algorithm described in the previous chapter. The night time, early morning and early evening measurements were discarded because of no or very low light levels. The spectral data was examined for variation in the trends of the D and then the average NO_2 concentrations were determined based on weather conditions and the typical concentrations recorded by the EPA CL monitor in Rathmines. The two sets of data were then compared for evidence of how the variation in concentration trends determined by each instrument showed any correlation.

The results are expected to have a good correlation between the trends of NO_2 concentrations determined by both instruments and also show that any substantial variations in the DOAS results data which are most likely related to the meteorological conditions, large variations in the local NO_2 profile and variations between the different

instruments used. The results gained, if successful, will lead to methods for calibrating the new instrument and further development of the device and its software.

5.8 Summary

The EPA monitors several pollutants including NO_x gases with a variety of sophisticated instruments. Annual concentrations of pollutants are typically higher in Dublin city and the greater Dublin area due to the higher population and traffic congestion levels. The Dublin Institute of Technology set up an OPSIS-DOAS system in the 1990's in various locations around Dublin City. Since then the system has been out of service, needs to be calibrated and several components need replacing. The emitter sites are no longer available due to the increased level of construction during the late 90's and early 21st century.

NO_x gases are typically monitored by the EPA using CL measurements the literature describes how comparisons have been made showing good correlation between this in-situ sampling instrument and different DOAS techniques. To test the ability of the novel optical system described in this research comparisons were made between it and two CL systems. Results are expected to show good correlation with any variation being the result of the methods employed and weather conditions. Although there are differences between CL and DOAS, particularly the novel portable USB spectrometer system described in this research, they could ultimately be used as comparative systems if it can be shown that the results obtained by both are complimentary. Chapter 6 presents the results of the

laboratory measurements and measurements taken using the ambient solar light. The results of the correlation of the novel-DOAS setup and CL are also presented and examined.

CHAPTER 6 RESULTS

6.1 Introduction

In this chapter, an examination of the experimental data obtained from the measurement of NO_2 concentrations by the novel-DOAS is described. Particular attention is given to how the results in the laboratory influenced the use of the DOAS instrument outside the laboratory. Initially testing was performed in the laboratory using three different spectrometers. Each one was tested with a view towards determining the one most suitable and the data acquisition parameters needed to accurately determine NO_2 concentration.

The laboratory results were obtained with NO_2 samples of different concentrations. Analysis was also made of the spectra taken from the local atmosphere. The results were analysed to determine NO_2 concentration using the attenuated features and a calculation of D. The atmospheric results were compared to established methods specifically CL used by the EPA. As described in the previous chapters, there are differences in the measurement using CL, which is a point sampling method, and the DOAS system, where open path remote sensing is employed. Therefore, it is accepted that the data from each method may not correlate exactly due to the different physics of each method. However, it is expected that, for clear bright days, there will be an acceptable correlation for each of the daily averages taken by each instrument. Some of the results were also compared to simultaneous measurements made by a CL monitor provided by Trinity College Dublin.

The results were used to determine how the portable optical system described here is suited for local measurements of an atmospheric pollutant using the DOAS method and if it is an ideal method for the determination of any local pollutant concentration with results that may justify closer monitoring by permanent *in situ* systems. Analysis of the quality of the results will inform the design and operation of the instrument and how the system will be used to determine NO_2 concentration levels in a practical situation. The results will also inform the nature of what future work could be done to further develop the system beyond the research described in this thesis.

6.2 Laboratory setup and equipment tests

6.2.1 Initial laboratory tests

The initial measurements were of concentrations of the analyte gas, NO_2, in PP bags. The spectra were analysed using a specifically written algorithm in Matlab software, as described in chapter 4 section 4.7. The absorption spectrum for each sample was determined using a reference bag filled with air and a measurement of a bag sample containing a mixture of air and concentrations of NO_2. The wavelength range between 430 nm and 437 nm, which was identified as containing NO_2 absorption features, was initially used to determine the absorption (A) and the differential absorption (D) values. The variations in concentration of the bags were closely examined for stability over time and how the sample concentration may have varied throughout the bags. Specially designed calibration cells were eventually used to replace the bags because of the more stable

concentrations of NO_2 (section 6.4). Further tests were also done using light emitting diodes as a spectrometer source to determine the changing intensity of the LED over increasing distance and the identification of NO_2 absorption features from the obtained narrow spectra. The results from these tests may inform future applications of the new system described in this research.

6.2.2 Laboratory tests

As described in chapter 4 section 4.8, the laboratory apparatus consisted of a miniature spectrometer and a tungsten lamp, each coupled to optical fibres and collimating lenses. Figure 6.1 shows how each sample was placed on the optical bench to ensure a collimated beam was used that passed through each sample with little adjustment of the apparatus.

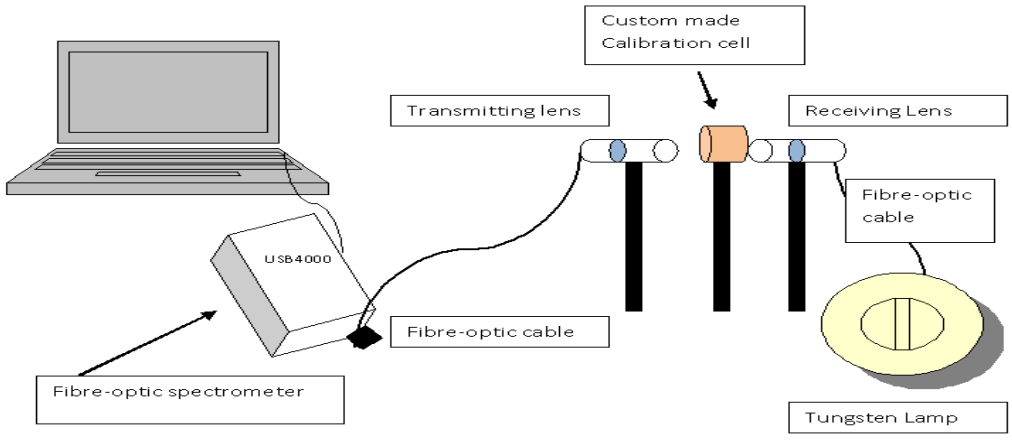

Figure 6.1 Diagram of laboratory bench top setup as seen in chapter 4

In chapter 4, the three different miniaturised spectrometers manufactured by Ocean Optics are described in detail. The USB2000 was used first, followed by the Maya2000 and then the USB4000. The USB4000 was used for calibration and field tests but the laboratory results are shown to compare the data acquisition and response of each spectrometer. For each spectroscopic measurement of a sample, the dark current spectrum was recorded. The signal to noise (S/N) of the spectrometer is proportional to the √n, where n is the number of scans for each integration time. For example, in figure 6.2, the dark current for averages of 1 scan and 500 scans with a 10 ms integration time is compared for the USB4000. Averaging 1 scan for 10 ms with a typical S/N of 300 for the USB4000 and a maximum signal of 60,000 counts produces noise of magnitude ~200 counts. Averaging over 500 scans for the same integration time and signal changes the magnitude of the noise to ~9.2 counts, resulting in a higher S/N of ~6500, increasing the S/N ratio by a factor of 21.6. In figure 6.2 the y-axes indicate the intensity of each dark current recorded. The intensity has no units but is represented by a digital number denoted by dn, this also represents the number of counts.

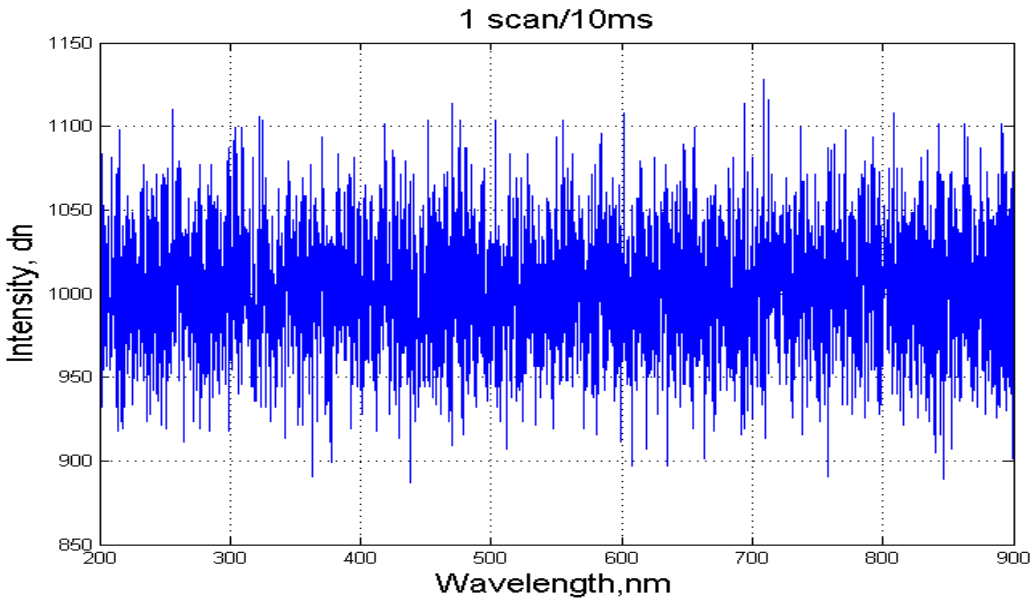

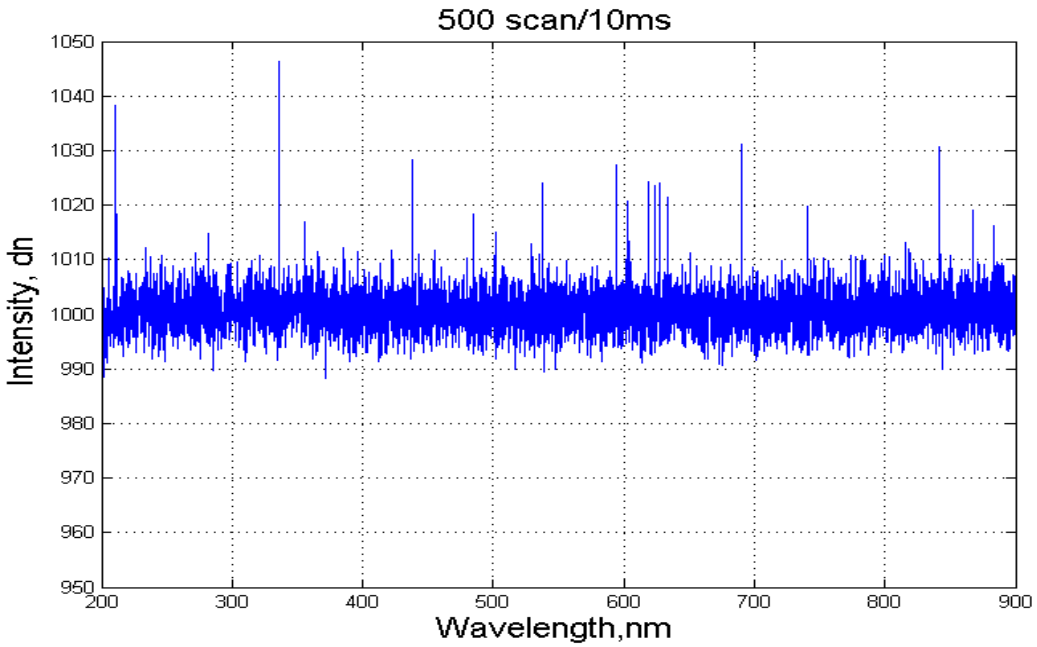

Figure 6.2. Comparison of the dark current signal, a digital number, for one and 500 scans. The top image is the dark current for 1 scan/ 10 ms and on the bottom image shows 500 scans/ 10 ms. Note the improved signal to noise when more scans are averaged.

In figure 6.3, the four different dark current signals illustrate how the intensity of each one increases over time when the spectrometer was in use for long periods. This was typically caused by the spectrometer heating up the longer it is kept operating. In general, the spectrometer was turned on and initially left operating for 20-30 minutes for the dark current to reach a stable intensity. For the field measurements, the spectrometer needed to be operating for long periods of time so the variation in dark current was corrected for by averaging numerous dark spectra, but in the laboratory, as the testing was usually conducted within a few hours, there was less variation in the dark current.

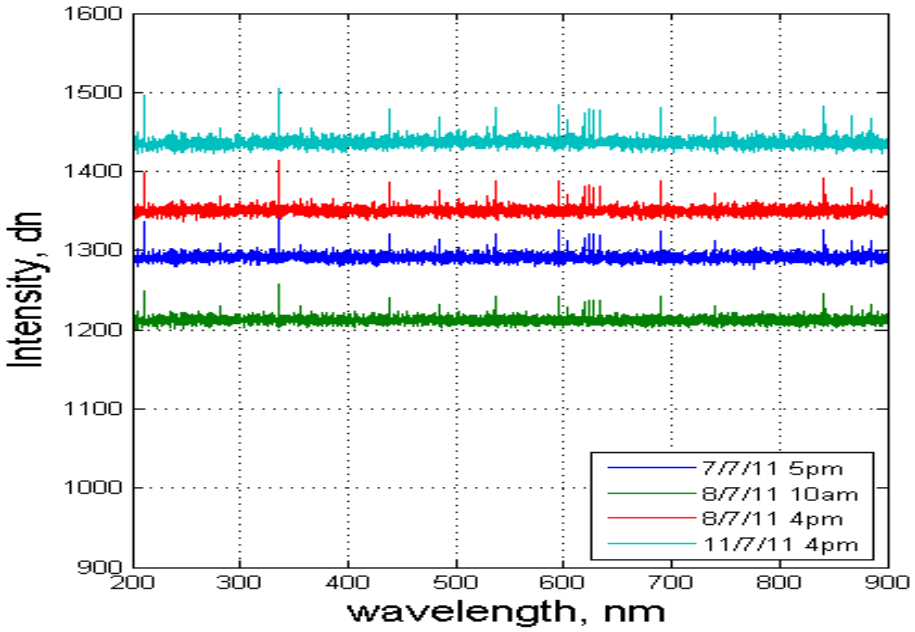

Figure 6.3 Variation in dark signal over time. The signal drops between the 7/7/11 (blue) and the morning of the 8/7/11 (green) then rises above it (red) before rising again (cyan). The variation is most likely due to the change in temperature of the spectrometer over time.

The experimental setup of the laboratory tests (see Ch. 4, section 4.8) included a 600 µm optical fibre which was used to maximise the light received by the spectrometer and was coupled to a 5 mm diameter collimating lens receiving light in the visible and near UV region of the e/m spectrum. The lens was aimed at an opposing uv/vis emitting lens. Both lenses could be fixed in position on a rail on the optical bench, see figure 6.4. The stands supporting the optical fibres and lenses were also adjustable to direct the collimated beam through the sample bag so that a maximum signal was obtained by the receiving optics without saturation.

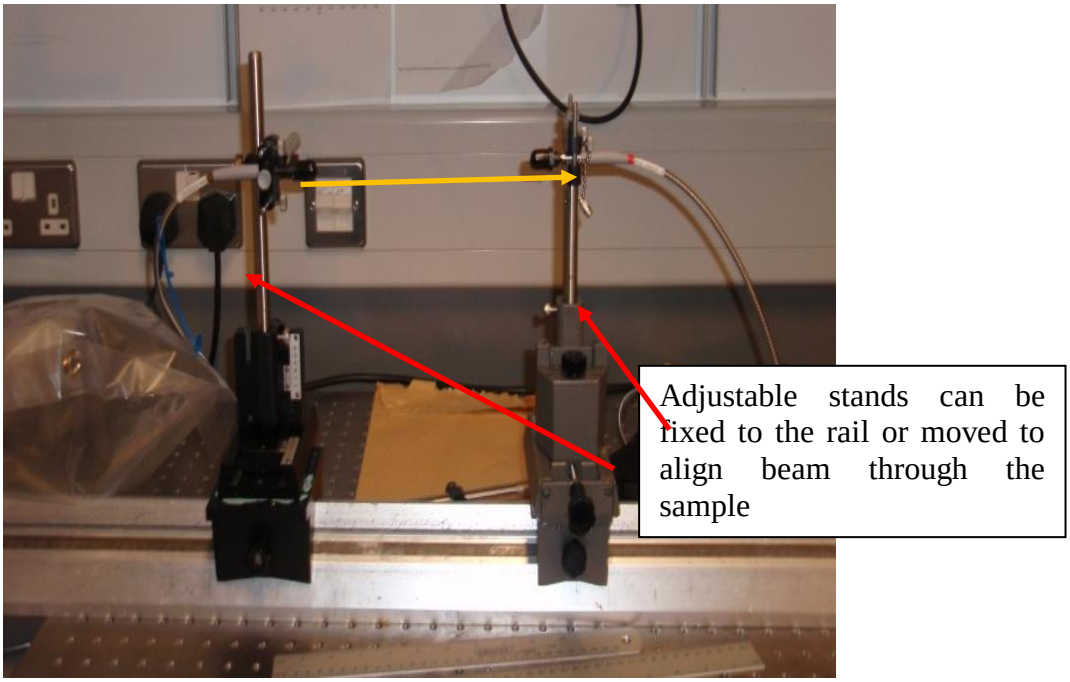

Figure 6.4 Optical setup of fibre optics with moveable stands on a rail without sample

The transmitting lens could be also connected to an optical fibre with a narrower diameter to reduce saturation. This transmitting optical fibre was connected to the tungsten halogen lamp which provided a broad band light source for the laboratory measurements. In figure 6.5, the setup is shown with the PP sample bag between the two lenses, in this image the emitting and receiving lenses are attached to permanent stands on the optical bench. Care was taken to keep the sample fixed between each stand to maintain the stability of the collimated beam so that the beam did not become misaligned when the sample was changed.

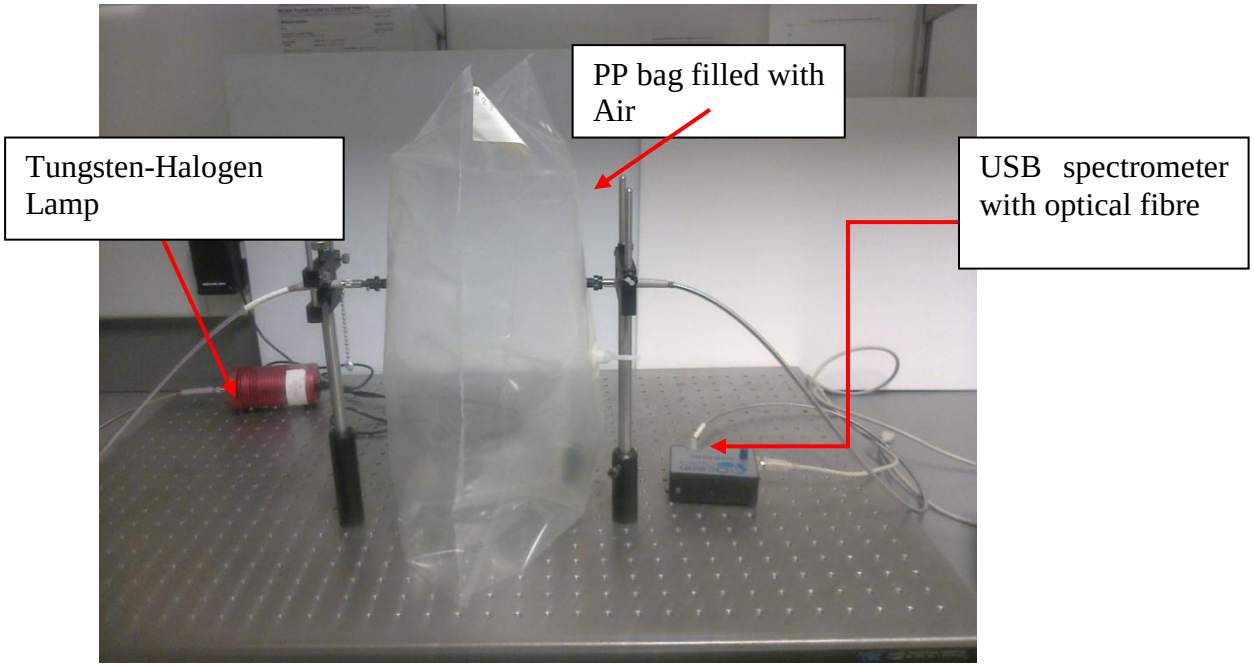

Figure 6.5 Polypropylene (PP) bag sample positioned between the two collimating lenses on the optical bench. Image is shown with the room lights on but measurements were taken in the dark to remove a prominent peak at 435 nm produced by the room lights.

Figure 6.6 shows the light passing through the bag sample. The room lights were turned off for each sample test because of an emission peak in the room's fluorescent lights at 435 nm.

To measure the absorption (A) and calculate the differential absorption (D), the choice of wavelengths is critical. An Ocean Optics calibration, mercury-argon lamp was used to measure the intensity of light received by the three miniaturised spectrometers and to examine their spectral response for the narrow wavelength range where NO_2 is known to absorb. These measurements were used to determine how well each spectrometer was suited to determine the concentration of NO_2 using the algorithm described in chapter 2.

Figure 6.6 shows the normalised intensity peaks (right hand side) for each spectrometer found using the calibration lamp. The peak shown was at 404 nm which is close to the spectral range where the prominent absorption features of NO_2 are found. The results illustrate the differences in the intensity profile detected by the USB4000 and the other two spectrometers. The USB2000 has a resolution of 2048 pixels/nm compared to the Maya2000 (2080 pixels/nm) and the USB4000 (3648 pixels/nm).

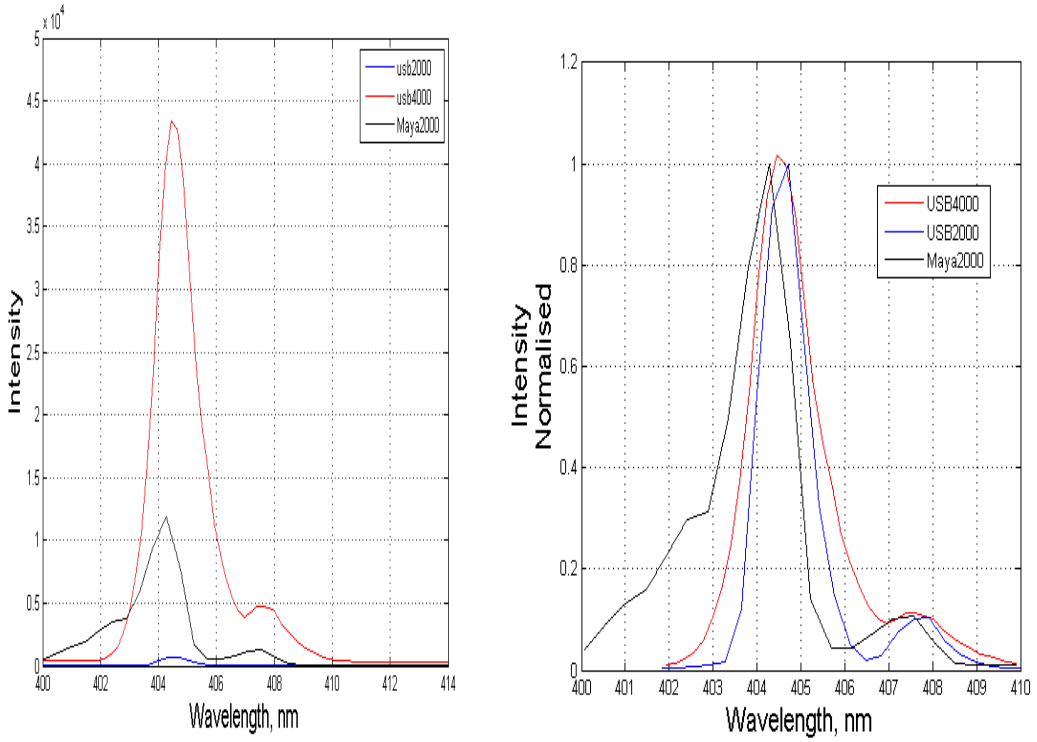

Figure 6.6 Hg peak detected by each spectrometer (left). The intensity on the y-axis is normalised (right) to illustrate the resolution of each peak. The Maya2000 has broadening (404 nm to ~ 400 nm) not present in the USB spectrometers.

The tungsten-halogen lamp is a broadband emission source used in the laboratory experiments had a central peak at 650 nm (see figure 6.7), unlike the calibration lamp which has numerous narrow peaks between 253 nm and 922 nm. The intensity of the source

is low between 400 nm and 500 nm but still proved adequate for the identification of NO_2 features when in absorption mode.

6.3 Laboratory tests using polypropylene bags

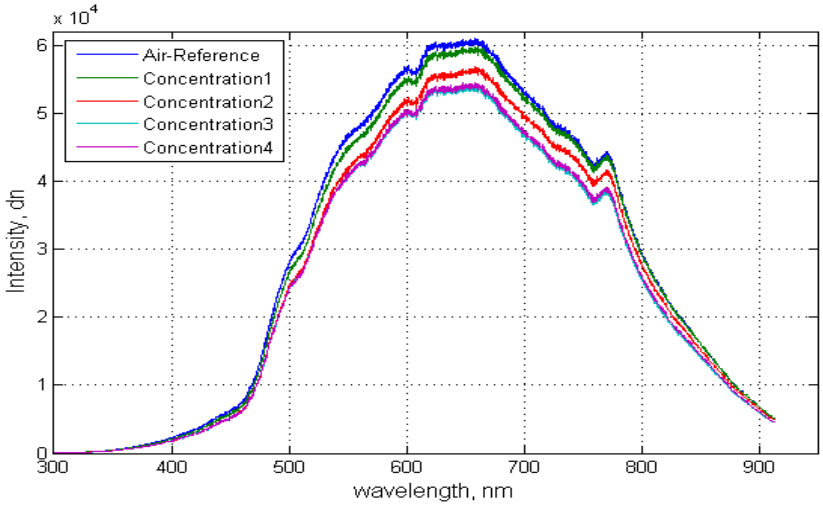

Figure 6.7 Spectral absorption data for four PP sample bags with different concentrations of NO_2 and one bag filled with air as a reference. The reference was used to determine the absorption spectra of the four sample bags, figure 6.10.

The first experiments were used to determine the correlation between the absorption of the light through each sample, then using the raw intensity measurements, the differential absorption for each of the samples. The first step performed to determine the absorption (A) of each bag involved recording the spectrum of an air-reference. The air-reference was then replaced firstly by the lowest concentration sample and then the other samples increasing in NO_2 concentration. Figure 6.8 shows how the reference spectrum and the increasing gas spectra compare in the intensity mode of the spectrometer note the NO_2

sample's intensity is lower than the reference. This is caused by the broad attenuation of the signal caused by the refraction through the denser gas sample. The effects of the broadband attenuation can be seen in figures 6.9 and 6.10 but only the narrow band features are of interest as they represent the absorption of the light by the NO_2 gas. The absorption spectrum for each sample is calculated using the Beer-Lambert law with the Matlab algorithm outlined in appendix II, where the wavelengths of the chosen feature are isolated and the related intensities are used to determine D (λ). In figure 6.8, a closer look is taken at how the air-reference and the higher NO_2 concentration (purple) in figure 6.7 compare. Any attenuation of the signal by the NO_2 at certain wavelengths is difficult to determine so the laboratory spectra were all carefully examined in the Scope mode of the SpectraSuite software first. Figure 6.9 shows the absorption spectra for 4 of the different concentrations with the NO_2 features clearly visible between 400 nm and 550 nm, where the dominant NO_2 absorption features are known to be present (see figure 6.9). Only four of the NO_2 spectra in figure 6.7 are used to develop the absorption spectra in figure 6.10 as two of the absorption spectra closely overlapped.

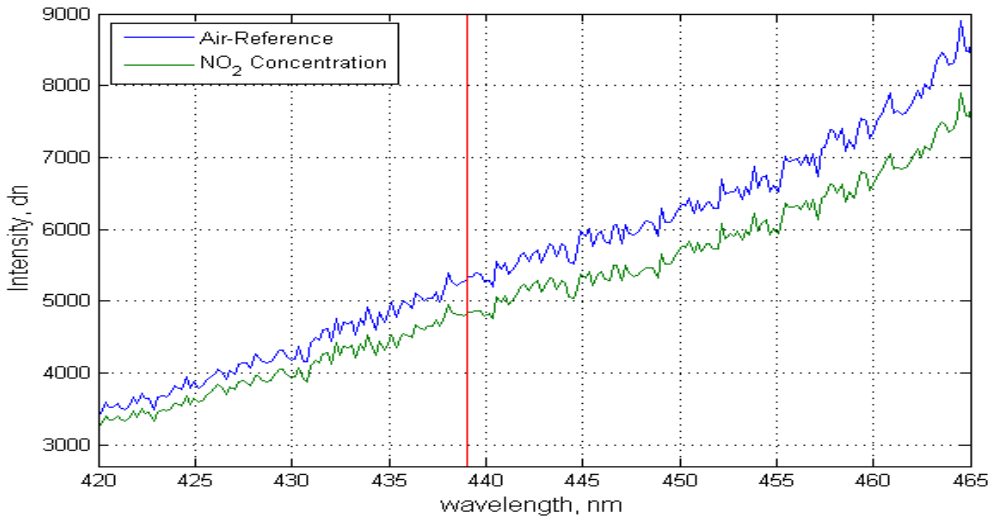

Figure 6.8 Close up image of the raw intensity of an air-reference and NO_2-Spectra. The red line indicates the location of the feature used to determine D for each sample. D was also determined for the air-reference to eliminate any error in the analysis.

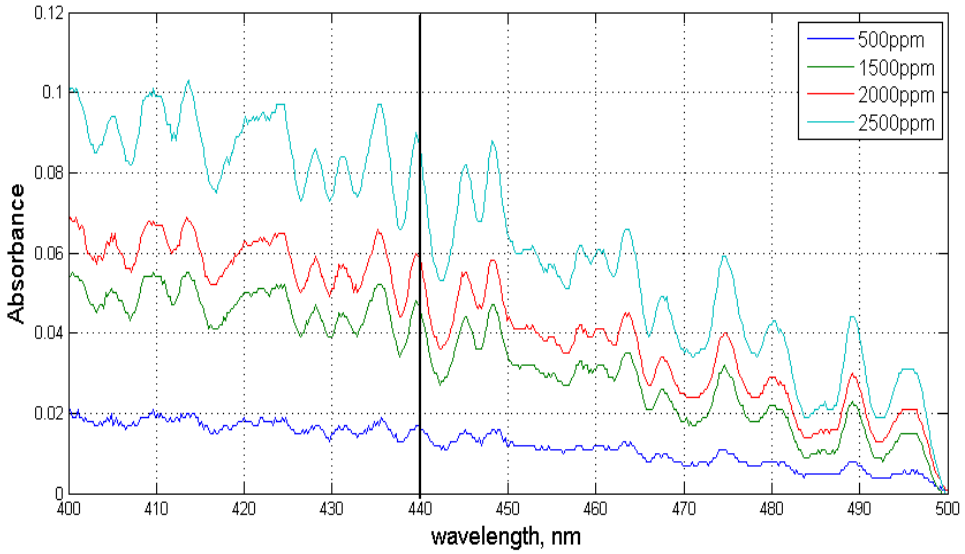

Figure 6.9 Absorption spectra for the four different bag samples shown in figure 6.7. The absorption feature at 440 nm was used to determine D. Each spectrum is normalised to 500 nm.

From each absorption spectrum, the concentration of each bag could be determined using the Beer-Lambert law (chapter 2). The concentrations were in the scale of 10^{-9} kg/m^3 but are presented here in figure 6.11, as μg/m^3 as they are the typical units used by the EPA. The absorption coefficient, α, determined using the USB4000 is shown in figure 6.10 alongside the absorption coefficient determined by Bogumil (2003, T=294 K). The units in the Bogumil data have been converted from cm^{2}molec^{-1} to m^{2}μg^{-1}.The spectra in figure 6.10 illustrate how well the two compare, even though the resolution of the instruments used are different. Bogumil et al. describe a double spectrometer with a 1024 pixel CCD and a resolution of 0.44 nm for 394 nm to 670 nm. In comparison, the USB4000 has a resolution of 0.18 nm and a 3648 pixel CCD.

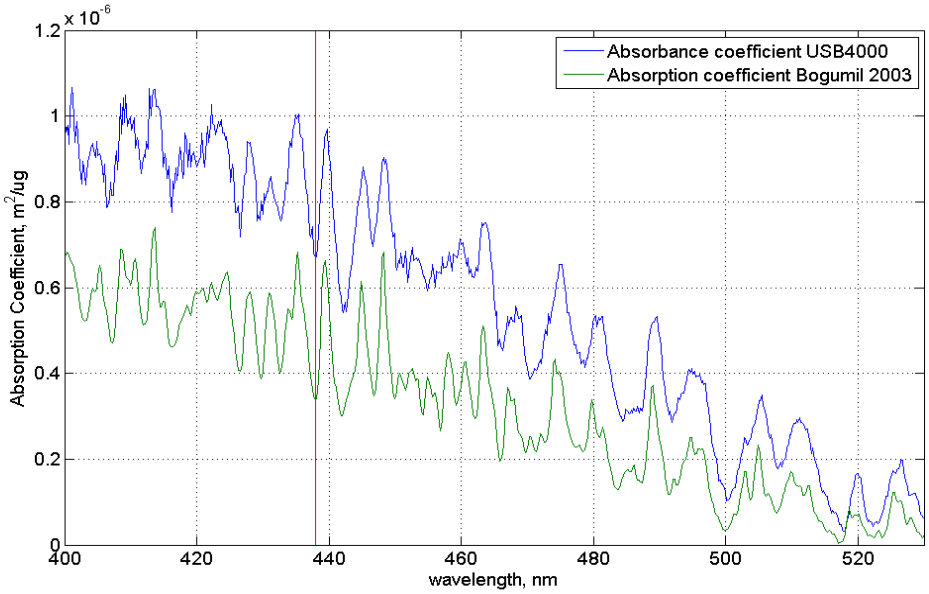

Figure 6.10 Absorption coefficient α (blue) for NO_2 determined using a USB4000 miniaturised spectrometer. A spectrum of the α obtained by Bogumil et al is shown for comparison[44].

The differential absorption (D) was determined for each individual spectrum using the wavelengths where the intensity was attenuated by the NO_2. The value of D from the air-reference sample was also calculated, and then compared to the value of D for each sample, to ensure that the air sample did not contain any NO_2,

In figure 6.11, the value of D for the air-reference sample is negative, as there is variation in the intensities of the chosen wavelengths. The values for A and D calculated for the higher concentration where determined using the two spectra shown in figure 6.8. The slope of the line in all the A versus D data can vary due to the choice of wavelengths and variation in noise. As a result some of the results show A with a higher slope, figure 6.11 and others where D has the higher values/slope, figure 6.14.

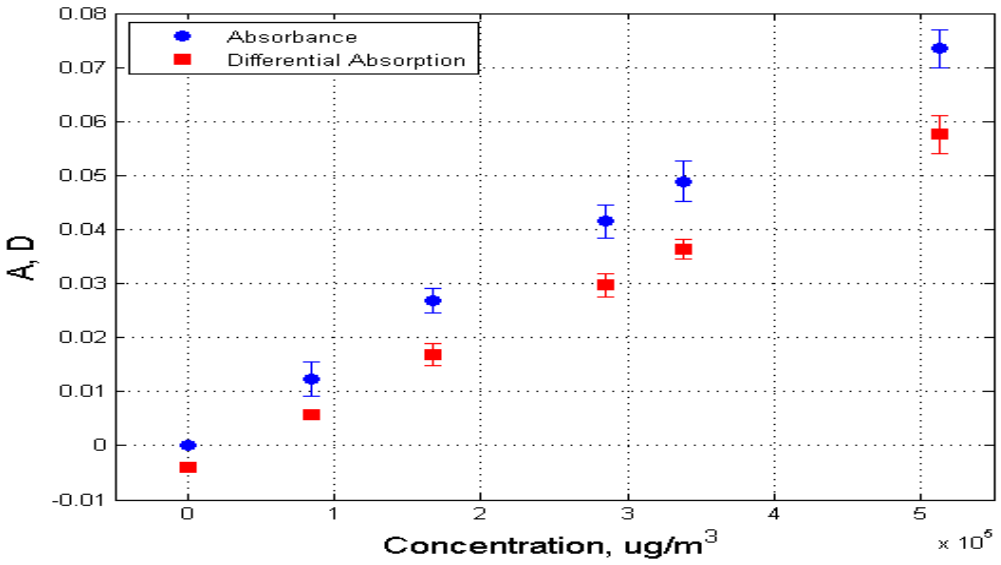

Figure 6.11 A and D, at 440 nm, determined from the intensity spectra in fig 6.8 and the results in fig 6.10. Note D is also shown for the air sample (zero concentration), this is only possible in the laboratory but its illustration here helps demonstrate the effectiveness of the algorithm.

The errorbars in figure 6.11 represent the standard deviation of the five bags tested. The measurements of each bag were taken within a two hour period, to reduce the magnitude of the error in each measurement. The results show a good correlation between D and A for each bag, but the concentration levels was much lower than those that were expected.

At first, the lower concentration was believed to be due to an error in the measurement, but comparison with laboratory CL measurements on diluted samples showed the bag concentration to be consistently lower than predicted. Table 6.1 shows the CL results on four PP bags filled with 2.5 ppm of NO_2. The measured concentration was approximately a third of what was expected.

Expected concentration, ppm	**Measured Concentration, ppm (after 2 hrs)**	**Percentage difference, %**
2.5	0.79	32
2.5	0.65	26
2.5	0.815	32.6
2.5	0.841	33.64

Table 6.1 Comparison of the expected NO_2 concentration and the measured concentration using a CL instrument in the laboratory

In figure 6.12, the results of tests on three bags which were filled from 17 L gas bottles containing NO, with the same concentration are shown. Each bag was tested five times each and the standard deviation error for each one is presented. These results show that the differences were substantial enough to be concerned about the estimated

concentrations in the bags making it difficult to accurately determine the absorption coefficient using the laboratory setup.

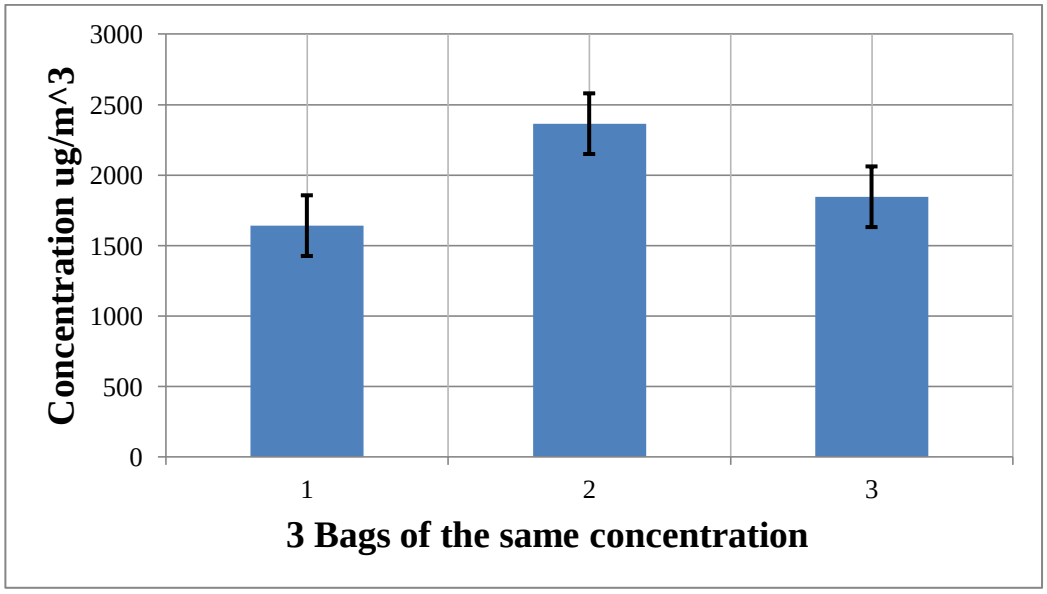

Figure 6.12 Comparison of 3 bags with approximately the same nominal concentration of (1900 µgm^{-3})

An old gas bottle of NO was compared to a new lecture bottle that was being used for the DOAS experiments. This was to determine if the bottle was releasing enough NO and if the filling procedure was different for two different bags when the same concentration was added. The result of these experiments showed that the bag filled using the old bottle, when checked by CL after two hours, had a concentration of 0.841 ppm and the bag filled by the new bottle was 0.815 ppm. These results are close enough statistically, allowing for an error in the determination of c, that the bag contents appeared to be filled with almost exactly the same amount from two different bottles.

There was a 2 hour mixing time after the bag was filled to allow the NO to fully mix with the air in each bag. Figures 6.13 and 6.14 illustrate the differences in a bag's absorption for different parts of the bag (using the USB2000 spectrometer) and the change in A and D over time for one bag respectively. In figure 6.14, the absorption is the same throughout the bag, which shows that there is a uniform distribution of NO_2 in the sample. Therefore, the positioning of the bag in the laboratory setup is not a factor in the lower concentrations determined by the analysis. In 6.14 the concentration is seen to be reduced by ~14% after five hours. Because of this, new samples needed to be prepared after every two days.

The mixing of the NO and air to produce NO_2 reaches a maximum after approximately 2 hours, so all the measurements performed with the bags were taken within this time frame. After 2 hours, the NO_2 concentration appears to decrease as the gas converts back to NO. Some of the gas also appears to form a deposit on the side of the bags and the NO_2 also breaks down when exposed to light, as described in chapter 1 (section 1.6).

The PP bag samples were eventually determined to be unsuitable for accurate calibration of the instrument, because of the unstable gas formation and the gradual decrease in concentrations. Another major disadvantage of the bag samples was that the high concentrations were not comparable to typical atmospheric NO_2 concentrations. However, the tests with the bags showed that determination of NO_2 concentration was possible and that the values for D correlated with the corresponding values for A essentially proving the principle of the laboratory tests.

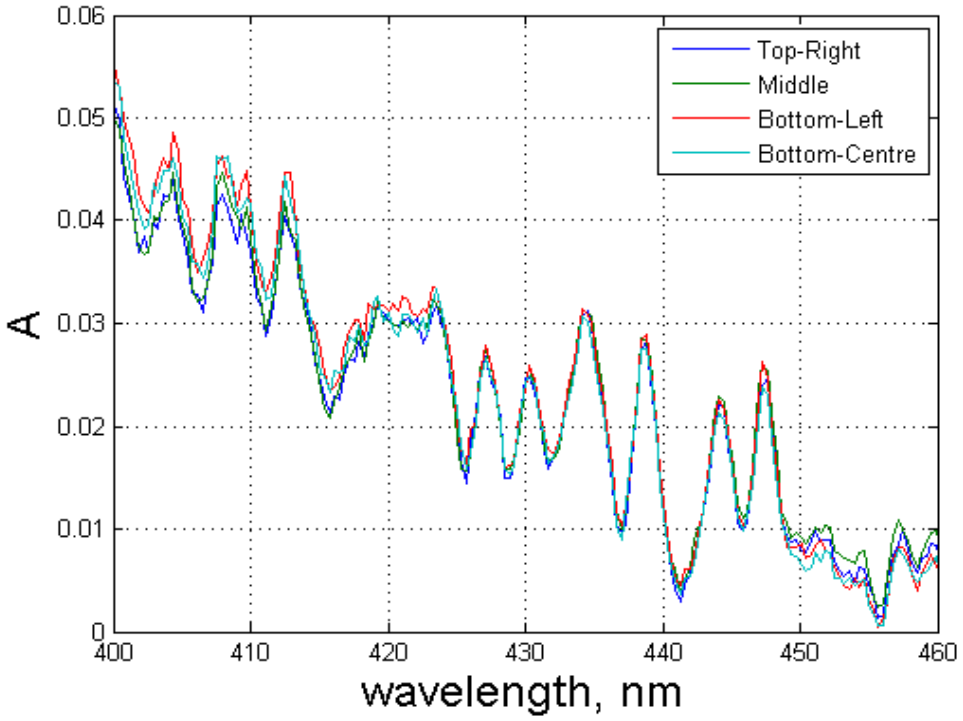

Figure 6.13 Variation in A for different parts of sample bag the results show that the NO_2 has a uniform concentration throughout the bag after it is mixed.

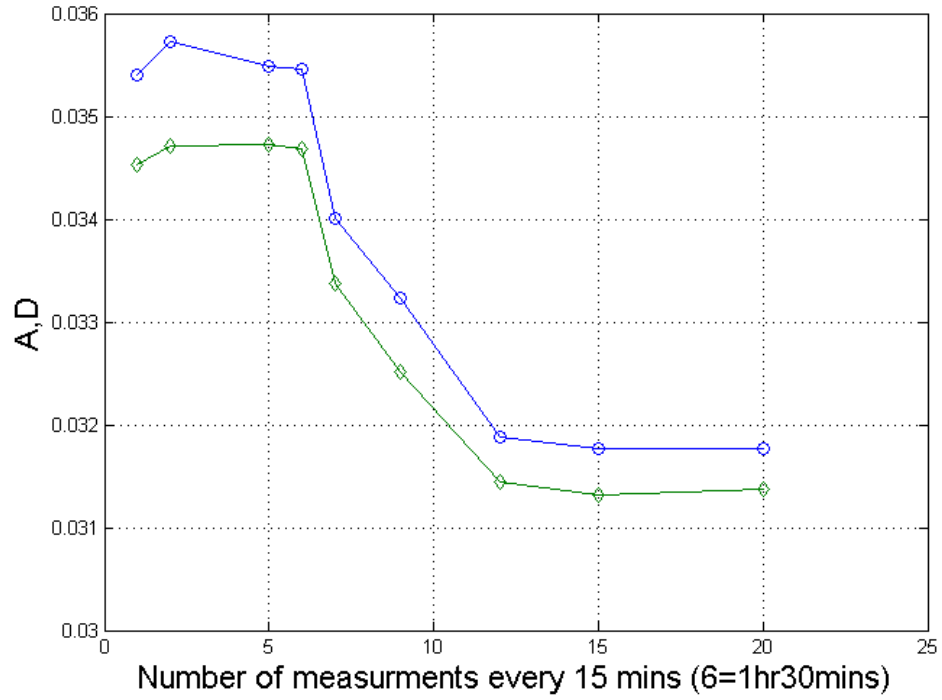

Figure 6.14 Decrease in D (blue) and A (green), (440 nm) after 5 hours for one bag sample of NO_2. The correlation between D and A remains but the concentration is reduced by ~ 14%

6.4 Laboratory tests with calibration cells

Custom made calibration cells were sourced from Resonance Ltd. (Canada). The concentrations for each one are listed in table 6.2, chapter 4, an air-reference, 5ppm-m, 20ppm-m and 50ppm-m concentrations, equivalent to 10 μgm^{-3}, 40 μgm^{-3} and 100 μgm^{-3} in a 1 km pathlength respectively (±10%).

	Cell concentration. Equivalent for 1m path length	10km path length	Concentration error %
1	Atmospheric air	0 ppb	0
2	5ppm-m	0.5ppb	±10
3	20ppm-m	2ppb	±10
4	50ppm-m	5ppb	±10

Table 6.2 (reproduced table 4.2) Concentrations of calibration cells for 1m in the laboratory (in ppm) and a 10km pathlength (in ppb) equivalent to those that can be measured in the atmosphere

The bench top setup was rearranged to accommodate the cells. This included an adjustable clamp to lightly hold each one by its stem for each measurement. Figure 6.15 shows the new setup with the lenses and optical fibres aligned on either side.

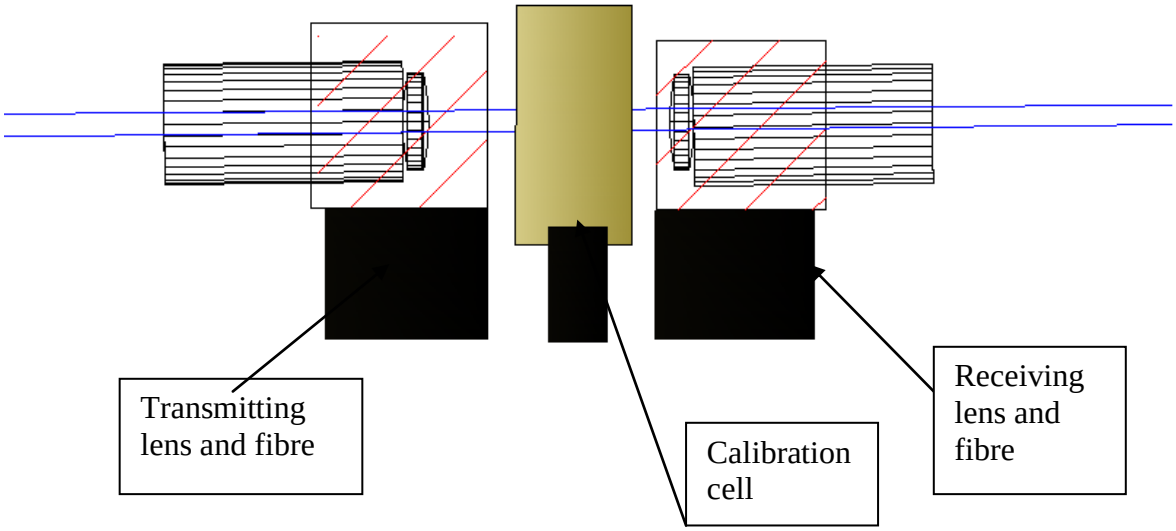

Figure 6.15 Calibration cell between source (transmitting lens and fibre) and detector (receiving lens and fibre) on the optical bench. The cells small size and stem allows precise alignment for each test.

The atmospheric air cell was used as a reference to determine the absorption of each NO_2 cell sample and this data was examined for correlation with the differential absorption for the other cells. The cell absorption results made it possible to accurately determine the concentration and the results were within a small percentage of the concentrations specified by the supplier. Figure 6.16 illustrates the absorption of each cell. The spectra data are normalised by subtraction to zero absorption at 499 nm where there are no absorption features. Note, the absorption features of NO_2 are visibly present in the measurement of the cell with the lowest concentration 5 ppm in 1 m.

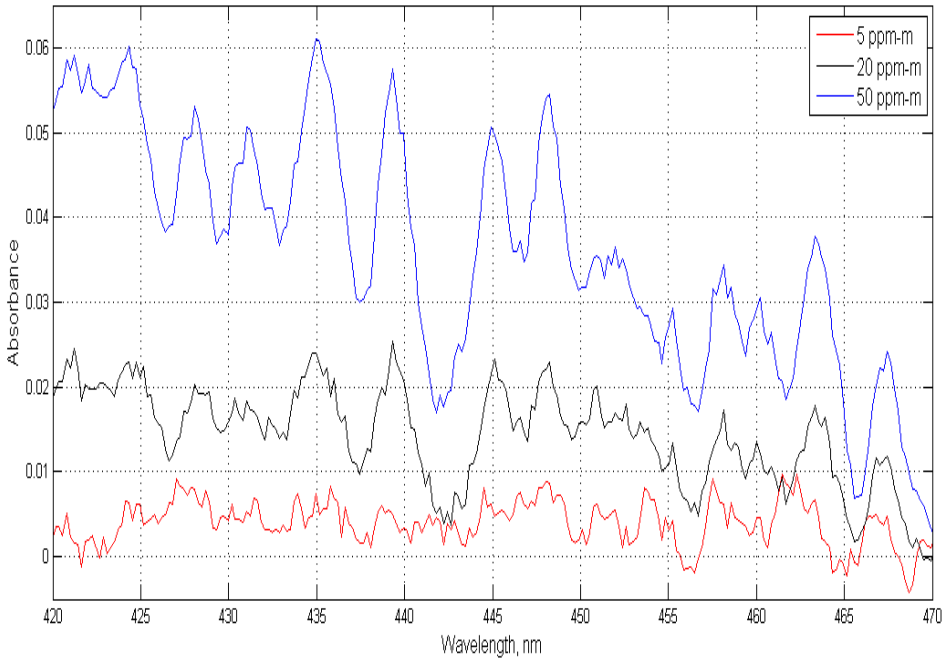

Figure 6.16 Absorption of each calibration cell using the USB4000 spectrometer Note the increase in size of the absorption features for increasing concentration.

This lowest concentration is equivalent to 1 μgm^{-3} in 1 km which provides an excellent example of what the LOD of the novel instrument is, these results were determined using the USB4000 spectrometer.

6.5 Comparison of each spectrometer for determination of differential absorption

Comparisons of each spectrometer are possible with the calibration cells because the concentrations are known. The USB2000 Ocean Optics spectrometer was used for the first set of laboratory tests. Figure 6.17 illustrates the result of tests on the three cells. The

results show a good correlation between A and D with each cell. Calculations using these A values to determine the concentrations resulted in values close to the concentrations provided by the manufacturer. It was found that the correlation of A and D could be affected by the wavelengths chosen in the analysis and the spectrometer being used for the tests. The air-reference sample cell was used to determine D without NO_2 and the result suggest a low value for absorption but this appears to be within the margin of error for each measurement.

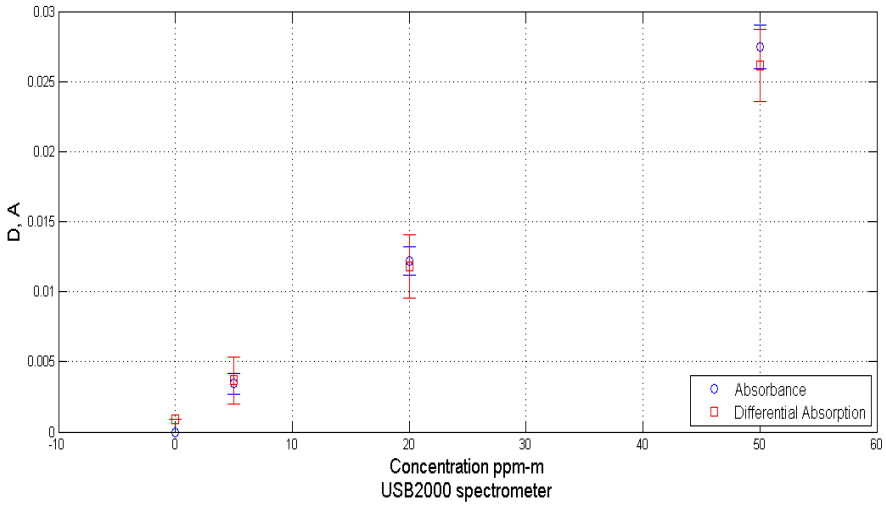

Figure 6.17 Results of A and D at 440 nm determined from USB2000 spectrometer results for each cell sample. There is a good correlation between the two sets of results but D has larger error bars than those for A.

The Maya spectrometer was initially chosen because it had much better low light level results than the USB2000, which would make it ideal for twilight measurements in the field, but the concentration results were always below what was predicted, as shown in figure 6.18. The results of the concentrations determined using both the Maya2000 and the USB4000 are shown in table 6.3. The expected values for each cell are also shown for

comparison. There was also an offset in the measurement of the wavelengths of each peak of the calibration lamp. This was likely an effect of the etalon features described in chapter 4 that are caused by the Maya's Back Illuminated CCD structure. This offset could be corrected in the analysis once the magnitude of the wavelength difference was found using the calibration lamp. The results show how much lower the Maya2000 concentrations were compared to the expected results and the USB4000. The results for the absorption determined using the USB4000 were also slightly less than those predicted, so the experiment was repeated for 10 sample tests (figures 6.22 to 6.23) and compared to D for each test.

USB4000, μgm^{-3}	**Maya2000, μgm^{-3}**	**Expected results, μgm^{-3}**
0	0	0
2.75×10^5	1.75×10^5	6.5×10^5
2.2×10^6	4×10^5	2.6×10^6
4.75×10^6	1.22×10^5	6.5×10^6

Table 6.3 Results of cell tests for the USB4000 and the Maya2000

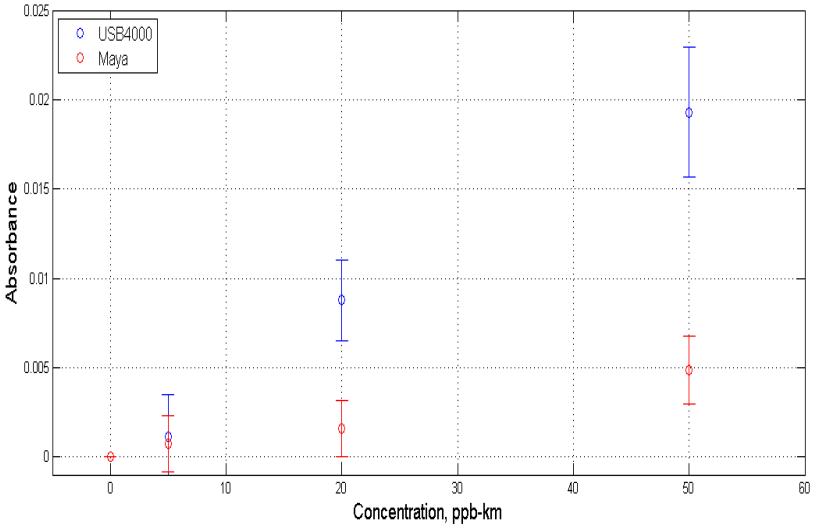

Figure 6.18 Absorption at 440 nm for each cell using the Maya2000 (red) compared to the USB4000 (blue). The Maya2000 results shown are below the results from the USB4000 and USB2000 this is likely caused by the BI-CCD of the Maya2000.

The USB4000 was ultimately chosen to perform the field measurements because of its larger resolution. The Maya2000 spectrometer made it easier to identify the attenuation features but greater accuracy was obtained with the USB spectrometers. The LOD of the USB4000 was examined using the cells by determining $A(\lambda)$ and $D(\lambda)$ at low light. To test this, an experiment was designed to measure the intensity (digital number, dn) of light passing through the reference cell and one NO_2 cell with a variable NDF (figure 6.19), decreasing the percentage of the intensity in fixed steps.

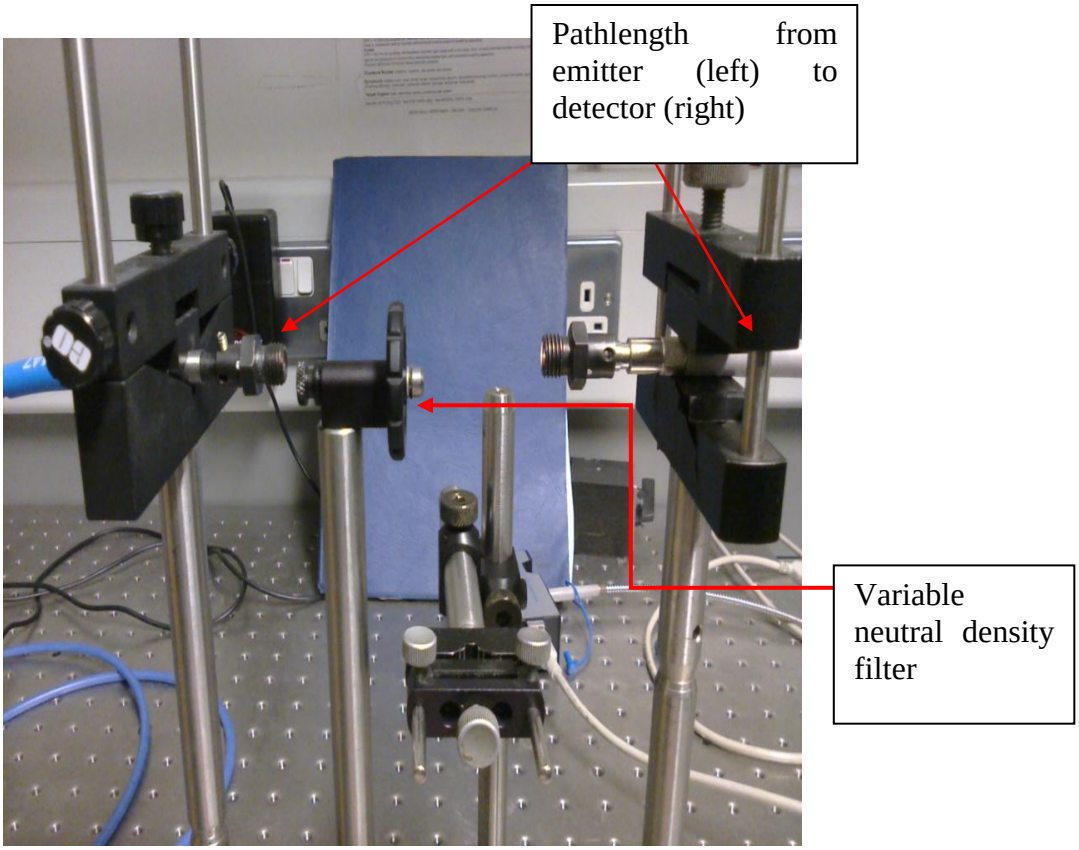

Figure 6.19 Alignment of the apparatus with a variable neutral density filter

Figure 6.20 shows the change in absorption at 440 nm on the left as the percentage of a maximum signal is reduced. On the left of figure 6.20, the absorption of light by a calibration cell only varies between 0.018 and 0.025 digital numbers but there is a much greater variation for the last two measurements which had the lowest signal intensity. As shown on the right hand side of figure 6.20, the signal at 440 nm is reduced to about 1.4% of the strength when the overall signal is at a maximum in the first measurement.

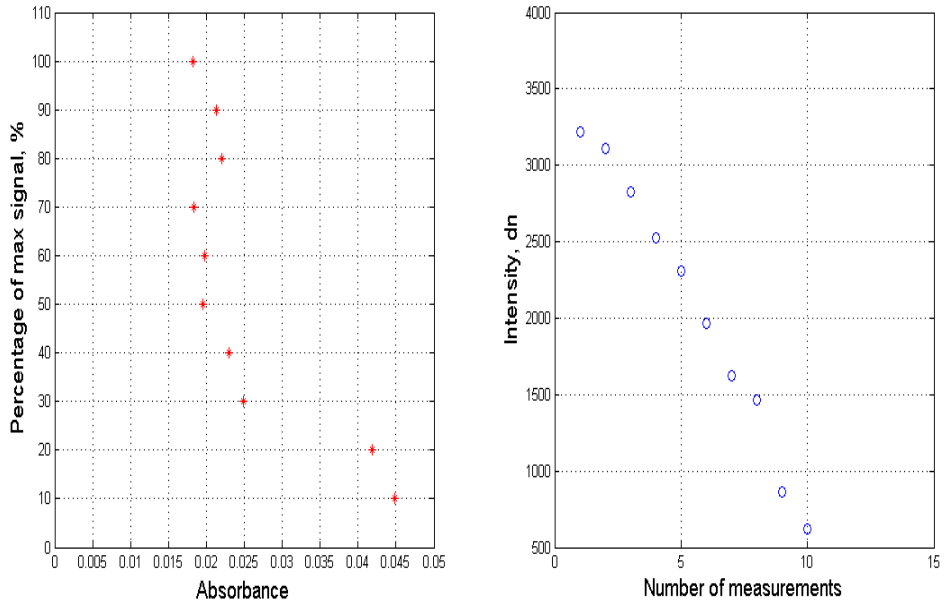

Figure 6.20 Change in A (440 nm) compared to the percentage of the maximum signal (left image) as the intensity (right image) is decreased by the NDF. The absorption (red) has a maximum variation when the max % is below 20%. The signal to noise at this low intensity is very low at the 440 nm feature.

6.6 Absorption and differential absorption determined using the USB4000

The absorption of each cell at the same wavelength (440 nm) was compared to the differential absorption for the USB4000 and produced a good correlation between the two, (figure 6.21). The cell concentration could be determined with greater accuracy, as the manufacturer provides concentration values within a 10% error so the scale of the A**(λ)** and D**(λ)** values can be predicted. In figure 6.21, the absorption and DOAS are compared for

each cell. The results of both methods show an excellent correlation which demonstrates the accuracy of the Matlab algorithm developed for the analysis. The value for D at 0 ppb-km represents the error in the DOAS calculation applied to a reference measurement with no NO_2 present. The values for D are offset by 0.0015 to account for variations in the chosen wavelengths. The accuracy of the results is improved by increasing the number of measurements. In figure 6.21, the errorbars represent the standard deviation of n=10 measurements on each sample. The absorption without NO_2 is taken as 0 ppb-km and the lowest concentration is 5 ppb in one kilometre which is equivalent to 5 ppm in one metre. Table 6.4 shows the results of the concentrations calculated from the experimental results compared to the expected results for the concentrations prepared by the manufacturer of the cells. The percentage difference for each result is within the 10% error claimed by the manufacturer.

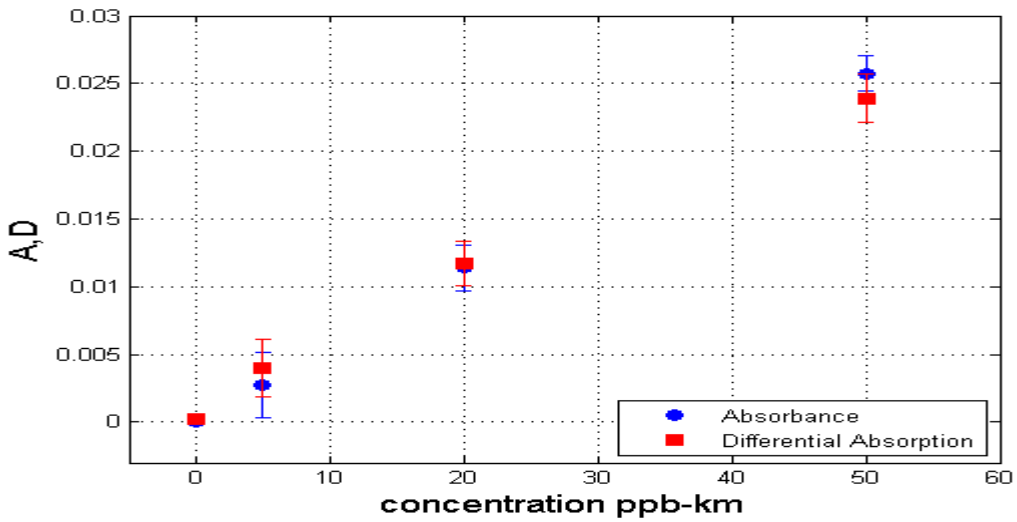

Figure 6.21 Correlation between A and D (440 nm) for each cell using the USB4000 spectrometer. These results demonstrate the effectiveness of the algorithm and the accuracy of the technique. DOAS data offset due to variation in chosen wavelengths.

USB4000, µgm^{-3}	Percentage difference between the two as a %	Expected results, µgm^{-3}
0	0	0
6.75 x 10^5	3.7	6.5 x 10^5
2.845 x 10^6	8.6	2.6 x 10^6
6.425 x 10^6	1.2	6.5 x 10^6

Table 6.4 Results of cell tests in µgm^{-3} for the USB4000 (N=10), the percentage differences are within the 10% parameter claimed by the manufacturer

Analysis of the results of D using the calibration cells is shown in figure 6.22 with a fitted line that shows how linear the data was. The slope of the line is 4.6x10^{-4} and the R^2 value for the mean is 0.9913 which indicates a strong correlation between the mean of each measurement of each cell when tested 10 times.

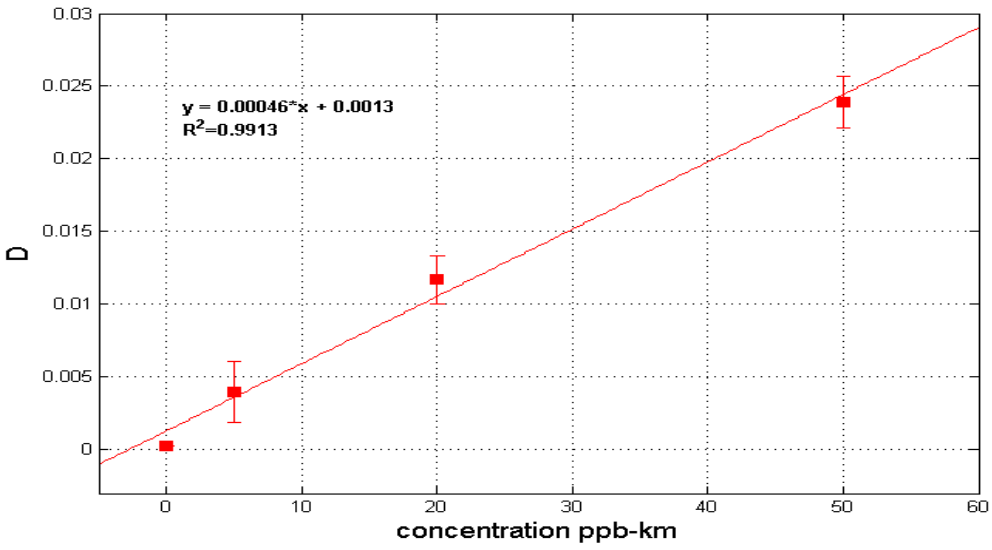

Figure 6.22 Cell concentration and D (440 nm) for n=10 tests on each cell. This shows the good repeatability of the measurements performed in the laboratory.

6.7 Initial measurements of the urban atmosphere to determine NO_2 concentration with the novel-DOAS

The apparatus used to monitor the atmospheric NO_2 concentrations was designed to measure a collimated beam of light using the small uv/vis lens attached to a collimating tube with an adjustable aperture to manually control the light entering the system, (see chapter 4 figure 4.10), as too much light directly received by the spectrometer would saturate the signal. The collimated design was necessary to ensure that the light was received from a single collimated beam and not from a wide beam that may include numerous reflections, and interfering sources. Figure 6.25 shows the design of the novel instrument that was attached to a rotational stage (below the collimating tube). The stage was then fixed to an adjustable camera stand which was ideal for ensuring the instrument stayed portable and controllable. The receiving optics can be directed to 180^0 in the vertical plane and 360^0 azimuthal. The setup shown in figure 6.25 is light, easy to use and portable. Attachments to increase the weight can easily be added in high winds and the whole system has a footprint of two square meters.

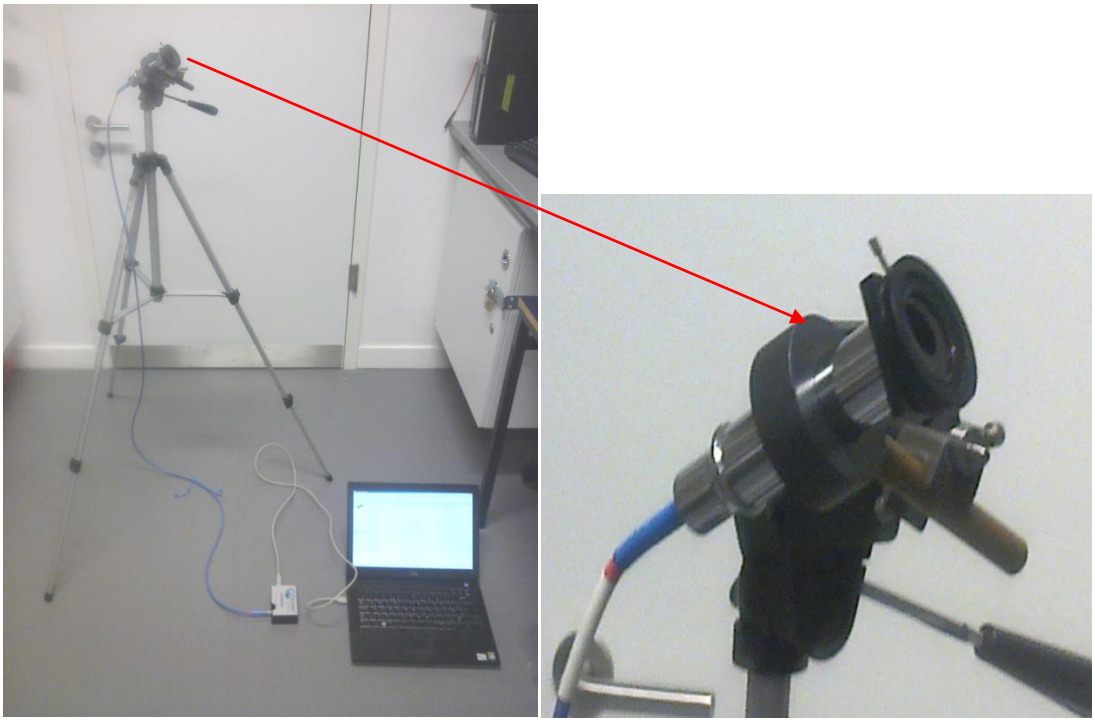

Figure 6.23 Novel-DOAS apparatus with camera stand. Close-up of collimating tube and 2m long optical fibre with mini-spectrometer and laptop

Initial tests of the spectrometer outside the laboratory were conducted in conjunction with the commercial DOAS apparatus on the roof of Kevin St. DIT. Figure 6.26(b) shows the smaller aperture fixed to the top of the commercial system's receiver with the aim of detecting the light emitted from the Cathal Brugha St. DIT source located 1.8 km to 2 km (see figure 6.26(a)) away, north of Kevin St. The emitter on the roof of Cathal Brugha St. was difficult to view from Kevin St. even with binoculars because of the Spire monument on O'Connell St., constructed after the emitter and detector were installed.

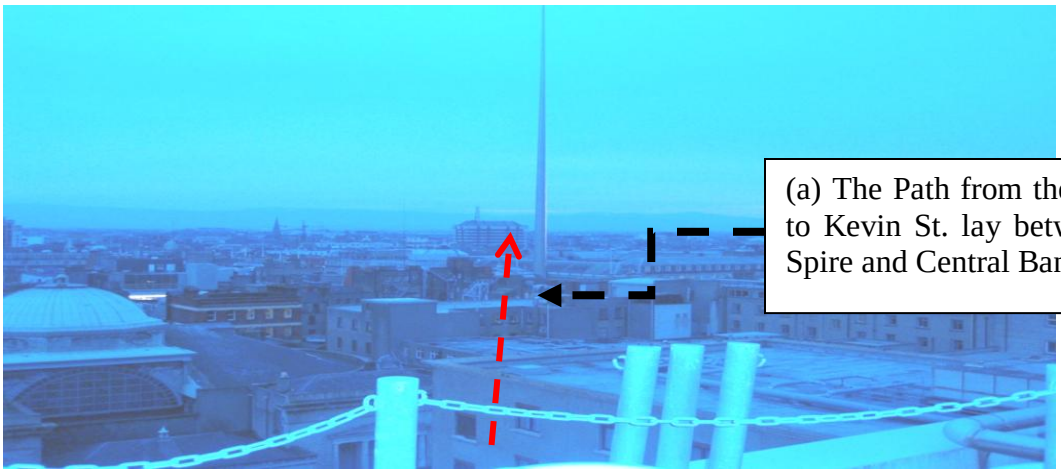

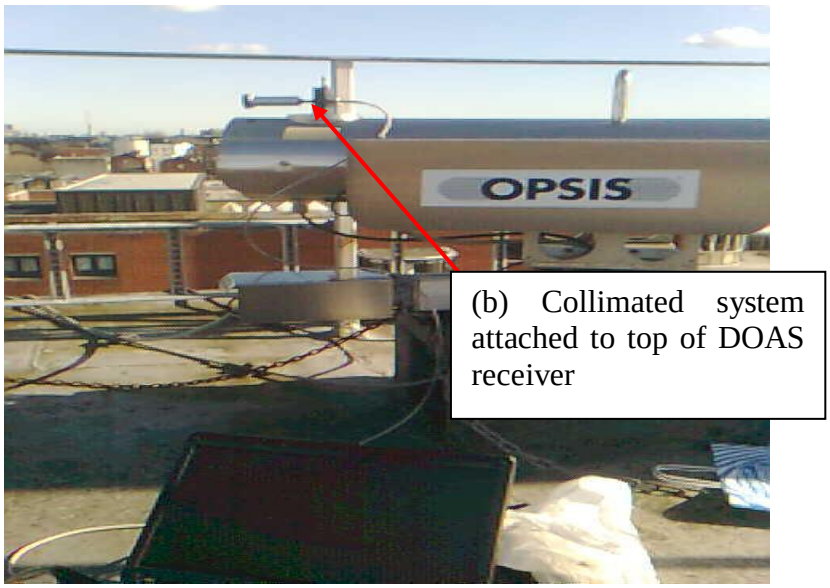

Figure 6.24(a) View from Cathal Brugha St. and (b) novel and commercial systems on Kevin St. roof. Note path in (a) passes between the Spire and Central Bank.

The spectrum of the Xenon lamp used by the OPSIS system, detected by a USB 2000 spectrometer, is shown in figure 6.27. The figure shows samples of two spectra over the 430 nm to 500 nm wavelength range. In commercial DOAS applications, the lamp and solar spectrum (blue) are divided by the lamp spectrum (red) and the result is a total absorption spectrum used to determine the NO_2 concentrations. As can be seen in the image, the spectrum of the 150 Watt lamp contains several distinctive peaks. However, at

460 nm, the small peak in the lamp spectrum (red) is difficult to observe in the lamp and solar spectrum (blue). For the Active DOAS analysis, this spectrum is divided into the measured spectrum of the light beam projected between the lamp and the spectrometer. For passive DOAS, only the solar spectrum is needed. An example of a solar spectrum recorded by the USB4000 is shown in figure 6.28, with an inset of wavelengths 340 to 460 nm.

Because the Cathal Brugha Street lamp had to traverse a pathlength of approximately 2 km to Kevin Street, the beam could not be detected by the USB spectrometer. Attempts were also made to detect the Xe lamp at night and low light levels and with varying integration times, but these were also unsuccessful.

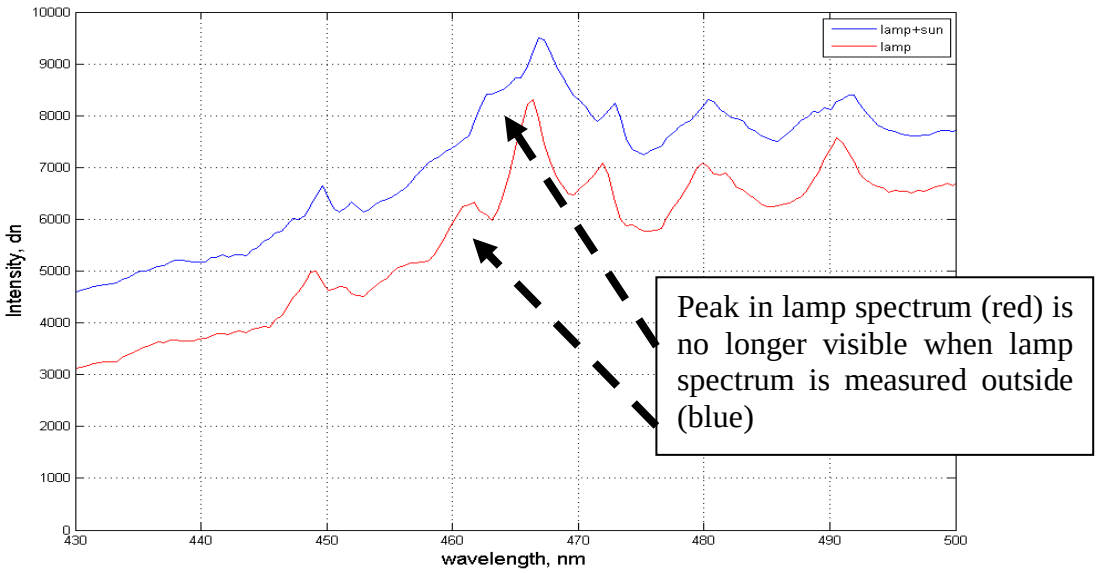

Figure 6.25 Spectra of Xe lamp (red) and lamp and Sun (blue) between 430 to 500 nm obtained from Cathal Brugha Street.

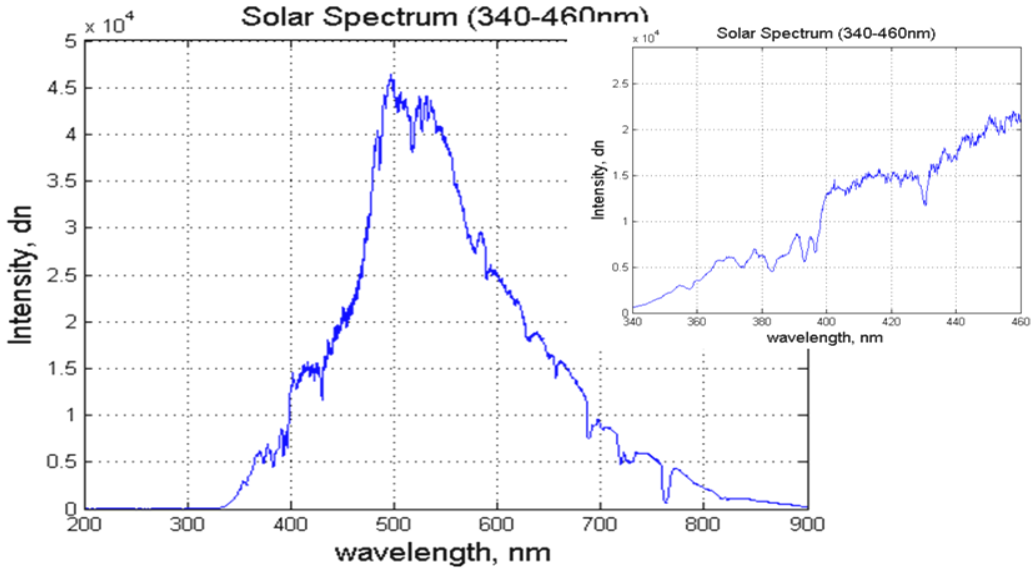

Figure 6.26 Solar spectrum with inset of 340 to 460 nm features recorded using the USB4000 spectrometer

Recommissioning the commercial system to measure NO_2 over a fixed pathlength proved to be beyond the capability of the project funding. The system required new software, calibration and possibly new components. The location of the monitor was not ideal and removing it would also involve the relocation of the datalogger and controller unit. An EPA CL monitor was used as an alternative system for comparisons of the NO_2 measurements made by the portable instrumentation, see chapter 5 for more detail. The nearest EPA monitor to Kevin Street was on Wynnefield Rd. in Rathmines, south of Dublin city centre. Figure 6.29 shows the monitoring site at Wynnefield Rd. at the top of an old public toilet building.

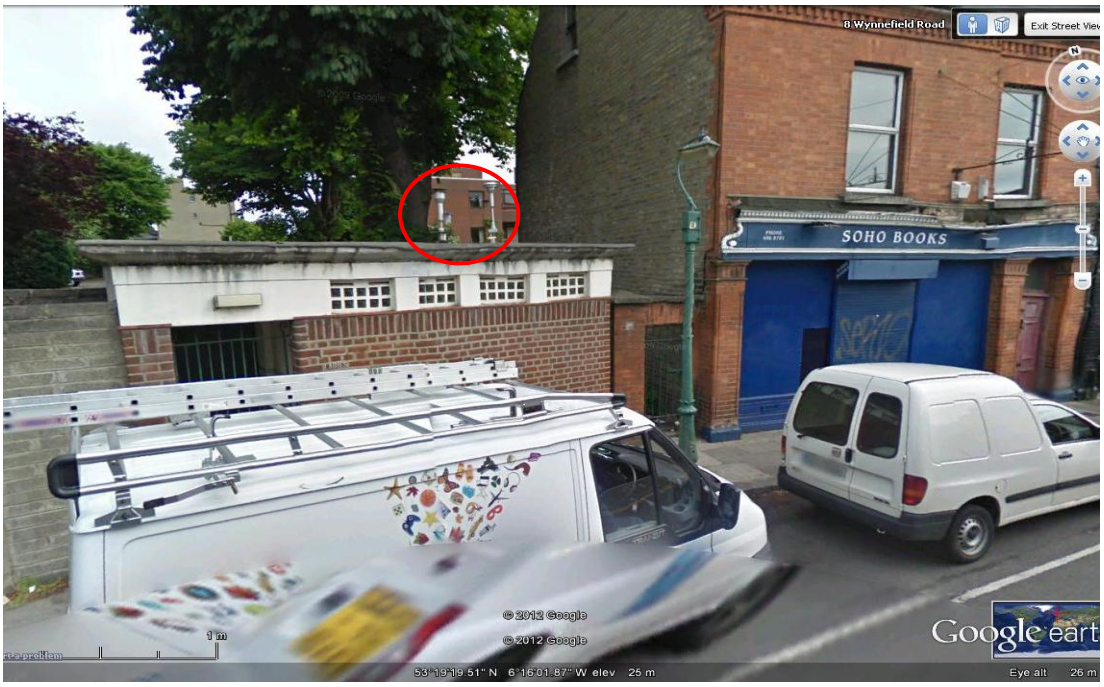

Figure 6.27 Location of EPA monitor in Rathmines. The red circle highlights the inlet tubes for the monitors.

6.8 Calibration of the *in-situ* novel-DOAS instrument with calibration cells

Early tests to calibrate the system involved placing bags containing different concentrations in front of the instrument which proved to be difficult largely due to the refraction of the light in each bag and the size of the bags compared to the instrument. The results of this test are shown in figure 6.30. The value for the concentration is larger with the NO_2-bags than with the no bag measurement, but there was very little difference between the bag containing only air and those with NO_2.

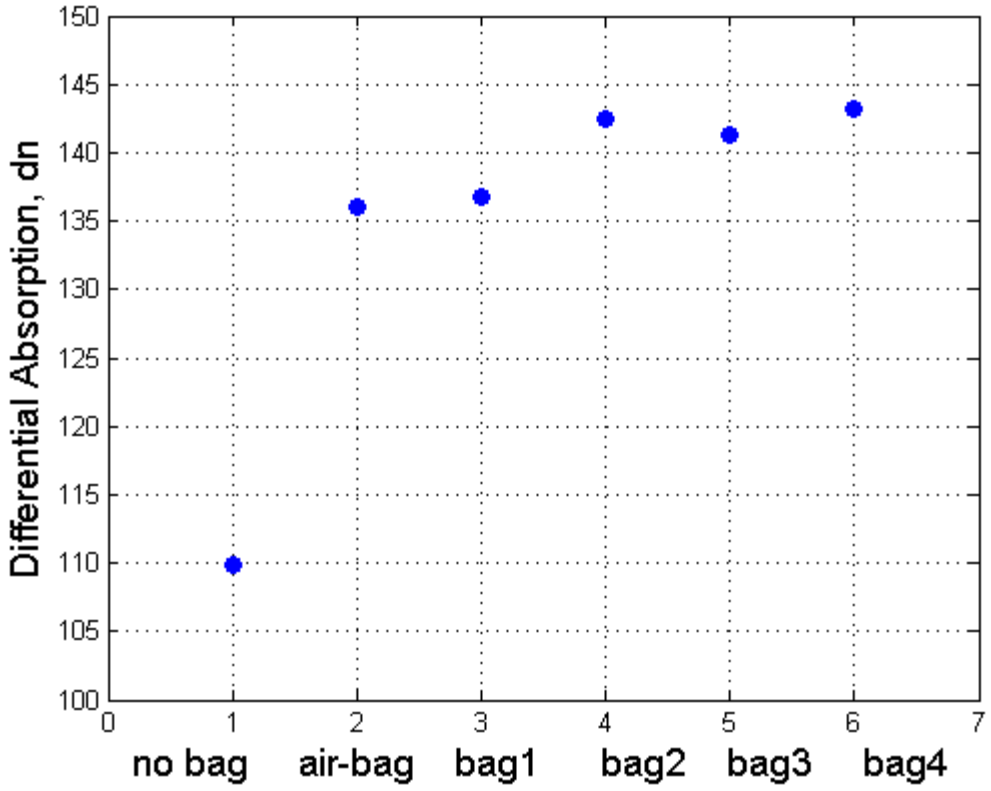

Figure 6.28 Variation of concentration when PP bags are placed in front of the detector. The first point on the graph represents the concentration without a bag.

The calibration cells were also used to test the accuracy of the algorithm used, to calculate D and the concentration of NO_2. Each calibration cell was placed in front of the aperture. It was expected that the value determined for D would increase as the cells with higher concentration were placed into the pathlength. The first cell has atmospheric air content, and could possibly show some variation compared to a D recorded without a cell present, but this measurement eliminates any error caused by light scattering in the cell. The variation expected would most likely be due to reflections from the quartz structure of the cell. The order of the cells in front of the collimator was 5 ppm-m, 20 ppm-m and 50

ppm-m. Figure 6.31 shows the results of this test and the change in D value for each atmosphere+cell measurement. On the x-axis, the numbers 1-5 represent the atmosphere, atmospheric cell and each cell concentration of NO_2 respectively. The results were recorded five times each to gain an average and standard deviation this would account for any subtle variations in the pathlength due to light scattering etc. The results confirm the aim of the research that the wavelengths and the NO_2 absorption feature at 440 nm can accurately identify changes in the NO_2 concentration within the instruments optical pathlength for an average integration time of 5 s.

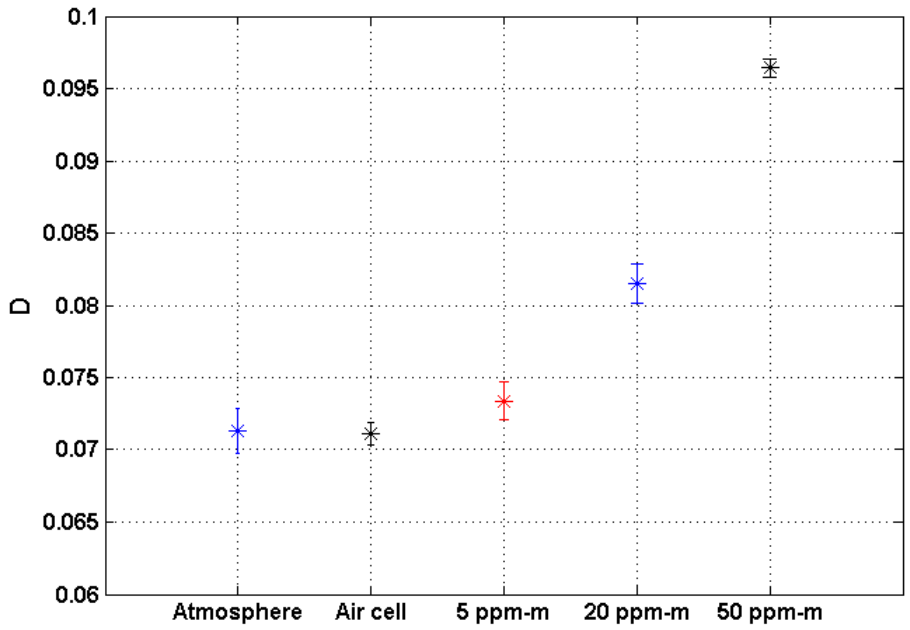

Figure 6.29 Increasing D for 5 measurements (1) no-cell, (2) air-cell and each calibration cell (3-5) containing NO_2 with ambient sunlight as a source. The results show that the increase in concentration from each subsequent sample results in an increase in absorption relative to the difference in concentration.

If the value for D in figure 6.31 for the Sun-no cell and atmospheric–air cell are taken as 0 the increase of approximately 0.003 for the next sample represents the 5 ppm/m cell. The next sample (20 ppm/m) should be 4 times greater at ~0.012 and the last cell (50 ppm/m) 10 times greater at ~0.03. The results show that the actual absorption increases is as much as ~0.011 and ~0.025 respectively, indicating that the increase in D can be attributed to the increasing sample concentrations place in front of the detector.

Figure 6.32 illustrates how D varies throughout the day when each cell is placed in front of the collimator. The broken blue line represents the changing atmosphere without a cell present, so the variation should represent atmospheric $NO_{2,}$ and the broken red line represents the atmospheric air cell. There is very little difference between the two as in figure 6.31 which suggests that the cell itself has very little effect on the DOAS calculation. In figure 6.32, seven measurements were taken using each cell every hour between 11am and 5pm. The green line in figure 6.32 represents the 5 ppm-m concentration, which is equivalent to 10 μgm^{-3} /1km which is near the values of the atmospheric air measurements. This implies that this cell concentration provides a relatively low increase to the atmospheric NO_2. The red and black lines indicate the changing D for the 20 ppm-m and 50 ppm-m cells which are equivalent to concentrations of 40 μgm^{-3} and 100 μgm^{-3} in 1 km respectively. The measurements were taken during daylight hours 11 am to 5 pm, the overall variation for each cell clearly shows that the DOAS method can detect variations of NO_2 throughout the day under clear sky conditions. Although the results for the low concentration cell also demonstrate that very small variations in the atmospheric NO_2 may be difficult to distinguish using the DOAS method on overcast days.

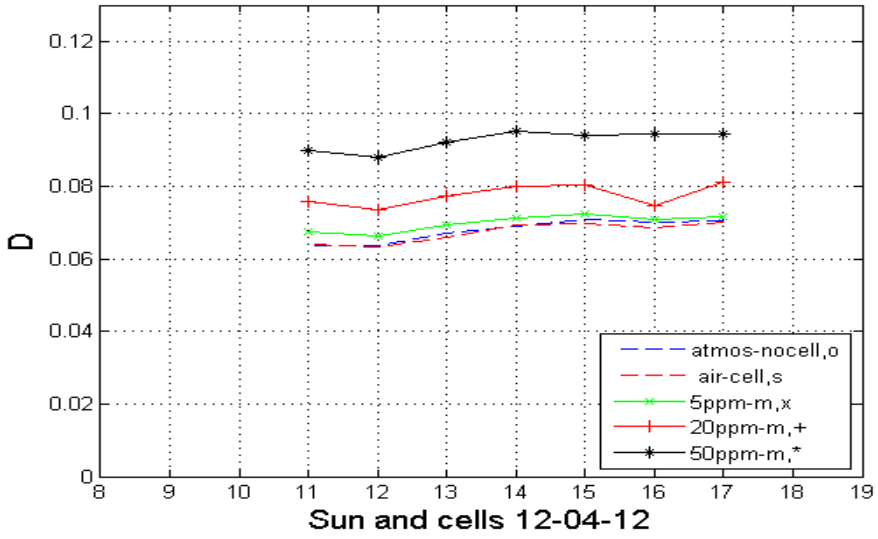

Figure 6.30 Diurnal variation of D for the atmosphere (blue) and each cell over a period of 6 hours. Note each NO_2 cell has a consistently higher D than the no-cell and air-cell data.

6.9 Measurements of NO_2 in urban environments and comparison to EPA-CL data

Initial attempts using the novel-DOAS setup were made from the roof top of the DIT-FOCAS building. Concentrations of NO_2 recorded by the EPA were then obtained at the end of the summer in 2010. Further data was collected using the USB4000 for the summer of 2011 and compared to the corresponding EPA data for the same dates and times. As the EPA data is recorded using a CL instrument, discrepancies between the two sets of data obtained are expected but it is hoped that an average discernible concentration for NO_2 may be found for a reasonable comparison of the two technologies (see section 5.3). The

factors affecting a good comparison include the measurement approach of each method, the CL monitor is placed in-situ, with the inlet tube located ~ 2 metres above the ground, whereas the DOAS instrument records spectra from the roof of the FOCAS building or from the second floor laboratory. The zenith measurements were taken from the streets near the CL monitor's location. Meteorological conditions can also affect the novel-DOAS measurements as cloudy days cause more scattering of the Sunlight as it passes through the atmosphere, which causes large variations in the optical pathlength [70, 111]. As explained in chapter 5 the transportation of NO_2 gas in the atmosphere can result in a more dynamic NO_2 variation than that expected from NO_2 photolysis and traffic congestion levels [111](section 5.5).

The DOAS data could be recorded automatically for several days. However, only the daylight hours were used for analysis and comparison as the signal at low light levels was too low to perform the DOAS calculation on without errors. The earliest results showed large variations in the D when 435 nm was used as the central wavelength for the DOAS calculations. This feature was close to a prominent Fraunhofer feature, so the smaller feature near 440 nm was used instead.

Each spectrum was dark subtracted and normalised for analysis. Figure 6.33 shows a comparison between the absorption determined using a horizontal measurement and a zenith reference (blue) and spectrum of the absorption cross section determined by Bogumil (green, 2003) corrected by 2×10^{17}. The determination of the absorption using this method was used by Morales and Walsh (with an S2000 spectrometer) in their paper, which was the foundation behind this work[5].

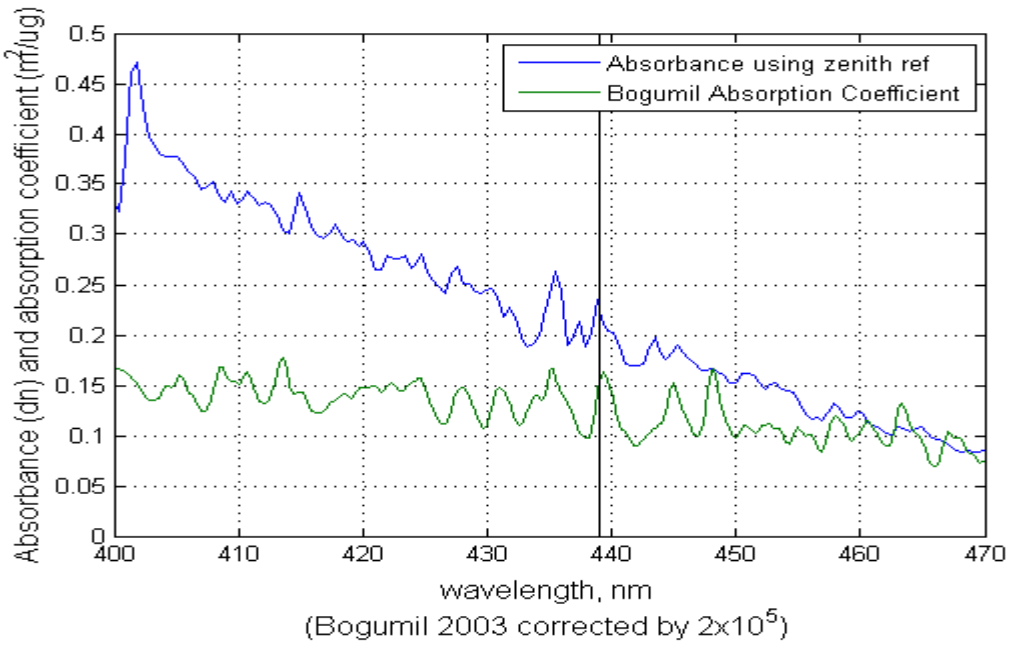

Figure 6.31 Absorption of Sunlight with zenith reference measurement and α (x $2x10^5$) determined by Bogumil_2003. Although there are NO_2 absorption features visible (at 440 nm) in the zenith reference measurement (blue), this zenith spectrum will still contain traces of atmospheric NO_2.

6.9.1 Correlation of novel-DOAS determined concentrations with EPA data

The concentration of the DOAS measurements were determined by estimation of the pathlength (L~ 10 km) based on the estimates of the height of the pollution boundary layer and the viewing geometry of the spectrometer and collimator. Additional estimates were made from the similarities between D to the pattern of the EPA data. The diurnal variation of NO_2 in most of the field results is comparable to the SCD variation described in section 2.9.3. Overall the results show some correlation between the two sets of data for

clear bright days. However there is data shown here where the correlation was weak most likely due to topographical and meteorological variations in the local atmosphere, but it is possible to make comparisons as shown in figure 5.4. In figure 6.34, the rise in NO_2 concentration at the beginning of the day and later (after 4 pm) is characteristic of the diurnal variation of NO_2 due to rush hour traffic congestion. In the example of the results comparing the DOAS measurement and EPA data shown, the concentrations are still relatively low with the maximum concentration determined by the EPA being slightly higher than 4 ppb, which is equivalent to ~7.52 μgm^{-3}.

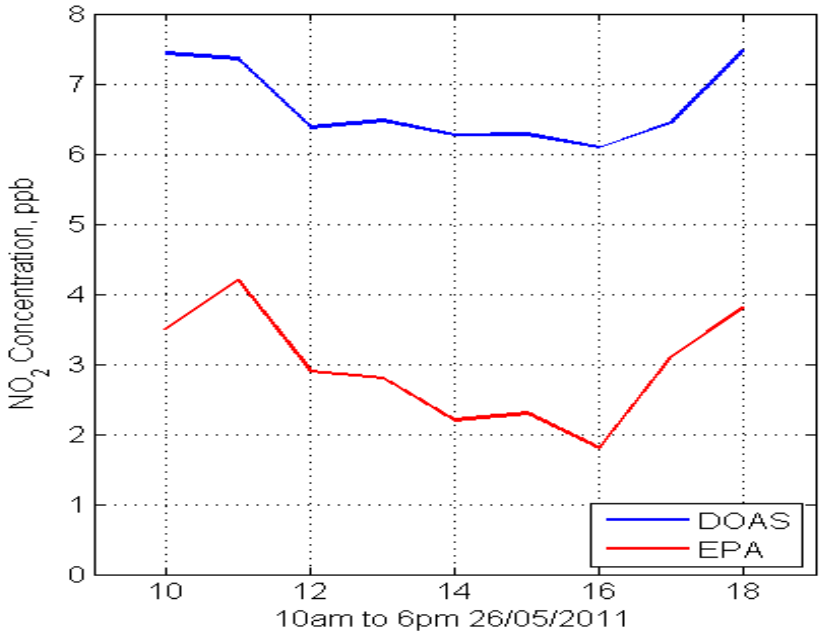

Figure 6.32 Variation of the concentration for NO_2 in ppb for 26/05/11 (L~10 km)

Initial measurements of the D of scattered sunlight at 435 nm and 440 nm were performed using the USB2000 spectrometer with a 600 µm fibre-optic. The concentration of NO_2 was then determined from the results and estimates of the pathlength based on the viewing geometry, see chapter 3. Measurements were made to determine the variation of D

for different elevation angles of the front end optics. Figure 6.35 illustrates the variation of D with changing angle θ. The angle 0^0 represents the zenith view and 90^0 the horizon. The gradual increase in D suggests more absorption of the sunlight in the lower troposphere compared to the upper troposphere and lower stratosphere.

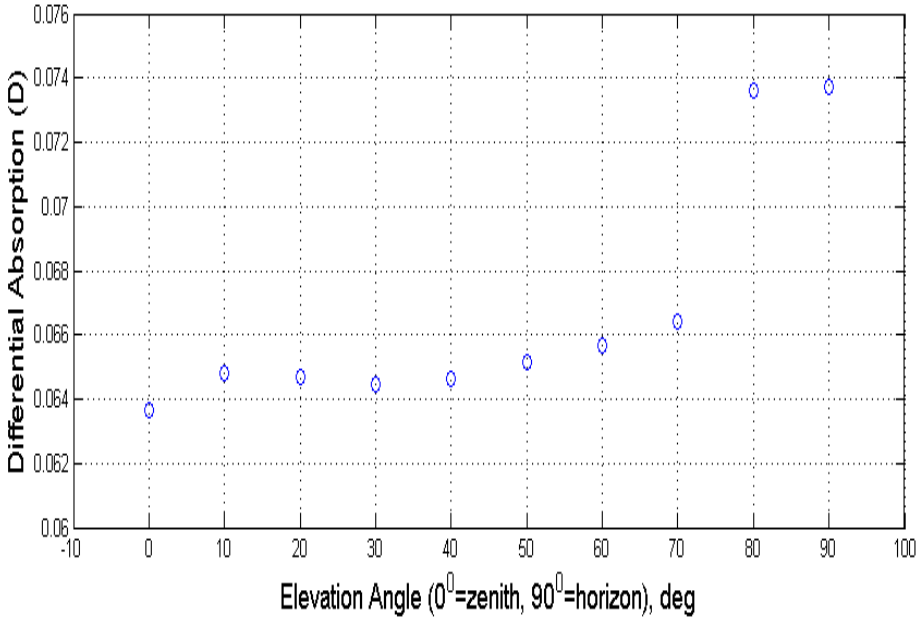

Figure 6.33 Variation of D with a changing elevation angle θ. An increase in D when the USB4000 is nearly parallel to the horizon suggests higher NO_2 concentrations closer to the Earth's surface.

This is representative of the higher concentrations of pollutants such as NO_2 produced by human activity. To determine the variation of D in different directions the instrument optics were directed at the available paths in the north, south, east and west azimuthal directions. These measurements were taken from the roof of the DIT/FOCAS institute where most of the East view was blocked by the top floor structure and the view

directly north was the rear of the DIT Kevin Street building. However, the results in figure 6.36 show that the variation of D for each azimuth was less than 0.02 when each measurement was taken within a few minutes of each other. It would be expected that larger variation between each direction would exist, depending on the sources of NO_2 in each direction and on days with higher winds which will affect the lateral transport of the NO_2. The highest concentrations would be expected for the north-east direction towards the city centre and dockland area, especially during times of day when traffic congestion is high [11].

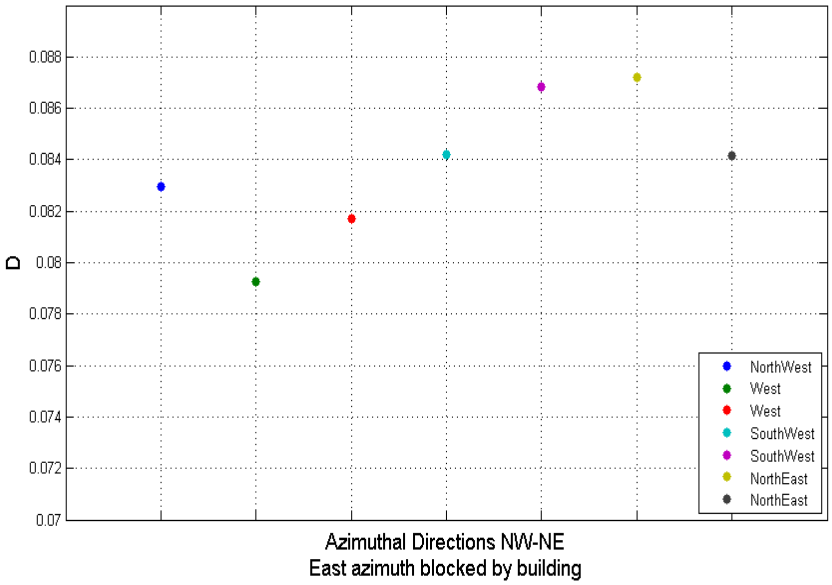

Figure 6.34 Variation of D for different azimuthal directions the values for D range between 0.078 and 0.088.

Measurements were also obtained of the optical pathlength south of the DIT-FOCAS building on Camden Row. The data was analysed for a variation in D that compared well with results in the literature [17] and the results obtained for the CL instrument located within the pathlength. The NO_2 feature at 440 nm was used to perform

the analysis with the differential absorption cross section $\sigma(\lambda)$' = 2.6 x 10^{-19}cm^2/molec. (3.4 x 10^{-7} m$^2\mu g^{-1}$). The pathlength was again estimated as 10 km and the results were compared to the data provided by the EPA. The measurements were recorded for full days between 9 am and 6 pm, weekends from Fridays to Mondays or for several week days. Any data recorded at night or at twilight were eliminated because there was no sunlight or there was not enough sunlight to determine an accurate D i.e. the signal was at the limits of detection (LOD).

Directing the collimator towards the zenith in theory measures the lower troposphere and some of the stratosphere. The variation of NO_2 concentration in the stratosphere typically has a pattern where the concentration is high in the morning and evening. The reasons for this variation include the increase in tropospheric concentrations at this time due to traffic congestion and the reduction in photolytic reactions during twilight hours when there is less direct sunlight on the Earth's surface. Some of the results from these tests are shown in figures 6.37 and 6.38.

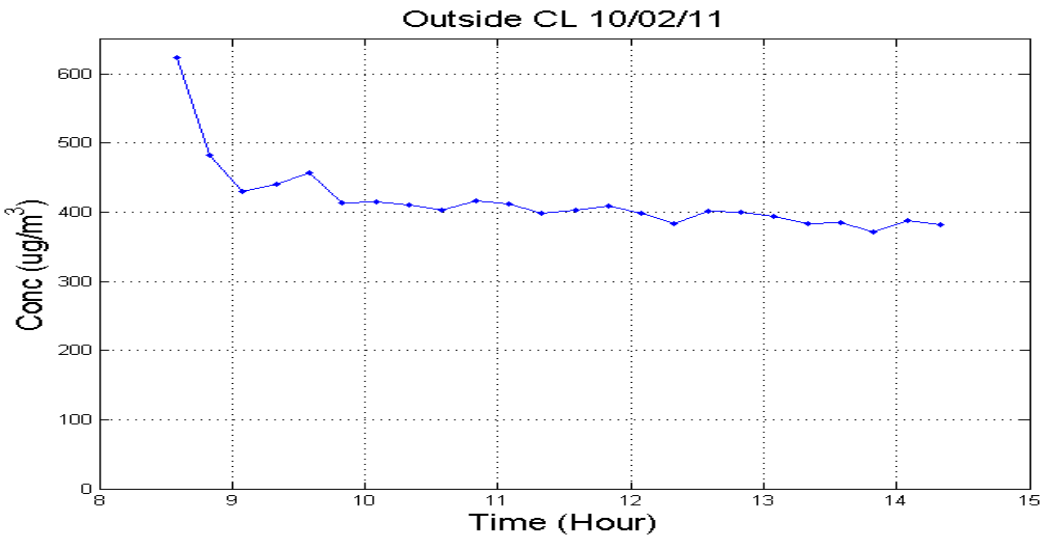

Figure 6.35 Variation in concentration for zenith directed measurements. There is higher concentration before 9am in the morning which can indicate high NO_2 concentrations from chemical mixing at twilight and morning rush hour traffic.

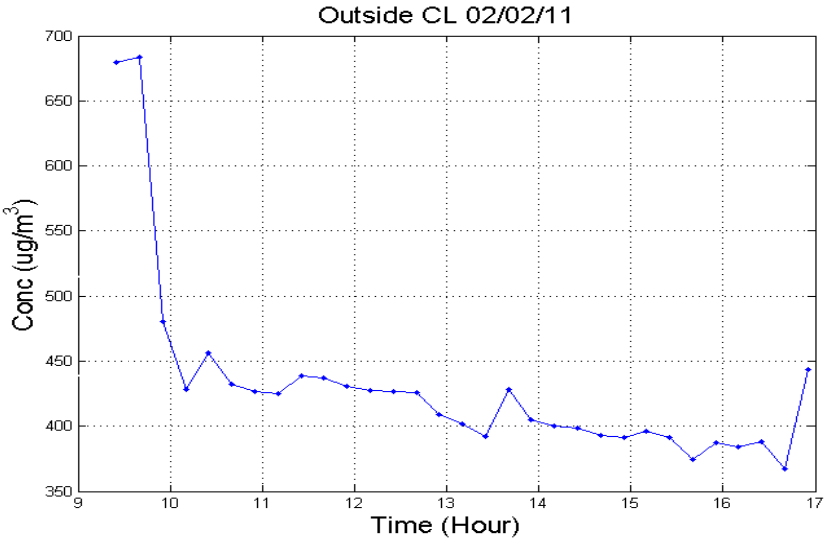

Figure 6.36 Variation in concentration for zenith directed measurements. As in figure 6.37 the data shows a high value for concentration in the early hours of the day and slight rise in the evening.

6.9.2 Results of comparison of novel-DOAS with EPA chemiluminescence

As described in chapter 5, section 5.5 there have been successful attempts comparing *in-situ* DOAS results to CL measurements. To test the effectiveness of the measurements made by the proposed novel-DOAS instrument the results obtained from the analysis were compared to results obtained using CL monitors. In figure 6.39, the blue data represents the concentration determined using the DOAS method and the red is the variation of NO_2 in Rathmines determined by an EPA CL instrument. The concentrations determined using DOAS were calculated using estimates of the average pathlength on the three days 02-04 June 2011. A pathlength of 6 km was estimated for each day. There is some correlation in the pattern of the data but the DOAS data shows less variation as can be seen in the peak in NO_2 recorded by the EPA in the late afternoon of June 3rd. This could be explained by the fact that the DOAS data represents the average NO_2 over a path of ~6 km unlike the CL data which can be influenced by local sources such as nearby traffic congestion. In the case of the Rathmines location, the traffic sources include a local school, and the car park in the adjacent apartment block. There is a rise in the NO_2 in both sets of data in the latter half of the each day most likely due to increased congestion.

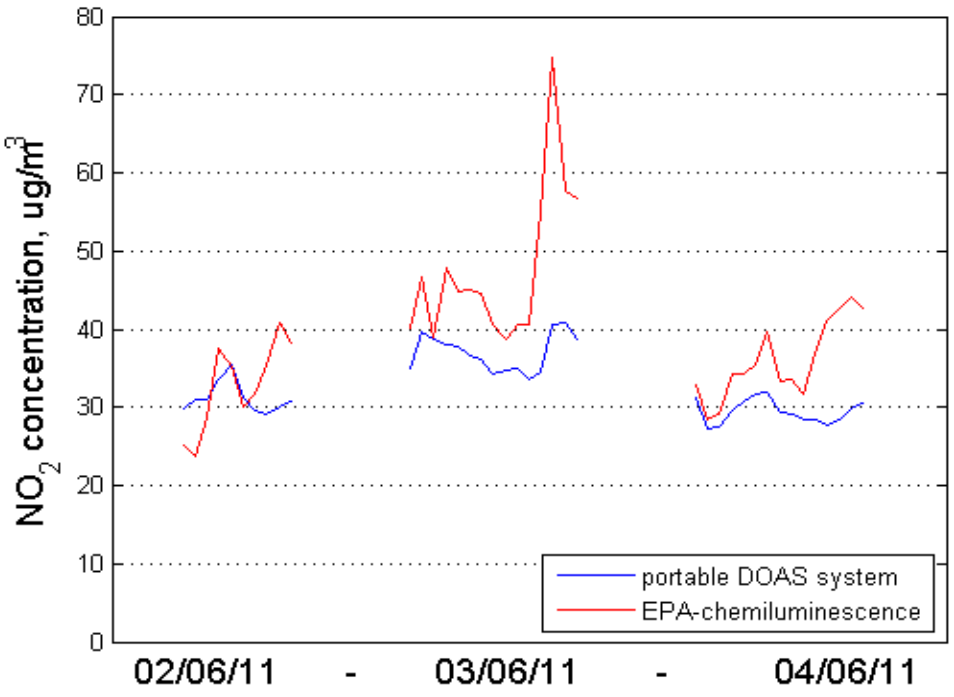

Figure 6.37 Three day comparison of EPA-CL and novel-DOAS data. The estimated optical pathlengths for the determination of the NO_2 concentration for each day were L~6 km respectively.

Data recorded for a bank holiday weekend from the 3/6/2011 to the 7/6/2011 in figure 6.40 show variation in NO_2 concentration with a decrease in concentration after the first day the 3/6/2011. The broad peak in the results on the third day the 6/6/2011 could suggest a large rise in traffic congestion in the morning of the bank holiday Monday. The weather was clear at the beginning of the weekend with some cloud and some showers on the 6th and 7th this can be attributed to a dependency on clear days with little or no cloud. This justifies the need for comparative data from a source such as the EPA CL results.

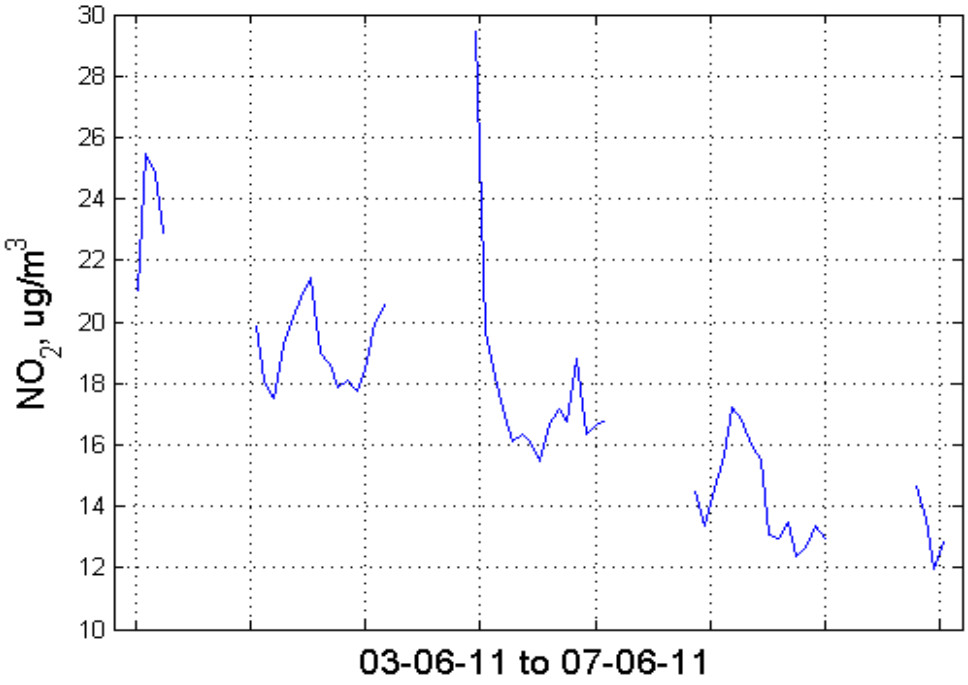

Figure 6.38 Concentrations of NO_2 determined for four days. A single estimated pathlength of 6 km was used.

As shown in figure 6.39, there can be some correlation between the DOAS method and local CL data for the overall NO_2 concentration throughout the day. But any correlations in the smaller variations of the data are harder to distinguish because of the spatial conditions and the variations in the optical pathlength due to light scattering effects. Figure 6.41 shows similarities between the DOAS and the EPA CL when the average pathlength is taken as ~ 10 km for each day.

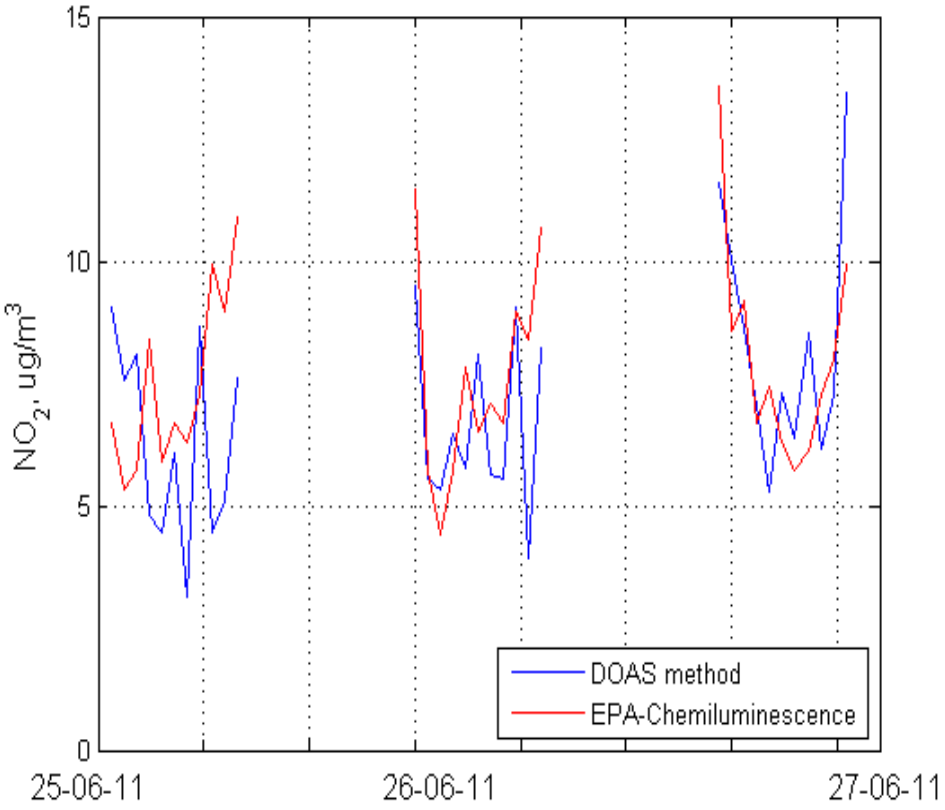

Figure 6.39 Comparison of 3 days of DOAS and EPA-CL (L~10 km). For the all three days the NO_2 concentration suggests a good correlation between the two methods.

However, in figure 6.42 the pathlength is estimated to be between 6 km and 10 km for the weekend of the 1st to the 4th of July in 2011. The data shown was collected between 8am and 8pm for mostly clear days with light winds. Shorter pathlengths were estimated for the 1st and 4th of July which may have been due to an increase in cloud cover and light showers [93]. The concentrations for the 3/7/2011 show a rise in the afternoon and a large decrease in NO_2 for most of the 4/7/2011 for both methods. The smaller features in the novel system data could be caused by the actual fluctuations of NO_2. But other influences could be responsible such as the light scattering in the field of view, which could affect the

length of L, and the length of time the spectrometer is used *e.g.* temperature effects on the dark current. The LOD of the system determined in the laboratory show that the analysis is capable of identifying concentrations of 10 μgm^{-3} in 1 km with signal > 20% of the maximum intensity. But these LOD can vary substantially on cloudy days when the intensity signal is lower and influenced by electronic noise (figure 6.20).

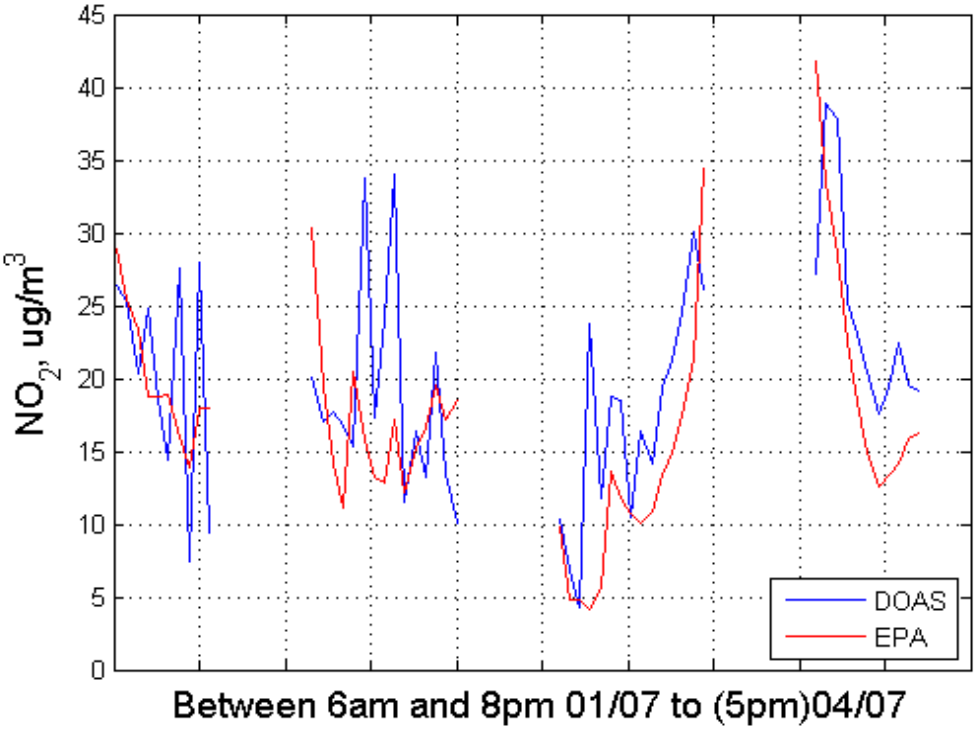

Figure 6.40 Comparison of 4 days of DOAS and EPA-CL data. (Average pathlength L ~ 8 km) The 3rd and 4th of July are similar but small fluctuations in the DOAS data could be the result of changeable weather conditions.

Comparing the DOAS data for days with very dynamic meteorological conditions (see sections 1.3 and 2.9.3) demonstrates the effects of light scattering in the atmosphere and pollution transport have on the DOAS data and NO_2 concentrations. The results in

figure 6.43(a) show greater differences in NO_2 concentration between four different days. Comparison of the DOAS method and the CL results of the 9th and 10th of July 2011 requires a large 20 km pathlength estimation. Displayed in 6.43(b) is the comparison of the novel DOAS system and EPA CL results. A possible reason for the larger pathlength estimated for the 9th and 10th is the changeable meteorological conditions over these few days. Comparing the weather of the 10th (L~20 km) and the 11th (L~6 km) shows that the 10th had 6 hours of sunshine recorded by Met Eireann whereas the 11th had 8 hours. On the Monday the 11th it was mostly dry, with only light breezes, whereas the 10th was a wet day with northwesterly winds. The Friday and Monday results are much higher this could be attributed to traffic emissions caused by increased congestion on weekdays.

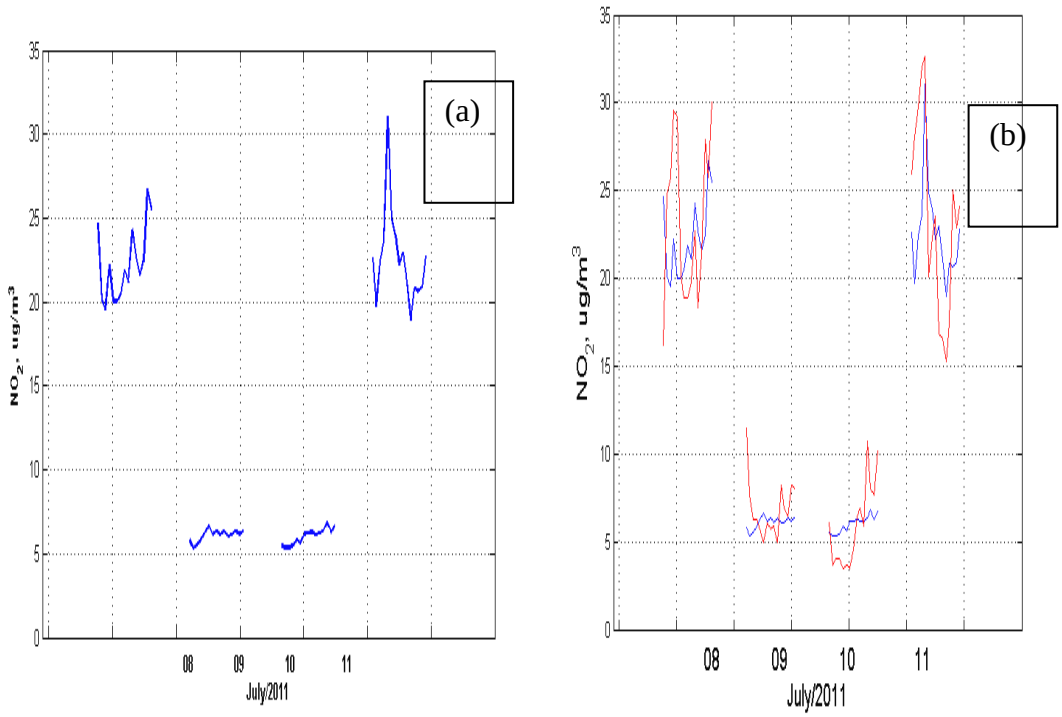

Figure 6.41 (a) Variation in NO_2 concentration using DOAS (L~6, 20, 20, 6 km)

(b) Comparison of the same data with EPA-CL results

6.9.3 Evaluation of CL and novel-DOAS data

In figure 6.44, the change in NO_2 (ppb) recorded by two CL monitors, the EPA monitor in Rathmines and the Trinity College Dublin Monitor on the roof of DIT Kevin Street are shown. The change in NO_2 recorded by the two CL monitors in different locations still has a very noticeable correlation. However, the weather on these days was very changeable, see table 6.5, which would have had more of an effect on the TCD CL monitor, as it was in a more exposed location and well above the ground. Still, the correlation between the data obtained from each monitor is enough to demonstrate that measurements of the average NO_2 by remote sensing along a fixed path should provide comparable results between novel-DOAS and the CL sampling if the atmospheric NO_2 concentration was stable. However as figure 6.45 illustrates, the variation of NO_2 concentration determined with the DOAS analysis compares poorly with the two CL monitors, this is attributed to the very dynamic meteorological conditions which can make remote sensing of NO_2 concentration by DOAS very difficult. The pathlengths used for each day to make the comparison shown are 6, 6, 10 and 8 km respectively, *i.e.* an average pathlength of ~7.5 km.

Date	**Wind Direction**	**Sunshine (national)**	**Weather**
29th July	NE	5 hours	Morning heavy Rain
30th July	SE	3 hours	Mostly Cloudy
31st July	SW	1 hour	Heavy rain, dry evening
1st August	Variable	4 hours	Cloudy

Table 6.5 Weather for the weekend of 29th of July to 1st of August 2011

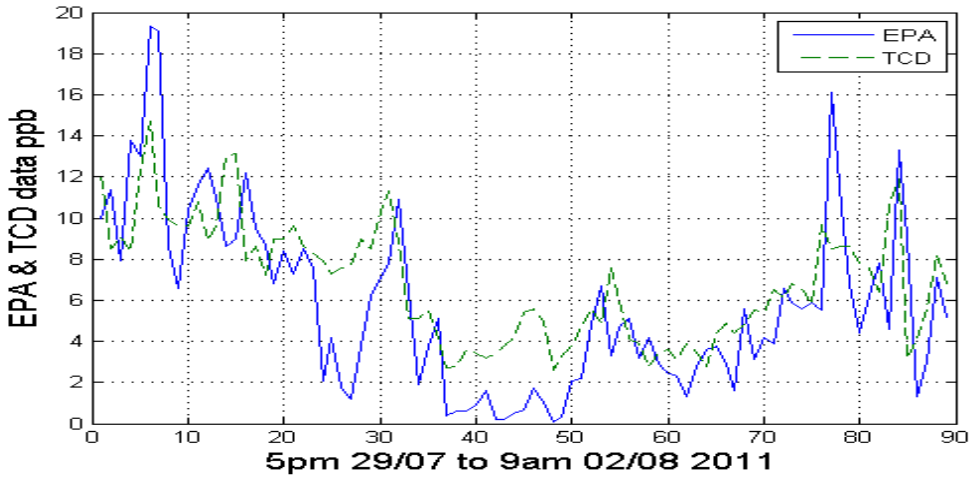

Figure 6.42 Change in NO_2 concentration in ppb using two CL monitors for the weekend 29/07 to 02/08 of 2011 (90hrs=3/4days). The overall change in the data obtained by the two monitors show some correlation which suggests that a CL monitor is capable of representing an average NO_2 concentration in an urban area.

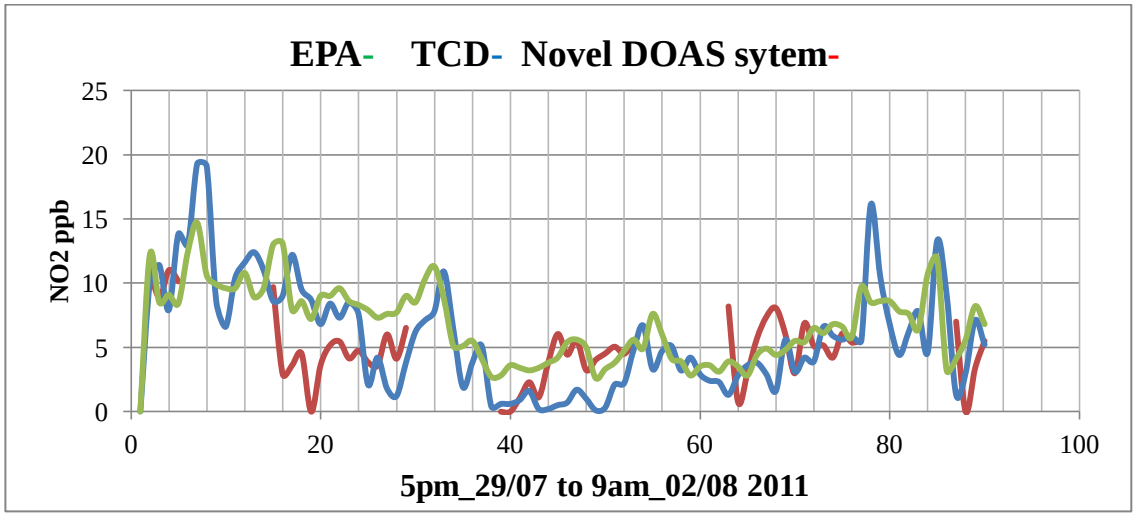

Figure 6.43 Data as shown in figure 6.45 but with the change in NO2 concentration determined by DOAS (red) added. The estimated pathlengths for each day are L~ 6, 6, 10, 8 km respectively. Heavy showers and dark cloud were also recorded for each day.

6.9.4 Further analysis of the EPA and DOAS data comparisons

Figures 6.43 and 6.45 showed how the DOAS data can vary in very different ways when compared to EPA data. Comparisons of the correlation of these results and others are shown in figures 6.46 to 6.48. In Figure 6.46, the concentration comparison is shown on the left and the correlation using a scatter plot on the right. The scatter plot indicates that there is a slight correlation between the two sets of data but the concentration determined by DOAS analysis is offset compared to the EPA data, the slope of the line through the plot is very large at 3.2. The calculated regression constant (R^2) for this data gives a good value of 0.539. Figure 6.47 illustrates the data in the same way for the August bank holiday weekend in 2011. The DOAS data here compares very well with the EPA data with the slope of line in the scatter plot at 1.3. An R^2 value of 0.708 indicates a very good correlation between each set of data for these four days. In figure 6.49 the slope of the scatter plot is 4.8 offset largely by the large difference between the EPA and DOAS data for the 30 of September 2011. The R^2 value is very low at 0.094 which indicates an extremely poor correlation between the DOAS and the CL data. All the DOAS results for figure 6.48 were calculated with a 10 km pathlength.

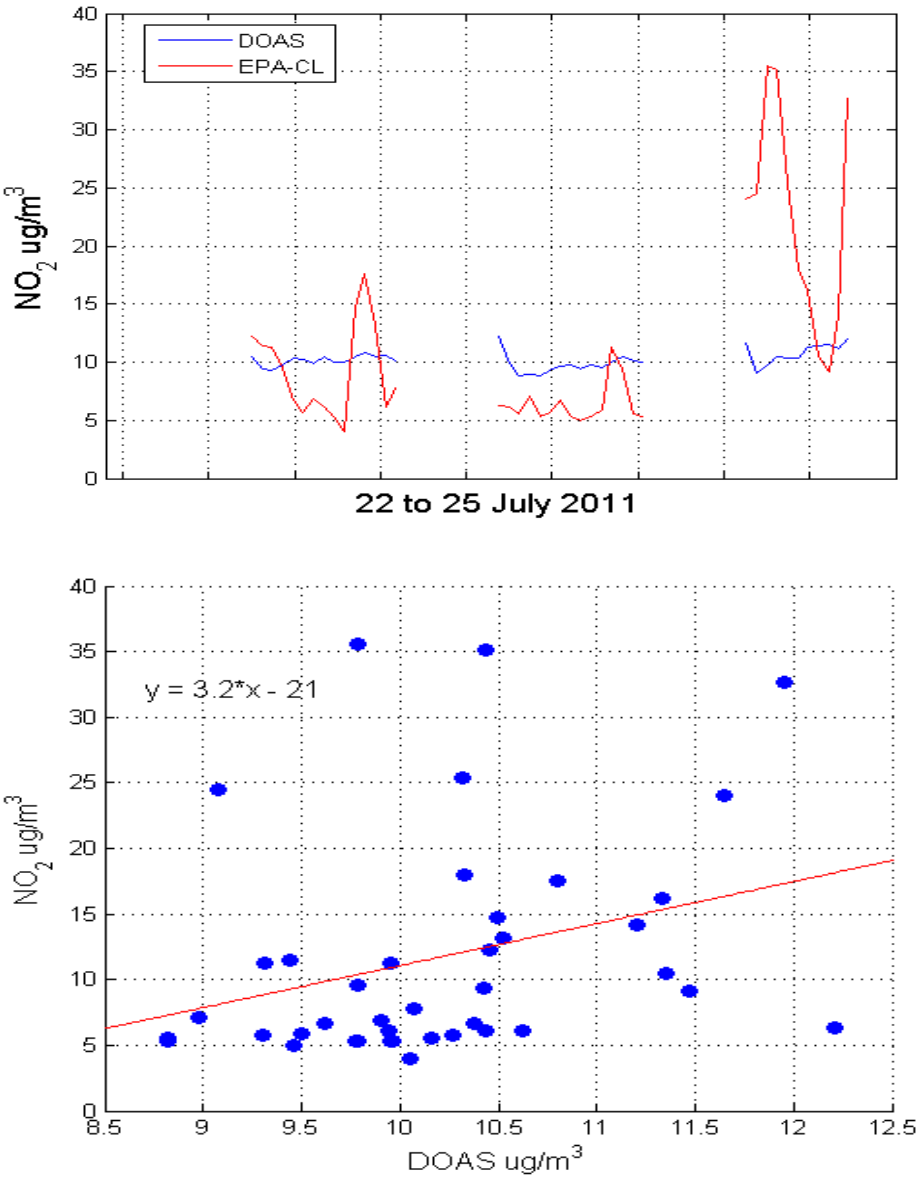

Figure 6.44 Comparison of in-situ DOAS (blue) and EPA-CL (red) for NO_2 and data correlation 23-25/07/11. The DOAS data is clearly not correlated well with the EPA-CL data. The slope of the line in the scatter plot is large ~3.2 indicating a weak correlation between the two methods on these 3 days.

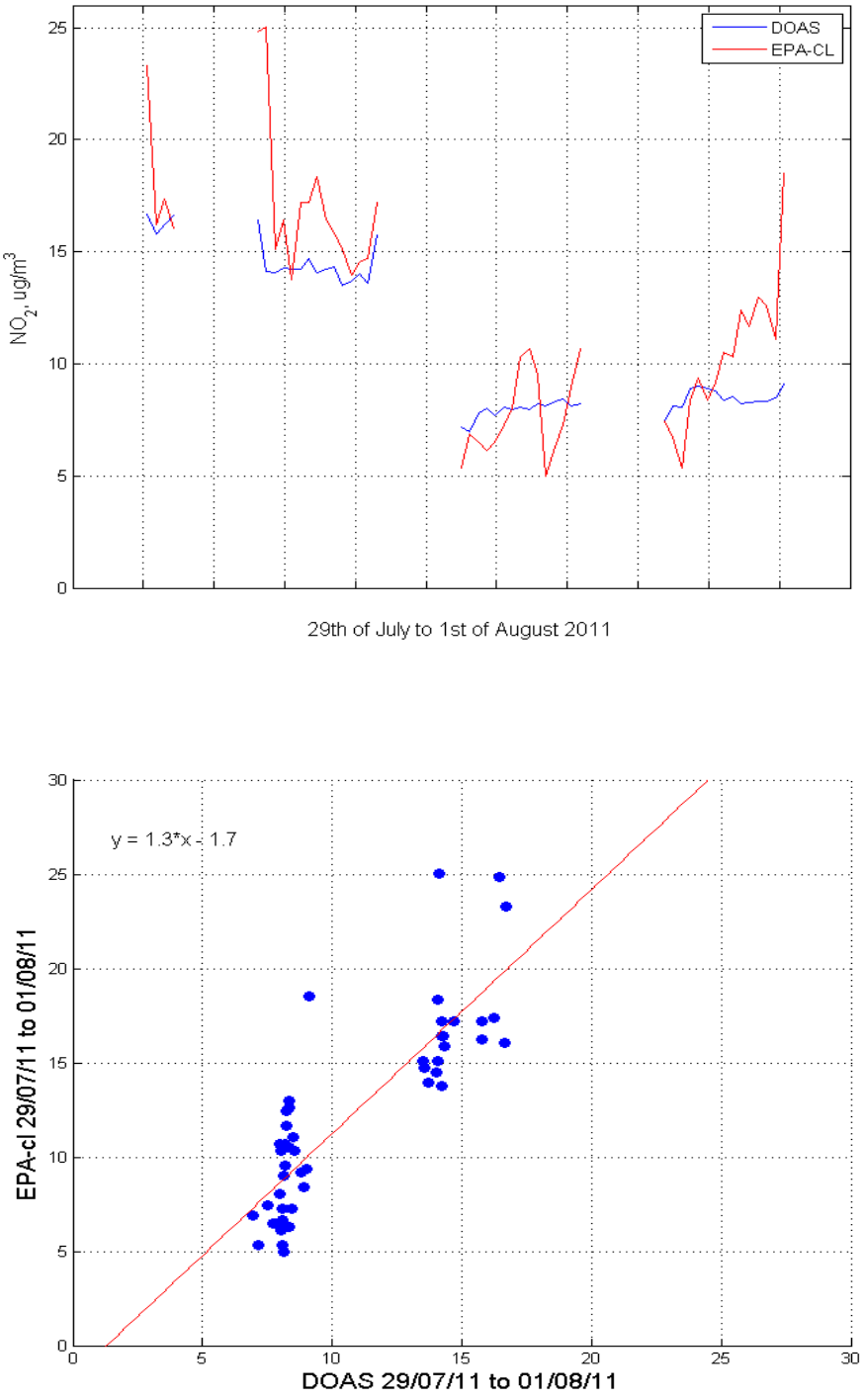

Figure 6.45 Comparison of in-situ DOAS (blue) and EPA-CL (red) for NO_2 and correlation 29/07/-01/08/11 the slope of the line in the scatter plot is 1.3 which indicates a good correlation between each set of data.

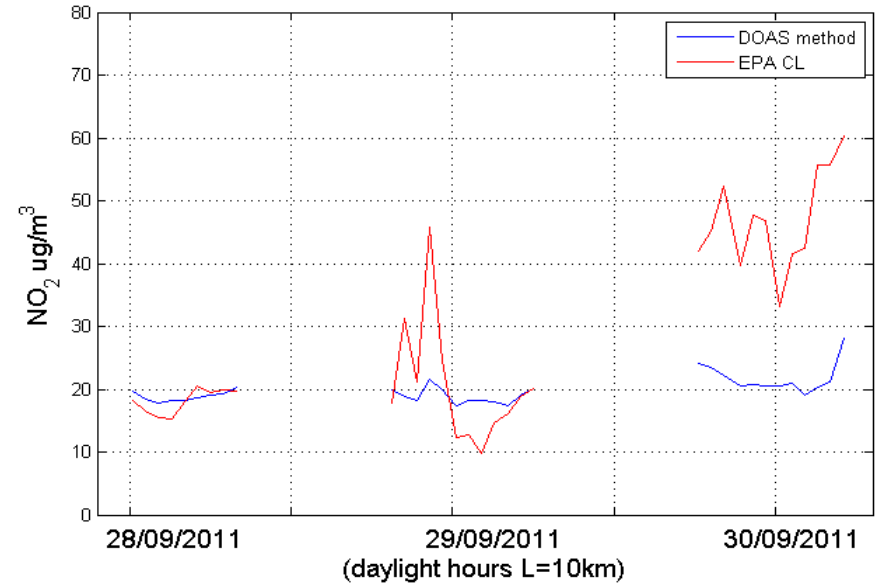

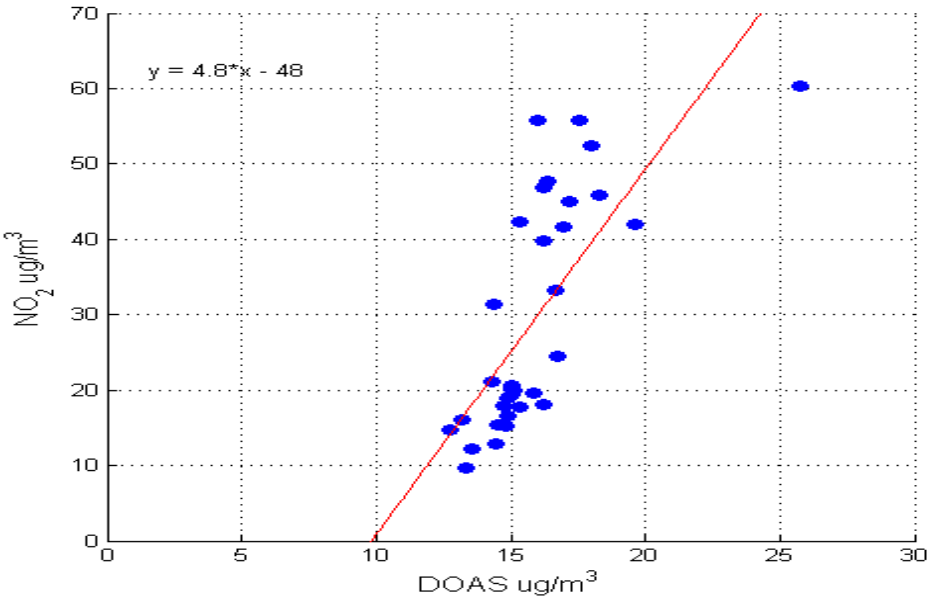

Figure 6.46 Comparison of in-situ DOAS (blue) and EPA-CL (red) for the concentration of NO_2 and correlation 28-30/09/11 the large difference on the third day (30/9/11) affects the data giving the line on the scatter plot a slope of 5.4.

By comparing the averages of CL and the *in-situ* novel-DOAS for different days, a more effective illustration of how the results compare is seen. The larger changes in NO_2 concentration demonstrate a much better comparison with each other and the smaller changes have less influence. Figures 6.49 and 6.50 show that the change in average concentration for 5 days in September 2011 with an estimated path of 10 km. In figure 6.49 the novel-DOAS data displays the variation in concentration of NO_2 in μgm^{-3} for an estimated pathlength of 10 km correlates almost exactly with the corresponding EPA data. This illustrates the effectiveness of the novel-DOAS system in the evaluation of the NO_2 in a local urban atmosphere.

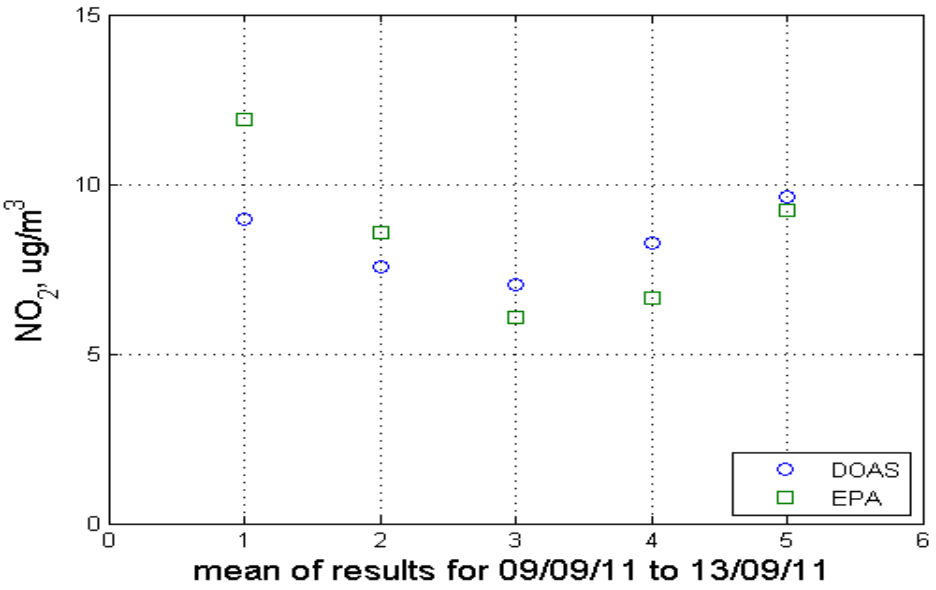

Figure 6.47 Comparison of the average EPA-CL and in-situ novel-DOAS data for 5 consecutive days (L~10 km). There is a clear correlation between both sets of data obtained by the two different methods.

In figure 6.50, the correlation illustrates less accuracy between the two methods. The average estimated pathlength for the four days was ~8 km ± 2 km. However, looking at

the individual data for each day, figure 6.51 shows that the pattern of the data for the 3rd and 4th of July are very similar even with the variation in the estimation of L. These results are clearly less conclusive than those in figure 6.49. The results make it plain that clear days provide better correlation between the in-situ novel-DOAS and the EPA-CL because of the variable pathlength caused by light scattering in the atmosphere by clouds and variations in the local traffic congestion.

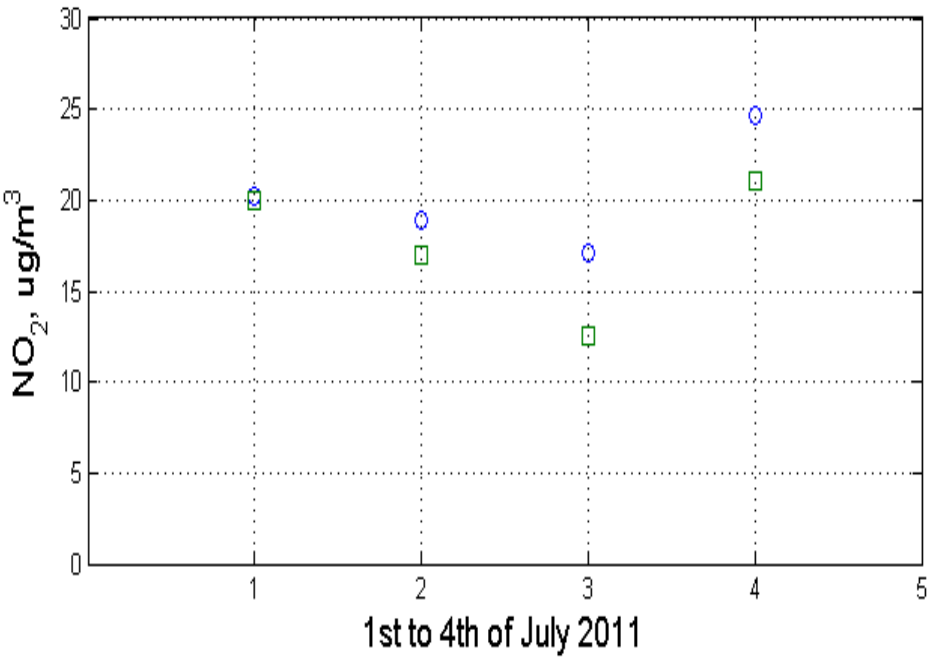

Figure 6.48 Comparison of average CL and in-situ novel-DOAS for 4 days (L~ 6 km 10 km 10 km 6 km respectively). Although there is some comparison in these results the variation in the estimated pathlength determined by comparing the two sets of data suggests the results were not conclusive.

6.10 Summary

Initial tests were designed to develop the Matlab algorithm and optical arrangement used to measure NO_2 concentrations for samples prepared in the laboratory. Polypropylene bags were filled with NO and reacted with air already in the bag to form NO_2.

Tests results show that an increase in concentration in different bags could be detected and the D compares with the A. Three different Ocean Optics, miniaturised spectrometers were used the USB2000, Maya2000 and the USB4000. Ultimately the USB4000 was chosen for further tests as it had a better resolution and signal to noise (~22.3 for 500 scans/10 ms) than the others and proved to be the most accurate in determination of NO_2 concentration with lab samples.

The PP bag NO_2 concentrations were consistently lower than the expected so calibration cells with known concentrations were sourced. Comparison of the concentration calculated from D and A, using the cells were successfully within the 10% error set by the manufacturer.

Measurements with the USB4000 were performed for several days with the results showing good correlations particularly for clear days with little changeable weather. The average results for each method were also compared. The portable system was tested with the calibration cells and Sunlight illumination by placing the cells in front of the instrument to determine if there is a change in the calculated novel-DOAS data and each cell was measured throughout one day and compared to the D variation without a cell. This was to

identify any variation due to the cell and if the cell in front of the instrument affected measurement without the cells.

Tests were performed outside the laboratory using one of the spectrometers and front end optics constructed to measure different elevation angles and azimuthal directions. Initial attempts with the OPSIS DOAS system in DIT could not be achieved because of the state of the OPSIS apparatus and the distance between Kevin St. DIT and Cathal Brugha St. DIT. An alternative method involved comparing the portable, novel-DOAS instrumentation to EPA CL. The results obtained show that comparisons can be made between the two methods but spatial, meteorological differences can affect the strength of any correlation. It is worth noting that each system the proposed novel-DOAS system and the CL monitor are designed to meet different accuracy and are expected to vary in their respective locations and function.

CHAPTER 7 Discussion and Conclusions

7.1 Project aims and background

The aim of this research was to develop a novel system for the detection of gaseous pollutants in an urban environment. The principle of operation of the system was based on the differential optical absorption spectroscopy (DOAS) method. The novel system developed in this research is inexpensive, capable of *in-situ* measurements, is user friendly and is also capable of comparable measurements with other pollutant detection methods.

The remote sensing technique known as DOAS is based on the principle where attenuated features in the spectral profile of a broadband source *e.g.* a tungsten lamp or Sunlight can be used to determine reference intensity, I_0, used to calculate the absorption in the Beer-Lambert law, see equation 2.10. The DOAS technique uses a variation of the Beer-Lambert law to determine a differential absorption that is equivalent to absorption with a reference value denoted by I_o'. This value is found mathematically using equation 2.14. With this approach it is possible to determine the concentration of the NO_2 gas. Two forms of the DOAS approach are described in detail in chapter 3 the active and passive methods using an artificial light source and naturally occurring sunlight respectively.

The active method has been successfully employed in commercial applications where it records the changes in concentrations for a variety of gases including organic compounds (VOC), ozone (O_3), sulphur dioxide(SO_2) as well as NO_2 although it is

expensive, requires mains power, in some scenarios more than one source, and fixed constructed locations.

The passive methods on the other hand utilize a variety of approaches including satellite measurements, plume measurements from smoke stacks and volcano SO_2 concentrations with large DOAS devices and miniaturised spectrometers. One of the objectives of this research is to demonstrate that, with both knowledge of the lower layers of the atmosphere and concurrent measurements by other instruments, it is possible to measure NO_2 concentrations comparable to local EPA chemiluminescence data using the novel-DOAS.

7.2 Laboratory work and discussion of the results

To test the validity of the use of a miniaturised spectrometer to measure NO_2 concentrations, tests were designed and developed in the laboratory on an optical bench to determine the correlation of absorption, (A), determined with a reference sample and differential absorption, (D), where no reference is needed. Along with the spectrometer an optical fibre coupled to a collimating lens were employed to measure the light passing through each sample. Using an algorithm developed the mathematical value for I_o' and hence D were calculated along with a value of A for each sample. The differential absorption and absorption were plotted against each other and the correlation between the two was excellent.

Three different miniaturised spectrometers were used; USB2000, Maya2000 with a back illuminated CCD and a USB4000. Ultimately the USB4000 was chosen which has an

optical resolution of ~1.5 nm and dispersion of ~0.18 nm/pixel. Initially PP bags were used as sample containers but it was discovered the concentrations were below the levels expected. From the results of measurements on the bags, the concentrations were approximately 33% of the expected concentrations. These samples were eventually replaced by custom made calibration cells sources from Resonance Ltd. The results using the bags showed that there was a good correlation between A and D but the calibration cells proved to be more accurate with both the correlation of the two values and the concentrations determined by the algorithm. These cells are more expensive than the bags but are far less expensive than the commercial DOAS calibration samples. Their small size also makes them ideal for alignment with the front end optics of the field measurement configuration i.e. the adjustable aperture and collimating tube, see figures 4.10 and 6.25.

Other tests were performed on the optical bench including a determination of the differential absorption coefficient, α', (equation 2.14) for the spectral resolution for the spectrometer and comparing them to the values described in the literature. A value of 3.4 x 10^{-7} m^2 μg^{-1} was determined, as the gravimetric equivalent to the absorption cross section σ', as an accurate value for the NO_2 molecule and is similar to values described in the literature [4], seen in figure 6.10.

The LOD in the laboratory were also tested for using the smallest concentration sample which was also comparable to 5 ppm in 1 m (equivalent to 1 μgm^{-3} in 10 km). A comparison of a decreasing raw intensity signal was compared to the value of D and A, determined while the amount of light received was decreased using a variable NDF. The results of this test showed that D could still be determined with some accuracy even at low light levels showing that the D was independent of the light intensity level.

7.3 Field work results

The final configuration of the novel system consisted of an adjustable aperture attached to a collimating tube which is coupled to the lens and optical fibre. The fibre is connected to a USB4000 miniaturised spectrometer which is connected via a USB cable to a Toshiba laptop. The analysis of the data recorded by the laptop is performed using the Matlab and SpectraSuite software. The key components are described in table 7.1.

Signal to noise of the USB4000 system, 300:1, was minimised by subtracting the dark signal from each measurement, see specifications table 7.1. By keeping the signal at a maximum the effects of electronic noise is reduced. This can be achieved by ensuring the front end optics is receiving as much light as possible. The integration time for the field measurements was 500 scans for 10 ms which averaged the signal over 5 seconds and increases the signal to noise ratio by a factor of ~22. This provides sufficient detector sensitivity during the day and matches the rate the ambient sunlight changes compared to commercial DOAS systems which average 30,000 scans over 5 minutes [105].

Large scale dimensions	Stand height	Collimating tube	Aperture maximum	Laptop type	
	Min: 54 cm Max: 140 cm	Length: 80 cm Diameter: 23 mm	23 mm	Dell E6400	
Optical components	Optical fibre	Length	Numerical aperture	Diameter	
	Ocean Optics	2 m	0.22	600 µm	
	Lens	Focal length	Optical Range	Diameter	
	Ocean Optics	10 mm	uv/vis	5 mm	
Optical spectrometer USB4000	CCD	S/N	No. of pixels	Resolution	Range
	Front Illuminated	300:1 (increases √n, n = no. scans) e.g. 500scans/10 ms √500 → S/N: ~6700	3648	~1.5 nm	650 nm (effective between 200 nm and 1100 nm)
Gas Species NO_2	Limits Of Detection	Absorption (visible range)	Differential absorption coefficient α'	Differential absorption cross-section σ'	
	1 μgm^{-3}/10 km	400 nm -500 nm	$3.4x10^{-}7m^2\mu g^{-1}$	$2.5x10-^{19}cm^2molec^{-1}$	
Calibration Materials	Type	Reference	Minimum conc.	Middle conc.	Maximum conc.
	Calibration cells (Source: Resonance Ltd.)	Atmospheric air	5 ppm-m (10 μgm^{-3}– 1 km)	20 ppm-m (40 μgm^{-3}– 1 km)	50 ppm-m (100 μgm^{-3}–1 km)

Table 7.1 Description of the key components of the final setup of the DOAS device with the USB4000 spectrometer and calibration cells specifications

Zenith measurements using the USB4000 showed that D changes very little in the middle of the day. It can be high at the beginning and the end of the day, as seen in figures 6.36 and 6.37, most likely due to increased traffic levels as described in the literature sources. Changing the elevation angle between the zenith and the horizon also reveals a much higher concentration closer to the horizon. This is expected because of the greater concentrations of NO_2 in the lower atmosphere[6].

Measurements of the atmosphere with the front end optics directed towards the horizon were conducted from the FOCAS building on Camden Row. Some of these results are shown in figures 6.41 to 6.42, which illustrate how the concentration varies throughout the day. Initially attempts were made to compare data obtained from the DIT/DOAS system described in chapter 5 using methods similar to those described by Dr. Alberto Morales and Dr. James Walsh in 2005 [5]. It was found, however, that the current DIT system requires an expensive recalibration and the once available paths are either obstructed by new buildings or are too long (~ 2 km) to perform an accurate calibration. Ultimately, the results determined by the novel DOAS system were compared to local CL data provided by the EPA. These results were compared with the EPA measurements if a reasonable pathlength of ~10 km is chosen. By comparing the results of the EPA monitor in Rathmines to another CL monitor placed on the roof of Kevin St. across from FOCAS (figure 6.44 and 6.45), it was demonstrated that there was a good comparison between the two even though these sampling monitors were separated by over 1 km. This demonstrates that the results of these instruments throughout the city are a good representation of the overall average NO_2 concentration and therefore it should be possible to gather comparable results with a novel

DOAS system which measures the average concentration along a fixed path. Further comparisons were also made between past EPA data [20].

Further analysis of the correlation of EPA data and the DOAS system demonstrated that the correlation was much better on clear sunny days. This was most likely due to the scattering of light long the measured pathlength on cloudy days where the scattered light can travel through the same part of the atmosphere more than once affecting the determination of the average NO_2. Analysis of the daily average for July and September 2011 (figures 6.49 and 6.50) illustrate how well the EPA data and the novel-DOAS system can correlate with an approximate pathlength of 10 km.

7.4 Summary of Conclusions

The novel system is constructed from components less expensive (€500) than the commercial DOAS (€130,000) and CL monitors (€50,000). Overall, the system consisting of the USB4000 setup costs approximately €3,500 with the front end optics and the four calibration cells described in chapter 4.

The algorithm developed in Matlab, shown in Appendix II, shows how effective the absorption data correlates to differential absorption. The value obtained for α' is the same as the values given in the literature obtained by other methods.

The portability of the novel system made it possible to record spectra from the roof tops of the DIT buildings and on the locations in Rathmines. The system can be calibrated in the laboratory with the cells containing different concentrations of NO_2. Calibration can also be achieved in the field by placing the cells in front of the instrument and calculating the increases in D for each cell and comparing the results to the D of the open atmosphere.

This approach is similar to the methods applied in the COSPEC DOAS application described in chapter 3. Table 7.2 summarises the conclusions that can be drawn from the overall research and results.

Laboratory results	Field results with novel-DOAS
• Excellent correlation between absorbance (A) and differential absorption (D) with custom made cells containing concentrations of NO_2	• Strong correlation between DOAS and EPA-CL measurements on clear days
• Absorption coefficient α' comparable to values determined from literature sources	• Weak correlation on cloudy days most likely due to light scattering in the optical path
• Limits of detection ~ 5ppm-m ≡ 1 μgm^{-3} -10km	• Strong correlation of DOAS and EPA-CL for daily averages
• S/N ~22	• Portable and adaptable setup

Table 7.2 Comparison of the laboratory and field results obtained with the novel-DOAS instrument

The results show the effectiveness and accuracy of the measurements in the laboratory and how the data recorded on clear days in the field is comparable to concurrent EPA data obtained using CL the existing standard monitoring technique outlined in European Union policy. The data analysis also compares well with results described in the literature which was studied in the extensive literature survey conducted at the beginning of the research.

7.5 Future work

The current system could be further developed by developing the algorithm to include radiative transfer equations to improve the estimation of the L being measured. Concurrent measurements with local commercial DOAS instruments would be ideal for correlation as the methodical approach is similar. However correlation with data obtained from CL monitors could be developed as well as with satellite data to develop a local profile of the NO_2 concentrations in different azimuthal directions and within the UBL of the troposphere. Further development of the software could also make the system more user friendly for various operators.

Detection of other pollutants could also be achieved, particularly O_3 and SO_2 which are also constantly monitored by the EPA. O_3 in particular contributes to the aerosol measurement data used to determine the AMF and can therefore be useful in the determination of the vertical height of NO_2 concentrations. The results show that cloudy days have an effect on L by scattering the light passing through the lower atmosphere as a result meteorological data gathered simultaneously with the DOAS data would add to the understanding of the pollutant profile.

Alternative designs to the setup could be achieved by the development of a weather protected casing for the system and an artificial light source like LEDs that would allow measurements to be undertaken when the light levels are low and during the night. A modest amount of work has already been achieved with LEDs in this research and in the literature. In figure 7.1 spectra are shown of the profiles between 300 nm and 600 nm of the Sun, an LED and the Xenon lamp that could be used for the detection of NO_2 in the laboratory or in the field. However, to be useful for DOAS measurements in the field, the ideal LED would need to be detectable over a distance of at least 300 m (OPSIS AB), the

LED. The commercial DOAS mirror for example produces a very bright, collimated beam, but does have a disadvantage of size setup of a certain length because of its relatively long focal length. The CCD miniaturised spectrometers could also be replaced by photodiode arrays designed to measure the light intensity at specific wavelengths could maximise the effectiveness of measurements of individual absorption features.

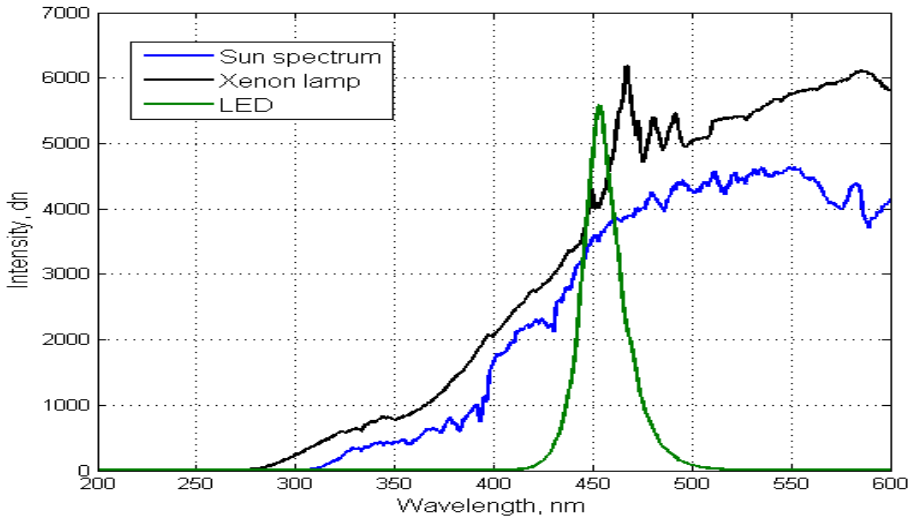

Figure 7.2 Profiles the Light Emitting Diode (green), the Sun (blue) and a Xenon lamp (black) in the UV/Vis range.

The versatility and variety of applications of the novel-DOAS method shows that it can be adapted and developed in numerous ways for many applications including the monitoring of industrial sites, monitoring areas of concentrated traffic congestion and scientific applications.

References:

1. Godish, T., *Air Quality*. 2004: Lewis Publishers. 460.

2. Association, S.M.H. *The vertical structure of the atmosphere.* cited 2012; Available from: http://smha.btck.co.uk/OriginoftheAtmosphere/VerticalStructure.

3. Vandaele 1998, S., Bogumil 2003, Burrows 1998. cited; Available from: http://www.atmosphere.mpg.de/enid/.../Spectra/Catalogue_Spectra_5p4.html.

4. Morales, J.A. and J.E. Walsh, *Detection of atmospheric nitrogen dioxide using a miniaturised fibre-optic spectroscopy system and the ambient sunlight.* Spectrochimica Acta Part A: Molecular and Biomolecular Spectroscopy, 2005. **61**(9): p. 2073-2079.

5. Platt, S., *Differential Optical Absorption Spectroscopy: Principles and Applications*. 2008: Wiley.

6. Bird, R.E. and C. Riordan, *Simple Solar Spectral Model for Direct and Diffuse Irradiance on Horizontal and Tilted Planes at the Earth's Surface for Cloudless Atmospheres.* Journal of Climate and Applied Meteorology, 1986. **25**(1): p. 87-97.

7. Fisher, B., J. Kukkonen, and M. Schatzmann, *Meteorology applied to urban air pollution problems: COST 715.* International Journal of Environment and Pollution, 2003. **16**(1-2): p. 560-570.

8. Union, E., *Clean Air for Europe (CAFE) Directive*. 21st of May 2008

9. API, T. *Technical Manual Teledyne Model 200E Nitrogen Oxide Analyser*. **Volume**,

10. Donnelly, A., B. Misstear, and B. Broderick, *Application of nonparametric regression methods to study the relationship between NO2 concentrations and local wind direction and speed at background sites.* Science of The Total Environment, 2011. **409**(6): p. 1134-1144.

11. Driscoll, S.O., *On imaging air pollutants in an urban street canyon using tomographic-DOAS*, in *Applied Physics and Instrumentation*. 2008, Cork Institute of Technology.

12. Platt, U., *Air monitoring by spectroscopic techniques*. 1994: Wiley-Interscience.

13. Brauer, M.E.A., *air pollution from traffic and the development of respiratory infections and asthmatic and allergic symptoms in children.* American journal respiratory and critical care medicine, 2002. **166**: p. 1092-1098.

14. Agency, I.E.P. *What we monitor*. present cited; Available from: http://www.epa.ie/whatwedo/monitoring/air/monitor/.

15. Brimblecombe, P., *Air composition and chemistry*. 2nd ed. Cambridge environmental chemistry series 6. 1986.

16. Commission, E. *Implementation of ambient air quality legislation*. 1999 [cited 2012 07-11-2012]; Understanding impact of individual pollutants]. Available from: http://ec.europa.eu/environment/air/quality/legislation/assessment.htm.

17. Bertram TH, C.R., et al, *Consistency of ozone and nitrogen oxides standards at tropospherically relevant mixing ratios.* J Air Waste Manag Assoc, 2005. **55**(10): p. 1473-9.

18. Dobson, G.M.B. and D.N. Harrison, *Measurements of the amount of ozone in the earth's atmosphere and its relation to other geophysical conditions.* Proceedings of the Royal Society of London. Series A, 1926. **110**(756): p. 660-693.

19. Instrumentation, T.A.P. *Instructional Manual: MODEL 300 CARBON MONOXIDE ANALYZER*. **Volume**, 111

20. Hönninger, G., C. von Friedeburg, and U. Platt, *Multi axis differential optical absorption spectroscopy (MAX-DOAS).* Atmos. Chem. Phys., 2004. **4**(1): p. 231-254.

21. Hecht Eugene, Z.A., *Optics*. 4th ed. 2002, USA and Canada: Addison-Wesley. 565.

22. Boeker, E., van Grondelle, *Environmental Physics*. 1996: Wiley and Sons. 448.

23. University, W. *Identifying elements in the Sun using spectral lines*. 2000 2002 [cited; Data description adapted from Learning astronomy by doing astronomy Ana Larson]. Available from: http://www.astro.washington.edu/courses/labs/clearinghouse/labs/Solarspec2/sunspec.html.

24. De Beek, R., et al., *The Ring effect in the cloudy atmosphere.* Geophysical research letters, 2001. **28**(4): p. 721-724.

25. Wagner, T., *Correction of the Ring effect and Io effect for DOAS observations of scattered sunlight.*

26. Chance, K.V. and R.J.D. Spurr, *Ring effect studies: Rayleigh scattering, including molecular parameters for rotational Raman scattering, and the Fraunhofer spectrum.* Applied Optics, 1997. **36**(21): p. 5224-5230.

27. Schneider, W., Moorgat, G.K., et al, *Absorption cross sections of NO_2 in the UV and visible region (200 - 700 nm)at 298 K.* Photochem. Photobiol., 1987(40): p. 195-217.

28. Bovensmann, H., et al., *SCIAMACHY: Mission Objectives and Measurement Modes.* Journal of the Atmospheric Sciences, 1999. **56**(2): p. 127-150.

29. Vandaele, A.C., Hermans, C., et al *Measurements of the NO_2 absorption cross section from 42000 cm^{-1} to 10000 cm^{-1} (238-1000 nm) at 220K and 294K.* Journal of Quantitative Spectroscopy and Radiative Transfer, 1998. **59**: p. 171-184.

30. Bogumil, K., Orphal, J., et al *Measurements of molecular absorption spectra with the SCIAMACHY pre-flight model: Instrument characterisation and reference data for atmospheric remote sensing in the 230-2380 nm region* J. Photochem. Photobiol A: photochemistry, 2003. **157**: p. 167-184.

31. Orphal, J., *A critical review of the absorption cross-sections of O3 and NO2 in the ultraviolet and visible.* Journal of Photochemistry and Photobiology A: Chemistry, 2003. **157**(2–3): p. 185-209.

32. Noxon, J.F., *Nitrogen Dioxide in the Stratosphere and Troposphere Measured by Ground-Based Absorption Spectroscopy*. Science, 1975. **189**(4202): p. 547-549.

33. Platt, U., D. Perner, and H.W. Pätz, *Simultaneous Measurement of Atmospheric CH2O, O3, and NO2 by Differential Optical Absorption.* J. Geophys. Res., 1979. **84**(C10): p. 6329-6335.

34. Roscoe, H.K., et al., *Intercomparison of slant column measurements of NO2 and O4 by MAX-DOAS and zenith-sky UV and visible spectrometers.* Atmos. Meas. Tech. Discuss., 2010. **3**(4): p. 3383-3423.

35. Chan, K.L., et al., *NO2 measurements in Hong Kong using LED based long path differential optical absorption spectroscopy.* Atmos. Meas. Tech., 2012. **5**(5): p. 901-912.

36. DOAS, U.o.B.I. *IUP-Bremen DOAS group*. [cited 2008; Summary of DOAS materials and research conducted by IUP-Bremen, specifically satellite projects]. Available from: http://www.iup.uni-bremen.de/doas/index.html.

37. Van Roozendael, M., et al., *Intercomparison of BrO measurements from ERS-2 GOME, ground-based and balloon platforms.* Advances in Space Research, 2002. **29**(11): p. 1661-1666.

38. Solomon, S., A.L. Schmeltekopf, and R.W. Sanders, *On the Interpretation of Zenith Sky Absorption Measurements.* J. Geophys. Res., 1987. **92**(D7): p. 8311-8319.

39. Zuo, H., et al., *Equiangular method: a technique of multiaxis DOAS.* J. Opt. Soc. Am. B, 2009. **26**(8): p. 1656-1662.

40. von Friedeburg, C., et al., *Derivation of tropospheric NO3 profiles using off-axis differential optical absorption spectroscopy measurements during sunrise and comparison with simulations.* J. Geophys. Res., 2002. **107**(D13): p. 4168.

41. Hendrick, F., et al., *Intercomparison exercise between different radiative transfer models used for the interpretation of ground-based zenith-sky and multi-axis DOAS observations.* Atmos. Chem. Phys., 2006. **6**(1): p. 93-108.

42. Iwabuchi, H., *Efficient Monte Carlo methods for radiative transfer modelling* Journal of atmospheric sciences, 2006.

43. Wagner, T., et al., *Comparison of box-air-mass-factors and radiances for Multiple-Axis Differential Optical Absorption Spectroscopy (MAX-DOAS) geometries calculated from different UV/visible radiative transfer models.* Atmos. Chem. Phys., 2007. **7**(7): p. 1809-1833.

44. Leigh, R.J., et al., *Concurrent multiaxis differential optical absorption spectroscopy system for the measurement of tropospheric nitrogen dioxide.* Appl. Opt., 2006. **45**(28): p. 7504-7518.

45. AB, O., *AR500 Opto-Analyser*. 1993, Furulund, Sweden: Opsis-AB.

46. Obinsk, P.T. *Commercial DOAS system*. cited; Available from: eridan.mega.ru/adr.htm.

47. GmbH, H.M. *Products*. cited; Available from: http://www.hmm.de/.

48. S.A., E. *Multi-Gas long path air quality monitoring system*. [cited 2012; Commercial DOAS system France]. Available from: http://www.environnement.it/public/articoli/53/Files/Sanoa_Scheda_tecnica_uk.pdf.

49. EPA, I., *Air Quality in Ireland 2011 key indicators of ambient air quality*. 2011, EPA 2012: Ireland.

50. Aliwell, S.R., et al., *Analysis for BrO in zenith-sky spectra: An intercomparison exercise for analysis improvement.* J. Geophys. Res., 2002. **107**(D14): p. 4199.

51. Eisinger, M., et al., *DOAS Zenith Sky Observations: 1. BrO Measurements over Bremen (53 N) 1993â€“1994.* Journal of atmospheric chemistry, 1997. **26**(1): p. 93-108.

52. Galle, B., et al., *A miniaturised ultraviolet spectrometer for remote sensing of SO2 fluxes: a new tool for volcano surveillance.* Journal of Volcanology and Geothermal Research, 2003. **119**(1–4): p. 241-254.

53. Petritoli, A., et al., *Off-axis measurements of atmospheric trace gases by use of an airborne ultraviolet-visible spectrometer.* Applied optics, 2002. **41**(27): p. 5593-5599.

54. Bobrowski, N., Honniger, G., Galle, B., Platt, U., *Detection of BrO in a volcanic plume.* Nature, 2002. **423**(6937): p. 3.

55. Melamed, M.L., et al., *Detection of pollution transport events southeast of Mexico City using ground-based visible spectroscopy measurements of nitrogen dioxide.* Atmos. Chem. Phys., 2009. **9**(14): p. 4827-4840.

56. Frins, E., et al., *Tomographic multiaxis-differential optical absorption spectroscopy observations of Sun-illuminated targets: a technique providing well-defined absorption paths in the boundary layer.* Appl. Opt., 2006. **45**(24): p. 6227-6240.

57. Takashima, H., et al., *NO2 observations over the western Pacific and Indian Ocean by MAX-DOAS on Kaiyo, a Japanese research vessel.* Atmos. Meas. Tech. Discuss., 2011. **4**(5): p. 6069-6095.

58. Kramer, L.J., et al., *Comparison of OMI and ground-based in situ and MAX-DOAS measurements of tropospheric nitrogen dioxide in an urban area.* J. Geophys. Res., 2008. **113**(D16): p. D16S39.

59. Pfeilsticker, K., et al., *Optical path modifications due to tropospheric clouds: Implications for zenith sky measurements of stratospheric gases.* J. Geophys. Res., 1998. **103**(D19): p. 25323-25335.

60. Frins, E., et al., *Tomographic MAX-DOAS observations of sun illuminated targets: a new technique providing well defined absorption paths in the boundary layer*. 2006.

61. Vlemmix, T., et al, *Potential and limitations of the MAX-DOAS method to retrieve the vertical distribution of tropospheric nitrogen dioxide.* Atmospheric Measurement techniques discussions, 2011. **4**: p. 4013-4072.

62. Richter, A. and J.P. Burrows, *Tropospheric NO2 from GOME measurements.* Advances in Space Research, 2002. **29**(11): p. 1673-1683.

63. Burrows, J., Dehn, A., et al, *Atmospheric remote-sensing reference data from GOME: part I. Temperature-dependent absorption cross-sections of NO_2 in the 231-794 nm range.* Journal Quant. Spectroscopic radiation transfer 1998. **60**: p. 1025-1031.

64. Streets, D.G., T. Canty, and e. al, *Emissions estimation from satellite retrievals: A review of current capability.* Atmospheric Environment, 2013.

65. Boeker, E., van Grondelle, *Environmental Physics*. 2011: Wiley and Sons. 448.

66. TEMIS. *Total and Tropospheric NO2 columns from GOME II*. 2013 cited; Available from: http://www.temis.nl/airpollution/no2col/no2monthgome2_v2.php?Year=2013&Month=05.

67. Elias, T., et al., *Comparison of COSPEC and two miniature ultraviolet spectrometer systems for SO₂ measurements using scattered sunlight.* Bulletin of Volcanology, 2006. **68**(4): p. 313-322.

68. Aeronomy, B.I.o.S. *WinDOAS*. 2012 cited 2011; Available from: http://uv-vis.aeronomie.be/software/WinDOAS/.

69. F. Gotz, A.R.M., G. Dobson, *The vertical distribution of Ozone in the Atmosphere*. Proceedings of the Royal Society Series A 1934. **145**(855): p. 416-466.

70. Andersen, A.H. and A.C. Kak, *Simultaneous Algebraic Reconstruction Technique (SART): A superior implementation of the ART algorithm.* Ultrasonic Imaging, 1984. **6**(1): p. 81-94.

71. Louban, I., et al, *Measurement of SO2 and NO2 applying ToTaL-DOAS from remote site.* Journal of Optics A: Pure adn Applied Optics, 2008. **10**(10).

72. Sinreich, R., et al., *Multi axis differential optical absorption spectroscopy (MAX-DOAS) of gas and aerosol distributions.* Faraday discussions, 2005. **130**: p. 153-64; discussion 241-64, 519-24.

73. Sinreich, R., et al., *Parameterising radiative transfer to convert MAX-DOAS dSCDs into near-surface box-averaged mixing ratios.* Atmospheric Measurement Techniques, 2013. **6**(6): p. 1521-1532.

74. Cohn, A., Angevine, W.M., *Boundary layer height and entrainment zone thickness measured by lidars and wind-profiling radars.* American meteorological society, 2000. **39**(8): p. 1233-1247.

75. Halla, J.D., et al., *Determination of tropospheric vertical columns of NO2 and aerosol optical properties in a rural setting using MAX-DOAS.* Atmos. Chem. Phys., 2011. **11**(23): p. 12475-12498.

76. Sinreich, R., et al., *Parameterising radiative transfer to convert MAX-DOAS dSCDs into near-surface box-averaged mixing ratios.* Atmospheric Measurement Techniques, 2013. **6**(6): p. 1521-1532.

77. Hao-yi, Z., et al., *Retrieval of the vertical column density of the atmospheric pollution gases by using the scattered solar radiation.* Journal of Quantitative Spectroscopy and Radiative Transfer, 2008. **109**(15): p. 2628-2634.

78. Williams, E.J., et al., *Comparison of Ultraviolet Absorption, Chemiluminescence, and DOAS Instruments for Ambient Ozone Monitoring.* Environmental Science & Technology, 2006. **40**(18): p. 5755-5762.

79. Lamsal, L.N., et al., *Ground-level nitrogen dioxide concentrations inferred from the satellite-borne Ozone Monitoring Instrument.* Journal of Geophysical Research, 2008. **113**(D16): p. D16308.

80. Wagner, T., et al., *Cloudy sky optical paths as derived from differential optical absorption spectroscopy observations.* Journal of Geophysical Research: Atmospheres, 1998. **103**(D19): p. 25307-25321.

81. Hertel*, O. and M. Evan Goodsite, *Chapter 1 Urban Air Pollution Climates throughout the World*, in *Air Quality in Urban Environments*. 2009, The Royal Society of Chemistry. p. 1-22.

82. Online, M.E.T.I.M.S. *Climate of Ireland*. 2013 cited; Available from: http://www.met.ie/climate-ireland/climate-of-ireland.asp.

83. Murphy, J.G., S. O'Driscoll, and N.J. Smith, *Multipath DOAS for tomographic measurements.* 2003: p. 875-885.

84. Optics, O. *Ocean Optics devices*. cited; Available from: http://www.oceanoptics.com.

85. Dooly, G., et al., *Low Concentration Monitoring of Exhaust Gases Using a UV-Based Optical Sensor.* Sensors Journal, IEEE, 2007. **7**(5): p. 685-691.

86. Fitzpatrick, C., O'Donoghue, C., Lewis, E., *A novel multi-point UV optical fibre sensor based on cladding luminescence.* Measurement science and technology, 2003. **14**: p. 1477-1483.

87. Chen, D., et al., *Tropospheric NO2 column densities deduced from zenith-sky DOAS measurements in Shanghai, China, and their application to satellite validation.* Atmos. Chem. Phys., 2009. **9**(11): p. 3641-3662.

88. Hecht Eugene, Z.A., *Optics*. 7th ed. 1982, USA and Canada: Addison-Wesley. 565.

89. Hamamatsu. *S10420 CCD*. cited; Available from: http://sales.hamamatsu.com/assets/pdf/parts_S/s10420-6_etc_kmpd1102e02.pdf.

90. O'Malley, M.J. and E. O'Mongain, *Charge-coupled devices: frame adding as an alternative to long integration times and cooling.* Optical Engineering, 1992. **31**(3): p. 522-526.

91. Scientific, R. *Spectroscopic etaloning in back illuminated CCDs*. cited 2012; Summary of Spectroscopic etaloning in BI-CCDs]. Available from: http://www.roperscientific.de/etaloning.html.

92. Walsh, J.E., et al., *Fibre-optic micro-spectrometers for biomedical sensing.* Transactions of the Institute of Measurement and Control, 2000. **22**(5): p. 355-369.

93. Ltd, R. *Calibration Cells*. cited; Available from: http://www.resonance.on.ca/calibration_cells.htm.

94. instruments, T. *Instruction Manual Model 200A Chemiluminescent analyzer*. **Volume**, 225

95. Morales, J.A., J. Treacy, and S. Coffey, *Urban ozone measurements using differential optical absorption spectroscopy.* Analytical and Bioanalytical Chemistry, 2004. **379**(1): p. 51-55.

96. Ireland, E.P.A., *Air Quality Annual Report 2011*, Environment, Editor. 2011: Ireland.

97. Council, D.C., *Air Quality monitoring and noise control Dublin Regional air quality management plan 2009-2012*, D.C. Council, Editor. 2009-2012.

98. Leigh, R.J., et al., *Spatially resolved measurements of nitrogen dioxide in an urban environment using concurrent multi-axis differential optical absorption spectroscopy.* Atmos. Chem. Phys., 2007. **7**(18): p. 4751-4762.

99. Dunlea, E.J., et al., *Evaluation of nitrogen dioxide chemiluminescence monitors in a polluted urban environment.* Atmos. Chem. Phys., 2007. **7**(10): p. 2691-2704.

100. Vlemmix, T,.et.al., *MAX-DOAS tropospheric nitrogen dioxide column measurements compared with the Lotos-Euros air quality model.* Atmos. Chem. Phys., 2011/10/26. **11**(10): p. 49.

101. Van Houcke, E., Garland, Wendy and Treacy Jack. *Measurement of SO_2 in Dublin City by Differential Optical Absorption Spectroscopy*. Facility for Optical Characterisation and Spectroscopy (FOCAS), Dublin Institute of Technology.

102. Rooney, J., Garland, Wendy and Treacy, Jack. *Formaldehyde in urban air*. Facility for Optical Characterisation and Spectroscopy (FOCAS), Dublin Institute of Technology.

103. Kambe, Y., et al., *Monitoring of atmospheric nitrogen dioxide by long-path pulsed differential optical absorption spectroscopy using two different light paths.* Journal of Environmental Monitoring, 2012. **14**(3): p. 944-950.

Appendix I Paper submitted for publication to the Atmospheric Measurement Techniques

Title: A portable spectroscopic detection system for pollution monitoring in an urban environment.

Brian Devine[1] and. James E. Walsh[2]

[1]Optical Sensors and Metrology Laboratory,

FOCAS,

Dublin Institute of Technology,

Camden Row, Dublin 8

[2]On leave from School of Physics,

College of Sciences and Health

Dublin Institute of Technology

Kevin Street, Dublin 8

Ireland

Currently

Director of Pre-University Studies,

MAHSA University College,

Jalan Universiti Campus,

Jalan Elmo, off Jalan Universiti,

59100 Kuala Lumpur, Malaysia

Abstract

Monitoring of air pollutants such as Nitrogen Dioxide (NO_2) that are toxic or environmentally damaging is a key metric for environmental protection agencies worldwide. There is a constant need to develop new technologies and methodologies that provide real-time, low cost pollution measurements over a broad range of sampling sites, particularly in urban and industrial areas.

Typically detection of pollutants in urban environments is performed using a variety of techniques many of which are expensive, require complex setups and are in fixed locations. The novel system presented here is designed for portable, low cost and in-situ detection of pollutants such as NO_2 using Differential Optical Absorption Spectroscopy (DOAS). The basis for the system is the new generation of miniature fibre optic spectrometers that provide measurement specifications close to that of more traditional high cost DOAS instruments which are used to cross calibrate the initial data. The system can also be calibrated against other NO_2 sampling techniques such as chemiluminescence (CL) monitors. Based on laboratory calibration the final measurement accuracy of the system in the field was less than ± 0.5 ppb over a calibration dynamic range of 0-50 ppb under typical daylight conditions. This level of accuracy was achieved with repeated measurements, n=10, of custom made calibration cells containing known concentrations of NO_2.

Laboratory experiments using a controlled light source were designed to examine the correlation between absorption and differential absorption using the calibration cells and a specifically developed algorithm based on the Beer-Lambert Law. These laboratory calibration tests verified that differential absorption determined using the novel system can be used to quantify NO_2 concentrations both in the laboratory and in the open atmosphere of a surrounding urban area. Field tests, using ambient sunlight as a source, were then conducted and compared to concurrent CL measurements. Good correlations have been confirmed between the novel systems data and the established NO_2 quantification methods.

Results prove that low cost fibre optic spectrometer systems can be used to identify and quantify gaseous pollutants in real-time using ambient sunlight and additional experiments using the new generation of high intensity light emitting diodes (LED) indicate that future systems can also be based around low cost LED arrays.

1. Introduction

1.1 Air pollution

Modern transport and industrial activities have resulted in the need to monitor gas pollutants produced in urban environments[21]. Several modern scientific methods have been utilised to accurately assess concentration levels, among these methods are those that directly sample gases and remote sensing of the average gas concentration[6]. The work presented here describes the development of a novel optical sensing system for monitoring gas pollution, based on differential optical absorption spectroscopy (DOAS) that is portable, inexpensive and will have reduced complexity compared to existing similar systems.

Monitoring the distribution and concentration of pollutants requires an understanding of the atmosphere, the types of pollutants, and the different methods of detection employed in their quantification. The atmosphere can be divided into different layers which are characterised by their changes in altitude, temperature and pressure. The natural composition of the atmosphere is primarily Nitrogen (78%), Oxygen (21%) and other gases e.g. Argon, CO_2, and Water[1, 6]. Natural sources such as volcanoes and plant decomposition as well as human activities contribute a broad range of gaseous pollutants to the atmosphere including nitrogen dioxide, sulphur dioxide, formaldehyde and particulate matter[6]. In the urban environment the primary source of these gasses is man-made and the distribution of pollution concentration throughout an urban environment and it's immediate atmosphere is primarily determined by factors such as the location of the emission sources, time of day and local weather conditions[34].

The optical system described here can technically quantify a broad range of polluting gases in the atmosphere but has been developed using nitrogen dioxide (NO_2) as the primary target test analyte due to its importance as a primary toxic pollutant and high spectral absorption coefficient at key/convenient visible wavelengths[5]. Nitrogen dioxide is a reddish brown gas and is present in the atmosphere, typically in the 0-100 ppb range, as a product of the naturally occurring nitrogen cycle and due to anthropogenic sources notably combustion[1, 6]. It's presence in the atmosphere is related to photochemical smog, acid rain and lower visibility[16] it is also partly responsible for the chemical formation of nitric oxide from photochemical reactions and the destruction of ozone by oxidation[16]. The standard set limits for the concentration of NO_2 in the atmosphere are usually determined by a country's respective Environmental Protection Agency (EPA), with EU regulations[9] allowing a mean annual concentration of 40 $\mu g\ m^{-3}$ at 20^0C, which is roughly 21 ppb.

In addition a maximum of 200 μg m^{-3} may not be exceeded more than 18 times a year as short term spikes in NO_2 will have public health implications[9].

The effect of NO_2 on human health includes respiratory complications and airway restrictions. Long-term exposure can increase the risk of these respiratory issues[112]. NO_2 has a lifetime in the atmosphere of ~2 days[6, 113] and known sources of NO_2 include the Nitrogen cycle in local eco-systems, industrial facilities and combustion engines. It is therefore essential that levels of toxic atmospheric gas such as NO_2 are accurately and frequently monitored in populated areas to ensure annual EPA standards are met and to provide alarm level detection when concentration spikes occur. NO_2 levels are also correlated with daily traffic congestion and industrial activity and can therefore be used as a monitor of urban pollution events by the EPA.

The accurate detection and monitoring of NO_2 concentrations and emissions in the atmosphere are achieved by a broad range of techniques that include direct sampling of the local atmosphere followed by chemical analysis in the field or laboratory. Direct sampling followed by optical analysis in a sampling chamber can be performed by using laser-induced fluorescence[114] or chemiluminescence (CL) and remote sensing by optical methods such as Differential Optical Absorption Spectroscopy (DOAS)[13]. NO_2 levels in Dublin are monitored by the Irish EPA, according to the EU standards, using a CL technique. A Teledyne NO_x Analyzer, model 200E (Teledyne Advanced Pollution Instrumentation, Cal. U.S.) is an example of the standard CL device used, it samples the atmosphere through an inlet approximately 2 metres above ground making it comparable to NO_x inhaled by humans[10]. The extracted sample typically contains nitric oxide, NO, and nitrogen oxides, NO_x that are detected by a photomultiplier tube after the sample chemically reacts with a molybdenum catalytic converter the concentration of NO_2 is found by subtraction[10]. Other forms of NO_x detection by CL may vary for different instruments. The method employed for this research is based solely on DOAS, which is a type of spectroscopy that can use a broad spectrum to detect several pollutants. This paper describes the design construction and testing of a novel, low cost DOAS system based around a fibre optic spectrometer system that overcomes many of the problems of the existing standard methods.

1.2 Atmospheric absorption spectroscopy

The absorption of electromagnetic radiation as a function of wavelength is a result of the interaction of the radiation with absorbing molecules in the path of the radiation. The chemical identity of an absorbing molecule can be determined from the unique spectral fingerprint it produces at specific wavelengths in the spectrum of incident radiation. Most absorption spectroscopy techniques require a reference spectrum of the test medium and the illuminating light source with no absorbing analyte present. If the reference spectrum is denoted by $I_0(\lambda)$ and the measurement spectrum with absorbing analyte present denoted by $I(\lambda)$, the sample absorption (A) is defined as:

$$A(\lambda) = \log(I_0(\lambda)/I(\lambda)) \qquad (1)$$

The Beer-Lambert Law then relates A(l) to key analyte metrics as follows:

$$A(l) = \alpha(\lambda)cL \qquad (2)$$

Where L is the optical path-length (m), c is the analyte concentration ($kg.m^{-3}$) and is α is the analyte specific absorption coefficient (m^2kg^{-1}) which is determined from the absorption cross section[5], σ, in $cm^2molecule^{-1}$.

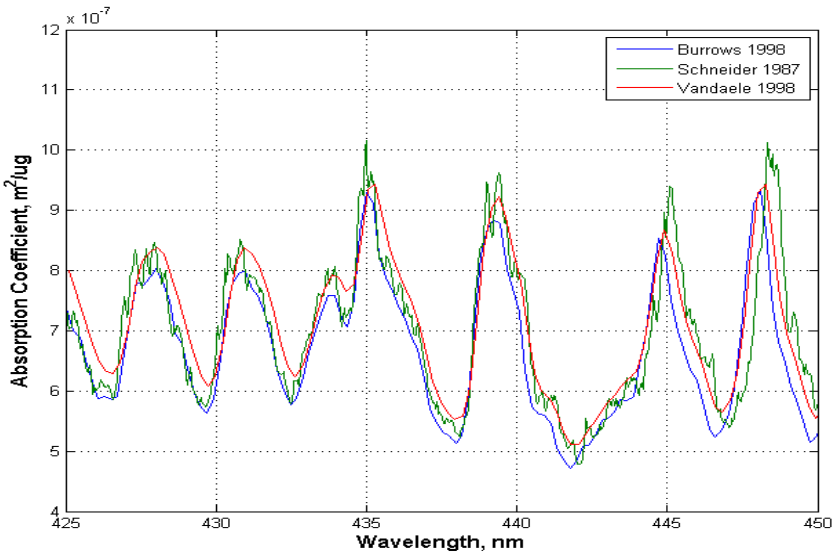

Figure 1 Absorption coefficient as a function of wavelength for NO_2 with spectral features of specific interest to this research highlighted [41, 43, 75].

For a known path-length analyte concentration is therefore directly related to specific absorption features in the absorption spectrum whose spectral fingerprint is contained in the specific absorption coefficient curve shown in fig. 1[41, 43, 75].

1.3 Differential optical absorption spectroscopy

In certain environmental monitoring situations, such as Tropospheric NO_2 quantification, it is very difficult to make a representative measurement of the reference intensity, I_0, as it requires a measurement virtually the same atmospheric path-length with no target analyte present. The DOAS method, developed in the 1970's by Noxon[46] and Platt[47], overcomes this by determining a differential absorption (D) at the selected target analyte fingerprint wavelengths in the measured spectrum. The principle behind the DOAS algorithm for the NO_2 spectral feature near 440 nm is shown in fig. 2, with the related calculations for determining the differential absorption, D, given equations. 3 to 5. The reference value used in the calculation of $I_0'(l)$ is related to the mean of the non absorbing regions either side of the analyte absorbing wavelength at $I_2(l)$, and the final values of D should be equivalent to absorption, A(l), values calculated using the reference I_o curve if available.

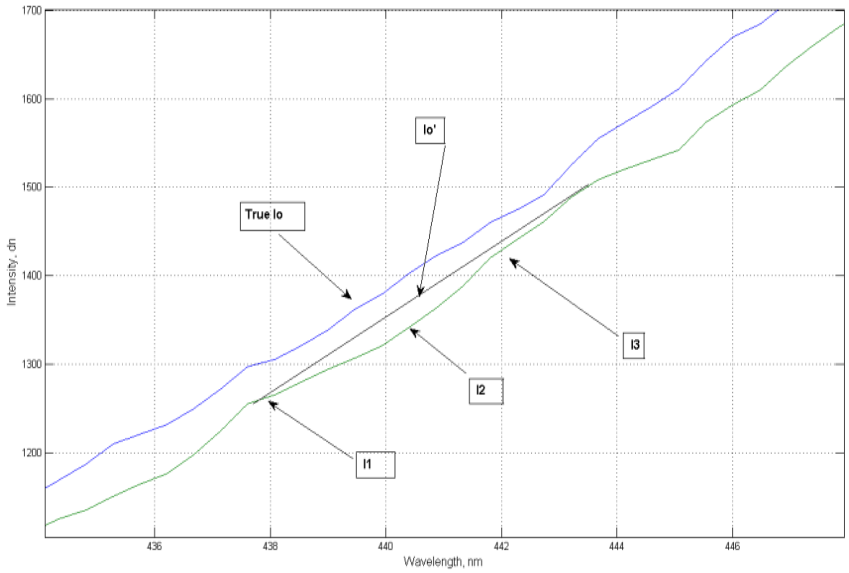

Figure 2 Comparison of reference (blue) and measured spectra (green) with labelled intensities of an attenuated feature used in the determination of D.

$$I_0' = I_1 + ((I_2 - I_1)(\lambda_2 - \lambda_1 / \lambda_3 - \lambda_1)) \quad (3)$$

$$I = I_2 \quad (4)$$

$$D = \log (I_0'/I) \quad (5)$$

$$D(\lambda) = \alpha'(\lambda)\, cL \quad (6)$$

The absorption coefficient α is wavelength dependent so a differential α' is approximated to be ~ 3.4 x $10^{-7} m^2 \mu g^{-1}$ for wavelength range of 350nm-500nm, see eq. (6). The concentration of the NO_2 is given in units of $\mu g m^{-3}$as specified by EU regulations alternatively the units can be in volumetric ratio ppm or ppb.

DOAS systems can be used to determine profiles of gases such as NO_2 and BrO in the local atmosphere using Multi-Axis DOAS or MAX-DOAS[32]. The MAX-DOAS measurements are more versatile than the commercial DOAS as miniaturised spectrometers are used and no artificial light source is required they are also comparable to other detection methods such as satellite measurements. However MAX-DOAS

may only provide data for column densities in molecules/m^2 and the cost and mobility of the instruments is limited when more than one detector is used for simultaneous measurements of different elevation angles.

One miniaturised portable spectrometer was used the USB4000 available from Ocean Optics[95]. The detection of NO_2 in the lower atmosphere above Dublin city involved the calculation of D from the recorded spectra with an algorithm designed in Matlab and a rigorously designed and tested optical set up. This system is demonstrated here to be portable, inexpensive and adaptable to a variety of applications e.g. traffic monitoring, location study, area surveys and continuous monitoring using ambient solar light and light emitting diodes.

2 Experimental: The novel detection system

The device will ideally will be portable and more affordable than the larger commercial DOAS system. The design will include optical components that maximise the light from various artificial and natural sources it will use a lens and collimating tube connected to the micro-spectrometer via an optical fibre. The following are proposed features of the system:

1. A narrow Field Of View, FOV. The FOV is the 3-Dimensional fraction of the area of the atmosphere viewed by the sytsems front end optics. The detector used for this research required a FOV with a comparable pathlength to a larger commercial DOAS system. The FOV should be parallel as too much divergence of the field can affect the volume being measured.
2. An adjustable aperture fixed to the collimating tube for a parallel FOV and to allow the measurement of a dark signal, which is subtracted to remove dark current and electronic noise, as the detected signal varies over time. The length of the collimating tube will also determine the field of view and the overall size of the detector.
3. A lens and fibre to detect enough light for a maximum signal. The sizes and spectral range of the lens and fibre must be compatible with the chosen wavelength range being investigated and the range of the spectrometer. These optical components will also need to detect light of the same wavelength emitted by broadband artificial sources.
4. A micro-spectrometer with a spectral resolution determined by the CCD detector and the width of the entrance slit. A bandwidth that allows the user to examine the detected signal for features that can be

used for the DOAS calculation eqns. 3-5. The spectrometer will need a wavelength range where features of NO_2 are present (350 nm to 550 nm). The spectrometer needs to have a signal to noise ratio and limits of detection comparable to larger DOAS system. The detection of real time spectra also requires the system to have a fast processing speed determined by a combination of the spectrometer and the laptop it's connected to.

The novel system has been developed so that it is comparable to the methods used by typical DOAS techniques. Its novel design will make it less accurate however, 'The design characteristics therefore have to be a compromise between flexibility and maximising the signal to noise', J.E. Walsh et al[103].. The USB4000 uses a Toshiba TCD1304AP CCD linear array also with a 25µm slit 3648 pixels and S/N of 300:1. The range of detection for the USB4000 is approximately 200nm-850nm and a FWHM of 1.5nm. The USB4000 with the optical fibre and front end optics arrives at a much lower cost than that of a larger commercial system.

2.1 Laboratory tests

The laboratory tests involved custom made quartz cells manufactured by Resonance Ltd[104], the cells were filled with known concentrations of NO_2 and one cell contained atmospheric air making it ideal as a reference. Each cell could be placed within a collimated beam of light, produced by a tungsten lamp the light is collimated by optical fibres and lenses directing the light beam through the sample. The receiving lens and fibre are coupled to the spectrometer. The complete apparatus is shown in fig. 3. The advantages of the calibration cells included the known concentrations provided by the manufacturer and the comparable concentrations to the expected NO_2 in equivalent pathlengths through the atmosphere. They are small, high quality quartz cells with a two year shelf life that have a diameter of 22mm and a thickness of 14.3mm with a stem. They are ideal for placing in front of the collimating lens and the adjustable aperture of the front end optics used in the field. From the experimental data the results obtained were used to determine the limits of detection and signal to noise (S/N) of the measurements. The spectrometer collected the light with a 5mm collimating lens and a 600µm diameter optical fibre. Integration times of 10ms for 100 scans and 500 scans

were used for the laboratory testing, the integration time of averages 5 scans per second. With these integration times the S/N increases by ~22.3.

A reference sample was used with other samples containing different concentrations of NO_2. Both A and D were determined from the measured spectra of these samples and the results compared. The spectral region for NO_2 absorption is between 330nm and 500nm with prominent features at 435nm and 441nm, the detection limits for NO_2 in the atmosphere are 0.2ppb for a 5km path length at 20^0C [6]. The features at 435nm although suitable for the laboratory tests were too close to a prominent Fraunhofer line in the solar spectrum however the 441nm feature proved adequate. Early testing showed a good correlation between D determined for each sample without the reference and A were results were calculated with the reference sample which are shown in fig. 5. The Ocean Optics USB4000 spectrometer operates with SpectraSuite software which controls the integration time and number of scans as well as displaying the spectra. D and A were calculated using the purposely written Matlab algorithm.

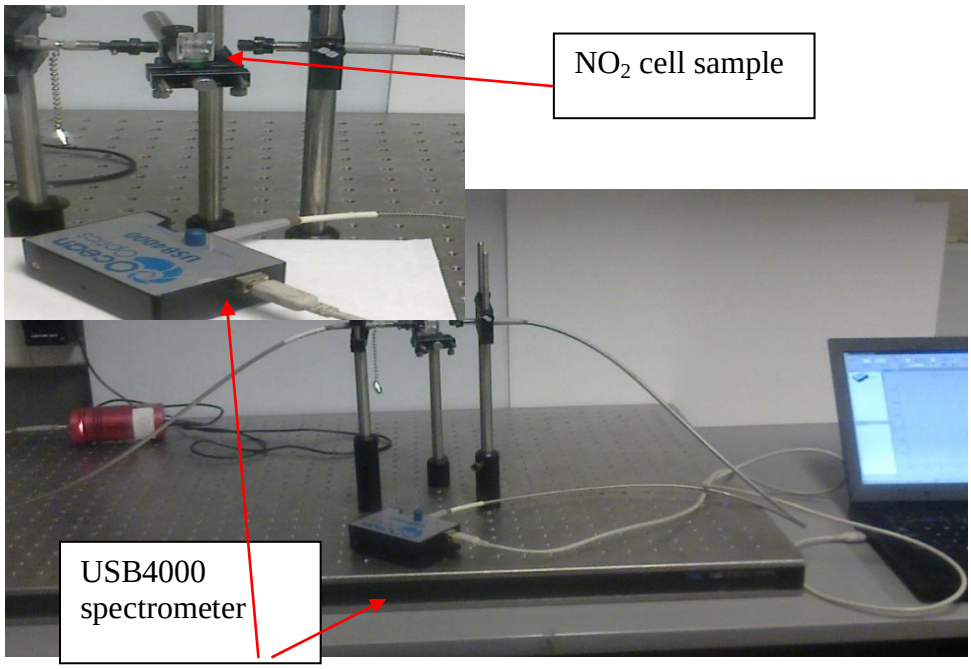

Figure 3 Calibration cell between source and detector (Main picture) on the optical bench. The cells small size and stem allows precise alignment for each test (inset)

The limit of detection of the technique was determined using the cells and showed that the cell with the lowest concentration 5ppm-m or 6.7 x $10^5 \mu gm^{-3}$ for 1.4cm cell was close to the minimum detectable limit of the system, this was equivalent to $0.94 \mu gm^{-3}$ in a 10km path as described in table 1 section 3.1.

2.2 Field Tests

Measurements taken with the spectrometer were of the atmosphere directly overhead i.e. the zenith direction and across the Dublin skyline at elevation angles ranging from 0^0 parallel to the ground to 30^0 (fig. 4). Measurements made from the FOCAS institute laboratory were of the sky above the south of Dublin city. For when the weather was not suitable to place the detector outside so the collimating tube and the aperture were adjusted to eliminate any reflections and light from within the room.

The recorded spectra were used to determine the differential absorption (D) of 438nm to 443nm to determine a value for D in eq. (5). Approximate pathlengths determined from the literature were10 km [5, 69] for the horizontal and 1km for zenith measurements of the planetary boundary layer. These were used to calculate the concentrations see figs. 5-7.

Measurements with the calibration cells involved placing the cells in front of the adjustable aperture at the end of the 100mm collimating tube starting with the atmospheric air sample. The expected results should show an increase in D for each cell except the air sample and the differences in magnitude between the increases should correspond to the differences in concentration between the cells, see fig. 10. For example the 50ppm-m cell would not show an increase less than that expected by the 5ppm-m cell when each one was placed in front of the detector.

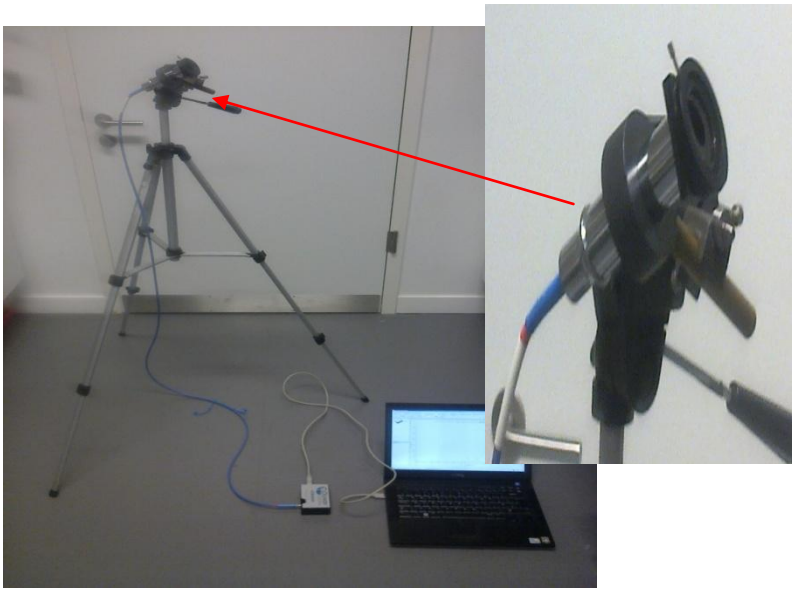

Figure 4: Novel-DOAS apparatus with camera stand, collimating tube, adjustable aperture (close up in inset) and 2m long optical fibre with (Maya2000) mini-spectrometer and laptop

3. Results and Discussion:

3.1.1 Laboratory Results

The cells concentrations including the reference cell filled with atmospheric air and three cells with different concentrations of NO_2 are shown in table 1.

	Cell concentration. Equivalent for 1 metre path length.	1km	Production Error %
1	Atmospheric Air	0ppb	0
2	5ppm-m	5ppb	±10
3	20ppm-m	20ppb	±10
4	50ppm-m	50ppb	±10

Table 1: Concentrations of Calibration Cells over 1m and equivalent over 1km

The results in fig. 5 were obtained when each cell was tested 10 times and the results plotted with errors because of the low concentration of the 5ppm-m cell it was ideal for an approximate determination of the limits of detection of the system. The concentrations in fig. 5 are shown in ppb-km to illustrate the scale of the cell concentration in relation to a commercial DOAS pathlength. The small size and stem of the cells

made it possible to place them in a lens holder in front of the detector for atmospheric measurements in the field.

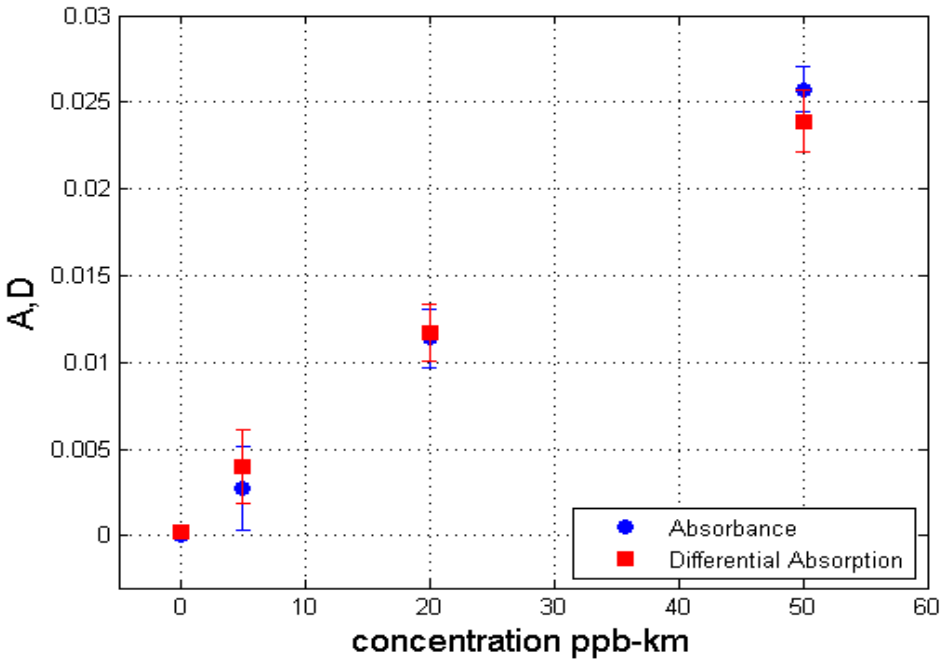

Figure 5: Correlation between A and D for each calibration cell using the USB4000 spectrometer. These results demonstrate the effectiveness of the algorithm and the accuracy of the technique.

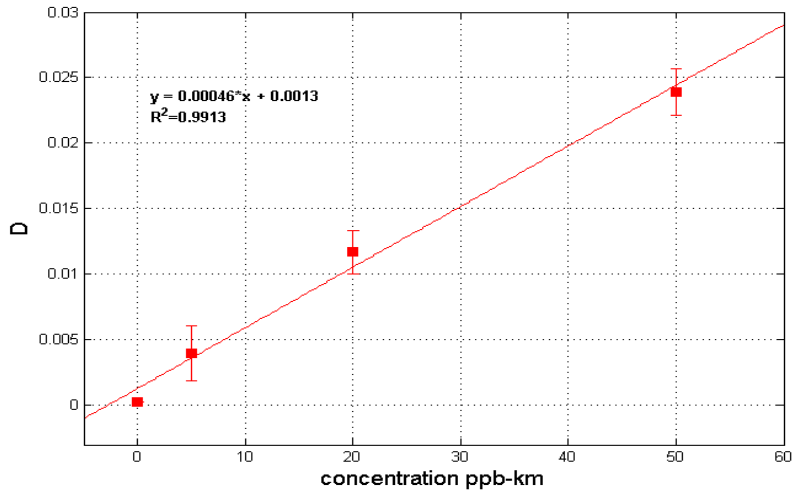

Figure 6 Cell concentration and D for n=10 tests on each cell. This shows the good repeatability of the measurements performed in the laboratory.

The values for A and D were determined using the path through the cell and the differential absorption coefficient α' was calculated to be ~3.4e-7 $m^2\mu g^{-1}$. The result of the tests in the laboratory with the tungsten-halogen lamp show there is a very good correlation between A and D (fig. 5). For each of the cells the measured concentration fell within the manufacturer's error of 10%. Therefore limits of detection showed that the system was capable of detecting concentrations of close to 0.5ppb in a 10km path, in fig. 6 the accuracy of the laboratory tests performed on each cell is determined using a regression line with R^2 value of 0.9913.

3.1.2 Detection of NO_2 in the atmosphere

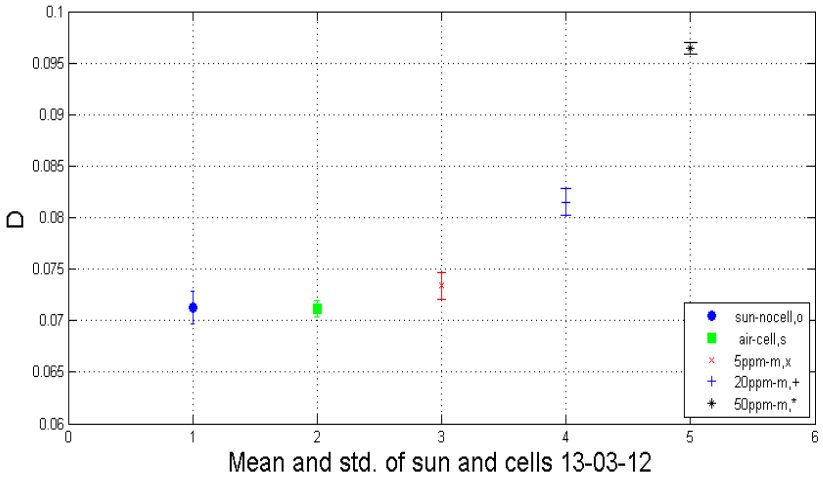

Figure 7 Increasing D for 5 measurements (1) no-cell, (2) air-cell and each calibration cell (3-5) containing NO_2 with ambient sunlight as a source.

Measurements of the atmosphere with the custom made cells placed in front of the detector throughout any day (fig. 7) show that the increase in NO_2 concentration to the path being measured is detectable by the DOAS method and the relative differences between the increases in concentration are comparable to the differences between the cells (fig. 5) once the outside concentration without the cells is subtracted. This is ideal for calibrating the system when measuring the local atmosphere.

Measurements of the atmosphere above DIT buildings were performed from the FOCAS building and from the roof of Kevin Street DIT. Fig.8 shows typical data taken for four consecutive days using the DOAS method with results compared with measurements made by a CL monitor placed in the path of the novel system. These results are inconclusive as the weather was cloudy and wet and not ideal for measurements of ambient sunlight. Clouds cause scattering effects which can vary the optical path of the light being measured[71]. However there is some correlation for an estimated pathlength of 5 km.

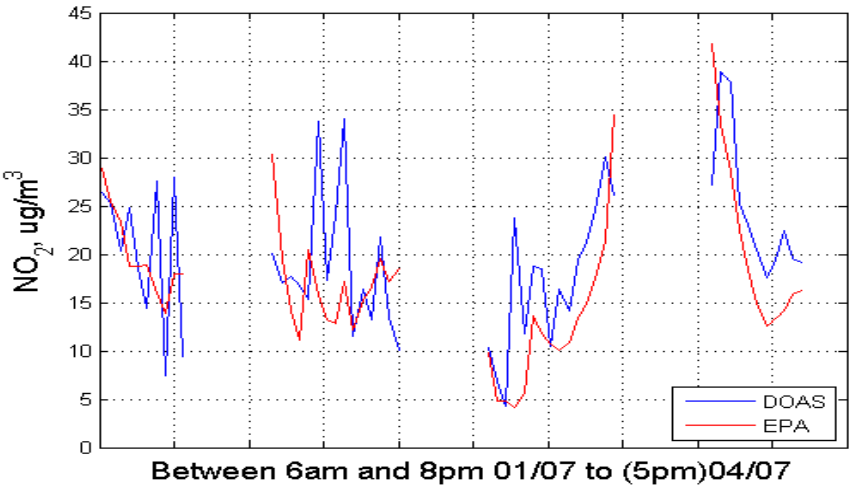

Figure 8 Four day comparison of EPA-CL and DOAS data. The estimated optical pathlengths for the determination of the NO_2 concentration for each day were l~5 km respectively.

Further comparisons of the DOAS method and CL reveal differences in data with sharp changes in the atmospheric NO_2 measured by CL. Fig. 9 illustrates how the data from each method compares. These results were obtained on a clearer day, although there are differences between CL and the DOAS techniques particularly that the CL is a point sampling technique which can be affected by local traffic congestion and the DOAS results are subject to variations in the optical pathlength by meteorological and topographical variations. A scatter plot of the data for late July 2011, (fig. 10), reveals that some correlation exists and by fitting a line to the data the slope is 1.3 which suggests the variation in NO_2 determined by CL and the novel DOAS are comparable between the two sets of recorded data for concentrations ranging between 5 μgm^{-3} and 25 μgm^{-3}. A correlation factor (R^2) obtained was very good at 0.708. The larger differences are likely due to

the differences in the types of measurement i.e. point sampling and remote sensing and the differences in the levels accuracy of each method.

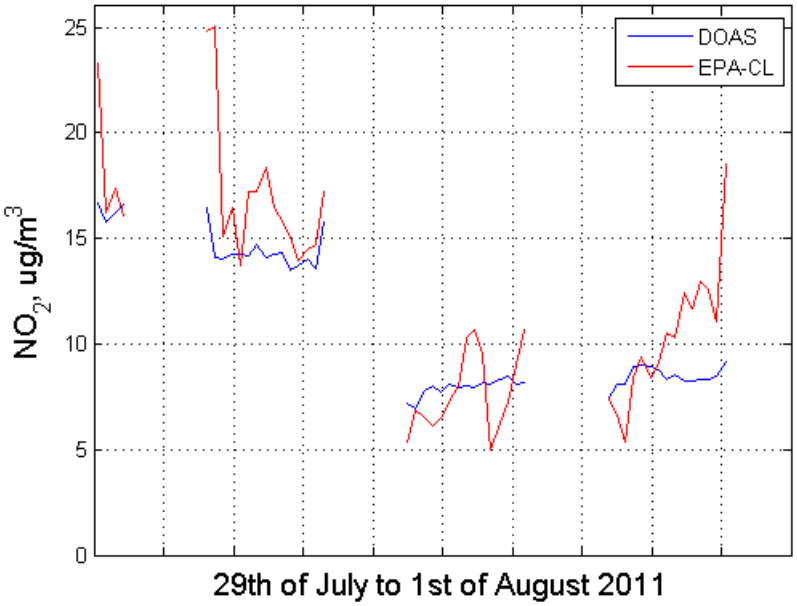

Figure 9 Comparison of in-situ DOAS and EPA for the concentration of NO_2 and correlation 30/07/11 to 01/08/11

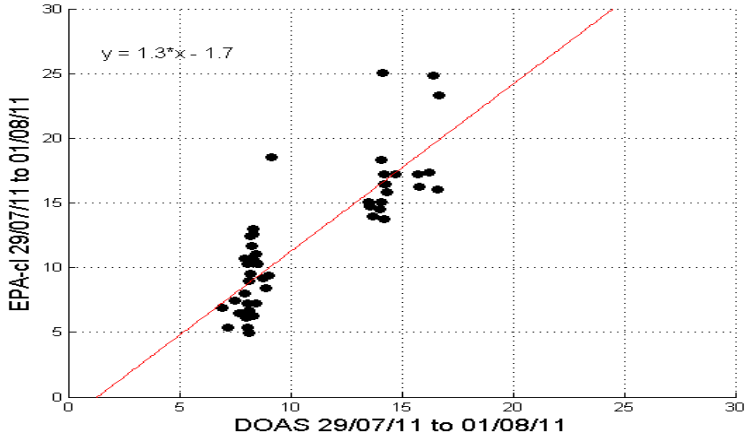

Figure 10 Scatter plot of the same data presented in fig. 8 with slope 1.3 and a correlation factor of R^2 = 0.708.

4. Conclusions

4.1 Summary of the results

To test the validity of the use of a miniaturised spectrometer to measure NO_2 concentrations, tests were designed and developed in the laboratory on an optical bench to determine the correlation of absorption, (A), determined with a reference sample and the differential absorption, (D), were no reference is needed. Using an algorithm developed the mathematical value for I_o' and hence D were calculated along with a value of A for each sample the results show that the correlation between the two was excellent. A value of 3.4×10^{-7} $m^2 \mu g^{-1}$ was determined for the absorption coefficient, α'. This was found to be an accurate value for the α' for NO_2 similar to values described in the literature [41]. The limits of detection were determined in the laboratory using the smallest concentration sample which was also comparable to 5 ppm in 1 m (equivalent to 1 $\mu g m^{-3}$ in 10 km).

The final configuration of the novel system consisted of an adjustable aperture attached to a collimating tube which is coupled to the lens and optical fibre. The fibre is connected to a USB4000 miniaturised spectrometer which is connected via a USB cable to a Toshiba laptop. The analysis of the data recorded by the laptop is performed using the Matlab and SpectraSuite software. The integration time for the field measurements 500 scans/10 ms which averaged the signal over 5 seconds increases the signal to noise ratio by a factor of ~22.

The results can be compared with the EPA measurements if a reasonable pathlength of ~10 km is chosen. Further analysis of the correlation of EPA data and the DOAS system demonstrated that the correlation was much better on clear sunny days. Figure 10 illustrates how well the EPA data and the DOAS system can correlate with an approximate pathlength of 10 km.

The novel system is constructed from relatively inexpensive components far less expensive than the commercial DOAS and CL monitors. The portability of the novel system made it possible to record spectra from the roof tops of the DIT buildings and on the locations in Rathmines. The system can be calibrated in the

laboratory with the cells containing different concentrations of NO_2. Calibration can also be achieved in the field by placing the cells in front of the instrument and calculating the increases in D for each cell and comparing the results to the D of the open atmosphere. The results show that the effectiveness and accuracy of the measurements on clear days in the field is comparable to concurrent EPA data obtained using CL the existing standard monitoring technique outlined in European Union policy.

4.2 Future Work

Concurrent measurements with local CL monitors could be taken with satellite data to develop a local profile of the NO_2 concentrations in different azimuthal directions and within the troposphere. Further development of the software could make the system more user friendly for various operators. Cheap alternative light sources would make the system more versatile allowing measurements to be taken at night and under various meteorological conditions.

Detection of other pollutants could also be achieved particularly O_3 and SO_2 which are also constantly monitored by the EPA. O_3 in particular contributes to the aerosol measurement data used to determine the AMF and can therefore be useful in the determination of the vertical height of NO_2 concentrations.

Acknowledgements

EPA STRIVE Research Program Grant

References:

1. Godish, T., *Air Quality*. 2004: Lewis Publishers. 460.
2. E.U., *Clean Air for Europe (CAFE) Directive*. 21st of May 2008 European Union.
3. Association, S.M.H. *The vertical structure of the atmosphere*. [cited 2012; Available from: http://smha.btck.co.uk/OriginoftheAtmosphere/VerticalStructure.
4. Vandaele 1998, S., Bogumil 2003, Burrows 1998. [cited; Available from: http://www.atmosphere.mpg.de/enid/.../Spectra/Catalogue_Spectra_5p4.html.
5. Morales, J.A. and J.E. Walsh, *Detection of atmospheric nitrogen dioxide using a miniaturised fibre-optic spectroscopy system and the ambient sunlight.* Spectrochimica Acta Part A: Molecular and Biomolecular Spectroscopy, 2005. **61**(9): p. 2073-2079.
6. Platt, S., *Differential Optical Absorption Spectroscopy: Principles and Applications*. 2008: Wiley.
7. Bird, R.E. and C. Riordan, *Simple Solar Spectral Model for Direct and Diffuse Irradiance on Horizontal and Tilted Planes at the Earth's Surface for Cloudless Atmospheres.* Journal of Climate and Applied Meteorology, 1986. **25**(1): p. 87-97.
8. Fisher, B., J. Kukkonen, and M. Schatzmann, *Meteorology applied to urban air pollution problems: COST 715.* International Journal of Environment and Pollution, 2003. **16**(1-2): p. 560-570.
9. Union, E., *Clean Air for Europe (CAFE) Directive*. 21st of May 2008
10. API, T. *Technical Manual Teledyne Model 200E Nitrogen Oxide Analyser*. **Volume**,
11. Donnelly, A., B. Misstear, and B. Broderick, *Application of nonparametric regression methods to study the relationship between NO2 concentrations and local wind direction and speed at background sites.* Science of The Total Environment, 2011. **409**(6): p. 1134-1144.
12. Driscoll, S.O., *On imaging air pollutants in an urban street canyon using tomographic-DOAS*, in *Applied Physics and Instrumentation*. 2008, Cork Institute of Technology.
13. Platt, U., *Air monitoring by spectroscopic techniques*. 1994: Wiley-Interscience.
14. Brauer, M.E.A.e.a., *Air pollution from traffic and the development of respiratory infections and asthmatic and allergic symptoms in children.* American journal respiratory and critical care medicine, 2002. **166**: p. 1092-1098.
15. Agency, I.E.P. *What we monitor*. present [cited; Available from: http://www.epa.ie/whatwedo/monitoring/air/monitor/.
16. Brimblecombe, P., *Air composition and chemistry*. 2nd ed. Cambridge environmental chemistry series 6. 1986.
17. EPA, I., *Air Quality in Ireland 2011 key indicators of ambient air quality*. 2011, EPA 2012: Ireland.
18. Commission, E. *Implementation of ambient air quality legislation*. 1999 [cited 2012 07-11-2012]; Understanding impact of individual pollutants]. Available from: http://ec.europa.eu/environment/air/quality/legislation/assessment.htm.

19. Ireland, E.P.A., *Air Quality Annual Report 2011*, Environment, Editor. 2011: Ireland.
20. Council, D.C., *Air Quality monitoring and noise control Dublin Regional air quality management plan 2009-2012*, D.C. Council, Editor. 2009-2012.
21. Holloway, A., Wayne, R, *Atmospheric Chemistry*, ed. R. publishing. 2010: RSC.
22. Harrison, R.M., Hester, R.E., Hertel, Ole, *Air Quality in urban environments*. 2009: Royal Society of Chemistry.
23. Wayne, R.P., *Chemistry of the Atmosphere*. 2000: Oxford University Press Inc.
24. instruments, T. *Instruction Manual Model 200A Chemiluminescent analyzer*. **Volume**, 225
25. Bertram TH, C.R., et al, *Consistency of ozone and nitrogen oxides standards at tropospherically relevant mixing ratios.* J Air Waste Manag Assoc, 2005. **55**(10): p. 1473-9.
26. Dobson, G.M.B. and D.N. Harrison, *Measurements of the amount of ozone in the earth's atmosphere and its relation to other geophysical conditions.* Proceedings of the Royal Society of London. Series A, 1926. **110**(756): p. 660-693.
27. Instrumentation, T.A.P. *Instructional Manual: MODEL 300 CARBON MONOXIDE ANALYZER*. **Volume**, 111
28. AB, O., *AR500 Opto-Analyser*. 1993, Furulund, Sweden: Opsis-AB.
29. Cohn, A., Angevine, W.M., *Boundary layer height and etrainment zone thickness measured by lidars and wind-profiling radars.* Amercian meteorological society, 2000. **39**(8): p. 1233-1247.
30. Harren, F.J.M., et al., *Photoacoustic spectroscopy in trace gas monitoring.* Encyclopedia of Analytical Chemistry, 2000.
31. Courtillot, I., et al., *Sub-ppb NO2 detection by optical feedback cavity-enhanced absorption spectroscopy with a blue diode laser.* Applied Physics B, 2006. **85**(2-3): p. 407-412.
32. Hönninger, G., C. von Friedeburg, and U. Platt, *Multi axis differential optical absorption spectroscopy (MAX-DOAS).* Atmos. Chem. Phys., 2004. **4**(1): p. 231-254.
33. Hecht Eugene, Z.A., *Optics*. 4th ed. 2002, USA and Canada: Addison-Wesley. 565.
34. Boeker, E., van Grondelle, *Environmental Physics*. 1996: Wiley and Sons. 448.
35. University, W. *Identifying elements in the Sun using spectral lines*. 2000 2002 [cited; Data description adapted from Learning astronomy by doing astronomy Ana Larson]. Available from: http://www.astro.washington.edu/courses/labs/clearinghouse/labs/Solarspec2/sunspec.html.
36. De Beek, R., et al., *The Ring effect in the cloudy atmosphere.* Geophysical research letters, 2001. **28**(4): p. 721-724.
37. Wagner, T., *Correction of the Ring effect and Io effect for DOAS observations of scattered sunlight.*
38. Chance, K.V. and R.J.D. Spurr, *Ring effect studies: Rayleigh scattering, including molecular parameters for rotational Raman scattering, and the Fraunhofer spectrum.* Applied Optics, 1997. **36**(21): p. 5224-5230.
39. Francis Rouessac, A.R., *Chemical Analysis, modern instrumental methods and techniques* 2000: John Wiley & sons.

40. E Haller, H.K., L.S. Cederbaum, *The visible absorption spectrum of NO_2: A three-mode nuclear dynamics investigation* Journal of Molecular spectroscopy, 1985. **111**(2): p. 377-397.
41. Schneider, W., Moorgat, G.K., et al, *Absorption cross sections of NO_2 in teh UV and visible region (200 - 700 nm)at 298 K.* Photochem. Photobiol., 1987(40): p. 195-217.
42. Bovensmann, H., et al., *SCIAMACHY: Mission Objectives and Measurement Modes.* Journal of the Atmospheric Sciences, 1999. **56**(2): p. 127-150.
43. Vandaele, A.C., Hermans, C., et al *Measurements of the NO_2 absorption cross section from 42000 cm^{-1} to 10000 cm^{-1} (238-1000 nm) at 220K and 294K.* Journal of Quantitative Spectroscopy and Radiative Transfer, 1998. **59**: p. 171-184.
44. Bogumil, K., Orphal, J., et al *Measurements of molecular absorption spectra with the SCIAMACHY pre-flight model: Instrument characterisation and reference data for atmospheric remote sensing in the 230-2380 nm region* J. Photochem. Photobiol A: photochemistry and photobiology, 2003. **157**: p. 167-184.
45. Orphal, J., *A critical review of the absorption cross-sections of O3 and NO2 in the ultraviolet and visible.* Journal of Photochemistry and Photobiology A: Chemistry, 2003. **157**(2–3): p. 185-209.
46. Noxon, J.F., *Nitrogen Dioxide in the Stratosphere and Troposphere Measured by Ground-Based Absorption Spectroscopy.* Science, 1975. **189**(4202): p. 547-549.
47. Platt, U., D. Perner, and H.W. Pätz, *Simultaneous Measurement of Atmospheric CH2O, O3, and NO2 by Differential Optical Absorption.* J. Geophys. Res., 1979. **84**(C10): p. 6329-6335.
48. Roscoe, H.K., et al., *Intercomparison of slant column measurements of NO2 and O4 by MAX-DOAS and zenith-sky UV and visible spectrometers.* Atmos. Meas. Tech. Discuss., 2010. **3**(4): p. 3383-3423.
49. Chan, K.L., et al., *NO2 measurements in Hong Kong using LED based long path differential optical absorption spectroscopy.* Atmos. Meas. Tech., 2012. **5**(5): p. 901-912.
50. DOAS, U.o.B.I. *IUP-Bremen DOAS group*. [cited 2008; Summary of DOAS materials and research conducted by IUP-Bremen, specifically satellite projects]. Available from: http://www.iup.uni-bremen.de/doas/index.html.
51. Van Roozendael, M., et al., *Intercomparison of BrO measurements from ERS-2 GOME, ground-based and balloon platforms.* Advances in Space Research, 2002. **29**(11): p. 1661-1666.
52. Solomon, S., A.L. Schmeltekopf, and R.W. Sanders, *On the Interpretation of Zenith Sky Absorption Measurements.* J. Geophys. Res., 1987. **92**(D7): p. 8311-8319.
53. Zuo, H., et al., *Equiangular method: a technique of multiaxis DOAS.* J. Opt. Soc. Am. B, 2009. **26**(8): p. 1656-1662.
54. von Friedeburg, C., et al., *Derivation of tropospheric NO3 profiles using off-axis differential optical absorption spectroscopy measurements during sunrise and comparison with simulations.* J. Geophys. Res., 2002. **107**(D13): p. 4168.
55. Hendrick, F., et al., *Intercomparison exercise between different radiative transfer models used for the interpretation of ground-based zenith-sky and multi-axis DOAS observations.* Atmos. Chem. Phys., 2006. **6**(1): p. 93-108.
56. Iwabuchi, H., *Efficient Monte Carlo methods for radiative transfer modelling* Journal of atmospheric sciences, 2006.

57. Wagner, T., et al., *Comparison of box-air-mass-factors and radiances for Multiple-Axis Differential Optical Absorption Spectroscopy (MAX-DOAS) geometries calculated from different UV/visible radiative transfer models.* Atmos. Chem. Phys., 2007. **7**(7): p. 1809-1833.
58. Leigh, R.J., et al., *Concurrent multiaxis differential optical absorption spectroscopy system for the measurement of tropospheric nitrogen dioxide.* Appl. Opt., 2006. **45**(28): p. 7504-7518.
59. Obinsk, P.T. *Commercial DOAS system*. [cited; Available from: eridan.mega.ru/adr.htm.
60. GmbH, H.M. *Products*. [cited; Available from: http://www.hmm.de/.
61. S.A., E. *Multi-Gas long path air quality monitoring system*. [cited 2012; Commerical DOAS system France]. Available from: http://www.environnement.it/public/articoli/53/Files/Sanoa_Scheda_tecnica_uk.pdf.
62. Aliwell, S.R., et al., *Analysis for BrO in zenith-sky spectra: An intercomparison exercise for analysis improvement.* J. Geophys. Res., 2002. **107**(D14): p. 4199.
63. Eisinger, M., et al., *DOAS Zenith Sky Observations: 1. BrO Measurements over Bremen (53 N) 1993â€“1994.* Journal of atmospheric chemistry, 1997. **26**(1): p. 93-108.
64. Galle, B., et al., *A miniaturised ultraviolet spectrometer for remote sensing of SO2 fluxes: a new tool for volcano surveillance.* Journal of Volcanology and Geothermal Research, 2003. **119**(1–4): p. 241-254.
65. Petritoli, A., et al., *Off-axis measurements of atmospheric trace gases by use of an airborne ultraviolet-visible spectrometer.* Applied optics, 2002. **41**(27): p. 5593-5599.
66. Bobrowski, N., Honniger, G., Galle, B., Platt, U., *Detection of BrO in a volcanic plume.* Nature, 2002. **423**(6937): p. 3.
67. Melamed, M.L., et al., *Detection of pollution transport events southeast of Mexico City using ground-based visible spectroscopy measurements of nitrogen dioxide.* Atmos. Chem. Phys., 2009. **9**(14): p. 4827-4840.
68. Frins, E., et al., *Tomographic multiaxis-differential optical absorption spectroscopy observations of Sun-illuminated targets: a technique providing well-defined absorption paths in the boundary layer.* Appl. Opt., 2006. **45**(24): p. 6227-6240.
69. Takashima, H., et al., *NO2 observations over the western Pacific and Indian Ocean by MAX-DOAS on Kaiyo, a Japanese research vessel.* Atmos. Meas. Tech. Discuss., 2011. **4**(5): p. 6069-6095.
70. Kramer, L.J., et al., *Comparison of OMI and ground-based in situ and MAX-DOAS measurements of tropospheric nitrogen dioxide in an urban area.* J. Geophys. Res., 2008. **113**(D16): p. D16S39.
71. Pfeilsticker, K., et al., *Optical path modifications due to tropospheric clouds: Implications for zenith sky measurements of stratospheric gases.* J. Geophys. Res., 1998. **103**(D19): p. 25323-25335.
72. Frins, E., et al., *Tomographic MAX-DOAS observations of sun illuminated targets: a new technique providing well defined absorption paths in the boundary layer*. 2006.
73. Vlemmix, T.E.A., et al, *Potential and limitations of the MAX-DOAS method to retrieve the vertical distribution of tropospheric nitrogen dioxide.* Atmospheric Measurement techniques discussions, 2011. **4**: p. 4013-4072.

74. Richter, A. and J.P. Burrows, *Tropospheric NO2 from GOME measurements.* Advances in Space Research, 2002. **29**(11): p. 1673-1683.
75. Burrows, J., Dehn, A., et al, *Atmospheric remote-sensing reference data from GOME: part I. Temperature-dependent absorption cross-sections of NO_2 in the 231-794 nm range.* Journal Quant. Spectroscopic radiation transfer 1998. **60**: p. 1025-1031.
76. Streets, D.G., T. Canty, and e. al, *Emissions estimation from satellite retrievals: A review of current capability.* Atmospheric Environment, 2013.
77. Boeker, E., van Grondelle, *Environmental Physics*. 2011: Wiley and Sons. 448.
78. TEMIS. *Total and Tropospheric NO2 columns from GOME II*. 2013 [cited; Available from: http://www.temis.nl/airpollution/no2col/no2monthgome2_v2.php?Year=2013&Month=05.
79. Elias, T., et al., *Comparison of COSPEC and two miniature ultraviolet spectrometer systems for SO₂ measurements using scattered sunlight.* Bulletin of Volcanology, 2006. **68**(4): p. 313-322.
80. Aeronomy, B.I.o.S. *WinDOAS*. 2012 [cited 2011; Available from: http://uv-vis.aeronomie.be/software/WinDOAS/.
81. F. Gotz, A.R.M., G. Dobson, *The vertical distribution of Ozone in the Atmosphere.* Proceedings of the Royal Society Series A 1934. **145**(855): p. 416-466.
82. Andersen, A.H. and A.C. Kak, *Simultaneous Algebraic Reconstruction Technique (SART): A superior implementation of the ART algorithm.* Ultrasonic Imaging, 1984. **6**(1): p. 81-94.
83. Louban, I., et al, *Measurement of SO2 and NO2 applying ToTaL-DOAS from remote site.* Journal of Optics A: Pure adn Applied Optics, 2008. **10**(10).
84. Sinreich, R., et al., *Multi axis differential optical absorption spectroscopy (MAX-DOAS) of gas and aerosol distributions.* Faraday discussions, 2005. **130**: p. 153-64; discussion 241-64, 519-24.
85. Sinreich, R., et al., *Parameterising radiative transfer to convert MAX-DOAS dSCDs into near-surface box-averaged mixing ratios.* Atmospheric Measurement Techniques, 2013. **6**(6): p. 1521-1532.
86. Halla, J.D., et al., *Determination of tropospheric vertical columns of NO2 and aerosol optical properties in a rural setting using MAX-DOAS.* Atmos. Chem. Phys., 2011. **11**(23): p. 12475-12498.
87. Sinreich, R., et al., *Parameterizing radiative transfer to convert MAX-DOAS dSCDs into near-surface box-averaged mixing ratios.* Atmospheric Measurement Techniques. **6**(6): p. 1521-1532.
88. Hao-yi, Z., et al., *Retrieval of the vertical column density of the atmospheric pollution gases by using the scattered solar radiation.* Journal of Quantitative Spectroscopy and Radiative Transfer, 2008. **109**(15): p. 2628-2634.
89. Williams, E.J., et al., *Comparison of Ultraviolet Absorbance, Chemiluminescence, and DOAS Instruments for Ambient Ozone Monitoring.* Environmental Science & Technology, 2006. **40**(18): p. 5755-5762.
90. Lamsal, L.N., et al., *Ground-level nitrogen dioxide concentrations inferred from the satellite-borne Ozone Monitoring Instrument.* Journal of Geophysical Research, 2008. **113**(D16): p. D16308.

91. Wagner, T., et al., *Cloudy sky optical paths as derived from differential optical absorption spectroscopy observations.* Journal of Geophysical Research: Atmospheres, 1998. **103**(D19): p. 25307-25321.
92. Hertel*, O. and M. Evan Goodsite, *Chapter 1 Urban Air Pollution Climates throughout the World*, in *Air Quality in Urban Environments*. 2009, The Royal Society of Chemistry. p. 1-22.
93. Online, M.E.T.I.M.S. *Climate of Ireland*. 2013 [cited; Available from: http://www.met.ie/climate-ireland/climate-of-ireland.asp.
94. Murphy, J.G., S. O'Driscoll, and N.J. Smith, *Multipath DOAS for tomographic measurements.* 2003: p. 875-885.
95. Optics, O. *Ocean Optics devices*. [cited; Available from: http://www.oceanoptics.com.
96. Dooly, G., et al., *Low Concentration Monitoring of Exhaust Gases Using a UV-Based Optical Sensor.* Sensors Journal, IEEE, 2007. **7**(5): p. 685-691.
97. Fitzpatrick, C., O'Donoghue, C., Lewis, E., *A novel multi-point UV optical fibre sensor based on cladding luminescence.* Measurement science and technology, 2003. **14**: p. 1477-1483.
98. Chen, D., et al., *Tropospheric NO2 column densities deduced from zenith-sky DOAS measurements in Shanghai, China, and their application to satellite validation.* Atmos. Chem. Phys., 2009. **9**(11): p. 3641-3662.
99. Hecht Eugene, Z.A., *Optics*. 7th ed. 1982, USA and Canada: Addison-Wesley. 565.
100. Hamamatsu. *S10420 CCD*. [cited; Available from: http://sales.hamamatsu.com/assets/pdf/parts_S/s10420-006_etc_kmpd1102e02.pdf.
101. O'Malley, M.J. and E. O'Mongain, *Charge-coupled devices: frame adding as an alternative to long integration times and cooling.* Optical Engineering, 1992. **31**(3): p. 522-526.
102. Scientific, R. *Spectroscopic etaloning in back illuminated CCDs*. [cited 2012; Summary of Spectroscopic etaloning in BI-CCDs]. Available from: http://www.roperscientific.de/etaloning.html.
103. Walsh, J.E., et al., *Fibre-optic micro-spectrometers for biomedical sensing.* Transactions of the Institute of Measurement and Control, 2000. **22**(5): p. 355-369.
104. Ltd, R. *Calibration Cells*. [cited; Available from: http://www.resonance.on.ca/calibration_cells.htm.
105. Morales, J.A., J. Treacy, and S. Coffey, *Urban ozone measurements using differential optical absorption spectroscopy.* Analytical and Bioanalytical Chemistry, 2004. **379**(1): p. 51-55.
106. Leigh, R.J., et al., *Spatially resolved measurements of nitrogen dioxide in an urban environment using concurrent multi-axis differential optical absorption spectroscopy.* Atmos. Chem. Phys., 2007. **7**(18): p. 4751-4762.
107. Dunlea, E.J., et al., *Evaluation of nitrogen dioxide chemiluminescence monitors in a polluted urban environment.* Atmos. Chem. Phys., 2007. **7**(10): p. 2691-2704.
108. Vlemmix, T.E.A.e.a., *MAX-DOAS tropospheric nitrogen dioxide column measurements compared with the Lotos-Euros air quality model.* Atmos. Chem. Phys., 2011/10/26. **11**(10): p. 49.
109. Van Houcke, E., Garland, Wendy and Treacy Jack. *Measurement of SO_2 in Dublin City by Differential Optical Absorption Spectroscopy*. Facility for Optical Characterisation and Spectroscopy (FOCAS), Dublin Institute of Technology.

110. Rooney, J., Garland, Wendy and Treacy, Jack. *Formaldehyde in urban air*. Facility for Optical Characterisation and Spectroscopy (FOCAS), Dublin Institute of Technology.
111. Kambe, Y., et al., *Monitoring of atmospheric nitrogen dioxide by long-path pulsed differential optical absorption spectroscopy using two different light paths.* Journal of Environmental Monitoring, 2012. **14**(3): p. 944-950.
112. EPA, U.S. *Air nitrogen oxides health*. [cited; Available from: http://www.epa.gov/air/nitrogenoxides/health.html.
113. Velders, G.J.M., et al., *Global tropospheric NO2 column distributions: Comparing three-dimensional model calculations with GOME measurements.* J. Geophys. Res., 2001. **106**(D12): p. 12643-12660.
114. Miyazaki, K., et al., *Development of atmospheric NO analyzer by using a laser-induced fluorescence NO2 detector.* Atmospheric Environment, 2008. **42**(33): p. 7812-7820.

Appendix II Matlab algorithm used for data analysis

```
% DOAS and EPA-CL data analysis
%load drk3.txt
load drk1.txt
wv=drk1(:,1);
drk1=drk1(:,2);
drk=(drk1+drk2+drk3)./3;
load scope00.txt
scope00=scope00(:,2);

nmspec=471;

%loads scope10 to scope540 text files
for i=10:nmspec;

    eval(['load scope',num2str(i),'.txt']);
i;
end
%assigns scope files 0-9 to 'array'
for i=1:9;

    eval(['array(:,',num2str(i),')=scope0',num2str(i),'(:,2);']);
end
%assigns scope files 10-540 to 'array'
for i=10:nmspec;

    eval(['array(:,',num2str(i),')=scope',num2str(i),'(:,2);']);
i;
end

wvnrm=20:40;
 for i=1:nmspec;

    eval(['arrayd(:,',num2str(i),')=array(:,',num2str(i),')-(   (drk1)   .*
(mean(array(wvnrm,',num2str(i),') ) ) ./mean(drk1(wvnrm)) );']);
i;
end

%DOAS calculation
b1=1129; %438 nm
p1=1137; %440 nm
b2=1149; %442 nm

dwv=(wv(p1)-wv(b1))/(wv(b2)-wv(b1));

for i=1:nmspec;

    eval(['DOAS(:,',num2str(i),')=log(    (    arrayd(b1,',num2str(i),')+(
(arrayd(b2,',num2str(i),')-arrayd(b1,',num2str(i),')
).*dwv))./arrayd(p1,',num2str(i),'));']);
i;
```

```
end

%hours
t01=[2 8 14 20 26 32 38 44 50 56];
%Differential absorption
d01=[DOAS(2) DOAS(8) DOAS(14) AS(38) DOAS(44) DOAS(50) DOAS(56)];
%EPA-CL data
n01=[30 40];
%pathlength of 10 km
plot(t01,d01./(3.4e-7*10e3),'b-')
grid on
ylabel('NO_2, ug/m^3')
xlabel('Between 6am - 8pm')
legend('DOAS','EPA-CL')
set(gca,'xticklabel',[])
scatter([d01./(3.4e-7*5e3)],[n01])
grid on
d=[d01 d03 d04];
n=[n01 n03 n04];
xlabel('DOAS ug/m^3')
ylabel('EPA-CL ug/m^3')

grid on
```

Appendix II Conference Paper 2012 STRIVE

An Optical Fibre System for the detection of Atmospheric Gaseous Pollutants in an Urban Environment.

Brian Devine[1], Dr. James Walsh[2]

1. FOCAS Research Institute, Dublin Institute of Technology.
2. Dublin Institute of Technology.

ABSTRACT

Detection of pollutants in urban environments is performed using a variety of techniques that are expensive, require large setups and are often in permanent locations. The novel system presented here is designed for in-situ detection of pollutants using absorption spectroscopy specifically Differential Optical Absorption Spectroscopy (DOAS). This work expands on earlier research[2] to develop a miniaturised in-situ fibre-optic system to measure Nitrogen Dioxide (NO_2) in an urban area.

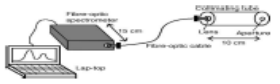

Figure 1 Ocean Optics Spectrometer instrument with Optical Fibre and Collimating tube

This system is designed to reduce costs and provide results that compare well to other systems. The principle of operation is based on Beer's Law:

Equation 1: $\mathbf{A = \log (I_0/I) = \alpha c l}$.

Laboratory tests were performed on polypropylene (PP) bags containing various concentrations of NO_2 and calibration cells filled with known concentrations.

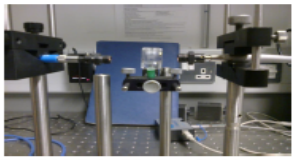

Figure 2 Typical calibration cell aligned between fibres for bench tests

Using an algorithm, based on the DOAS method, these tests have verified that Beer's Law correlates well with absorbance for different concentrations of the gas. Data has also been recorded on the roofs of DIT buildings to detect the differential absorption of NO_2. To perform these tests rigorous optical set-ups have been designed and tested. Tests have also been performed with Light Emitting Diodes[4] for use as alternative light sources

Differential Optical Absorption Spectroscopy

Developed in the 1970's DOAS[1,3] has been used for the detection of gaseous pollutants in the Earths atmosphere. DOAS involves the detection of pollutant concentration (μgm^{-3}) using a variation of Beer's Law. A reference intensity I_0 measurement taken when no analyte is present cannot be determined for the atmosphere because of background concentrations, so a baseline atmospheric measurement (i.e. no analyte present) cannot be quantified. The DOAS method overcomes this by determining a Differential Absorption with a calculated reference intensity I_0' from each measured spectrum. For this research an algorithm was developed to calculate I_0' (fig. 2) for each measurement. The absorption coefficient α is wavelength dependent so a differential α' was found in the literature sources[3].

DOAS Algorithm

The method used for the DOAS algorithm is illustrated in fig. 3. where the true I_0 is shown (blue) above the measured intensity (green) which is used to determine the I_0' with the following algorithm:

$$\mathbf{I_0' = I_1 + [I_3 - I_1] \cdot (\lambda_2 - \lambda_1) / (\lambda_3 - \lambda_1)}$$

$\mathbf{I = I_2}$, Differential Absorption: $\mathbf{D = \log(I_0'/I) = \alpha' cl}$

Where c is the concentration and l the path length.

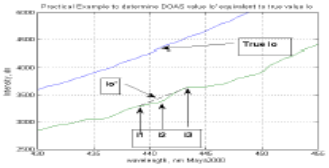

Figure 3 Determination of the differential reference I_0' from a raw intensity measurement (green) with an example of a true reference (blue). Spectrum of MAYA 2000 spectrometer.

Laboratory Test Results

Experiments were performed in the laboratory using PP bags with different concentrations of NO_2. The results shown in figure 4. compare the values obtained for the absorbance, "o", using a reference sample and those obtained using the DOAS algorithm, "squares".

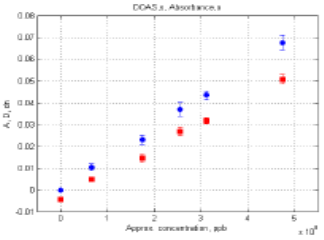

Figure 4 Average DOAS α and Absorbance o for 5 concentrations of Polypropylene Bag samples.

The results show a good correlation between absorbance and DOAS for both the PP-bags and the calibration cells which verifies that the DOAS algorithm can be used for determination of gas concentration. The novel system is being developed in accordance with EU regulations for monitoring gaseous pollutants[5].

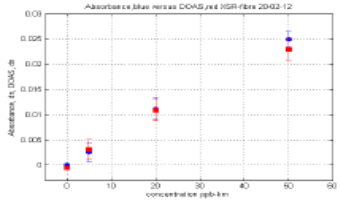

Figure 5 Average DOAS red and Absorbance blue for the 4 calibration cell concentrations including air cell at 0.

Acknowledgements

I would like to thank Dr. Walsh and the STRIVE research Programme for providing the funding for this project.

Light Emitting Diodes : Alternative Light Sources

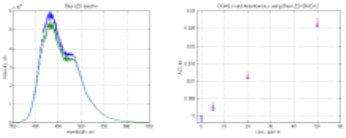

Figure 6 Spectra of LED light passed through calibration cell and reference (blue), Figure 7 Calculated Differential Absorption and absorbance for 3 concentrations.

Measurements using ambient Solar Light

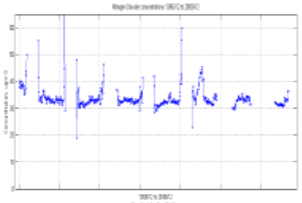

Figure 8 Concentration for 8 days in $\mu g/m^3$ for a 10km light-path

Conclusions

- Laboratory results show that the Differential Absorption algorithm and Absorbance are the same metric for measuring NO_2 concentration when applied to low cost spectrometer systems. This means that baseline atmospheric measurements (i.e. no analyte present) do not have to be quantified.
- Laboratory calibration has been successfully transferred to field based measurements and spectrometer specific algorithm variations determined.
- Testing of atmosphere above Dublin city show detailed analysis of Solar spectrum under various weather conditions, illumination levels and times which can be used to field calibrate the spectrometer systems.
- Preliminary testing of low cost, rugged LED sources has opened up several possibilities for a fixed path length, independent of Solar illumination when required.

Future Work

- Further testing of the novel system for the detection of NO_2 in atmosphere using the calibration cells and DOAS algorithm.
- Further analysis of the Solar spectrum for different times, illumination and weather conditions.
- Detection of NO_2 with calibrated novel system in various locations in Dublin city.
- Further development of LED light sources over fixed path lengths.

References

1. Platt & Stutz 2008 Differential Optical Absorption Spectroscopy: principles and applications, Springer.
2. Morales, J.A., & Walsh, J.E. 2005, Detection of atmospheric nitrogen dioxide using a miniaturized fibre-optic spectroscopy system and the ambient sunlight. Spectrochimica acta. Part A, Molecular and Biomolecular Spectroscopy, pp. 61[9], 2073-9.
3. Signiel, M.W. (ed.) 1994 Air Monitoring by Spectroscopic Techniques, Chemical Analysis Series, Wiley-Interscience
4. Kern, C. Platt, U. 2006 Applicability of light-emitting –diodes as light sources for active differential optical absorption spectroscopy measurements, Appl. Opt. 45, 2073-2088
5. EU Legislation (EU directive 2008/50/EC)

Appendix IV List of presentations & publications:

- 7th Annual STRIVE EPA researchers seminar

  Oral presentation

  12th - 13th November 2009 Gresham Hotel, Dublin

- 8th Annual STRIVE EPA researchers seminar

  Poster presentation

  11th - 12th November 2010 National Convention Centre, Dublin

- ESAI: 21st Irish Environmental Researchers Colloquium

  Poster presentation

  6h - 8h April 2011 University College Cork, Cork

- 9h Annual STRIVE EPA researchers seminar

  Oral presentation

  17h - 18h November 2011 Gresham Hotel, Dublin

- Rosse Medal – Institute of Physics researchers seminar

  Poster presentation

  30th March 2012 Royal College of Surgeons

- 2012 Strive Research Conference

  Poster presentation

  28th June 2012 Trinity College

- Research Paper: Atmospheric Measurement Techniques (September 2013)